IN-VIVO TESTING OF BIOLOGICAL BULK SOFT TISSUES BY A NON-AXISYMMETRIC TIP INDENTER USING DISPLACEMENT AND FORCE CONTROL

A THESIS SUBMITTED TO
THE GRADUATE SCHOOL OF NATURAL AND APPLIED SCIENCES
OF
MIDDLE EAST TECHNICAL UNIVERSITY

BY

PARINAZ ASHRAFI

IN PARTIAL FULFILLMENT OF THE REQUIREMENTS
FOR
THE DEGREE OF MASTER OF SCIENCE
IN
BIOMEDICAL ENGINEERING

FEBRUARY 2015

Approval of the thesis:

IN-VIVO TESTING OF BIOLOGICAL BULK SOFT TISSUES BY A NON-AXISYMMETRIC TIP INDENTER USING DISPLACEMENT AND FORCE CONTROL

Submitted by **PARINAZ ASHRAFI** in partial fulfillment of the requirements for the degree of **Master of Science in Biomedical Engineering Department, Middle East Technical University** by,

Prof. Dr. Gülbin Dural Ünver _____
Dean, Graduate School of **Natural and Applied Sciences**

Prof. Dr. Hakan Işık Tarman _____
Head of Department, **Biomedical Engineering**

Assist. Prof. Dr. Ergin Tönük _____
Supervisor, **Mechanical Engineering Dept., METU**

Prof. Dr. Murat Bozkurt _____
Co-Supervisor, **Department of Orthopedy and Traumatology, Atatürk Research and Education Hospital**

Examining Committee Members:

Prof. Dr. R. Orhan Yıldırım _____
Mechanical Engineering Dept., METU

Asst. Prof. Dr. Ergin Tönük _____
Mechanical Engineering Dept., METU

Prof. Dr. Suat Kadıoğlu _____
Mechanical Engineering Dept., METU

Assoc. Prof. Dr. Yeşim Serinağaoğlu Doğrusöz _____
Electrical and Electronics Dept., METU

Assist. Prof. Dr. Kıvanç Azgın _____
Mechanical Engineering Dept., METU

Date: 6.02.2015

I hereby declare that all information in this document has been obtained and presented in accordance with academic rules and ethical conduct. I also declare that, as required by these rules and conduct, I have fully cited and referenced all material and results that are not original to this work.

Name, Last name: Parinaz Ashrafi

Signature:

ABSTRACT

IN-VIVO TESTING OF BIOLOGICAL BULK SOFT TISSUES BY A NON-AXISYMMETRIC TIP INDENTER USING DISPLACEMENT AND FORCE CONTROL

Parinaz Ashrafi
M.S., Department of Biomedical Engineering
Supervisor: Assist. Prof. Dr. Ergin Tönük
Co-supervisor: Prof. Dr. Murat Bozkurt

February 2015, 195 pages

Soft tissues of human body have complex structures and different mechanical behaviors than those of traditional engineering materials. There is a great urge to understand tissue behavior of human body. Experimental data is needed for improvement of soft tissue modeling and advancement in implants and prosthesis, as well as diagnosis of diseases. Mechanical behavior and responses change when tissue loses its liveliness and viability. One of the techniques for soft tissue testing is indentation, which is applied on live tissue in its physiological environment. Indentation affords several advantages over other types of tests such as uniaxial tension, biaxial tension, and simple shear and suction, thus it is of interest to develop new indentation techniques from which precise data can be extracted. In this study experimental data was acquired using a soft tissue indenter designed and manufactured in METU. For real time data collection computer codes with a

graphical user interface was developed in LabVIEW programming software. The in-vivo force rate controlled cyclic loading test method which is novel is compared with the traditional displacement controlled cyclic loading tests. Displacement and force rate cyclic loading, and relaxation experiments were conducted on human arm. In addition to viscoelastic behavior of soft tissue, the anisotropic behavior and preconditioning behavior of human arm soft tissues were examined. Anisotropic behavior of tissue cannot be determined by axi-symmetric tips, therefore ellipsoid tips were designed and used for examining in-plane anisotropy of bulk soft tissues. Finally, precise experimental data, to be used in the computer simulations, were obtained.

ÖZ

YUMUŞAK BİYOLOJİK DOKULAR ÜSTÜNDE AKSİSIMETRİK OLMAYAN UÇLARLA YER DEĞİŞTİRME VE KUVVET KONTROLLÜ YERİNDE-CANLI İNDENTÖR DENEYLERİ

Parinaz Ashrafi
Yüksek Lisans, Biyomedikal Mühendisliği Bölümü
Tez Yöneticisi: Yrd.Doç. Dr. Ergin Tönük
Ortak Tez Yönetici: Prof. Dr. Murat Bozkurt

Şubat 2015, 195 sayfa

İnsan bedenindeki yumuşak dokular karmaşık yapıları nedeniyle geleneksel mühedislik malzemelerinden farklı davranışa sahiptir. İnsan bedenindeki dokuların davranışının anlaşılmasına büyük gereksinim vardır. Yumuşak doku bünye denklemleri için deneysel veriye gereksinim vardır ve bu sayede implantlar, protezler ve hastalıkların tanılanmasında gelişme sağlanabilir. Doku yerinden çıkarıldığında ve canlılığını kaybettiğinde mekanik yanıtı da değişir. Yumuşak doku deneylerinde kullanılan yöntemlerden birisi de indentasyondur ve dokuyu kendi fizyolojik ortamında ve canlı olarak test edebilir. İndentasyon tekniğinin tek eksenli veya iki eksenli çekme, basit kayma, emme deneylerinden belirgin üstünlükleri vardır, bundan dolayı yeni indentsayon yöntemleri ilgi görmüştür ve hassas veriler sağlamıştır. Bu çalışmada ODTÜ Makine Mühendisliği Bölümünde

tasarlanıp üretilen bir cihaz kullanılmış, cihaza gerekli kodlar LabVIEW ortamında yazılmıştır. Kuvvet denetimli devirli yükleme deneyleri bu çalışmada özgün olarak kullanılmıştır. Yer değiştirme ve kuvvet denetimli devirli deneyler, sünme ve gevşeme deneyleri insan kolu üzerinde uygulanmıştır. Yumuşak dokunun viskoelastik özelliklerine ek olarak eşyönsüzlüğüne ve alışma etkisine de bakılmıştır. Eşyönsüzlük için eksenel simetrik uçlar kullanılamayacağı için eliptik uçlar kullanılarak düzlemsel eşyönsüzlüğe bakılmıştır. Sonuçta, bilgisayar andırımları için kullanılabilecek hassas veri elde edilmiştir.

ACKNOWLEDGEMENTS

I would like to express my sincerest appreciation to all those people who has supported me either physically or morally throughout this study.

I am fully grateful to my supervisor Assist. Prof. Dr. M. Ergin Tönük for his unmatched guidance, encouragement, support, criticism and invaluable supervision. I am also thankful to him for being a reason for me to learn precious values for my future life. It was an honor for me to study with him throughout my graduate education.

I would also like to express my sincere thanks to dear Bilgehan Erdoğan (Mechanical Engineering Department) for his guidance and patience for my numerous questions during my study.

I need to express my thanks to all my friends and all the contributors who helped me with conducting experiments as subjects. I have been very lucky to share unforgettable moments in Biomechanics Lab with them.

My very special thanks go to my parents, Ali Ashrafi and Pari Haghighi for their eternal trust and unconditional support. Without their belief in me, this study could not have been realized.

Finally I would like to thank Gürhan Özkayar for his patience, love, support and never leaving me alone in this period of my life.

To my parents

TABLE OF CONTENTS

LIST OF TABLES

TABLES

LIST OF FIGURES

FIGURES

CHAPTER 1

AIM OF STUDY AND FIELD OF USE

For engineering materials such as steel, aluminum, titanium alloys etc. the material parameters and constitutive relations of them are known thus, the material behavior under the action of force and displacement is predictable. Therefore constructing buildings, making machines and, going to space, etc. is possible, but for soft tissues, because of complexity and lack of reliable and realistic experimental data, material model formulation of them is still in progress and there is not an accurate model yet. Thus our knowledge about mechanical properties of soft biological tissues should be improved.

Soft tissue property identification and material modelling is necessary for

- Improved surgical simulations
- Haptic virtual medical training
- Minimally invasive surgery (MIS)
- Identification of tissue abnormalities
- Improved prosthetics, orthotics and implants design
- Diagnosing disease and degeneration of tissue
- Pathobiology studying
- Finite element (FE) simulations of mechanical interaction of soft tissues with surrounding

Thus the mechanical interaction of biological materials with environment does hold keen interest for scientists, for this, experimental data is needed. These mechanical

behavior and responses change when tissue loses its liveliness and viability, hence ex vivo experiments in laboratory on a piece of soft tissue do not give us a reliable result, in vivo bulk soft tissue experiments that can be applied on live tissue in its physiological environment and in its original place in body, provide us this proper result then, more realistic simulations can be performed on the virtual world via soft-ware packages. Thus in this study, the indentation method (for the sake of reasons explained in Chapter 2) was chosen for doing experiments on live soft tissues, in its original location, and without any harm to the subjects. Indentation affords several advantages over other types of tests such as uniaxial tension, biaxial tension, and simple shear and suction, thus it is of interest to develop new indentation techniques from which more precise data can be extracted.

In this study experimental data that is needed for improvement of soft tissue modeling was acquired using a soft tissue indenter device, designed and manufactured in Middle East Technical University, (METU) Department of Mechanical Engineering, Biomechanics Laboratory. For real time data collection computer codes with a graphical user interface was developed in LabVIEW programming software. After preparing the set up for being able to do tests, improved test protocols was also developed in order to conduct more trustworthy and advanced in-vivo experiments on human arm. An elliptic tip was used for indenting tissue during anisotropy experiments, since the use of axially symmetric tips like spherical or cylindrical tips ignores pronounced tissue anisotropy. This tip is made of a polymer for preventing tissue harm.

The reason that a specific tissue such as skin or muscle was not chosen for our study was that in most of biomechanical designs, such as prosthetics, orthotics and implant design, the engineers are engaged with the whole bulk tissue of body, and the reaction of whole tissue together with skin, muscles, tendons, vessels and even with supporting bone in it is what they need. In addition to this, conducting experiments on human without any harm and intervention is an important factor in this selection.

It is hoped that this study could be a trustworthy experimental data source for soft tissue simulating and modeling, better understanding the mechanical behavior of live soft biological tissues, and also a guide for new researchers in this field.

CHAPTER 2

INTRODUCTION

2.1 An Introduction to Mechanical Behavior of Materials

2.1.1 Linear and nonlinear elastic material behavior

Elastic behavior is characterized by the following two provision: (1) where the stress in a material is a unique function of the strain, and (2) where the material has the characteristic for full recovery to a "natural" configuration after removal of the imposed forces. If the behavior of a material is not elastic, it is said that it is inelastic.

Also that elastic behavior may be linear or non-linear. Figure (2.1-1) presents these behavior patterns by simple stress-strain curves, with the relevant loading and unloading paths indicated. For many engineering applications theory of elasticity is a reliable model for design.

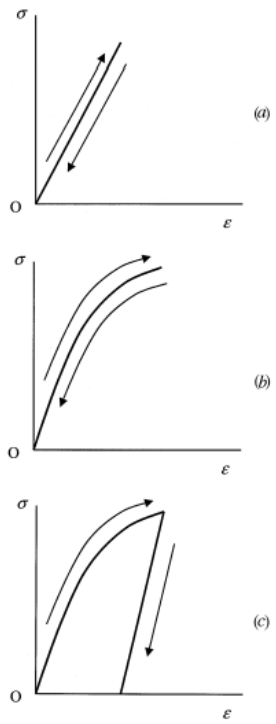

Figure 2.1-1. "Uniaxial loading-unloading stress-strain curves for (a) linear elastic; (b) nonlinear elastic; and (c) inelastic behavior."(MECHANICAL PROPERTIES OF MATERIALS ,David Roylance 2008)

2.1.1.1 Linear elastic

The relation between load and displacement in linear elastic materials, generally known as Hooke's Law, that can be written algebraically as

$$P = k\delta \qquad 2.1\text{-}1$$

Where k is a constant of proportionality called the stiffness and having units of N/m. Using more general measures of force per unit area and displacement per unit length, Hooke's Law becomes:

$$\sigma = E\epsilon \qquad 2.1\text{-}2$$

The constant of proportionality E, called "**Young's modulus**" or the "modulus of elasticity", is one of the most important mechanical descriptors of a material

independent from the geometry of the structural member. It has the same units as stress, Pa since strain is dimensionless (or elongation per unit length).

A material that obeys Hooke's Law is called a Hookean material. Such a material is elastic according to the description of elasticity given earlier (immediate response, full recovery), and it is also linear in its relation between stress and strain (or equivalently, force and deformation). Therefore a Hookean material is linear elastic. It is important to keep in mind that not all elastic materials are linear (rubber is elastic but nonlinear), and not all linear materials are elastic (viscoelastic materials can be linear in the mathematical sense, but do not respond immediately and are thus not elastic). It should be mentioned that all real materials have some sort of internal friction therefore deviate from ideal elasticity.

2.1.1.2 Poisson's ratio

A positive (tensile) strain in one direction will also contribute a negative (compressive) strain in the perpendicular direction, just as stretching a rubber band to make it longer in one direction makes it thinner in the other perpendicular directions. This lateral contraction accompanying a longitudinal extension is called the Poisson effect, and the Poisson's ratio is a material property defined as

$$\nu = \frac{-\epsilon_{lateral}}{\epsilon_{longitudinal}} \qquad 2.1\text{-}3$$

2.1.1.3 Shear modulus

The strain accompanying the shear stress τ_{xy} is a shear strain denoted γ_{xy}. This quantity is a deformation per unit length just as was the normal strain, but now the displacement is transverse to the length over which it is distributed. This is also the distortion or change in the right angle:

This angular distortion is found experimentally to be linearly proportional to the shear stress at sufficiently small loads, and the shearing counterpart of Hooke's Law can be written as

$$\tau_{xy} = G\gamma_{xy} \qquad 2.1\text{-}4$$

Where G is a material property called the shear modulus. For isotropic materials (properties same in all directions), there is no Poisson-type effect to consider in shear.

For isotropic linear elastic materials simple relations exist between elastic constants (Young's modulus E, shear modulus G, bulk modulus K, and Poisson's ratio ν) that allow calculating them all as long as two are known:

$$E = 2G(1 + \nu) \qquad 2.1\text{-}5$$

2.1.2 Constitutive relations:

The kinematic equations relate strains to displacement gradients, and the equilibrium equations relate stress to the applied tractions on loaded boundaries and also govern the relations among stress gradients within the material. In three dimensions there are six kinematic equations and three equilibrium equations, for a total of nine. However, there are fifteen variables: three displacements, six strains, and six stress. There is a need for six more equations, and these are provided by the material's constitutive relations: six expressions relating the stresses to the strains. These are a sort of mechanical equation of state, and describe how the material is constituted mechanically.

2.1.3 Viscoelastic material behavior

One of the principal features of elastic behavior is the capacity for materials to store mechanical energy when deformed by loading, and to release this energy totally

upon removal of the loads (in a thermodynamic sense, deformation process is fully reversible). Conversely, in viscous flow, mechanical energy is continuously dissipated with none stored. A number of important engineering materials simultaneously store and dissipate mechanical energy when subjected to applied forces. In fact, all actual materials store and dissipate energy in varying degrees during a loading/unloading cycle. This behavior is referred to as viscoelastic. In general, viscoelastic behavior may be imagined as a spectrum with elastic deformation as one limiting case and viscous flow the other extreme case, with varying combinations of the two spread over the range between. Thus, valid constitutive equations for viscoelastic behavior embody elastic deformation and viscous flow as special cases, and at the same time provide for response patterns that characterize behavior blends of the two. Intrinsically, such equations will involve not only stress and strain, but time-rates of both stress and strain as well.

2.2 Anisotropic and Isotropic Behavior of Material

If a body's elastic properties are the same in every set of reference axes at any point for a given situation, we call it an isotropic elastic material. For such materials, the constitutive equation has only two independent elastic constants. A material that is not isotropic is called anisotropic. In the simplest case of an isotropic material, whose stiffness is the same in all directions, only two elements are independent. We have earlier shown that in two dimensions the relations between strains and stresses in isotropic materials can be written as:

$$\begin{Bmatrix} \epsilon_x \\ \epsilon_y \\ \epsilon_z \\ \gamma_{yz} \\ \gamma_{xz} \\ \gamma_{xy} \end{Bmatrix} = \begin{bmatrix} \frac{1}{E} & \frac{-\nu}{E} & \frac{-\nu}{E} & 0 & 0 & 0 \\ \frac{-\nu}{E} & \frac{1}{E} & \frac{-\nu}{E} & 0 & 0 & 0 \\ \frac{-\nu}{E} & \frac{-\nu}{E} & \frac{1}{E} & 0 & 0 & 0 \\ 0 & 0 & 0 & \frac{1}{G} & 0 & 0 \\ 0 & 0 & 0 & 0 & \frac{1}{G} & 0 \\ 0 & 0 & 0 & 0 & 0 & \frac{1}{G} \end{bmatrix} \begin{Bmatrix} \sigma_x \\ \sigma_y \\ \sigma_z \\ \tau_{yz} \\ \tau xz \\ \tau_{xy} \end{Bmatrix} \qquad 2.2\text{-}1$$

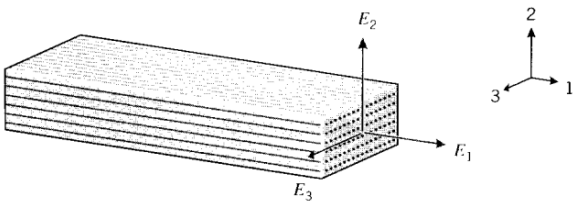

Figure 2.2-1. An orthotropic material (MECHANICAL PROPERTIES OF MATERIALS David Roylance, 2008)

If the material has a texture like wood or unidirectionally-reinforced fiber composites as shown in Fig (2.2-1), the modulus E_1 in the fiber direction will typically be larger than those in the transverse directions (E_2 and E_3). When E1 = E2 = E3, the material is said to be orthotropic. It is common, however, for the properties in the plane transverse to the fiber direction to be isotropic to a good approximation (E2 = E3); such a material is called transversely isotropic. The elastic constitutive laws must be modified to account for this anisotropy, and the following form is an extension of Eqn. 2.2-2 for transversely isotropic materials:

$$\begin{Bmatrix} \epsilon_1 \\ \epsilon_2 \\ \gamma_{12} \end{Bmatrix} = \begin{bmatrix} 1/E_1 & -\nu_{21}/E_2 & 0 \\ -\nu_{12}/E_1 & 1/E_2 & 0 \\ 0 & 0 & 1/G_{12} \end{bmatrix} \begin{Bmatrix} \sigma_1 \\ \sigma_2 \\ \tau_{12} \end{Bmatrix} \qquad 2.2\text{-}2$$

The parameter ν_{12} is the principal Poisson's ratio; it is the ratio of the strain induced in the 2-direction by a strain applied in the 1-direction. This parameter is not limited to values less than 0.5 as in isotropic materials. Generally $\nu_{12} > \nu_{21}$.

The simple form of Eqn. 2.2-2 with zeroes in the terms representing coupling between normal and shearing components, is obtained only when the axes are aligned along the principal material directions; i.e. along and transverse to the fiber axes. If the axes are oriented along some other direction, all terms of the compliance matrix will be populated, and the symmetry of the material will not be evident. If

for instance the fiber direction is off-axis from the loading direction, the material will develop shear strain as the fibers try to orient along the loading direction. There will therefore be a coupling between a normal stress and a shearing strain, which never occurs in an isotropic material.
This explanation was for a typical material where there is no direction, for more information about isotropy definition of a tensor refer to any continuum mechanics book.

2.2.1 Strain and displacement theories

Depending on the amount of strain, or local deformation, the analysis of deformation is subdivided into three deformation theories:

- **Infinitesimal strain theory**, also called small strain theory, small deformation theory, small displacement theory, or small displacement-gradient theory where strains and rotations are both small (to be exact, infinitesimal). In this case, the un-deformed and deformed configurations of the body can be assumed identical. The infinitesimal strain theory is used in the analysis of deformations of materials exhibiting elastic behavior, such as materials found in mechanical and civil engineering applications, e.g. concrete and steel.
- **Large-displacement or large-rotation theory**, which assumes small strains but large rotations and displacements.
- **Finite strain theory**, also called large strain theory, large deformation theory, relates to deformations in which both rotations and strains are arbitrarily large. In this specific case, the un-deformed and deformed configurations of the continuum are significantly different and a clear distinction needs to be made between them. This can be commonly the case along with elastomers, plastically-deforming materials along with fluids and biological soft tissue.

In each of these theories the strain is then defined differently. The engineering strain is the most common definition applied to materials used in mechanical and structural engineering, which are subjected to very small deformations. On the other hand, for some materials, e.g. elastomers and polymers, subjected to large deformations, the engineering definition of strain is not applicable, e.g. typical engineering strains greater than 1%, (Rees, David, 2006) thus other more complex definitions of strain are required, such as stretch, logarithmic strain, Green (Green_Lagrange), or Almansi strain tensors. (Adopted from Inelastic Analysis of Structures by Milan Jirasek, Zdenek P. Bazant)

2.3 Mechanical Behavior of Soft Biological Tissues

According to Fung (1993) soft tissues have nonlinear, non-homogenous, anisotropic behavior that is dependent on time and rate (Roan & Vemaganti, 2011). Although it has different degrees for different tissues, it is certain to observe nonlinear stress-strain relation in soft tissues. The quasilinear viscoelastic theory developed by Fung, models the nonlinear viscoelastic behaviour of soft tissues within the framework of a linear theory. There are two viscoelastic properties of interest: stress relaxation, the decrease in load with the tissue under repeated or constant elongation; and creep, the increase in elongation of the tissue under repeated or constant load.

Since soft organs are composed of different materials, like elastin and collagen, in different combinations, soft tissue properties are both coordinate and direction dependent (Holzapfel et al. 2004, Hrapko et al., 2008a). Time and rate dependent behavior is also common and explained by viscoelasticity.

Soft tissues in a human body are defined as tissues which are capable to go into finite deformations. They are differentiated from hard tissues, such as bones in the human body, with this capability they possess. Soft tissues also behave highly different from traditional engineering materials, such as steel or aluminum. Although, the linear elastic theory for infinitesimal strains applies well for most of the engineering materials and hard tissues, this theory could not be applied for soft biological tissues which can undergo large deformations. For soft tissues

undergoing large deformations, nonlinear elastic (large/finite strain) theory should be applied to analyze their stress-strain behavior.

Almost all of the soft tissues are composed of a mixture of solid and liquid medium, e.g. cells and extracellular matrix. Therefore, they are classified as viscoelastic materials. In this regard, the nonlinear elastic theory which is suggested for soft biological tissues under large deformations is necessary but not sufficient. To model the nonlinear elastic and the viscoelastic properties of soft tissues, nonlinear elastic theory and the viscoelasticity theory should be applied together. For improving this methodology for material modeling of soft there is a need to learn more about the mechanical characteristics of living materials.

2.4 Different Types of Tests on Biological Tissues

There are types of biological tissue mechanical testing according to the physiological state and condition of the tissue, which are;

2.4.1 In-vitro

In vitro (Latin word for within the glass) refers to the technique of performing a given procedure in a controlled environment outside of a living organism. Many experiments in cellular biology are conducted outside of organisms or cells. One of the abiding weaknesses of in vitro experiments is that they fail to replicate the precise cellular conditions of an organism. Because of this, in vitro studies may lead to results that do not correspond to the circumstances occurring around a living organism.

2.4.2 In-vivo

In vivo (Latin word for “within the living”) refers to experimentation using a whole, living organism as opposed to a partial or dead organism. Animal studies and clinical trials are two forms of in vivo research. In vivo testing is often employed over in vitro because it is better suited for observing the overall effects of an

experiment on a living subject. Testing the tissue in its natural state is ideal for ensuring accurate representations of the mechanical behavior, but difficult to achieve due to accessibility, ethical, variability, noise, and uncontrolled boundary condition issues.

2.4.3 In-silico

In silico is an expression used to mean “performed on computer or via computer simulation”. This term is used to characterize biological experiments carried out entirely in a computer by simulations with models reflecting the real world.

2.4.4 Ex-vivo

Ex vivo means outside the living body; denoting removal of an organ (e.g., the kidney) for reparative surgery, after which it is returned to the original site. In another word ex-vivo means that something is experimented on or investigated outside its natural in-vivo environment, while in vitro means in the test tube. As an example ex-vivo gene therapy means that cells are taken directly from the body, transduced with the gene in vitro and then returned to the body. If one is primarily interested in how that organ behaves outside its natural environment, the expression ex vivo seems to be more appropriate. On the other hand, work on some cell line, which originally developed from the primary culture long time ago, is usually described as in-vitro experiment.

2.4.5 In-situ

In Latin in-situ means located at a native or original site. The state can be a dead body. Differing from the in-vivo tests, the donor and therefore the tissue is not alive (Adopted from Skeletal Muscle Damage and Repair edited by Peter M. Tiidus)

2.5 Different methods of mechanical tests on soft biological tissues

The testing of soft biological tissues is usually similar to testing of traditional engineering materials. However the testing methods should include comprehensive testing protocols when complex nonlinear tissues are considered.

There are a number of methods used for investigation of soft tissue mechanical properties. Some examples are tensile testing, confined and unconfined compression testing, shear testing, and indentation testing (localized compression) (Fig 2.5-1).

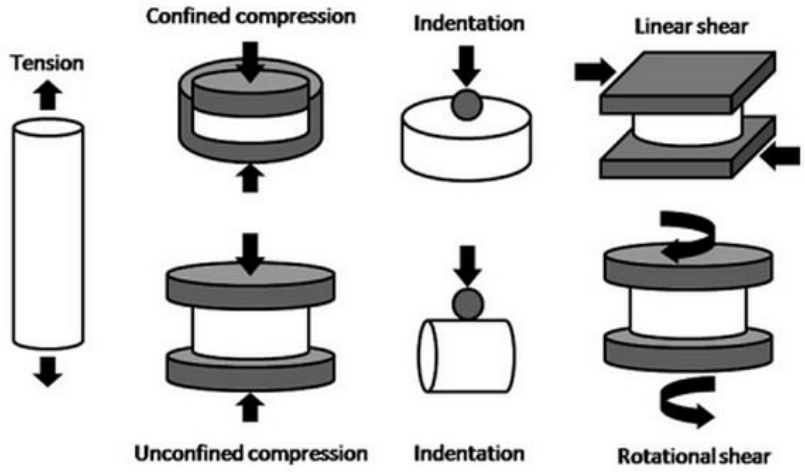

Figure 2.5-1."*Typical test methods using to investigate mechanical properties of soft tissues"(adopted from Neural Tissue Biomechanics by Lynne E. Bilston p.27)*

As the name suggests, tensile testing involves applying tension to stretching the specimen that can be applied in three types; uniaxial tensile tests, biaxial tensile tests, and suction cub. Confined compression testing applies compression to the specimen within an enclosed chamber, while unconfined compression testing applies compression along one axis of specimen leaving it free to deform along the other axes. These latter two typically apply the compression over the whole of one face of the specimen whereas indentation testing applies a compressive load to a localized area of the specimen through a probe (tip). Soft tissues can also be tested

under shear loading, which can be applied in a linear or rotational manner. Apart from indentation and suction cub methods, none of the presented classical testing methods is usable under in-vivo conditions. In suction cub method, viscoelastic behaviors creep and relaxation properties of the soft biological tissues, cannot be observed. Also observing of anisotropy behavior is difficult in this method.
For the other methods used in-vitro the tests require the excision of tissue samples and consequently result to be very sensitive to the geometry of the samples. Cutting samples from soft tissues and obtaining an accurate geometry is a challenging task. After excision, the samples are often stored in saline solutions and this affects the mechanical behavior of sample.

2.6 The Importance of Soft Biological Tissue Material Modelling

Determining the mechanical behavior of soft biological tissues is required for material modeling of them. Soft-tissue modelling is an important problem, dealing with predicting mechanical interaction of soft tissues with the environment. Soft-tissue models are enhanced in order to model and inspect the interactions between tissue and surgical tools. It may be useful for minimally invasive surgery (MIS) and in order to measure tissue stiffness of patients who are in need of clinical palpation. This modeling and inspection also allows for users to detect and identify tumors. In order to have athletic and orthopedic shoes, one needs to know the properties of heel pad soft tissue. Prosthetic and orthotic devices to fit in the best way, we need to specify the conditions of the soft tissue which is remained after an amputation. Specification of the features and properties of tissues is important and required for establishment of biomechanical systems, such as foot's finite element modeling (Luo, et al., 2011)and for covering the burns by harvesting the skin (Duchemin, et al, 2005), grasping and for soft organ manipulation for haptic surgery (Tholey, et al., 2003). Measurement of the features of 'force displacement' can be handled beneficially by the usage of variable-diameter indentation tools where these methods are used in some medical applications such as "fitting orthotic shoes for diabetic feet, prosthetic sockets for amputees, tumor detection and clinical

palpation" and obtained positive results. (Al-ja'afreh et al., 2008; Zhang,et al., 1997).

Although different models are established for live soft biological tissues and these models take place in the literature, none of these models can be widely accepted, because the behavioral structure of these issues are particular to different cases. As there are many different distinct experimentally observed properties of these tissues, it does not seem to be possible for a model to cover all these properties, but some of the models in the literature cannot even have numerous basic features observed experimentally (Zheng et al., 1999). There are several methods of mechanical experiments in the area of soft biological tissues. It can be seen that most of existent experiments in literature conducted ex vivo and data collected from these experiments constitute large part of the information we have in the area (Ahn & Kim, 2010; Carson et al., 2011; Fu & Chui, 2014; Seifzadeh et al., 2012; Zhang et al., 2014). This kind of measurements are chosen as it is possible for this measurements to be conducted in repetitive conditions and more easily. Despite this easiness and ability of repetition, it is also clear that, the data obtained from these measurements are mostly impossible to be applied to the realistic mechanical modeling, because removing a living organ from its natural location with blood perfusion and sufficient water content, will change the mechanical behavior of it. (Nava et al., 2008).

In our study, in-vivo tests were conducted. In in-vivo tests organ is studied at its original place and while it is alive. As the organ is in its own place and alive, this method of test is more realistic and ideal whereas mentioned above, organ changing its place and liveliness can exhibit different forms of behaviors which results in unsuccessful measurements. Moreover, not only the tissue itself but also the environment that surrounds the organ or tissue in its original place is determinant in this situation where this is described by Fung (1984) through the example of blood vessel testing.

2.7 Indentation method

As each tissue is composed of different contents and these contents are organized in different forms and also these components interact with each other in different ways mechanical properties of soft connective tissues' characteristics are complex. Numerous planar soft tissue has type I collagen fibers as their main basis of their structure. A network which constituted from type I collagen fibers play a role of imparting "strength and stiffness" under tensile load. When we consider the resistance against non-tensile loading or in other words indentation, we must regard the important role of non-collagenous proteins like "proteoglycans, and glycosaminoglycans" Moving from this information we can assess that, in order to get knowledge about the biomechanical characteristics of specific tissues and to understand the way of organization that results in a specific list of responses to a mechanical stimulus in a tissue, indentation testing is efficient and straightforward way (Lake & Barocas, 2012). In addition to this efficiency, indentation testing is preferred due to closer proximity to physiological loading.

Foot (Chao,et al. 2010) articular cartilage, skin, together with subcutaneous tissues (Pailler-Mattei, Bec, & Zahouani, 2008), corneal tissue (Ahearne, et al., 2007) white and gray matter of brain (van Dommelen, et al, 2010), and liver and spleen (Wang, et al, 2013) are examples of biological soft tissues that indentation is generally used to get necessary information about the mechanical properties of these tissues.

In comparison to the "confined and unconfined compression tests" of tissues, the advantage of the indentation test is that in vitro (Al-ja'afreh, et al., 2008, van Dommelen et al., 2010, Ahearne, et al., 2007) and in vivo (Mak et al., 1994; Zheng et al., 2000; Toyras et al., 2001; Sun et al., 2001) usage is possible.

In addition indentation testing is advantageous as it does not require a huge homogenous volume of tissue where it is different from standard rheological testing in this sense which makes this form of testing beneficial to use in organs like brain if a comparison between gray and white matter tissues is tried to be held. In this case, the comparison can only be possible when we use indentation method because

it is not possible to reach a high volume of homogenous tissues in these areas of the brain (van Dommelen et al., 2010)

Indentation method permits to obtain the tissue mechanical properties, in normal direction, without pre-stressing the tissue before the test .Moreover, it permits to determine the bulk and surface properties of the tissue, which reflect the physico-chemical properties of the skin/indenter interface.

Moreover indentation testing, is different from methods like suction, traction and torsion, as they require modification of natural stress state of the tissue, because in other test methods, the requirement of fixation of the tissue sample to the device used in the testing process, changes the natural state of stress in the tissue tested. In physiological state soft tissues usually present residual stress that may be released when the tissue is excised. This retraction usually causes an error in results. It is possible for this interference with the natural state to affect the consequent measurements of mechanical properties and also consideration and estimation of the level of inducement of the pre-stress value applied to the tissue is not possible in many cases. As a consequence when soft tissue testing is applied by different devices and methods, results differ prominently, which allows these results to be only serving for a descriptive purpose. For example the Young's modulus of the skin can be given as an example to this case where this modulus, E, has various values from 0.42MPa to 0.85MPa when torsion tests are applied, from 4.6MPa to 20MPa when tensile tests are applied and from 0.05MPa to 0.15MPa when suction tests are applied (Pailler-Mattei et al., 2008).

2.7.1 Disadvantages of indentation

There are several disadvantages of using indentation method. Firstly, the results obtained are difficult to interpret since obtaining stress-strain curves for the purpose of establishing a constitutive equation is not straight forward as in the case of simple tension or torsion tests. In addition different contact conditions between indenter and the tissue tested can lead to different results.

2.7.2 Advantages of computer controlled indenters

In vivo studies on humans are not as common as the studies on animals since possible damages in the tissues can happen. In this sense, different mechanical devices are developed in order to have these negativities reduced to a minimum while measuring the properties of the material in-vivo. Currently "free-form" and robotic measurements are the approaches developed.

For safety reasons, a hand-held probe is used in the measurement process of any free-form measurement. Human factor in the usage of these probes makes movements of device on the tissue, expected and nonhazardous. Although these are the positive sides of this approach, there are also negative sides of this approach, which contains three main issues (Holzapfel, G. A., 2004):

1- The experiments are carried out manually, thus they are not repeatable.
2- The determination of a reference point in experiments is a problem.
3- An unwanted initial stress can be applied by the hand of user prior to test.

When we consider the computer controlled indenter usage as another approach to the issue of in vivo measurements the advantageous side of this usage can be resolution of the problem of actuation and position sensing which are problematic in free-form measurements. This resolution can be reached through the pre-programming in computer controlled indenters. In free-form indentation, different users can result in different results, in robotic indentation; this problem is also resolved by programming the device for each different case. In this sense the same conditions and same usage can be possible for repetitive usages. In other hand more controlled indentations can be performed on tissue and the indenter can be programmed to apply different experiments. Thus, dependency to a user is eliminated and repeatability is possible (Holzapfel, G. A., 2004).

"Transient Ultrasound Elastography and Magnetic Resonance Elastography, (MRE)" are different techniques which allows for measurement of the dynamic material properties non-invasively in a way that does not interfere with the natural

form of the tissue as direct contact (Sandrin et al., 2003). In addition the elasticity amounts reported in these studies are typically measured at a certain frequency rather than a range of frequencies as in the case of dynamic loading test.

2.7.3 Compression experiments

As aforementioned compression methods (e.g. indentation) are popular methods in compare to the other experiment methods such as suction, torsion and traction. Three major types of this method are unconfined compression, and nano-indentation, micro-indentation. These groups are categorized due to heterogeneousity level of soft tissue to detect local or global difference in mechanical properties such as stiffness. In this part of the literature review, these categories and their preferences will be given with their examples from the literature:

2.7.3.1 Unconfined compression

This method of compression is conducted by placing the samples between two metal plates. Here, the top plate stays still, having a load measure device adhered to it. In this starting point of the compression, the samples are collected to be smaller than the plates they are put on. As the top plate stays still, we can move the lower plate with an input speed and through an input position that is set before the measurement. In this test displacement and force can be considered as loading conditions of the measurement. Through this form of compression test, it is aimed to determine the characteristics of the tissue sample at "large, physiologically relevant strain". It is also clear that loading conditions for this test can be chosen to be static or dynamic where through static conditions, stiffness of the material can be established and through dynamic conditions, like cyclic unconfined compression tests with different frequencies, dynamic characteristics that are directly related to frequency can be measured. As an example, Walraevens et al. (2008) and Lee et al.

(1992), using unconfined compression method to test the compressive mechanical properties of human aorta plaques can be given.

As the plates used in the compression are large, the results obtained of the measurement does not get so accurate in terms of classification of the sample, thus only the global categorization of fibrous, non-fibrous and calcified tissue can be detected for the tissue, resulting in a wide domain in reported mechanical properties within each categorized group in literature (Raghunathan, et al, 2010).

2.7.3.2 Microindentation

In order to have measurements of small and inhomogeneous samples, micro-indentation tests are used where local material stiffness of this material is measured. Due to geometrical shape of indenter and tissue surface and thickness, force-depth curves is not enough to have measurements around tissue stiffness. In order to have the values accurate about the tissue stiffness, inverse finite element method is also used. As an example to the usage of this measurement, in Barrett et al. (2009), a micro-indentation device with spherical indenter with a diameter of 1 mm was used. Homogenous sample is required in this measurement method of micro-indentation in order to have accurate results that can be produced for several times.

2.7.3.3 Nanoindentation

When we consider the stiffness measurement of single collagen fibers and cells at small strains nano-indentation is a method used generally. For the samples from soft tissues that are too heterogeneous even for micro-indentation, nano-indentation is used to specify the differences between different localities in terms of their mechanical properties, and large displacements cannot be applied when we use this technique. Hayenga et al. (2011), Tracqui et al. (2011) and Ebenstein et al. (2009) used this technique in their studies.

As the dimensions of the indenter tip is too small in this measurement method, many complex and advanced algorithms are also developed to get over the hardness and

complex process of reconstructing the data collected into the mechanical stiffness. In addition, we can apply nano-indentation to really thin tissue, for example 16 μm is a thickness of a sample that can be measured by nano-indenters.

Since in nano-indentation really small displacements can be applied, it cannot be used for measuring most of the physiological strains due to tissue thickness. This requirement of low strain in measurement makes nano-indentation unable to capture non-linear mechanical behavior and underestimate the stiffness of the sample, at the same time (Chai, et al, 2014). Nano-indentation is more efficient in specifying mechanical characteristics of bone like osteons and trabeculae individually (Rho, et al., 1999, Tai, et al., 2005, Zhang, et al., 2010, Zhang, et al., 2008, Zysset, et al., 1999, Wu, et al., 2012).

2.8 Some Indentation Tests and Set ups Recently Used in Literature

Indentation tests are frequently used in the investigation of the mechanical properties of soft biological tissues (Choi & Zheng, 2005; Korhonen, 2003; Yin et al., 2004). Pailler-Mattei et al. (2008) used an original light load indentation device to study in vivo the mechanical properties of human skin in order to purpose of a two-layer elastic model. In the part (a) of the Figure 2.8-1, schematic representation of the indentation device is given. And in the second part, part (b) of Figure 2.8-1, the system of indentation and the way the subject's arm is positioned in the device is given. In this example, indenter device attain a displacement of 15 mm with a resolution of 10μm during the loading–unloading cycle and also the velocity used in the measurement range from 5μm/s to 1500μm/s.

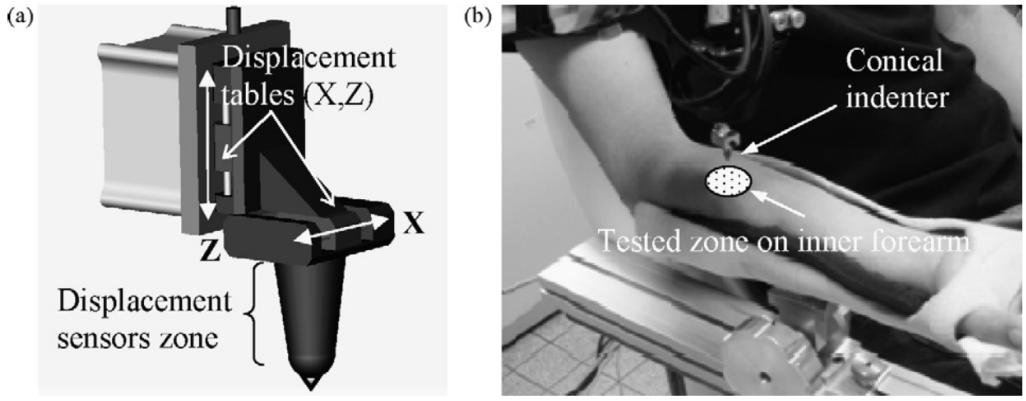

Figure 2.8-1. "Skin tribometer device: (a) Indentation device's schematic representation; (b) the system of indentation and the way the subject's arm is positioned in the device. The tests were conducted on the inner forearm." Pailler-Mattei et al. (2008)

Cox et al. (2008) used indentation tests with varying indenter sizes on linear elastic rubbers and compared to tensile tests on the same specimen for modeling of synthetic heart valve. The whole setup (surface force apparatus) was mounted on top of an inverted confocal laser scanning microscope (CLSM) to enable visualization of the deformations in the bottom plane of the sample during indentation. Digital image correlation (DIC) was used to quantify these deformations.

The elastic mechanical properties of carotid atherothrombotic plaque samples were studied by indentation tests by Barrett et al. (2009). In this text the specifications of the usage is given as: "A Zwick 3103 hardness testing machine (Zwick/Roell, Leominster, UK) was used to indent the specimens with a tungsten sphere of radius r = 0.5mm. The approach speed of the indenter was 20mm/min. Indentations were carried out until a force F of 0.2N was reached or when an indentation depth of 0.5mm was exceeded."

In Ahn & Kim, (2010), porcine livers are used to measure the deformation and force-response on the surface of the organ when different indentation depths by two different tip shapes are applied to the tissue; flat ended and hemisphere cylindrical tips. Since even small changes in an indenter tip shape can yield large differences in the mechanical responses of the tissues, the shape of the indenter tips is an

important factor (Mahvash and Hayward, 2004). The difference in obtained results by different two tips were shown in Figure (2.7-2) as anticipated the force response for the flat tip was larger than the force response for the other tip.

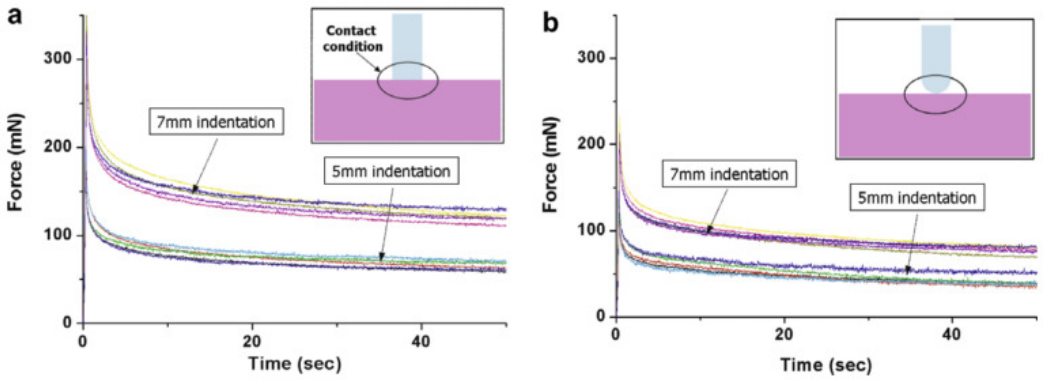

Figure 2.8-2. "Indentation experimental results and contact conditions (upper and right box) for (a) flat and (b) hemisphere tips" (adopted from Ahn&Kim 2010)

For surface deformation measurement, in the study, additionally an optical 3D deformation analyzer (GOM co. ARAMIS, Germany) and for measuring of the force responses, a one-dimensional indentation device was used.

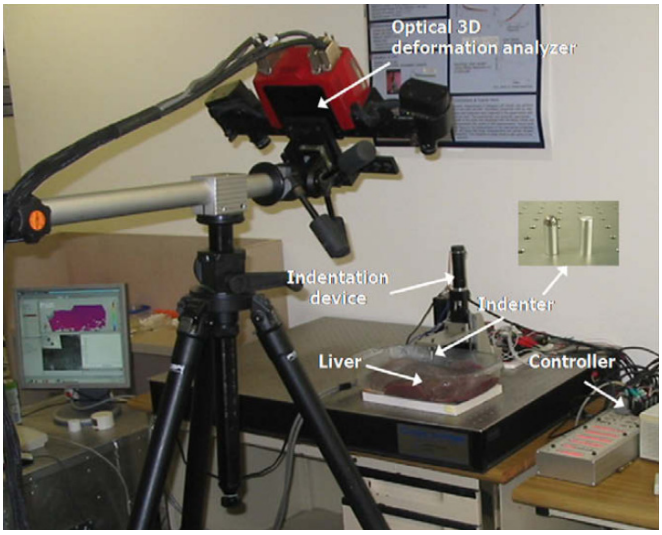

Figure 2.8-3. "Optical three-dimensional deformation analyzer (ARAMIS, GOM co., Germany) and indentation device (flat and hemisphere tip indenters)". Ahn & Kim, (2010)

Carson et al., (2011) for an ex vivo material characterization process, for a prostate tissue, used spherical indentation tests. Chao et al. (2010) made a comparison between the results he obtained from investigation of a forefoot plantar soft tissue, separately using a tomography-based air-jet indentation system, and using a tissue ultrasound palpation system. In the work of W.-M. Chen et al., (2011), they came up with a tissue tester which is driven by instruments such as a portable motorized indenter and used this tester in in vivo tests with a specific foot positioning apparatus. The study of Van Dommelen et al. (2010) was focused on comparison of white and gray matter tissues from brain through making indentation experiments. Iivarinen et al., (2011) used a hand held stiffness meter in order to come up with the differences between "relaxed, physically stressed and oedemic" human forearm in terms of their indentation stiffness. Luo et al. (2011), while conducting experiments on human heel, used an optoelectromechanical tissue indenter. In this study the in-vivo indentation is used for finite element analysis of heel pad.

In a study by Moerman et al, (2013) an "MRI compatible soft tissue indenter" has been introduced; specification about a novel MRI compatible soft tissue indenter, which controlled by a computer. Forces up to 15N were able to be sensed by an optical Fibre Bragg Grating (FBG) force sensor that has the acquisition rate of 100 Hz. Indentation tests which were conducted on a silicone gel phantom and the upper arm of a subject were used to verifying the performance of the system. In Figure 2.8-4, the complete soft tissue indentation system is revised. This revision is given in detail as: "In the control room, a computer linked with data acquisition units and custom electronics controls the motion of a hydraulic master cylinder (Fig.2.8-4C) whose motion is linked with the MRI compatible indenter assembly (Fig.2.8-4D) in the MRI room. The force sensor data is acquired using an optical interrogator system (Fig.2.8-4E)."

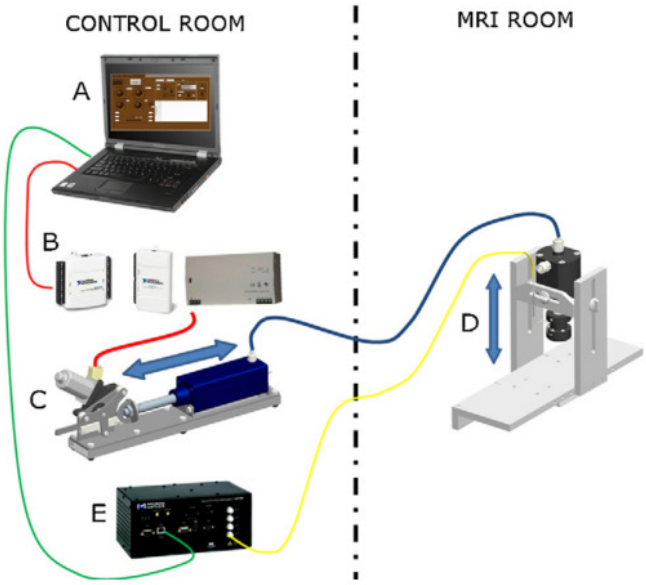

Figure 2.8-4. "Overview of the MRI compatible indentor and control system." Moerman et al, (2013)

A comparison between "in-vitro, in-vivo and in-situ" indenter tests were conducted in Prevost et al., (2011) through experimenting on porcine brain tissue. Fu & Chui (2014) also used animal tissue, porcine liver for an experiment that constitutes of a

combination of compression and elongation and the resulting in vitro data was used to the examination of indentation testing.

In a study by Chen et al (2011) a setup named MPEAI was introduced. This setup consists of a motorized indenter that is aimed to get the necessary information of plantar soft tissue pads below the metatarsal heads through in-vivo foot indentation tests. It constitutes of "a closed-housing linear actuator comprising a 500-step per revolution stepper motor (MYCOM) and a 1.25mm pitch tangential screw unit to drive a 5mm diameter hemispherically tipped probe" (Figure 2.8 5).

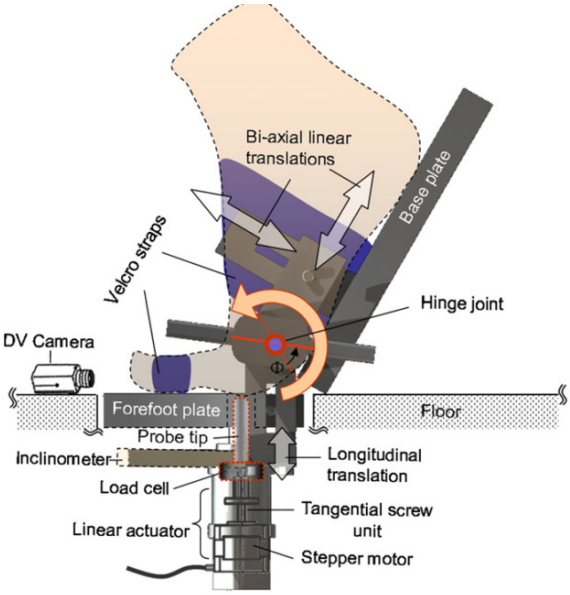

Figure 2.8-5. "Schematic diagram of the sub-Metatarsal Pad Elasticity Acquisition Instrument (MPEAI), showing details of probe tip, accommodation of sub-MTH pad, and inside components of actuator to drive probe tip." Chen et al,(2011)

2.9 Anisotropic Behavior of Soft Biological Tissues

Material anisotropy concept is used to determine the fact that direction of the load applied to the soft biological tissue directly affects viscoelastic response.

Anisotropy is the characteristic of most of the biological tissues (Kroon & Holzapfel, 2008; Pandolfi & Vasta, 2012; Peña et al., 2008). The direct effect of loading direction on the mechanical behavior is based on different microstructural

features where collagen fiber bundles can be counted as one of these features (Samur et al, 2007 , Lokshin & Lanir, 2009) For instance, nanofibrillar collagen scaffold which simulate blood vessel's collagen organization is examined to have transverse anisotropy (Huang et al., 2013; Argatov et al., 2015).

For anisotropic materials to determine the material coefficients, combination of more than one loading is necessary even to develop linear elastic mechanical characteristics of that material. Because of this requirement, it is really a huge challenge for researchers to come up with the mechanical behavior of anisotropic materials. Circular indenter tips are not efficient for observation and examination of these important characteristics of anisotropy. The use of axially symmetric tips for estimating material properties ignores pronounced anisotropy. In literature, flat-ended cylindrical (Choi et al., 2008), spherical (Dimitriadiset al., 2002), conical (Pelletier et al., 2006), pyramidal (Borodich et al., 2003) and cylindrical lateral (Argatov et al., 2015) that uses the lateral contact of a cylindrical indenter tips are widely used.

The anisotropic characteristics of material can be obtained from indentation tests through the information related to the direction; indenting and stretching the tissue sample at the same time can result in this kind of an information extraction as an example (Karduna et al., 1997). Another option is the approach by Bischoff (2004), who showed in a computational study that using several tests in different angles with axially asymmetric indenter tips (elliptic indenters), in-plane anisotropic tissue behavior may be revealed. Then Petekkaya (2008) used these ellipsoidal tips in his experimental study.

In addition to that, in a study by Cox et al. (2006) gradient data of force and deformation was combined and this combination resulted in adequate information just from a single indentation tests, about the local anisotropic characteristics of aortic valve leaflet. In another study of Cox et al (2008) small deformations were applied through quantitative validation, which involves comparison of the results obtained from different sized indenters were compared to the uniaxial tensile test results where all these tests were conducted on same rubber material.

In the study of Cox, et al (2008) a combination of force-displacement curve that is obtained from the symmetric indentation, and the principal stretches which are specified through viewing the material under an optical microscope, and also a computational model, was used to obtain anisotropic hyperelastic parameters through an inverse algorithm. The difficulties in determination of reliability of principal stretches make it insufficient to use this method, and need additional instrumentation. Instead, force-displacement curves interpreted in numerical simulations, are enough for the method of axially asymmetric indentation

Recently Namani et al., (2012) demonstrated the combined shear-indentation approach by applying it to characterize the linear elastic properties of an anisotropic fibrin gel. In this study also an axially asymmetric tip was used in indentation experiments that was rectangular (Figure 2.9 1). Then, as there were differences between the stiffness of the aligned fibrin gels, these differences were clarified through a linear transversely anisotropic elastic material model. However it must be mentioned that in indenter experiments of this study on fibrin gel only elastic properties were examined and viscoelastic properties were not considered.

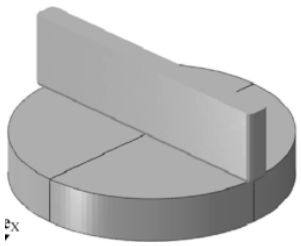

Figure 2.9-1. Rectangular indenter tip

The indentation experiments results are shown in Figure 2.5-3 It can be seen in (Fig.2.9-2-b) that in force-displacement curves of aligned fibrin gels the response force is larger in the direction perpendicular to the aligned fibers (open circles, indenter perpendicular to dominant fiber direction; closed squares, indenter aligned with dominant fiber direction).

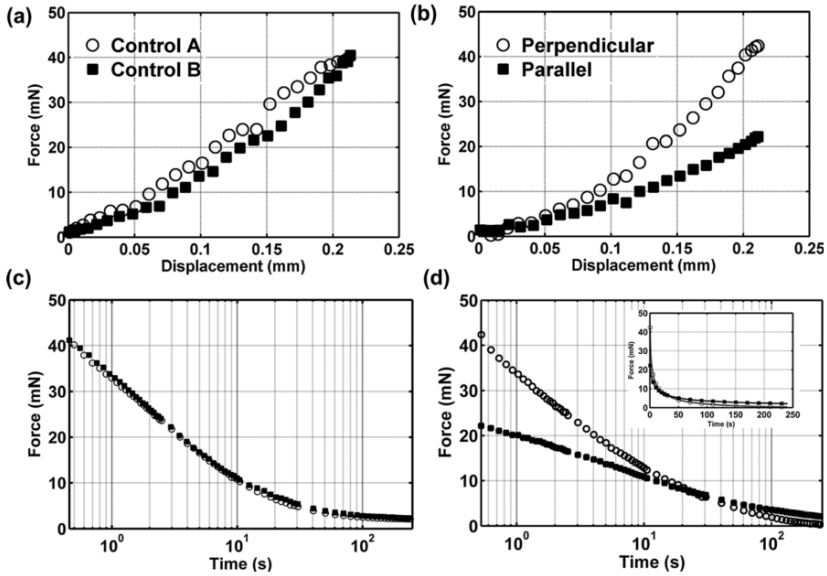

Figure 2.9-2. "(a) and (b) Force-displacement measurements during indentation of (a) control (nonaligned) fibrin gels (open circles, first test; closed squares, second test) and (b) aligned fibrin gels (open circles, indenter perpendicular to dominant fiber direction; closed squares, indenter aligned with dominant fiber direction). The indentation loading ramp duration was 0.33 s. (c) and (d) Force relaxation for 240 s after indentation of control fibrin gels and aligned fibrin gels. Relaxation time is plotted on a logarithmic scale. Both control and aligned fibrin gels lose more than 90% of their peak indentation force after 240 s. Inset in panel (d) shows force relaxation for aligned gels on a linear time scale" (Namani et al., 2012)

Moreover, Feng et al., (2013), applied combination of a 3-step indentation, with dynamic shear tests, on the white matter in order to understand the mechanical anisotropy or the transverse isotropy of this sample (Namani et al., 2012). In this specific application, a rectangular stainless steel indenter was used with a head in 19.1mm long*1.6mm wide.

In another study by Chai et al., (2014) artery plaque samples which were of examined by a spherical (2mm diameter) micro-indentation system to capture the anisotropy behavior of this tissue. The set-up of this study can be seen in the Figure 9. Samples were sliced radially and axially in the process of these tests (Chai et al., 2013).

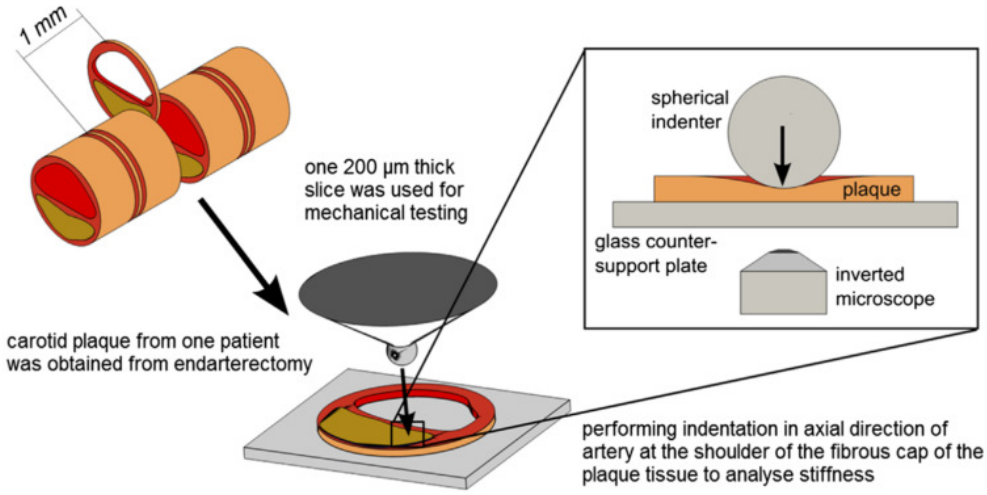

Figure 2.9-3. "Sectioning of plaque tissue"(Chai, et al., 2014)

In this experiment while indentation was conducted, visualization of collagen deformation could be observed through an inverted confocal microscope. Force response, indentation depth and collagen deformation were the data obtained from this process of indentation and in addition local displacement field was also acquired through the usage of digital image correlation (DIC). Figure 2.9-4 summarizes the process briefly.

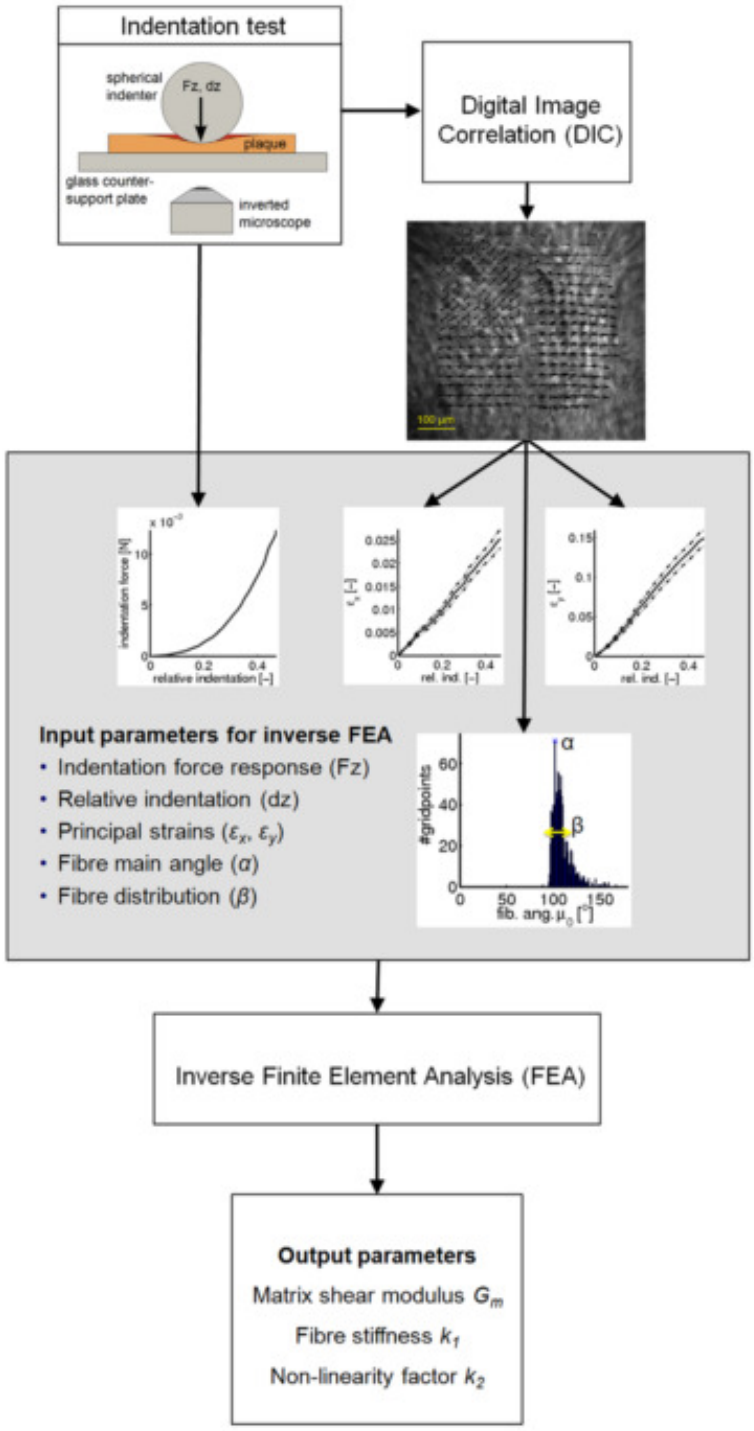

Figure 2.9-4.Process of experiment. Chai, et al., (2014)

The necessary information of local deformations and principal strain directions were acquired through the analysis of displacement field. “The displacements, local first (ε_x) and second (ε_y) principal strain magnitude and direction of the collagen fibres were assumed as a function of indentation displacement. The anisotropic behavior of the sample can clearly be observed through the Figure 2.9-5 where the relationship between the fibre displacement and the global stress is given. The final observation can be summarized to be “the tissue offers much more resistance in the direction of the fibre alignment whereas perpendicular to the fibre direction much higher strain occurred during indentation.”

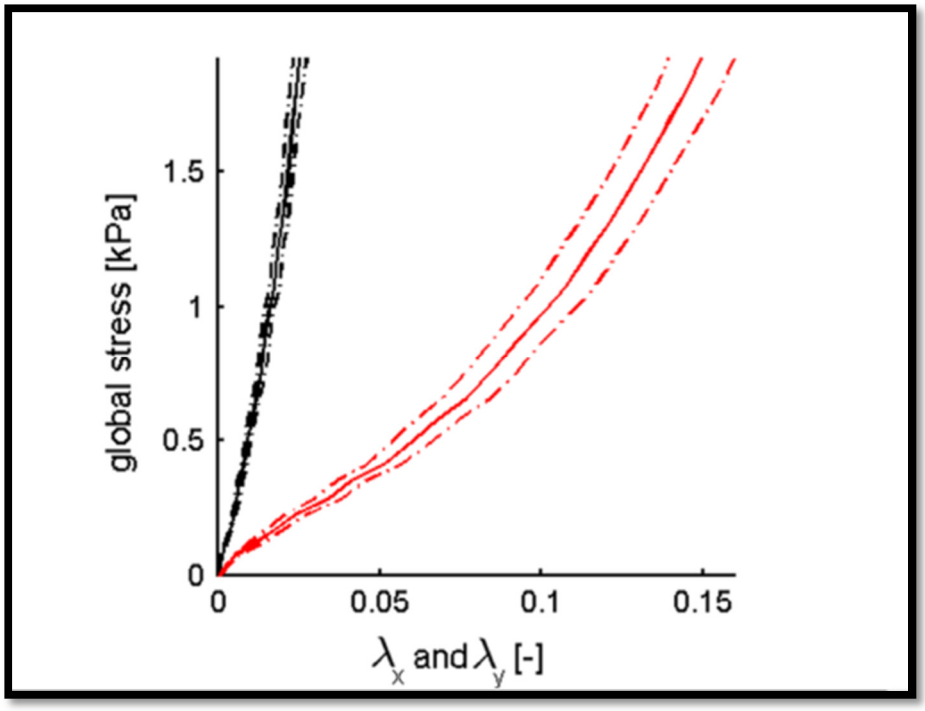

Figure 2.9-5. “The global stress against the collagen fibre displacement: λ_x fibre stretch: λ_y displacement perpendicular to fibre alignment. It shows again highly anisotropic behaviour of the tissue. The stiffness in the direction of the fibres is much higher, whereas much higher strain appears perpendicular to the fibre direction.” [Adopted from Chai, et al., 2014]

It should be mentioned that Chai et al's study was carried out in-vitro on a thin sample that the direction of collagen fibers are homogeneous and predictable over thickness for finite element analysis then in bulk tissue it is not applicable, on the other hand the slicing may also disrupt the coherence in the collagen fibre architecture. Since the collagen fibres are the load-bearing structure of the blood vessel, this might have an impact on the mechanical properties. Also only the elastic parameters were extracted, however in our in-vivo study on bulk biceps muscle the opposite of this result was concluded by observing response forces in different directions.

2.10 Preconditioning

In both in vitro and in vivo cases, one of the core response characteristics of soft issue is preconditioning. This characteristic can be observed in soft biological tissues when strain softening (Mullins effect) is exhibited and when fiber reference length is increased. In addition, in all estimations, fact of elastic fibers to be predominant at low strains is supported and this situation shows that in time, increase in the strain results in collagen to become predominant where this situation does not affect the important position of elastic fibers in discussion.

Soft tissues undergo preconditioning adaptation during loading. We can observe linearity in the stress-strain curves when strain level is low, this situation changes to nonlinearity in the strain's "toe" region. At high strains, again a linear curve can be observed about the relation between strain and stress. In addition to this, viscoelasticity and preconditioning are factors that clearly points out the fact that the soft biological tissues are highly dependent to time, where strain history of a material affects the stress in any time, which concludes to viscoelasticity behavior. It can be manifested by "relaxation at constant strain, creep at constant stress, hysteresis under cyclic loading, strain-rate dependence of the elastic moduli, and stress-strain phase lag under harmonic loading." Under repeated loading, a gradual change occurs in response of viscoelastic tissue because of the phenomena of preconditioning (Lokshin & Lanir, 2009). This change is shown up as a decrease in

the maximum response force under repeated loading, and also a decrease in hysteresis area of the loading and unloading cycles, up to a steady amount after several cycles.

Strain level is accepted to be affecting preconditioning directly. In this sense, when a change in strain level occurs, the preconditioning process changes which also affect the steady response to have a different value. Thus repeating cycles should be conducted again in new strain level.

In a study by Lokshin & Lanir, (2009) the required time for completely recovery of preconditioned skin following cyclic loading tests is claimed to be several hours.

Mechanical properties are usually collected from the examination of preconditioned tissues, it is not really clear if these properties are acquired from non-preconditioned tissue. Preconditioning is used to have a more stable statistical output in a process that can be produced repetitively. (Fung, 1973, 1993).

In most cases, it must be expressed that shear moduli is reduced by preconditioning and this effect can be observed more in experiments on the dead tissues such as in situ or in vitro. As an example, in the study of Gefen & Margulies, (2004), it was observed that in a process of 4mm indentations on the both non-preconditioned and preconditioned porcine brain, applied in vivo, in situ and in vitro, obtained relaxation responses were shear moduli was less in preconditioned examination.

2.11 Finite element method

Apart from some very simple situations the partial differential equations resulting from a continuum-mechanical boundary value problem can only be solved with numerical methods. The complex geometry of the studied organs and the employed constitutive equations additionally complicate the solution of the problem. Finite element methods have become the standard method in solving continuum mechanical problems with complex geometry and complex material laws, especially when non-linear situations are encountered as soft biological tissues. Since soft tissues often undergo large deformations and in many cases show a

strongly non-linear material behavior non-linear finite element methods are required for a correct simulation of their behavior.

Finite element analysis of indentation experiments are widely studied in the literature. In 1992, Spilker et al., investigated the indentation problem on a thin layer of soft tissue such as cartilage with a circular plane-ended indenter. The bone is modeled by attaching a layer of soft tissue to the bone. In the indentation test a plane-ended cylindrical indenter was used. Bischoff, (2004), applied finite element method to investigate soft tissue mechanical properties axially asymmetric indenters. Choi and Zheng (2005), investigated the finite element of indentation with two different-sized indenters by employing an axisymmetric finite element model of the tissue with rigid-cylindrical flat ended indenters. The tissue is assumed to be linearly elastic. Feng, et al, (2013), used finite element analysis for interpreting the indentation experiment results on brain tissue. Eder et al., (2013),Seifzadeh, et al., (2012), Fu & Chui, (2014),Spilker,(2014) are among the articles that recently used finite element method for soft tissue modeling and simulation.

2.12 Inverse finite element method

The Inverse Finite Element Method is a numerical approach in which an optimization algorithm is coupled with a finite element method in order to find optimal values for a set of target parameters which enter the finite element simulation. A user defined objective function serves to measure the optimality of the parameters. The finite element method is used to simulate the physical process which depends on the target parameters. The target parameters can be various physical quantities like material parameters in inverse material parameter estimation related to experimental testing. In this case an optimal fit of the simulated data to the experimental data is searched. In the case of the tissue indentation experiment, the target parameters cannot be determined by solving simple relations between the experimental data and the target parameters. Therefore, the inverse finite element method is used to evaluate the experiments. Inverse finite element modeling is used to fit the mathematical formulation in the form of constitutive

equation to the experimental data. Major drawback of inverse FEM is that, selected constitutive law is a priori. It cannot predict which constitutive equation is proper to model the existing experimental data. It only determines the coefficients of selected constitutive equation. Determining a precise and proper constitutive response and using the finite element methodology means the ability to simulate different modes of deformation that are not possible with experimentation.

In Kauer, et al, (2002) A finite element simulation of the aspiration experiment on soft tissue, is used together with a curve fitting algorithm to estimate the material model parameters through an inverse finite element method. In Nava, (2008)the parameters of a quasi-linear viscoelastic model of human liver have been determined from the experimental data by means of inverse finite element calculations. Recently Yao et al., (2014) presented an inverse finite element analysis to optimizing material parameters of a viscoelastic material model to fit the stress–relaxation response of human cervical tissue samples to spherical indentation. Tönük & Silver-Thorn, (2004) applied inverse finite element model for to simulate force-relaxation and creep data obtained during in vivo indentation of the residual limb soft tissues.

CHAPTER 3

IN VIVO SOFT TISSUE INDENTER DEVICE UPGRADES AND IMPROVEMENTS

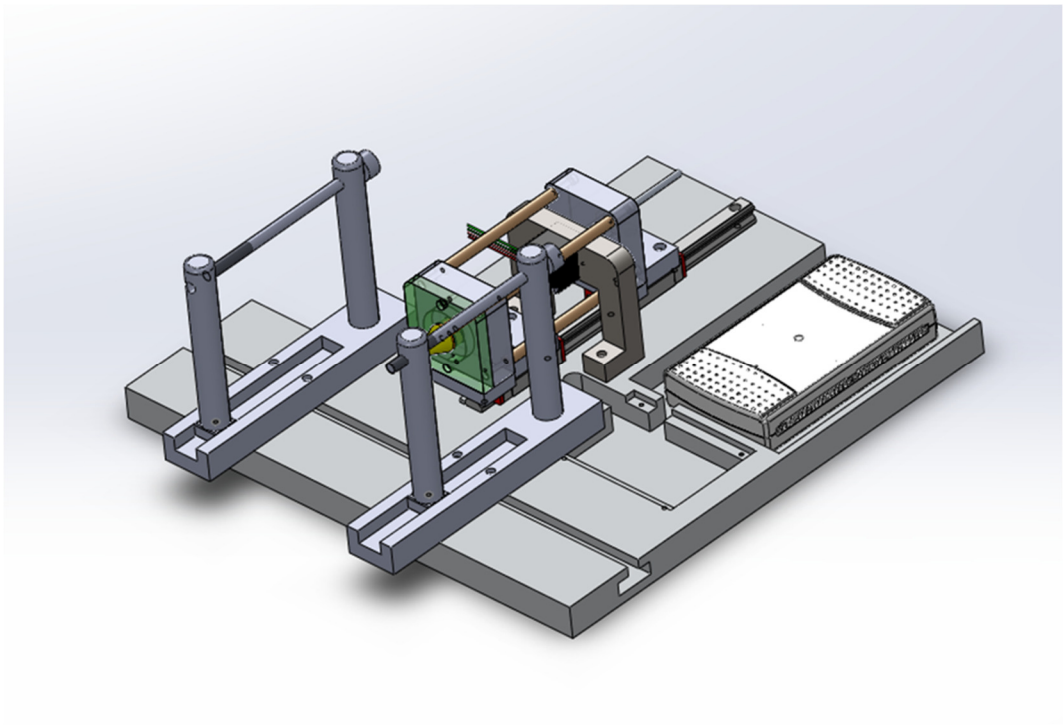

Figure 3-1.The (schematic) indenter device (ME407 Project)

3.1 Indenter Device and Experiment Set Up

An original indentation device has been developed during a project in METU for studying in-vivo the mechanical properties of human soft tissue.
The indentation tests were designed to carry out on the forearm. Fig (3.1-1) shows the indentation system and the positioning of the subject's arm schematically and Fig (3.1-2) simply shows working principle of the indenter device:

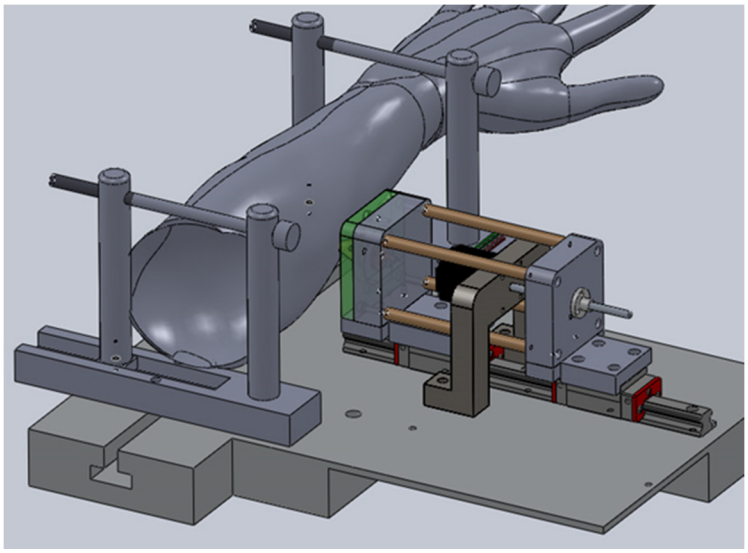

Figure 3.1-1.The indentation system and the positioning of the subject's arm (schematically)(ME 407 Project)

Briefly, in new design with the help of a step motor, which is operated under different frequency, the basic indenter operations, such as cyclic test, relaxation test, and creep test, will be performed to extract the response of soft tissue under different circumstances. To drive the motor and show the results LabVIEW environment is utilized. Load cell as a second important piece gives different voltage values in mV order. Load cell is a transducer converting the tissue reaction force into voltage which can be converted into digital data by the data acquisition card that may be read and recorded by the computer. Continuation of the process these crucial data is collected in NI-6121 DAQ and displayed on the interface of LabVIEW. For detail information about codes see Appendix B.

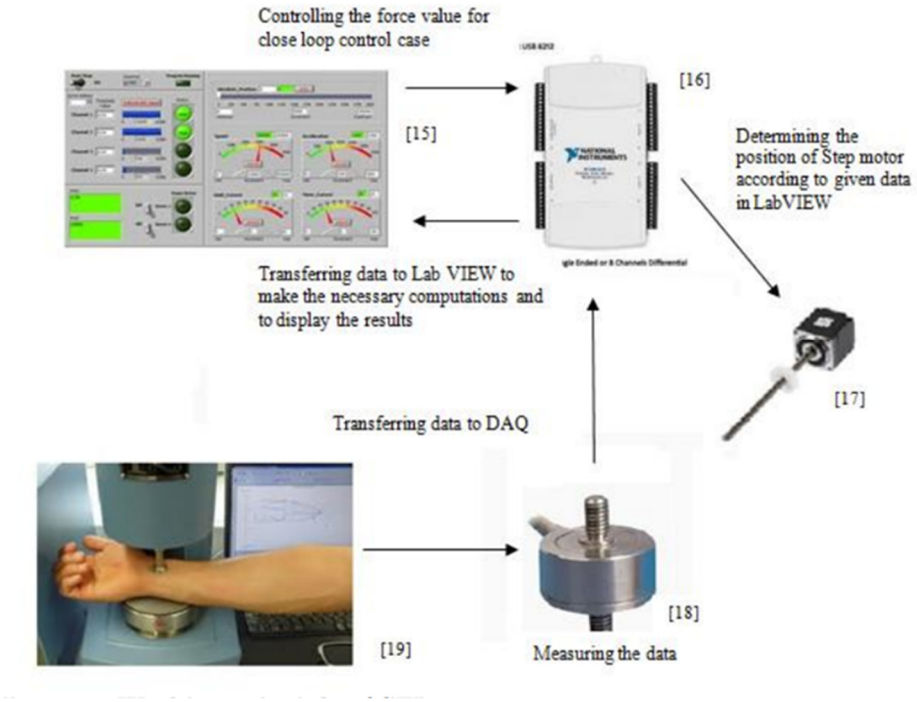

Figure 3.1-2. Working principle of the indenter device

3.1.1 Equipment

Experimental data was acquired using an original in-house soft tissue indenter.
It is designed in Middle East University (Biomechanics Laboratory) to make in vivo (on live body) measurements on human arm. After fixing the arm device indents a predetermined point on it with forward and backward movements. The arm is at rest and lay on a mechanical support during each experiment. Indenter set up and indentation regions on arm are presented in Figure (3.1-3) and figure (3.1-4) respectively. The indentation force was measured via a load cell, the step motor displacement, and experiment time are measured and controlled via Labview software for being able to read and record by computer. Data acquisition card was used to digitize the data. For this Haydon switch hybrid stepper motor (28000 series size 11), Honeywell ELPF-T1-M-50N load-cell and AD620 amplifier was selected. For real time data collection a computer code with a graphical user interface was developed in LabVIEW programming software (version 11.0) and NI-6212 (16-bit

resolution) data acquisition card was used. In this study's measurements, in this study's experiments, indenter velocity changes from 1mm/s to 10 mm/s. The step resolution of stepper motor is 0.0127 mm. Ellipsoidal tip made of a polymer (polyamide) was used for indenting tissue during experiments. For detailed information about the equipment refer to Appendix A.

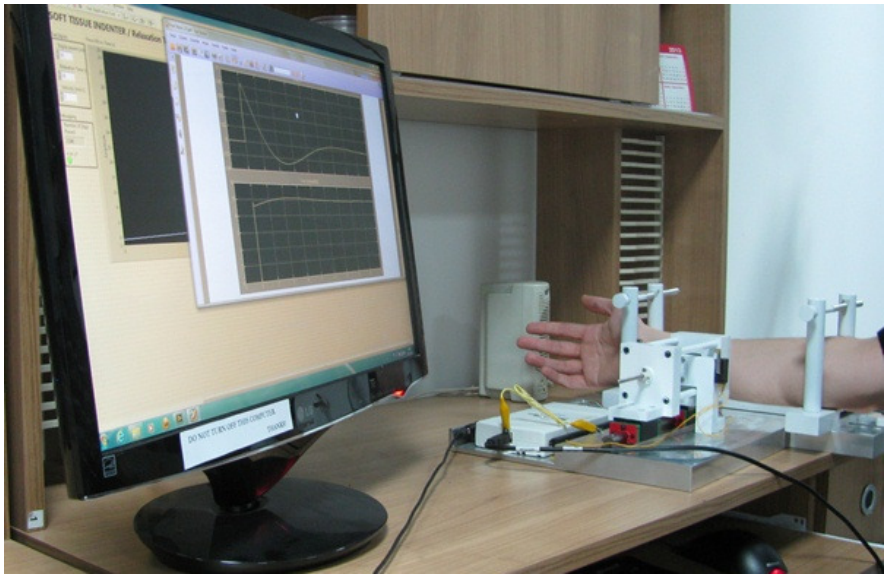

Figure 3.1-3. Indenter set up

The indentation experiments have been conducted mostly on the inner forearm region of subject (Fig.3.1-4). This region is easily accessible, relatively flat and less disturbed by the natural movements of the body.

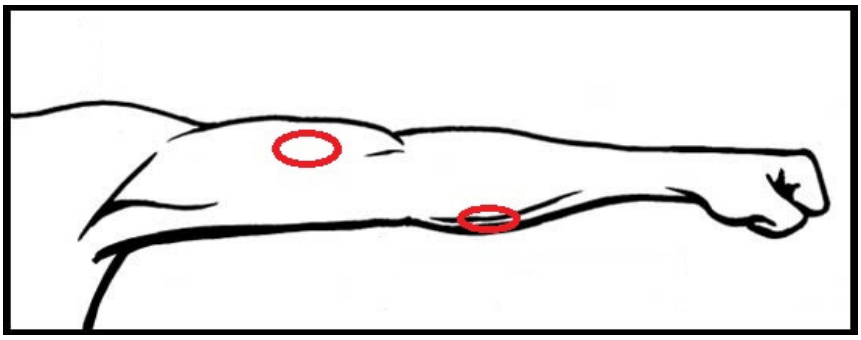

Figure 3.1-4. Indentation regions on arm

3.1.2 Indenter tips

In addition to a cylindrical tip, elliptical tips were used for soft tissue indentation experiments. The details and SolidWorks sketches are provided in Appendix A. The dimensions of elliptic tips and the top and front view of tip surface are demonstrated in Figure (3.1-5) and Figure (3.1-6) shows a 3D shape of a sample elliptic tip (C) used in anisotropy tests. The top and front view of the contact surface of tip C is also illustrated in this figure .The dimensions are: Rx=6mm, Ry=1.5 mm, Rz=1.5 mm.

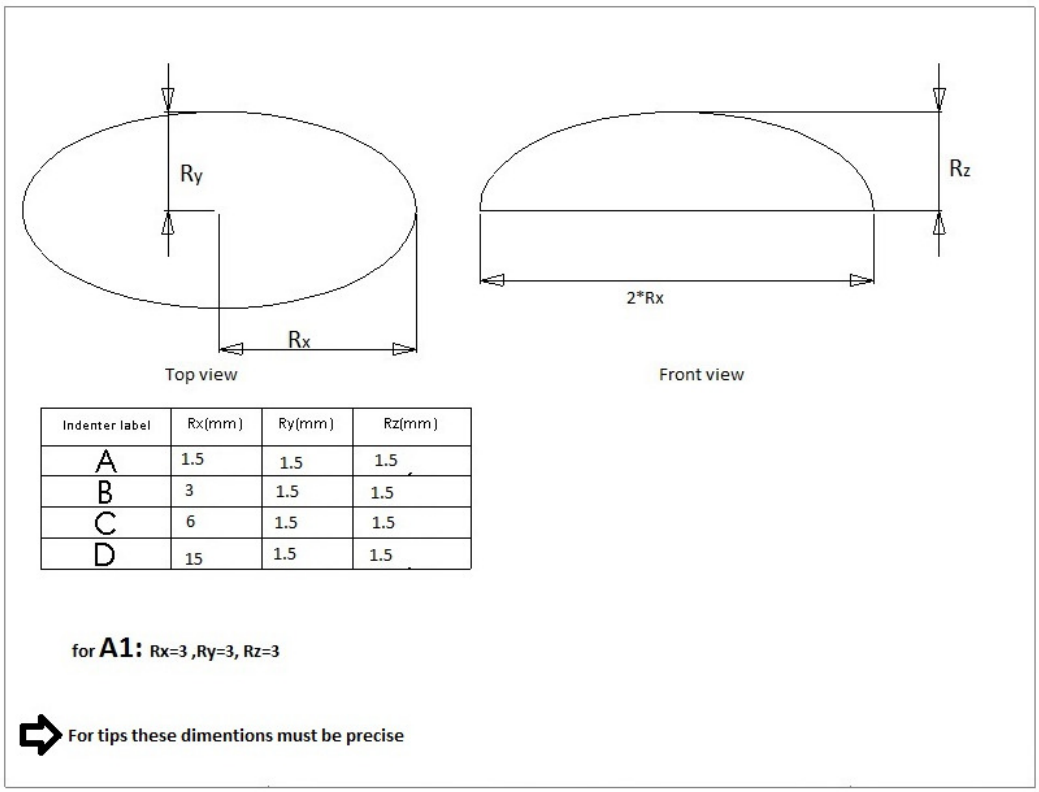

Figure 3.1-5. The dimensions of elliptic tips and the top and front view of tip surface

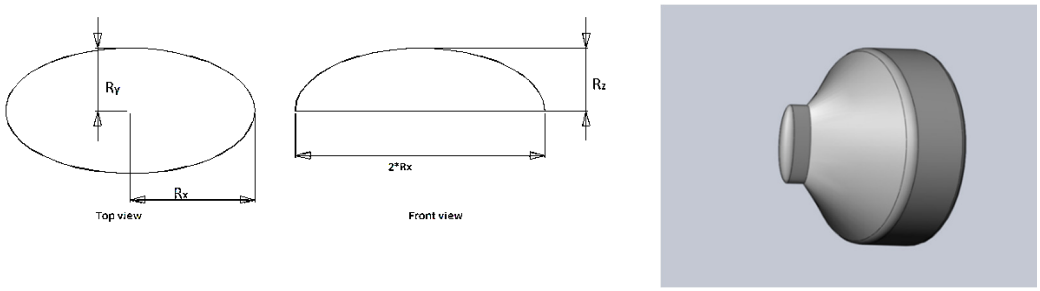

Figure 3.1-6. Indenter Tip used in anisotropy tests; R_x=6mm, R_y=1.5 mm, R_z=1.5 mm

All four different measurements with different aspect ratios which is used in Bischoff (2004) with scaling variation is chosen to design and manufacturing compatible tips of device for further comparing and examining the results.

In the indenter tips used by Petekkaya (2008) in previous version of the indenter device all the applied ratios of “x “to “y” are 4. For examining anisotropy axially asymmetric tips with different ratios of 2, 4, and 10 was designed, and used. For examining in plane-isotropy two axisymmetric tip (cylindrical) was used (ratio=1)

Ellipsoidal indenter tips have been manufactured for examining the anisotropy characteristic of soft tissues that means different alignment or orientation of the tips on the tissue shows different results. So conducting experiments by different angle intervals is feasible. For aligning the tips in different directions the part shown in Figure (3.1-7) was designed.

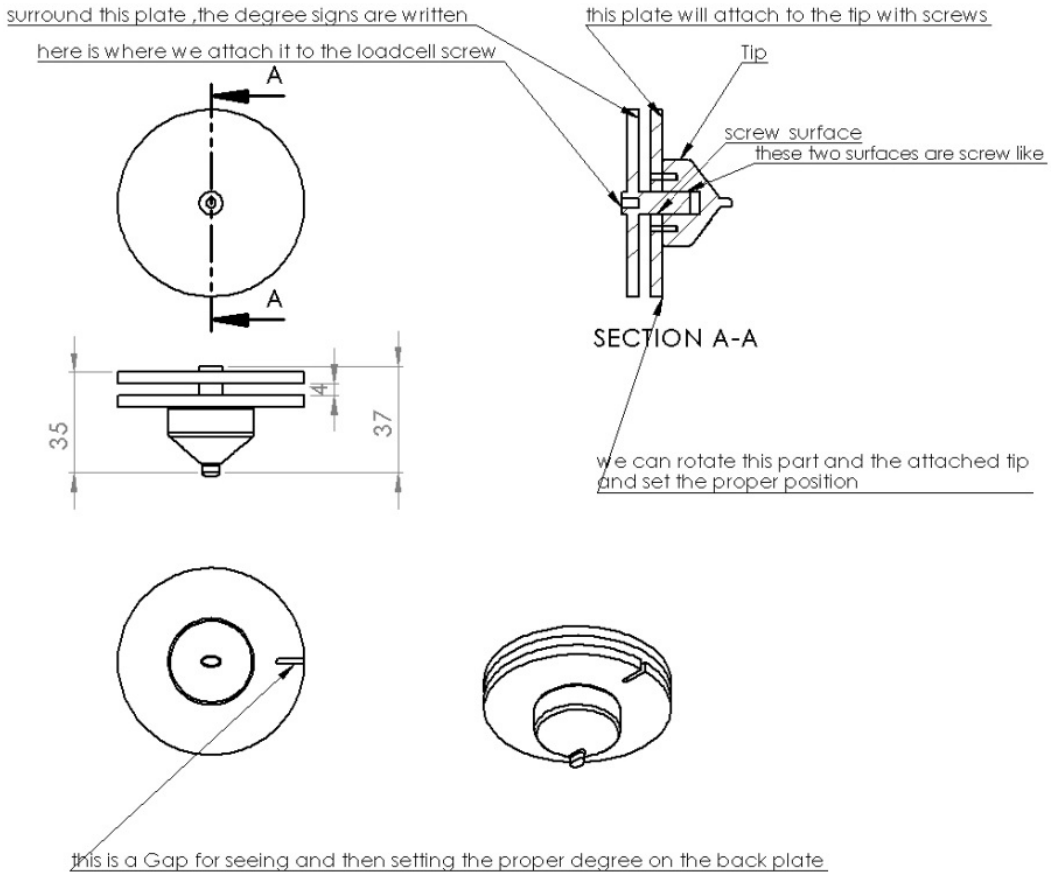

Figure 3.1-7. The designed part for aligning the tips in different directions

3.2 Experimental Procedures/Protocols

3.2.1 Displacement Rate Controlled Cyclic Loading Experiments:

In cyclic loading test, soft tissue (on the forearm) is loaded and unloaded periodically as the indenter tip moves forward and backward in each cycle. This movement is repeated until the desired number of cycles is reached.

In displacement rate controlled test, various scrutiny were made using two groups of data that are force-time and force-displacement. Soft biological tissues display preconditioning effect (Mullin's effect) under cyclic loading. During first few

cycles, tissue is more stiff, by repeating the cycles the reaction force of tissue changes and shows repeatable and comparatively compliant response.

In “displacement rate controlled mode”, the amount of displacement is kept constant with constant rate, and force versus time and force versus displacement characteristics of the soft tissue are examined. In other words, the stepper motor is driven in forward direction by constant speed until the desired displacement is reached and it is retracted back again with the same displacement amount. The test is repeated until the desired number of cycles is reached. Motor speed [mm/s], the displacement [mm] and number of cycles have to be taken as inputs by the help of the graphical user interface in LabVIEW.

The graphical user interface of this test (in LabVIEW) is illustrated in figure (3.2-1);

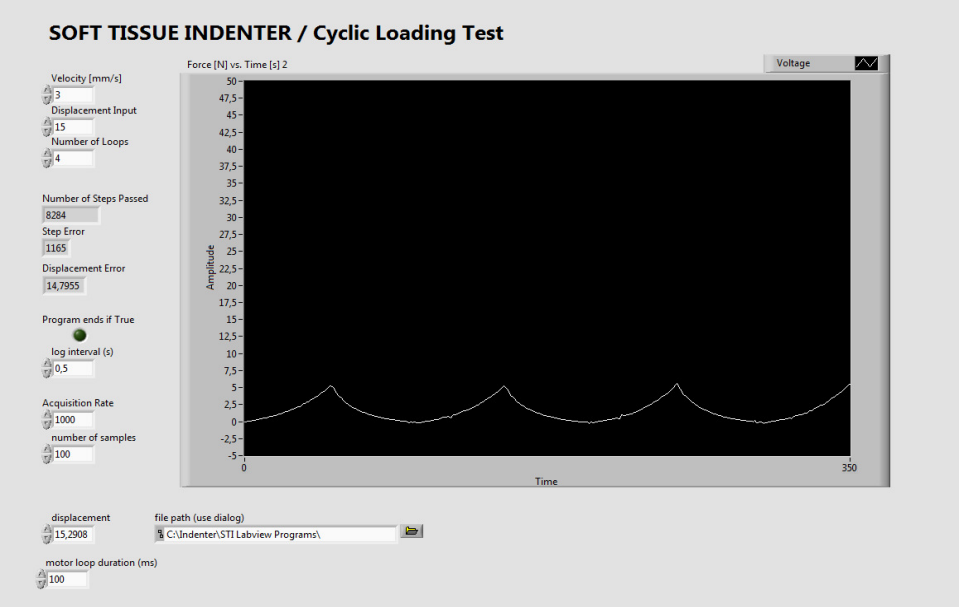

Figure 3.2-1. The graphical user interface of displacement rate controlled cyclic loading

3.2.2 Force Rate Controlled Cyclic Loading Experiments:

Through this study in addition to displacement rate controlled measurements, the implementation of the force rate controlled cyclic loading test method also was possible. The displacement rate controlled cyclic loading test is open loop control system. There is neither position nor force correction in the system and there is no feedback in that. Force Controlled Cyclic Loading Test includes a feedback information from the output which makes it a closed loop system.

In “force rate controlled mode”, the amount of force rate is kept constant [N/s], and displacement-time and force-displacement characteristics of the soft tissue are examined. For example if input is 1 N/s and the cycle duration time is 10 s , in 5 s the indenting force linearly increases to 5 N (the peak force of cycle) and then it linearly decreases back to zero force. The test is repeated until the desired number of cycles is reached. Therefore, in order to perform this test, parameters such as force rate [N/s], the time duration for every cycle, and number of cycles have to be taken as inputs by the help of the graphical user interface. In addition to these inputs the value of threshold to define tolerance domain of target force is also defined as user’s input parameter. It defines an acceptable error zone for force variations due to time. The graphical user interface of this test (in LabVIEW) is shown in Figure (3.2-2).

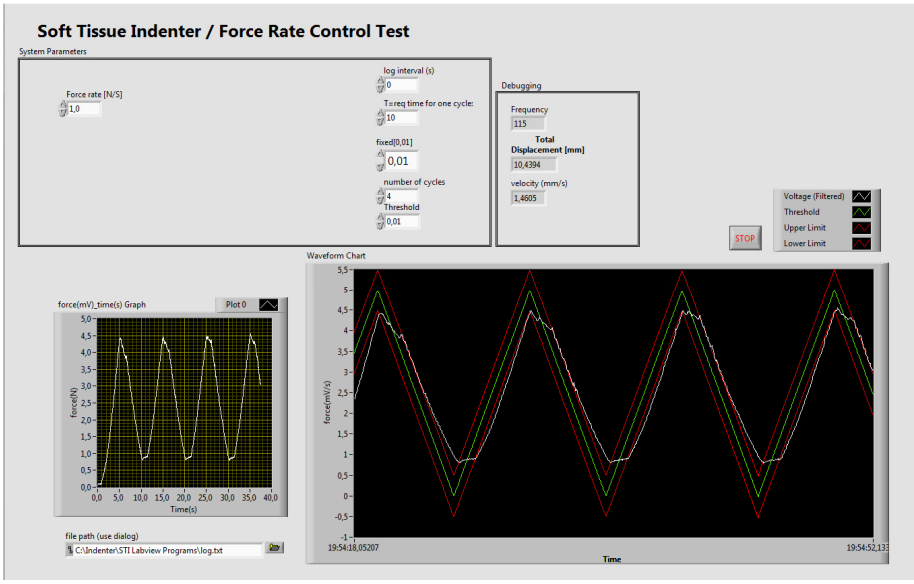

Figure 3.2-2. The graphical user interface of force rate controlled cyclic loading

One of the counter pins of NI USB-6212 of data acquisition card is used for driving the stepper motor. Two different analog pins are used to read load cell data continuously. After receiving the data, in order to get rid of its noise acquired voltage values from the load cell (in mV) are filtered (see appendix A). Those filtered values are converted into newton [N] and compared with the target force value. After comparing these a signal is generated and sent to the motor direction pin in order to choose the desired direction (Forward or Reverse), if the applied force is not in the desired range (that was defined with threshold value input) a digital I/O pin is triggered which enables pulse generation from the counter pin for driving motor.

3.2.3 Relaxation experiments:

In this test, after initial rate controlled indentation the amount of displacement (penetration into tissue) was kept constant and the response of tissue was observed. After going forward and reaching the required input displacement into the soft tissue, the stepper motor and indenter tip was dwelled until input relaxation time is reached and then at the end of this time indenter device is retracted. The input

parameters to this test are the amount of displacement [mm], the speed of the motor [mm/s] and relaxation time [s]. Due to sensitivity, relaxation experiments should be conducted in a noiseless (Electrical, Magnetic, Acoustic, Mechanical, etc.) environment. Even mobile phone noises can affect the results. Also they are extremely influenced by muscle movements during relaxation time. The graphical user interface of this test (in LabVIEW) is illustrated in Figure (3.2-3) ;

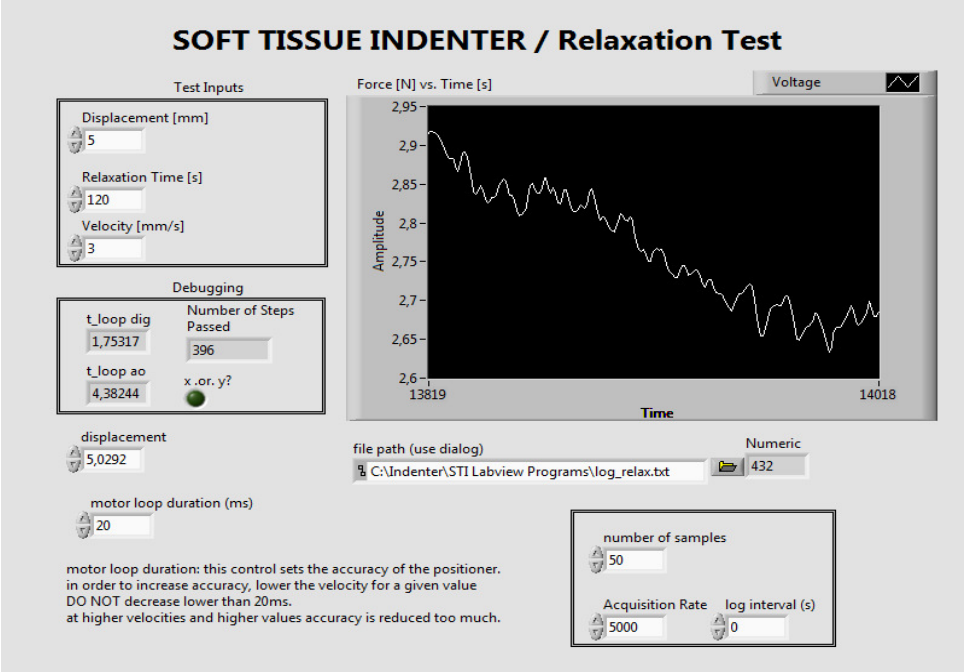

Figure 3.2-3. . The graphical user interface of Relaxation test

3.2.4 Creep Experiments

In creep test also, the system works in a closed loop form. Here the amount of force that will be applied on the soft tissue is tried to be kept constant. The target force value is defined by the user as input. At the beginning the step motor begins to move with a constant speed [mm/s] that is another input parameter of the experiment. It continues moving until it enters to the threshold domain of the target force. After this point the movement of the motor is force controlled and the speed changes due

to the force thus if the force applied on the indenter tip is below that value, motor goes forward and indents more. If the applied force is greater than target force value, the motor is retracted, so the soft tissue is unloaded until the target force is reached. By loading and unloading the tissue, the force on the indenter tip is tried to be kept constant. The difference between the load on the indenter tip and the target force value is fed back to the motor and motor reacts to this difference by changing its frequency (speed). In other words, if there is a big difference between the target force and the value read from the load cell, motor moves faster and as the indenter indents, motor slows down and even stops when the target force is reached. The test is continued until the desired input experiment time is reached. Again with the same flow of operation, load cell sends the force readings to NI-6212 and in LabVIEW environment, the force vs. time and displacement vs. time characteristics of the soft tissue is examined. The input parameters for this test are simply the target force value [N], initial constant velocity of the stepper motor [mm/s], experiment time [t], and threshold. Log interval is optional for variations in number of written samples. The graphical user interface of this test (in LabVIEW) is illustrated in Figure (3.2-4). In this experiment displacement vs. time and force vs. time characteristics of the soft tissue are examined.

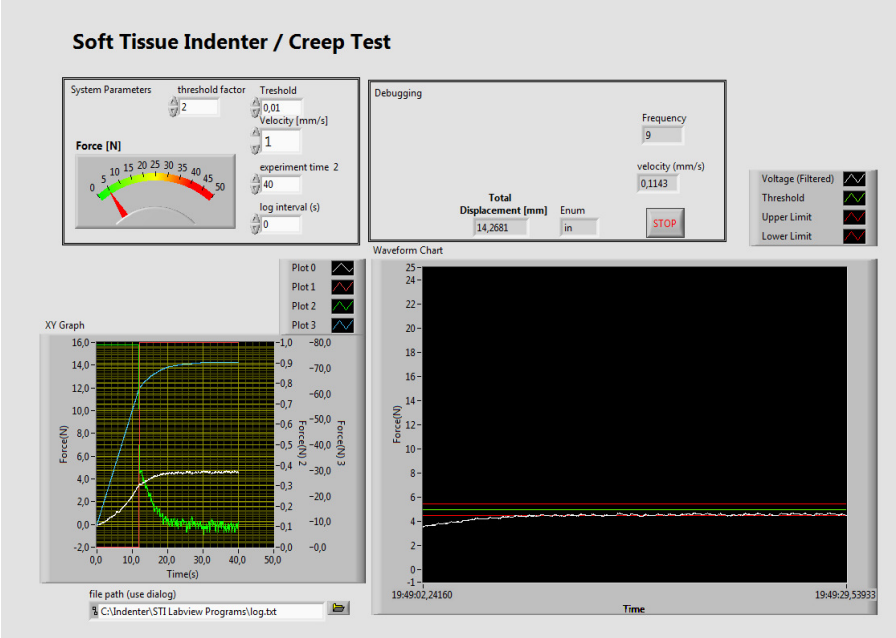

Figure 3.2-4. . The graphical user interface of creep test

3.2.5 Determination of material directions and in-plane anisotropy:

In literature, flat-ended cylindrical (Choi et al., 2008), spherical (Dimitriadiset al., 2002), conical (Pelletier et al., 2006), pyramidal (Borodich et al., 2003) and cylindrical lateral (Argatov et al., 2015) that uses the lateral contact of a cylindrical indenter are widely used. The response of tissue to loads are different depend on the direction, this behavior cannot be determined by axi-symmetric tips, therefore ellipsoid tips which are theoretically examined by Bischoff (2004), and first experimentally used by Petekkaya et al (2010) were used.

The long axis of the ellipsoidal indenter tips was placed parallel to the longer axis of the biceps muscle and cyclic loading tests were conducted in every 30 degree up to 180 and a 210 degree for control. In these tests, for eliminating the preconditioning effect at first, 20 loops of cyclic loading were conducted at a pre-determined point of muscle then the real tests were conducted consequently without waiting for the soft tissue to recover. Response of biceps muscle in different indenter tip alignments, to the same displacement controlled cyclic loading test

were examined .The tests were carried out at same point ellipsoidal indenter tips. Moreover displacement values of biceps muscle in every 30 degree indenter tip alignments, to the same force controlled cyclic loading test also were examined. The tests were carried out at same point.

3.3 Study of the Indenter Force and Movement Sensitivity

The movement accuracy of device up to required distance was controlled before conducting any experiment on human soft tissue by using a dial gauge. The comparator device has a resolution of 1/100 mm accuracy, and maximum 10 mm displacement measurements are feasible with this set up. The measured traveled distance of the device during sample experiments was compared with the input displacement amounts. Controlled tests were repeated in different rates and displacements, and the errors was found,

Moreover some trial experiments were conducted on dummy objects and the results were analyzed.

3.3.1 Examining displacement and time accuracy of cyclic loading

In Table (3.3-1) the input and output displacement amount of cyclic loading test with different displacements and rates in both forward and backward directions were collected.

Table 3.3-1. Displacement accuracy in displacement rate-controlled cyclic loading with 50 number of samples and 5000 data points (100 sample per second)

Input displacement(mm) (LabVIEW)		**Output displacement (mm) (Comparator)**		**Speed (mm/s)**	$Error/input$	
forward	**Back ward**	**forward**	**backward**		**forward**	**backward**
1	1	0,95	0,98	1	5%	2%
3	3	2,93	2,90	1	2.3%	3.3%
5	5	4,93	4.94	1	1.4%	1.2%
9	9	8,85	8.87	1	1.6%	1.4%
3	3	2,90	2,85	3	3.33%	5%
5	5	4,85	4,90	3	3%	2%
9	9	8,75	8,79	3	2.77%	2.33%
3	3	2,95	3.05	5	1.6%	-1.6%
5	5	4,85	4,80	5	3%	4%
9	9	8,85	8.73	5	1.6%	3%
5	5	4,85	5,10	10	3%	-2%
9	9	9,20	9,25	10	-2.2%	-2.7%

For time accuracy examining in cyclic loading tests the calculated required time for one cycle due to speed and displacement input, was compared with the time measured with a chronometer. Manual chronometer has an accuracy of slightly less than a second therefore the obtained time for 6 cycle was divided to 6 for minimizing this error (table 3.3-2)

Table 3.3-2. Time accuracy in displacement rate-controlled cyclic loading with 100 sample per second

Input Duration(sec) For one cycle due to speed	**Output real For one cycle duration(sec)**	**Speed(mm/s)**	**Input displacement (mm) (LabVIEW)**	**(Output-input)/input**
2	2,02	1	1	-1%
6	6,1	1	3	-1.6%
10	9,94	1	5	0.6%
18	18,46	1	9	2.5%
2	1,85	3	3	-7.5%
3,33	3,10	3	5	-6%
6	5,7	3	9	-5%
1,20	1,20	5	3	0
2	2,04	5	5	2%
3,60	3,69	5	9	2.5%
1	1,06	10	5	6%
1,80	1,86	10	9	3.33%

.

3.3.2 Examining displacement and time accuracy of relaxation experiment

Table 3.3-3.Displacement accuracy in forward direction for relaxation test with 20 seconds relaxation time.

Input displacement(mm) (LabVIEW)	**Output displacement(mm) (Comparator)**	**Speed(mm/s)**	
5	4,90	1	0,02
5	5	3	0
5	5	5	0
5	5,10	8	0,02
8	7,95	8	0,00625
8	7,97	1	0,00375
8	8,20	3	0,025
8	8,20	5	0,025

For examining the displacement accuracy and time accuracy in relaxation tests again some tests on different rates and displacements were carried out. The results are collected in table (3.3-3) and table (3.3-4) for displacement accuracy and time accuracy respectively.

Here just value for forward direction of the indenter device was analyzed. For time accuracy analyzing, the duration for whole experiment was predicted from the input speed and summed with input relaxation time. Then obtained time was compared with the obtained time of chronometer. The chronometer has an accuracy less than 1 sec, therefore this error should be added to the calculated values.

Table 3.3-4.Time accuracy of relaxation tests with different displacement and rates and 20 seconds relaxation time

Input Duration(sec) For one cycle due to speed: **(forward+relax time+backward)** **(T_i)**	**Real Output For one cycle duration(sec)** **(T_R)**	**Speed** **(mm/s)**	**Input displacement** **(mm)** **(LabVIEW)**	**(Ti-Tr)/Ti**
10+20	30,5	1	5	-1.6 %
3,33+20	23,9	3	5	2.4%
2+20	22,47	5	5	-2.1%
1,25+20	21,47	8	5	-1%
2+20	21,5	8	8	2.2%
16+20	36,38	1	8	-1%
5,33+20	25,45	3	8	-0.4 %
3,2+20	24,19	5	8	-4.2%

3.3.3 Examining displacement accuracy of creep experiment

During conducting of the tests it was observed that the displacement travelled by creep test after catching the target force was different than what was reported in labview. The accuracy of displacement was checked and the problem was solved then again the accuracy of measured displacement was controlled by conducting trial tests with 30 seconds creep time and different target forces. Movement of the tip was achieved by applying force to the tip during the experiment.

The travelled displacement was measured with the same displacement comparator (MITUTOYO) the measured time at the end of the experiment , was compared with the recorded measurement in labview code and the errors of these values were found . The results were provided at table (3.3-5)

Table 3.3-5. Measured displacements at the end of 30 seconds creep time.

$D_{comparator}$(mm)	$D_{LabVIEW}$ (mm)	$(D_l-D_c)/D_l$
3,15	3,297949	4,48%
1,5	1,444777	-3,82%
3,8	3,946437	3,71%
6,7	6,739508	0,58%
3,05	3,225241	5,43%
5,3	5,325771	0,48%
2,8	2,970378	5,7%
4,2	4,389665	4,3%
3,2	3,333395	4%
2,4	2,5	4%

3.3.4 Tests on dummy objects

In order to examine the movement style of indenter device a dummy object with similar viscoelastic behavior was chosen to conducting some trial tests.

During in-vivo tests on human arm the motions originated from breathing, heart beating, and muscle movements were shown up as fluctuations in experiments. Thus examining of the movement of device on a motionless dummy object, in order to being able to make certain conclusions about the fluctuations were decided. For this the tests were conducted on a flexible ball. This ball had a whole that in case of applying pressure the inside air exits and after removing the force again it recovers to the initial form of it.

Firstly relaxation experiment was carried out. The indenter went forward and indented the ball for 6mm displacement and then stopped there for until the relaxation time was over. As can be seen in Figure (3.3-1) the result is very smooth and noiseless. The reason for dropping of force during relaxation time is going the air inside out.

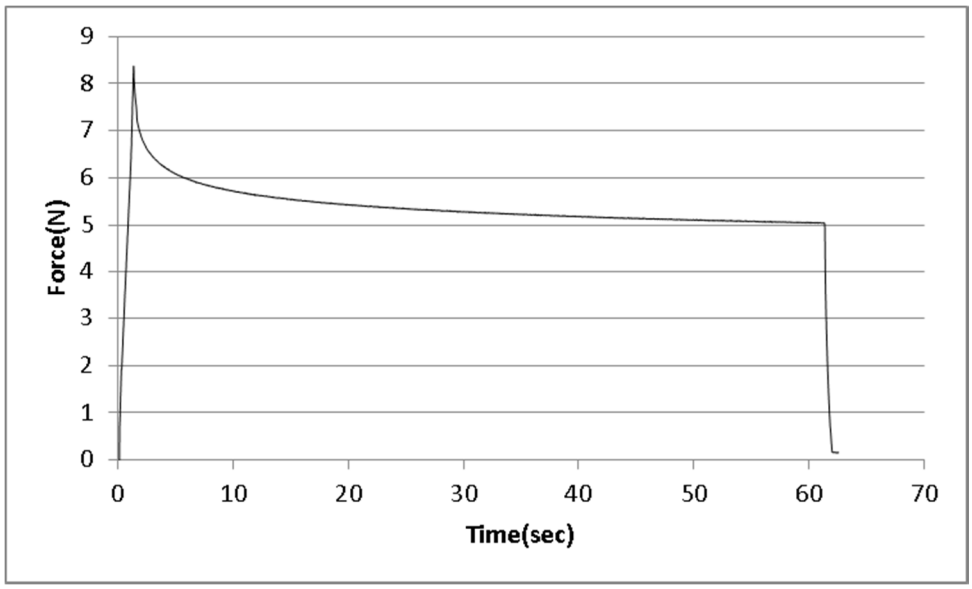

Figure 3.3-1.Relaxation test on dummy object. The result is a noiseless and very smooth data.

Then the creep tests were tried on this object. The indenter goes forward and indents the ball until it reaches to target force, then stops there during experiment's input time. The result (Figure 3.3-2) showed again a smooth movement of step motor without fluctuations originated from muscle tonus. The step motor keeps moving forward because of transpiration of air inside. Indenter tries to catch the target force.

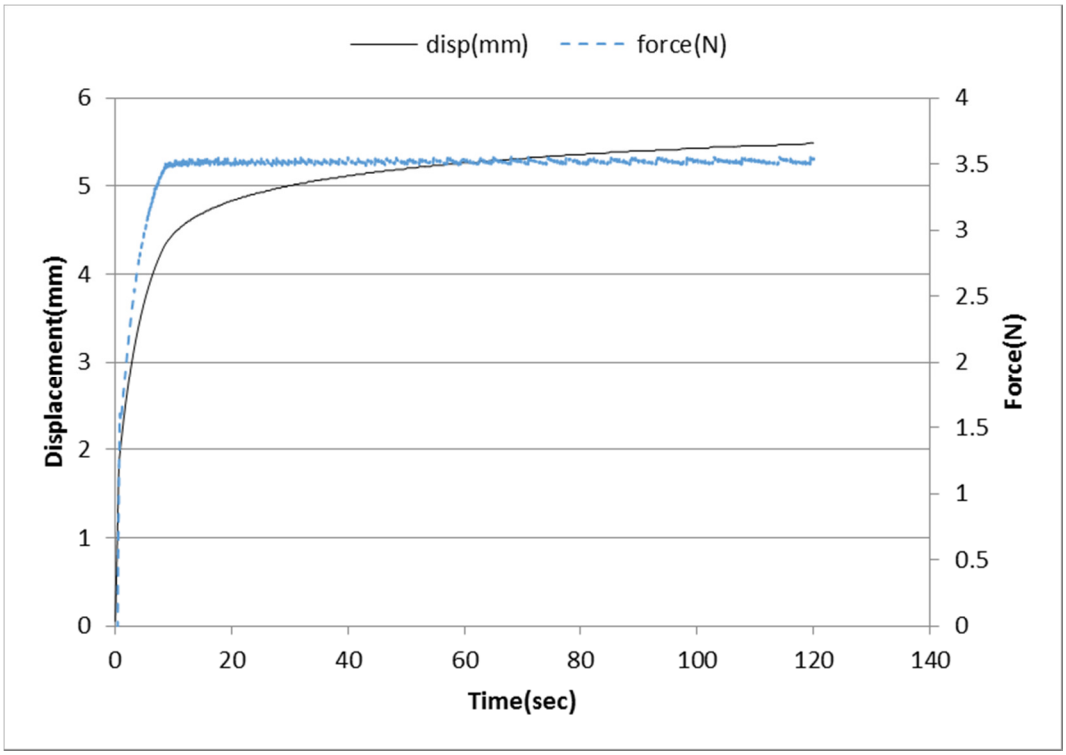

Figure 3.3-2.Creep test on the dummy object.

3.3.5 Examining the force accuracy of load-cell

In order to study the sensitivity of the load-cell and the accuracy of measurements, a number of pre-determined weights (deadweights) were used. The accuracy of these weights were checked using electronic scale, then the measured gram values converted to kg and multiplied by 9.806 to obtain the values in Newtons. The results were shown in Table (3.3-6) where, the deadweight defined force is our Labelled force and Mass is the measured weight in electronic scale.

Table 3.3-6.Deadweights accuracy studying; output measured forces of deadweights and labeled forces of them

Labelled (N)	Mass (Kg)	Weight (N)
5	0.51196	5.020
5	0.51179	5.018
5	0.51198	5.020
5	0.51200	5.022
2	0.20462	2.006
2	0.20458	2.005
2	0.20446	2.0049

Since the difference between stamped and weighed values are very small, thus the labeled values of weights (inputs) were accepted for measurements.

Then the indenter device was positioned in such a way that the tip and loadcell was perpendicular to the ground. The device was turned on to energize the sensor. After 1 hour of giving energy to sensor, the weights were put on the loadcell and the measured force in LabVIEW was recorded.

The sensor was loaded and unloaded in two styles; in an order and also randomly. Firstly the weight was increased in 8 steps from zero to 26 N. the measured forces were demonstrated in Figure (3.3-3) and Table (3.3-7). The average of errors was -0.5205 and the standard deviation of errors was 0.21892595.

In this case the closeness of slop of trend-line to one shows that the calibration of sensor is acceptable. Y-intercept originates from the fact that, load-cell has an offset when there is no load on it. Force data correctness can be achieved by subtracting this offset value from the measured values (Refer to section 4.1.1).

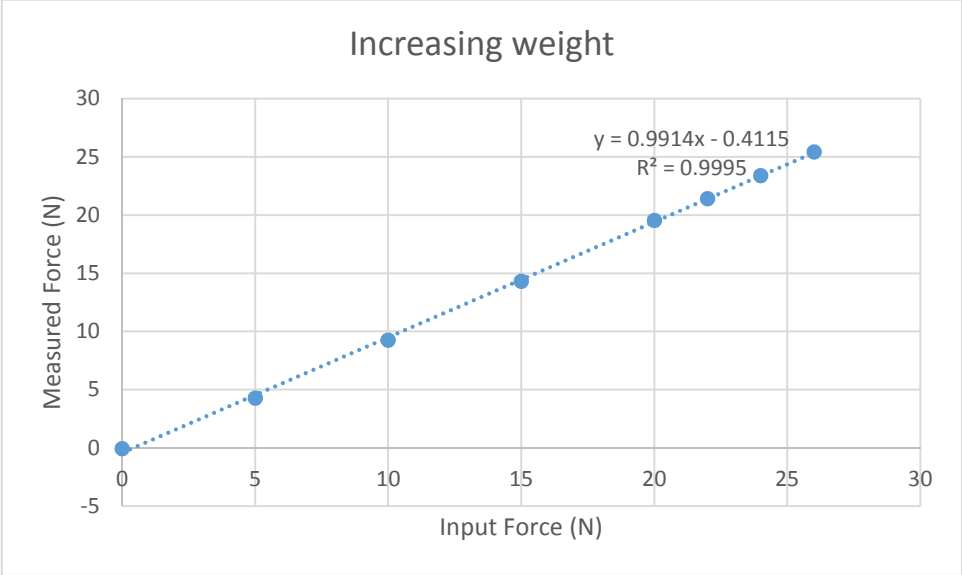

Figure 3.3-3. Load-cell measured forces vs. input forces

Table 3.3-7. Input and output weights as weight increased. The average error was -0.5205 and the standard deviation of errors was 0.21892595

Dead weights(N)	Measured forces (N)	Errors (output-input)	Error distance from the mean
0	-0.045	-0.045	0.4975
5	4.29	-0.71	-0.1675
10	9.27	-0.73	-0.1875
15	14.34	-0.66	-0.1175
20	19.54	-0.46	0.0825
22	21.42	-0.58	-0.0375
24	23.41	-0.59	-0.0475
26	25.435	-0.565	-0.0225

In another set of experiments the behavior of sensor was analyzed as the weight was decreased from 26 N to 0 N (Figure3.3-4 and Table 3.3-8). The average error was -0.29125 and the standard deviation was 0.104736063. Again in this case also

the slope of fitted line to measured force data is very close to one which means that the sensor was calibrated properly.

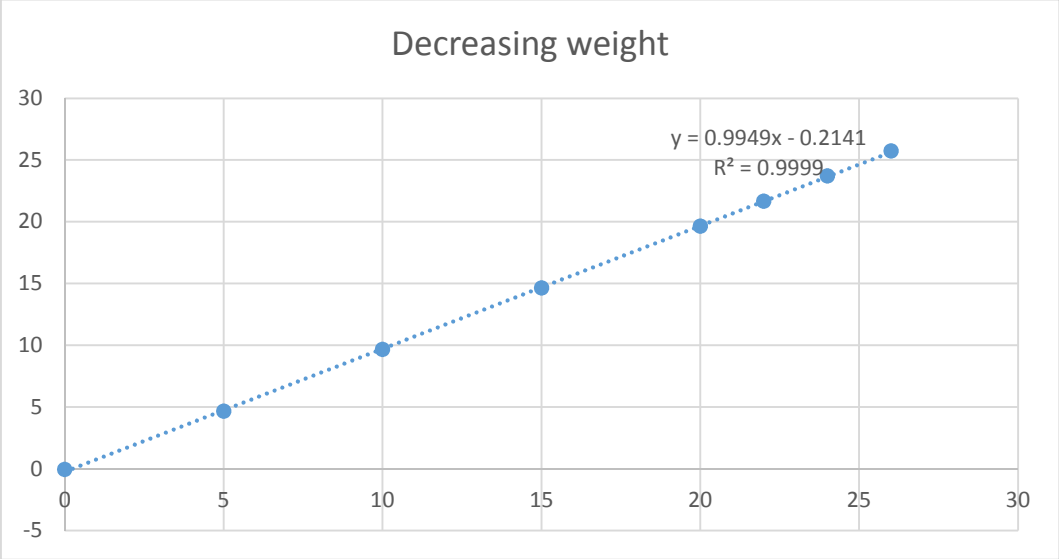

Figure 3.3-4. Load-cell measured forces vs. input forces

Table 3.3-8. Input and output weights as weight decreased. The average of errors was -0.29125 and the standard deviation of errors was 0.104736063

Dead weights(N)	Measured forces (N)	Errors (output-input)	Error distance from the mean
26	25.73	-0.27	0.02125
24	23.71	-0.29	0.00125
22	21.68	-0.32	-0.02875
20	19.645	-0.355	-0.06375
15	14.635	-0.365	-0.07375
10	9.665	-0.335	-0.04375
5	4.65	-0.35	-0.05875
0	-0.045	-0.045	0.24625

The third set of experiment was carried out as the weights was randomly increased or decreased (2, 7, 17, 12, 21, etc.) and the results are shown in Figure (3.3-5) and

Table (3.3-9). The average of absolute errors was 0.026875 and the standard deviation of absolute errors was 0.157976886.

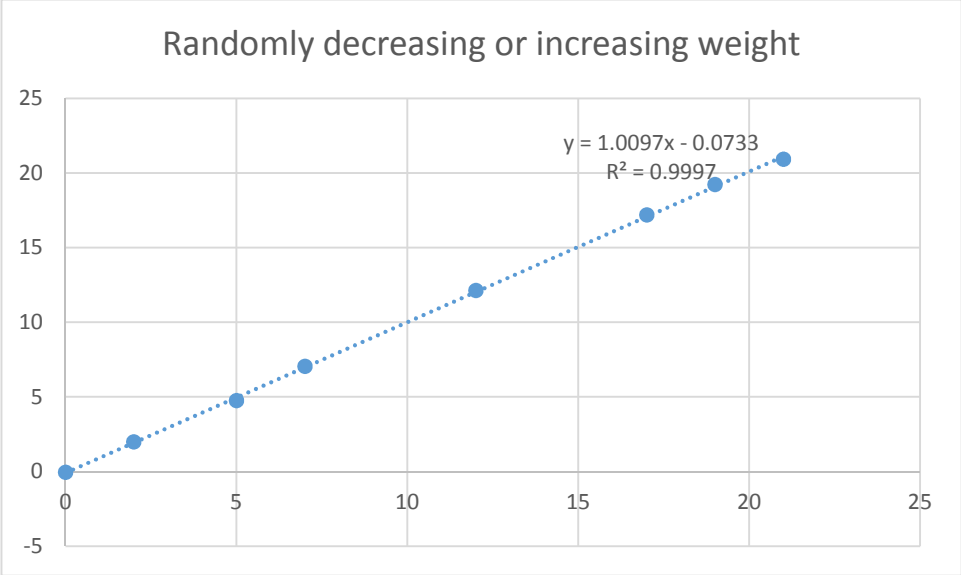

Figure 3.3-5. Load-cell measured forces vs. input forces

Table 3.3-9. Input and output weights as weight increased, the average of errors was 0.026875 and the standard deviation of absolute errors was 0.157976886

Dead weights(N)	Measured forces (N)	Errors (output-input)	Error distance from the mean
0	-0.045	-0.045	-0.07188
2	1.99	-0.01	-0.03688
5	4.75	-0.25	-0.27688
7	7.05	0.05	0.023125
12	12.125	0.125	0.098125
17	17.19	0.19	0.163125
19	19.235	0.235	0.208125
21	20.92	-0.08	-0.10687

The maximum difference of slope of trend-lines of explained three set of experiments is 0.0183, thus expected error value is around 1.8% which is fairly precise for our measurements.

Moreover the **zero drift** of sensor was checked. The signal level may vary from its set zero value when the sensor works. This may cause an error in force measuring equal to the amount of variation, or drift as it is usually termed. Zero drift may result from changes of temperature, electronics stabilizing, or aging of the transducer or electronic components.

Zero drift was studied with comparing the first no-load condition with completely unloaded conditions (zero-loaded or no-load conditions) of sensor during the process of decreasing or increasing of weights. The measured force changes between 0.035 to 0.045 N, but mostly 0.045 value was seen as force in no-load case.

CHAPTER 4

IN VIVO EXPERIMENTS ON HUMAN ARM

A group of six young subjects all having a normal healthy condition (age 25-29) voluntarily contributed to the study (Table 4.1-1). The experiments were performed under the approval of the Ethics Committee of Middle East Technical University (Ankara- Turkey). (Appendix C)

After a great number of exhaustive experiments and troubleshooting and solving the observed problems and bugs in codes and graphs, a chosen summary of experiments was provided in this chapter. Because of ease, more control and facility in conducting tests and obtaining more precise results in consequence, the subject's arm was chosen for in-vivo indentation experiments.

.Table.4.1-1.Volunteer subjects for experiments

Experiment subjects	**Gender**	**Age**
G	M	28
N	M	29
Z	F	25
B	F	26
S	F	26
P	F	28

4.1 Points to be considered for conducting experiments:

Experiments were started while the surface of indenter tip was positioned in tangency with a predetermined point of arm but without any pre-strain or pre-force. This is an important point which should be considered. After conducting tests the zero-strain and zero-force data were separated from recorded data and the remained data was analyzed. In these experiments we used three part of subjects' arms; Flexor carpi radialis, Flexor digitorum superficialis, and biceps muscle as shown in Figure (4.1-1). It was tried to repeat the points in different subjects and use the same location for tests.

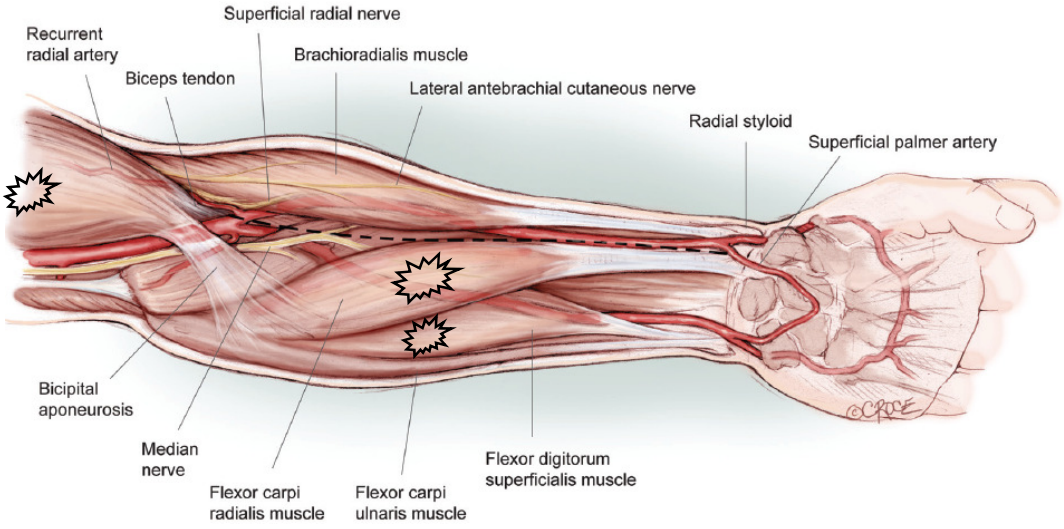

Figure 4.1-1 Three determined points for indenter experiments. Adopted from: www.annalscts.com

It will be beneficial to mention some issues about the experiment procedures: firstly after entering input parameters of each protocol into LabVIEW interface, the subject's arm is fixed and secured in indenter arm encasement. Then indenter tip's position is manipulated and fixed in preferred alignment using tip positioner part. Tangency and perpendicularity of the tip to the tissue surface should be taken into consideration in this stage. Force zeroing are also important points that should be carried out. The tests are initiated by a button in labview interface. During the

experiments the subject must avoid any activity. This involves speaking, head motion, fingers motion, and irregular intense breathing.
Moreover after each experiment the position of tip, device and arm should be checked in order to conducting precise experiments.
Another significant issue is that during the experiments arm must be at rest and must not be squeezed. Finally if the aim is utilizing data in future computer simulations therefore the points which indentation is applied should be marked and mentioned in text.

4.1.1 Force zeroing

In order to remove any (negative or positive) offset of load cell from recorded data, prior to tests, data was recorded for a specific duration and the mean value of the existent load was calculated, using a Labview code that is provided in Appendix B. Then this value was subtracted from recorded force data of followed experiment. This process was done prior to every experiment separately.

4.2 Displacement Controlled Cyclic loading Tests

The details about this experiment's procedure and the input parameters are explained in Chapter 3. Here two data categories should be observed; Force vs. time and force vs. displacement. Our input loading and unloading displacement is constant thus observing the displacement vs. time graph can be carried out just for controlling the performance of the device. The same information can be extracted from force-displacement graph also. Before analyzing the results I prefer to explain two principal definitions related to cyclic loading experiments on soft biological tissues; preconditioning and hysteresis.
Preconditioning is a process that the sequential cyclic loading is applied to the soft tissue until the mechanical properties of it are unaltered and constant. Preconditioning is generally be conducted in "load controlled" and "displacement controlled" experiments.

Hysteresis: At the point when viscoelastic materials have a force applied to them and after that uprooted, it takes more energy to dislocate the material than it does to return back where it is due to its unique setup. As such, it expends more energy during the loading stage (applying a load and extending the material) contrasted with the unloading stage (taking the load away and permitting the material to come back to its first configuration). This energy contrast is brought about by the material losing energy during the loading stage, because of heat dissipation or rearrangement inside the material. The area between the loading and unloading bend represents the energy lost.

Figure (4.2-1) and Figure (4.2-2) illustrate force-time and force–displacement relations of a "displacement controlled cyclic loading "test conducted on forearm of (Flexor digitorum superficialis muscle) of a female with 5 mm/s velocity,15 mm displacement and 15 loops inputs. It has been experimentally detected that the maximum response force gradually decrease from 5.75 N to 4.75 N during preconditioning in sequential loading-unloading cycles and they progressively remain unaltered when the tissues are completely preconditioned. Preconditioning in this experiment can be seen after 7th cycle. Additionally as shown in force vs. displacement graph, the preconditioning phenomenon appears by decreasing in hysteresis area eventually up to a constant area amount during sequential cycles. The downward shift of the hysteresis curves and finally remaining in a repeatable pattern demonstrate this fact (Figure 4.2-2).

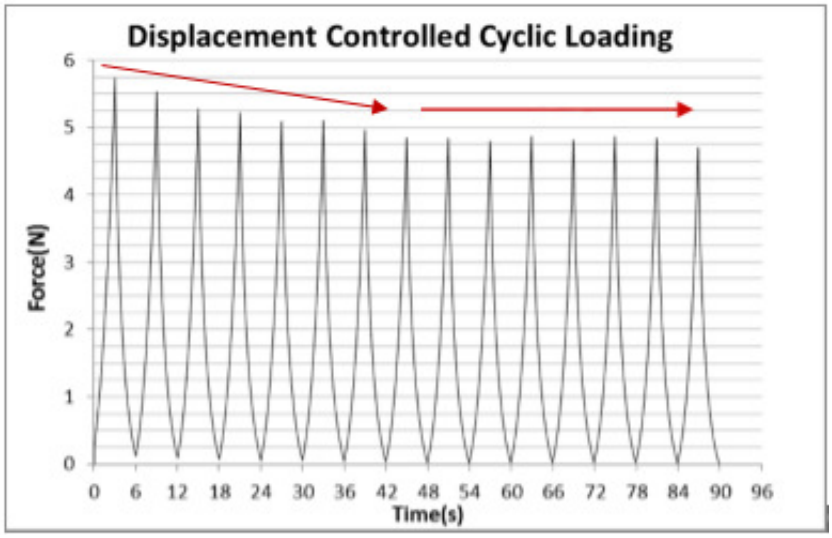

Figure 4.2-1. Displacement controlled cyclic loading test with 5 mm/s velocity, 15 mm displacement and 15 loops

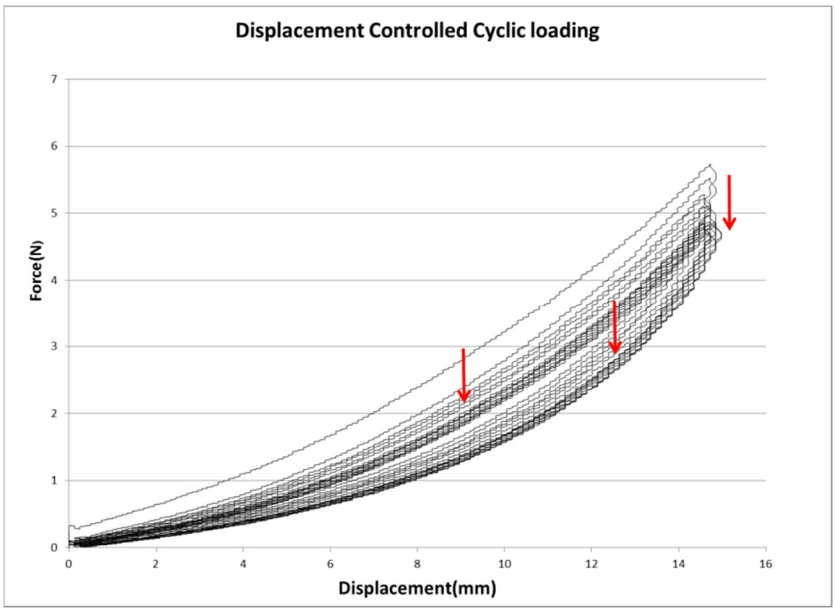

Figure 4.2-2.The observed downward shift in Hysteresis of cyclic loading test

4.2.1 Rate-dependency of hysteresis area and preconditioning analyzing by calculating hysteresis area

In this section displacement rate controlled cyclic loading on forearm were conducted in four different rates of 10 mm/s, 5 mm/s, 3 mm/s and 1 mm/s. The experiments were conducted on different rate orders like, 1, 3, 5, 10 mm/s and 10, 1, 5, 3 mm/s. After each experiment the tissue allowed to partially recover again to its initial configuration for 15 minutes. The reason for applying random order speeds was to check the preconditioning effect on the results also. In other words in a series of experiments with regular speed order, tissue may be preconditioned by repeating cycles during tests, and this effect appears gradually, thus the real results cannot be observed.

In these tests the purpose is to studying both "rate-dependency" and the "preconditioning effect". 20 mm displacement and 15 loops are the other input parameters of these experiments. Experiments were done by the same indenter tip (ellipsoidal c). The results of both two mentioned displacement-rate orders were the same, so the obtained data from random rate order were provided here.

As illustrated in Figure (4.2-3) in the force-time graph of this test although there seen the decrease in force until 4^{th} cycle but the decreasing amount is small and the preconditioning is not so clear, nonetheless in force-displacement graph (Figure.4.2-4) the downward shift of curves and decreasing of hysteresis show the existent preconditioning very clearly. For more precise analyzing, the hysteresis area of each loop was calculated, using the recorded data and "Trapezoidal Rule". As shown in Figure (4.2-5) the hysteresis area deacreases during progressing cycles and eventually tends to a constant amount (from above 10 mJ to around 6 mJ).

The figures up to 4.2-14 shows the results of these experiments. Calculated hysteresis area (mJ) in each cycle of displacement rate controlled experiment with 15 loop, 20 mm displacement, and 10 mm/s speed inputs (figure.4.2-5), decreased through repeating cycles.

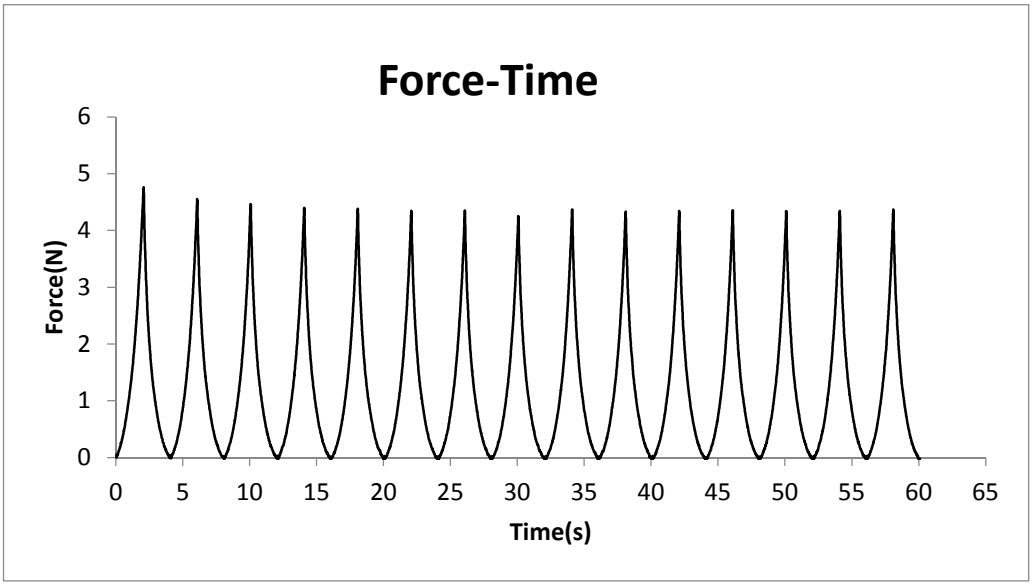

Figure 4.2-3.Force vs. time relation of displacement rate controlled experiment with 15 loop ,20mm displacement, and 10 mm/s speed inputs.

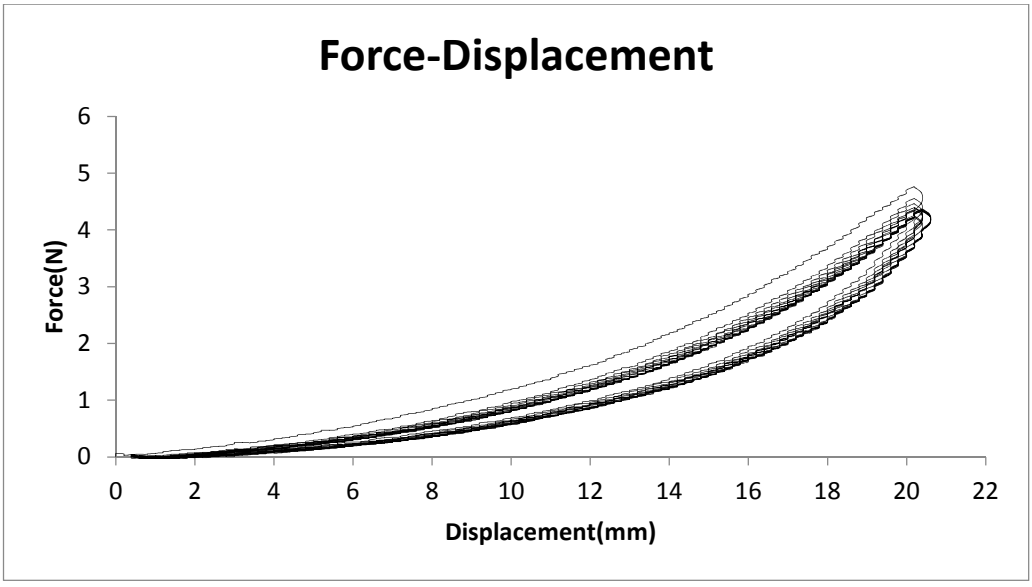

Figure 4.2-4. Force vs. displacement relation of displacement rate controlled experiment with 15 loop, 20mm displacement, and 10 mm/s speed inputs

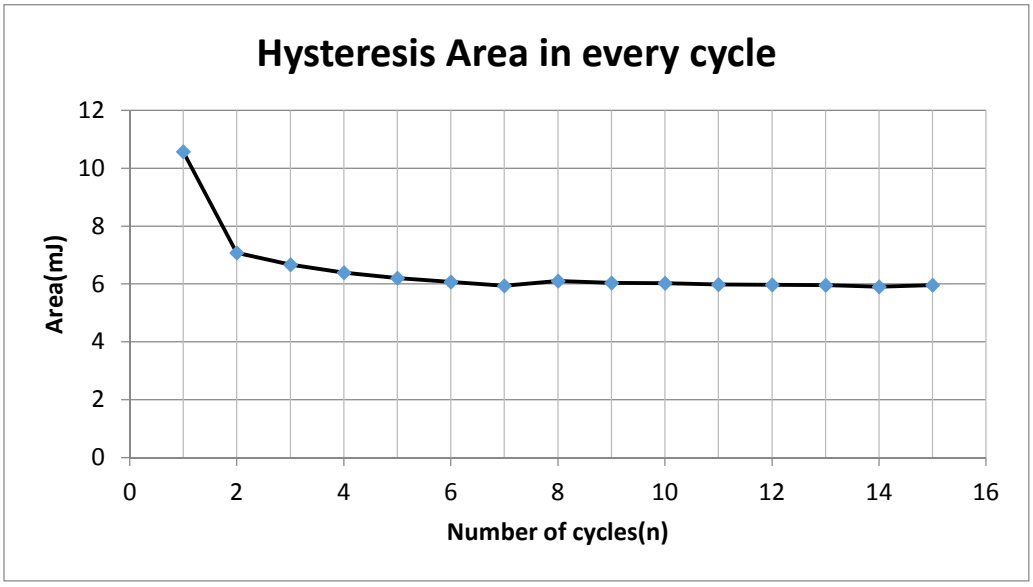

Figure 4.2-5. Appeared hysteresis area (m J) in each cycle of displacement rate controlled experiment with 15 loop, 20mm displacement, and 10 mm/s speed inputs

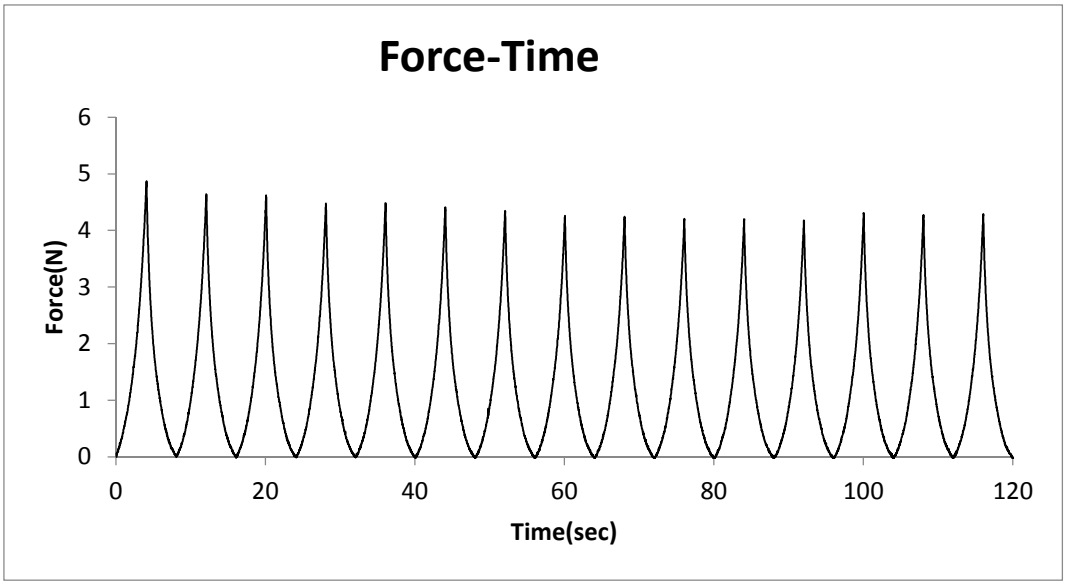

Figure 4.2-6. Force vs. time relation of displacement rate controlled experiment with 15 loop, 20mm displacement, and 5 mm/s speed inputs.

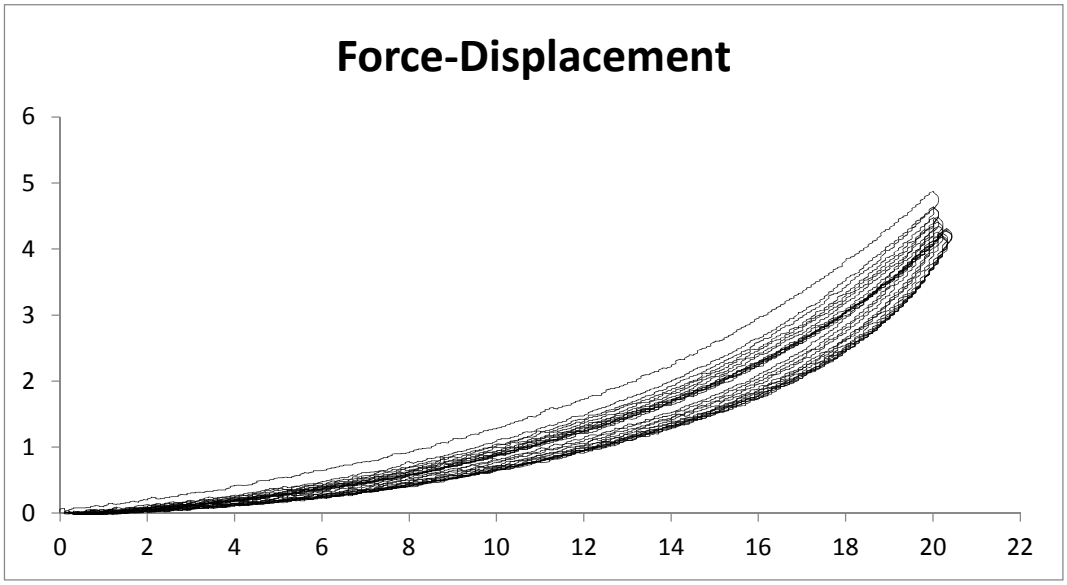

Figure 4.2-7. Force vs. displacement relation of displacement rate controlled experiment with 15 loop, 20mm displacement, and 5mm/s speed inputs

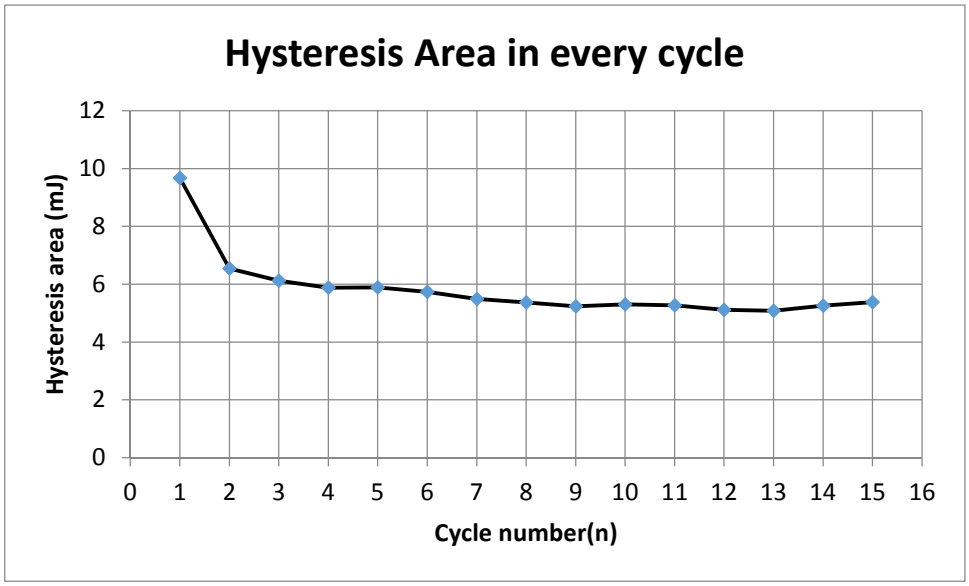

Figure 4.2-8. Appeared hysteresis area (mJ) in each cycle of displacement rate controlled experiment with 15 loop, 20mm displacement, and 5mm/s speed inputs

Calculated hysteresis area (mJ) in each cycle of displacement rate controlled experiment with 15 loop, 20 mm displacement, and 5 mm/s speed inputs (figure 4.2-8) clearly decreased until 9th cycle.

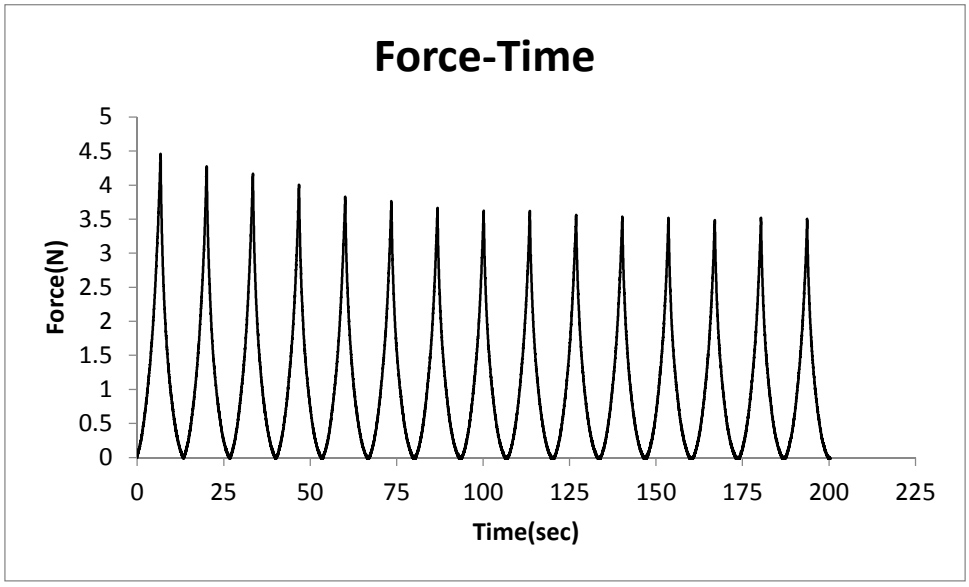

Figure 4.2-9. Force vs. time relation of displacement rate controlled experiment with 15 loop, 20mm displacement, and 3 mm/s speed inputs.

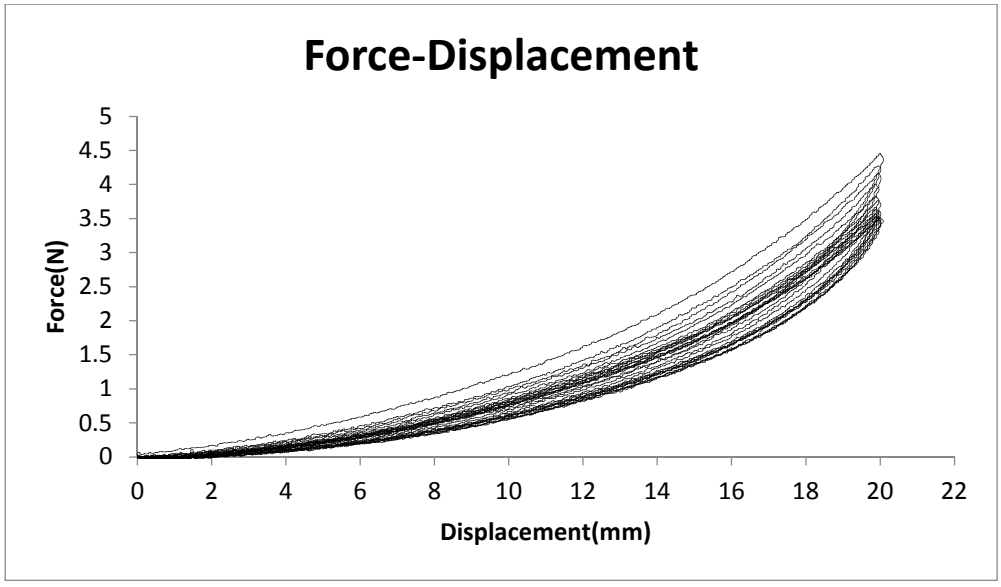

Figure 4.2-10. Force vs. displacement relation of displacement rate controlled experiment with 15 loop, 20mm displacement, and 3mm/s speed inputs

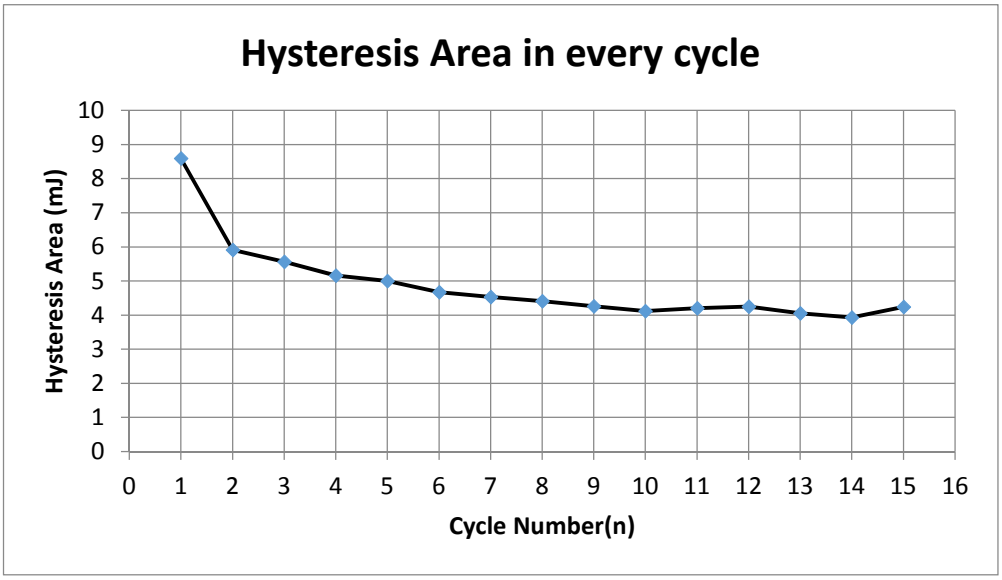

Figure 4.2-11. Appeared hysteresis area (mJ) in each cycle of displacement rate controlled experiment with 15 loop, 20mm displacement, and 3mm/s speed inputs

Calculated hysteresis area (mJ) in each cycle of displacement rate controlled experiment with 15 loop, 20mm displacement, and 3mm/s speed inputs decreased significantly until 10^{th} cycle.

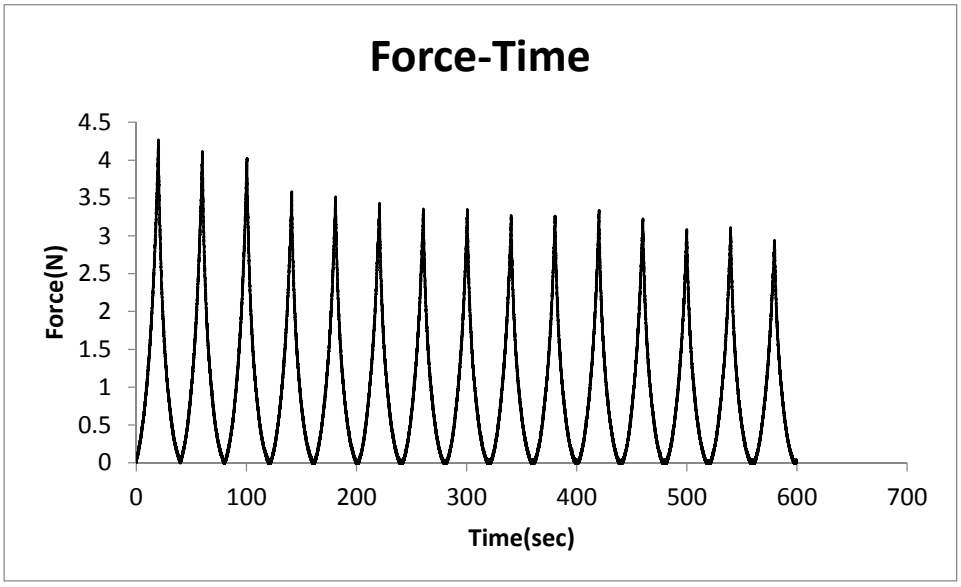

Figure 4.2-12. Force vs. time relation of displacement rate controlled experiment with 15 loop, 20mm displacement, and 1 mm/s speed inputs

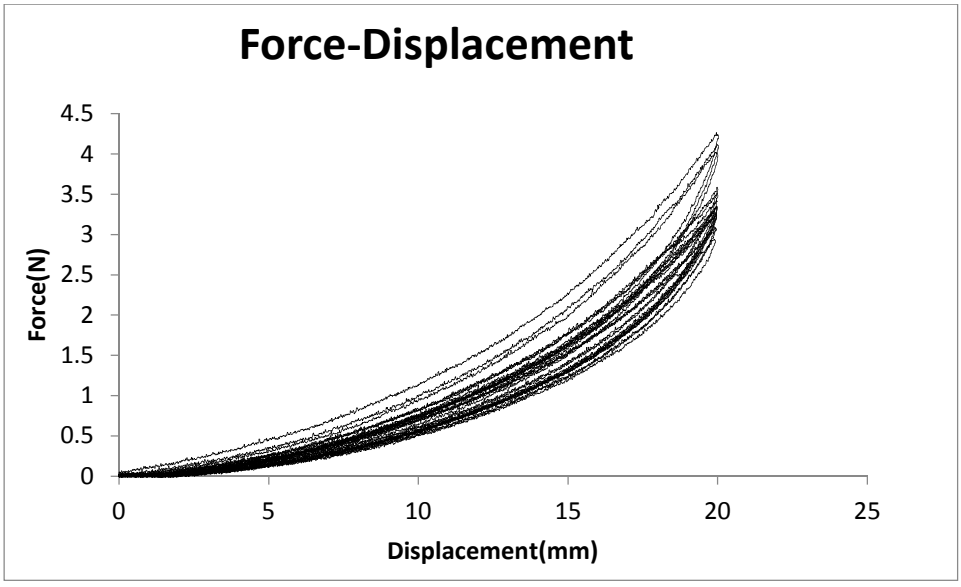

Figure 4.2-13. Force vs. displacement relation of displacement rate controlled experiment with 15 loop, 20mm displacement, and 3mm/s speed inputs.

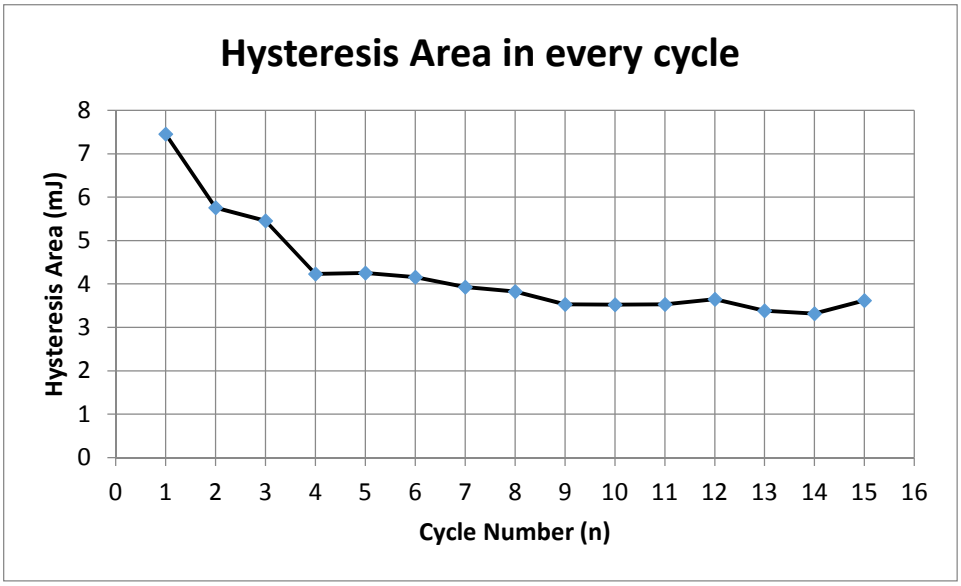

Figure 4.2-14. Appeared hysteresis area (mJ) in each cycle of displacement rate controlled experiment with 15 loop, 20mm displacement, and 3mm/s speed inputs.

In Figure (4.2-15) the hysteresis the trend of conducted different displacement rate experiments were compared. In all tests the difference of maximum and minimum hysteresis is 4 mJ- 4.25 mJ, Thus rate-dependency is not seen very clearly about the decreasing of hysteresis amount. But it can be seen that maximum energy loss happens in faster indentations (Around 10.5 mJ) in experiment with 10 mm/s speed. In this experiment hysteresis amount starts from Around 10.5 mJ, and drops to 6 mJ in 6^{th} cycle, then steadily continuous. This means preconditioning happens after 6^{th} cycle, which this issue was not clear enough in force-time graph of this experiment.

In the tests with 5 mm/s, 3 mm/s, and 1 mm/s speed, preconditioning appears approximately after 9^{th} cycle. As the displacement-rate reduces, the amount of energy loss in each loop reduces also.

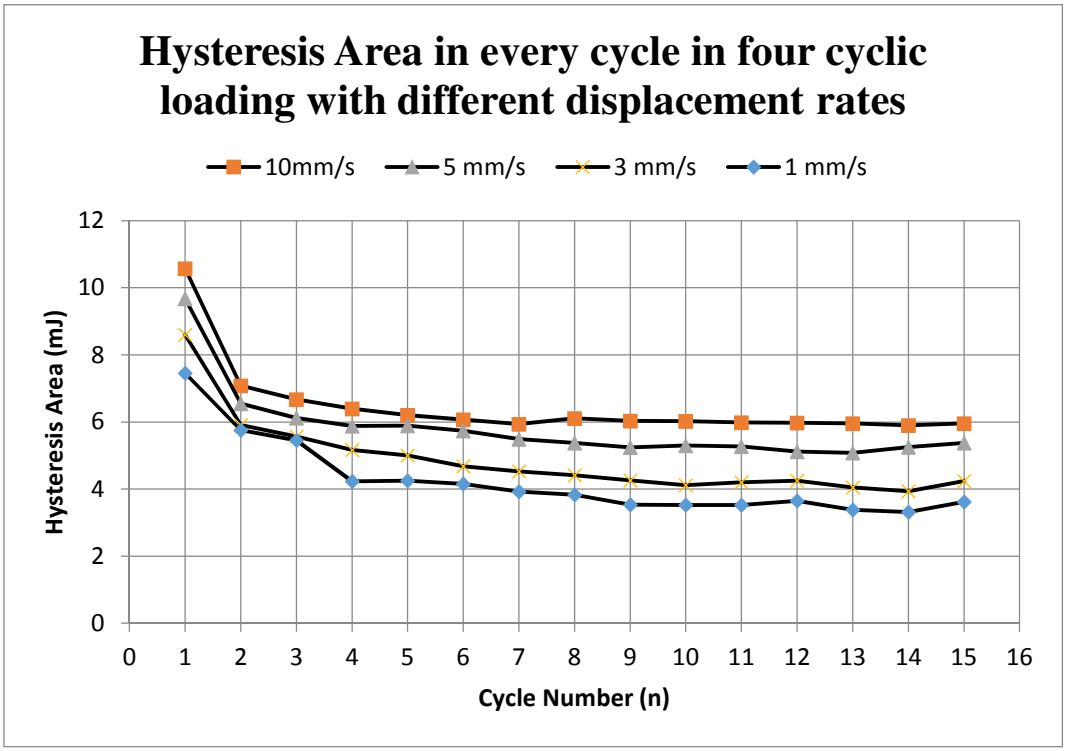

Figure 4.2-15.comparing the fall trend of hysteresis area in displacement-controlled cyclic loading tests with different displacement- rate of 1mm/s ,3 mm/s, 5 mm/s, and 10 mm/s.

For analyzing rate dependency of the hysteresis area, the average hysteresis of 15 cycles of each experiments were obtained and compared in Figure (4.2.16). It is clear from this set of experiments and our other conducted repeated in-vivo experiments by indenter device, that there is a proportional dependency between hysteresis and displacement rate of the loading and unloading process. It can be observed that the faster a cyclic loading-unloading conducted, the larger hysteresis area resulted, and that means higher energy loss. This fact is already mentioned by Petekkaya (2008) and is in contrast to Fung's observations (Fung 1993, page 281) and the other studies referred to Fung (1993) such as Zhang et al., (2007) and Rubin and Bodner, (2002) which claim independency and insensitivity of hysteresis magnitude, on displacement rate of experiment in the same stress level over a wide range of rates.. This result is very important outcome and should be considered in modeling of soft tissue.

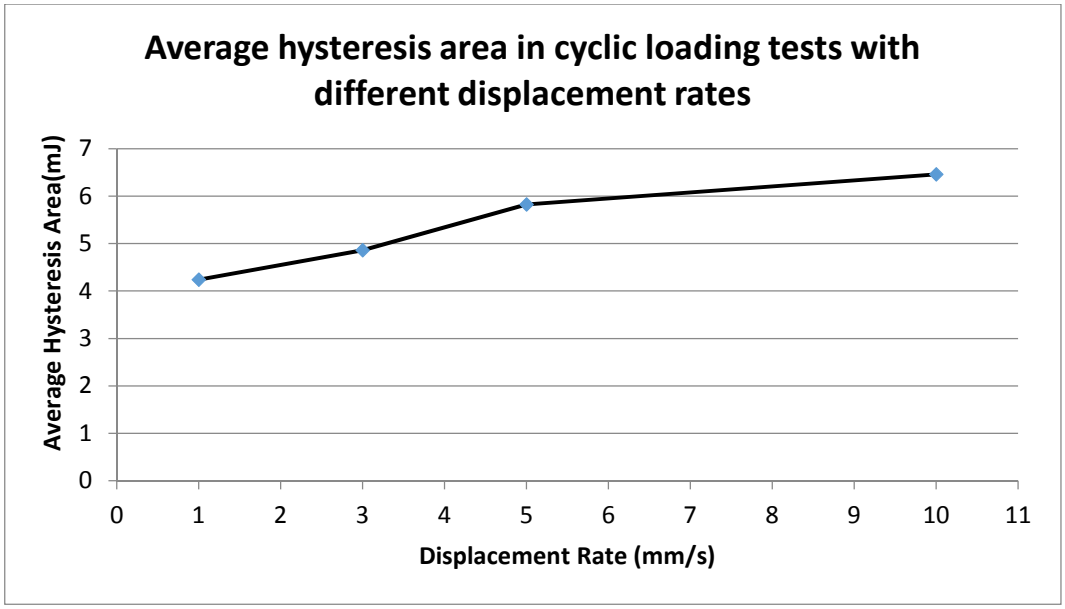

Figure 4.2-16.Average hysteresis area of four cyclic loading tests with different displacement rates (1, 3,5,10 mm/s)

For better analyzing of the obtained result, the hysteresis areas of 6 first cycles of each experiment were extracted prior to obtaining the average hysteresis amount in each rate. In this way only the average hysteresis magnitudes of cycles which approximately reached to steady maximum force amounts, were calculated. The result was shown in Figure (4.2 17). It can be seen that the trend of values again is so similar to the previous result (without extracting cycles).

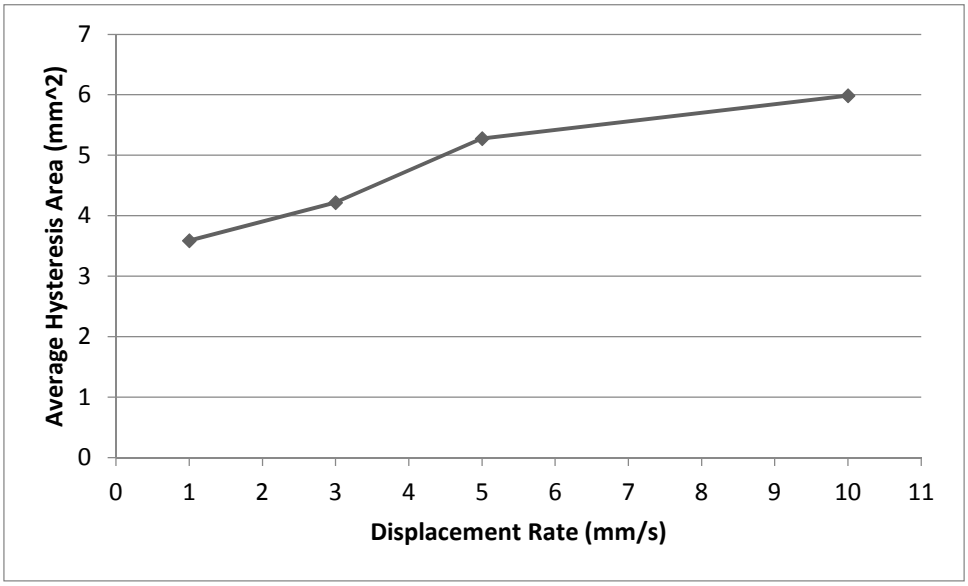

Figure 4.2-17. Average hysteresis areas after extracting the preconditioning cycles

Exceptions:

Sometimes exceptions were seen in results which were because of difficulties in conducting in-vivo tests on human and existence of mistakes of operator or movements of subject. For instance in experiments conducted for preconditioning studying, we were to wait after each test for tissue to recover itself. Because of the limited time of subjects and large number of experiments the waiting duration was not enough in some case, which was clear from results (4.2-18). As shown in the force-time graph of this example experiment, no preconditioning in terms of maximum force exists, and maximum force values of loops are approximately the same, due to not enough waiting for tissue recovery before experiment.

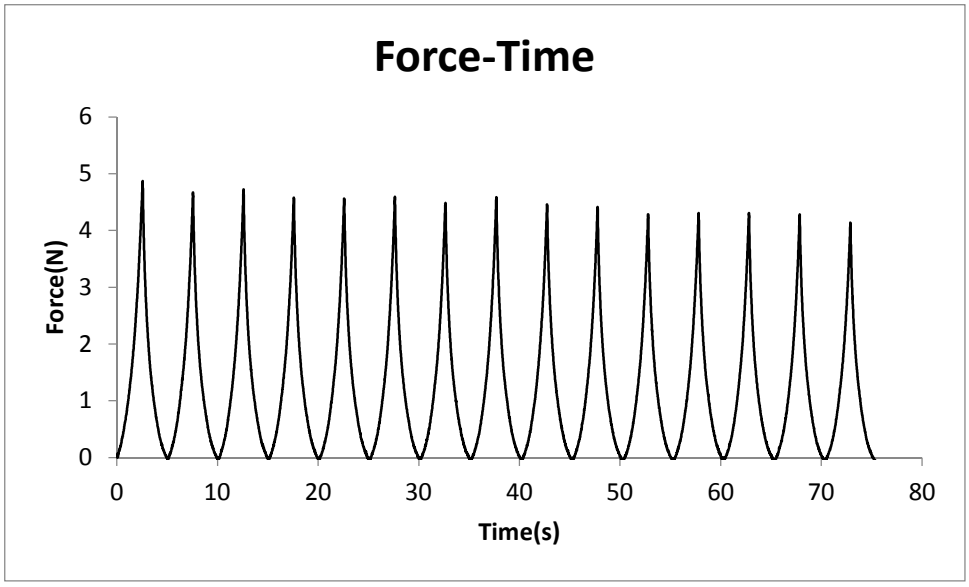

Figure 4.2-18. No preconditioning was observed in terms of maximum force.

Calculated hysteresis area magnitude in this test was as following (Figure 4.2 19):

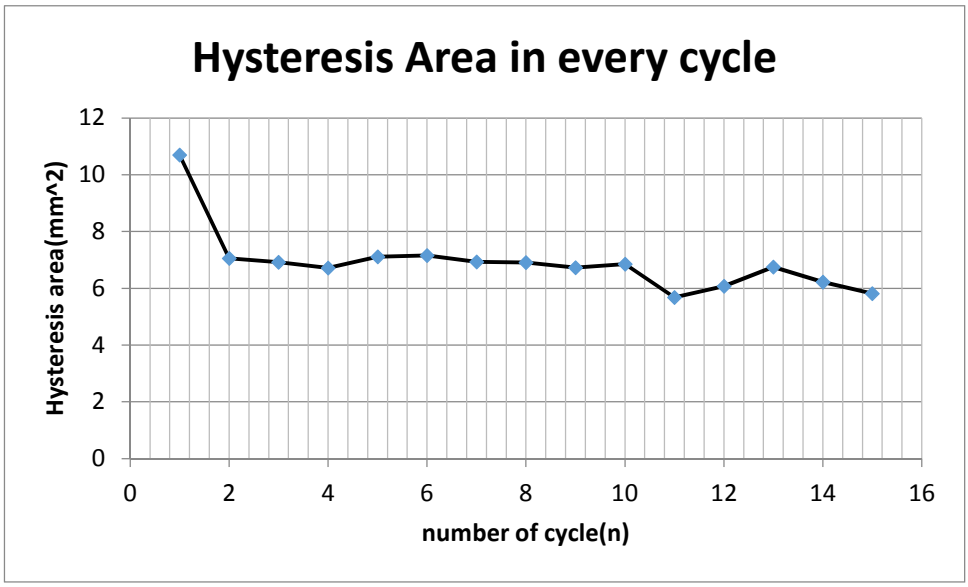

Figure 4.2-19. Calculated hysteresis area magnitudes of experiment illustrated in Figure (4.2-18).

As shown in graph the magnitudes of hysteresis areas does not have any regular trend and there are increasing tendency in cycle 4 and 11, but if the first value and the last value is considered, decreasing of the hysteresis magnitude was observed from above 10 to around 6 mJ, however this decrease mostly is only in first cycle and during the other repeating cycles, hysteresis had a value around 7 mJ with small deviations. another important observation was about 11^{th} cycle, which although in maximum force value of this cycle there was not any large deviation but in terms of hysteresis area there was a minimum deviation. As a result there is no firm relation between maximum force values trend and the hysteresis area magnitudes trend.

In addition to this, some experiments were to repeat again and again to check the validation of results or eliminating the encountered problems. In these cases because of subject's tiredness and unconscious muscle tonus or movements, obtained result were different. Figure 4.2-18 a, b, and c were provided as an example experiment for muscle movement for clear explanation. The experiment inputs were 20 mm, 8 mm/s, 15 cycles. In force-time graph (a) the irregular increase in maximum force values after 7^{th} cycle was appeared as irregular hysteresis repeating in force-displacement graph. The repeated curves in precise and successful tests were in down part of both loading and unloading group curves. But here the repeated curves were located in the middle of each loading and unloading group curves. That means the hysteresis magnitude decreased until the 7^{th} cycle and then started to increase progressively due to muscle motion. This result shows that hysteresis areas are not completely independent of maximum force values irregularities. They are also influenced but still hysteresis magnitudes are more dependable in compare to maximum response values for using in computer simulation or modeling.

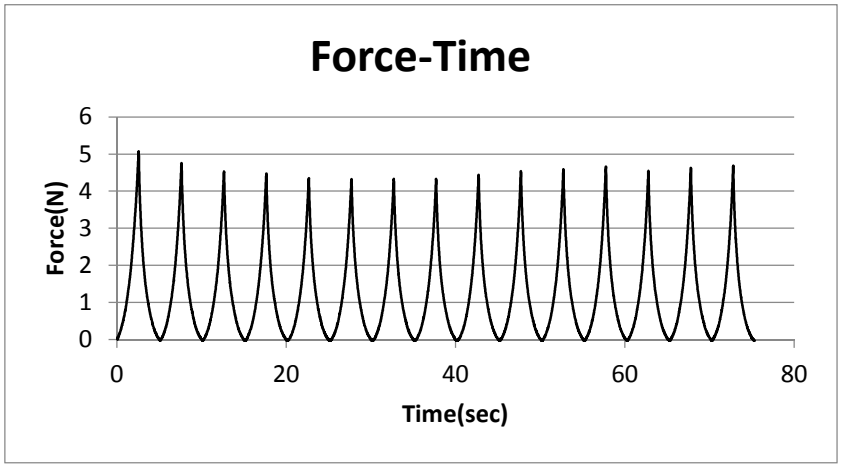
Force-Time
Force(N)
0
1
2
3
4
5
6
0
20
40
60
80
Time(sec)

a)

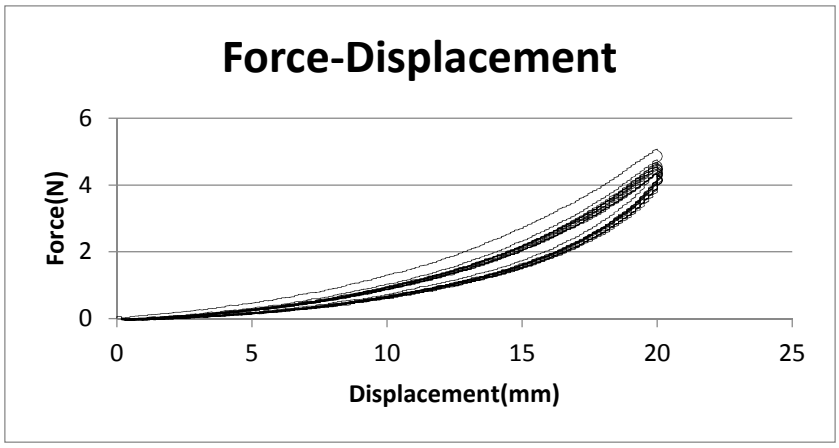
Force-Displacement
Force(N)
0
2
4
6
0
5
10
15
20
25
Displacement(mm)

b)

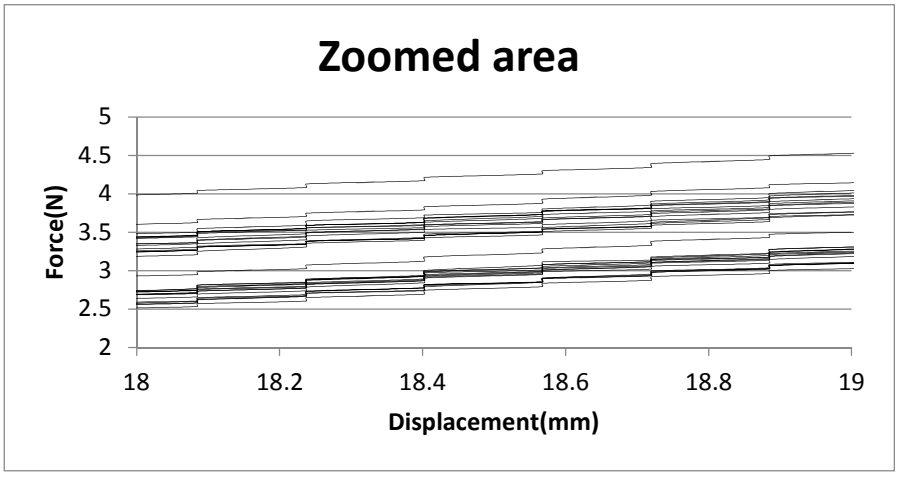

c)

Figure 4.2-20. An example experiment (20 mm,8 mm/s,15loop) with observed muscle tonus due to (a) weird increase in maximum force values in force-time graph. (b). observed irregular hysteresis in force-displacement graph. (c). repeating curves can be seen in middle loading curves and middle unloading curves in zoomed area of force-displacement graph.

4.3 Force Rate Controlled Cyclic Loading Tests

In this section, the results of in-vivo force rate controlled cyclic loading experiments, which are novel, are provided and compared with the traditional displacement controlled cyclic loading tests.

Mullin's effect (preconditioning effect) on soft tissue during force controlled cyclic loading test was examined. The illustrated preconditioning effect observed in displacement-time and force-displacement graph is different from that in displacement rate controlled cyclic loading tests.

In displacement-time graph, as expected there was an increase in the displacement with progressing cycles, which means a decrease in stiffness of tissue. Here we were trying to keep the force rate constant. In every cycle, indenter sets out the movements in order to catch the target force pertinent to that current time thus, the peak forces were the same. The target force rate is 1.8 N/s. The indenter device sets out its movement to catch this rate, thus the traveled displacements in tissue changes progressively depending on the softness. At first cycle the displacement was around

14 mm, then following a gradual increase, it remained steady after 8th cycle in above 16 mm displacement. That means the tissue becomes more compliant by repeating cycles until a specific number of cycles is reached. This is due to preconditioning phenomenon in viscoelastic materials or specifically soft tissues. Due to breathing, difficulties of in vivo tests, and good sensitivity of load-cell, we normally cannot see the exact equilibrium displacement (Fig.4.3-1).

In force-displacement graph of this experiment preconditioning was illustrated distinctly. There was a shift to right in curves by repeating cycles and during the last cycles, almost repeated curves occurred. In addition to increase in the maximum displacements of the tissue (stretch), a decrease was observed in magnitude of hysteresis as the number of cycles increased, which approaches to a repeatable pattern (Fig.4.3-2).

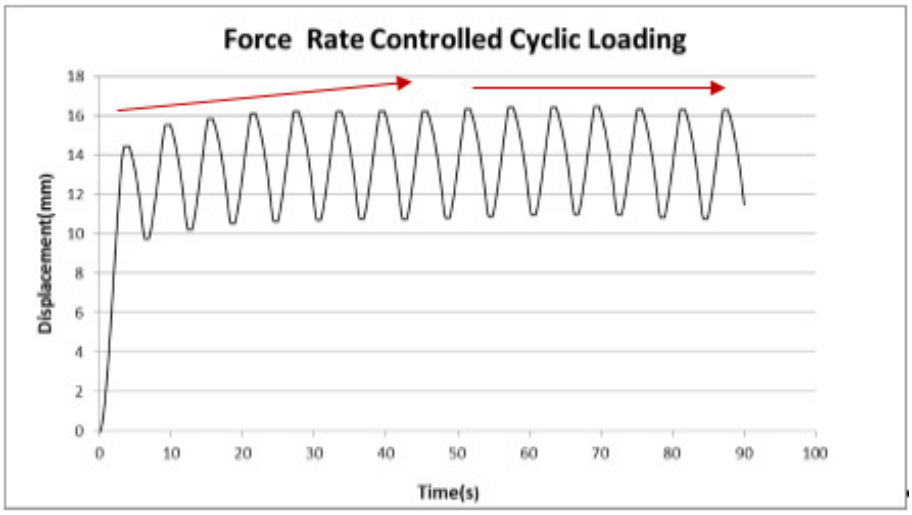

Figure 4.3-1. Force rate controlled cyclic loading test with 1.8N/s, 6s for every cycle and15 loop

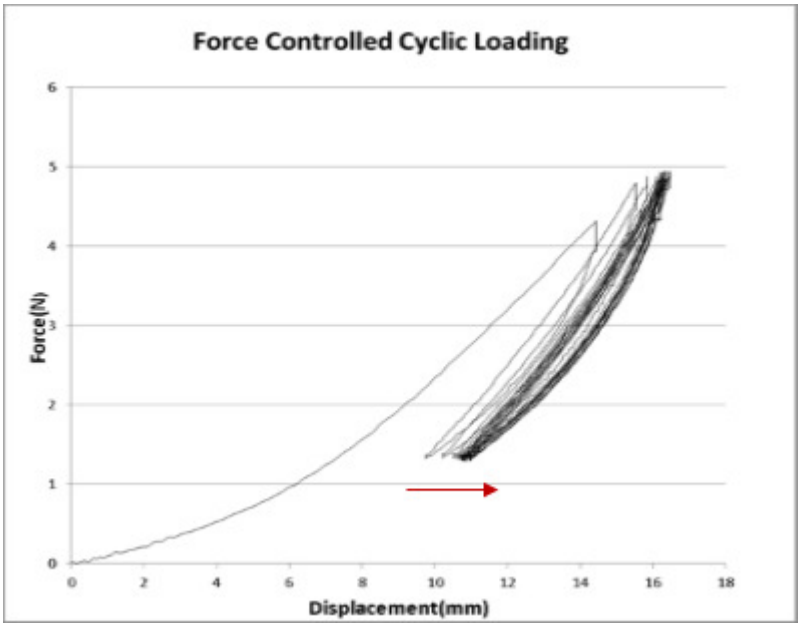

Figure 4.3-2. Obvious shift to right in maximum displacements by repeating cycles

For summary and for clearer explanation force-displacement relation under displacement rate control and load rate control for fifteen cycles is illustrated in figure (4.3-3). The period of both experiment was 90 s but on different subjects. The resulting force values were tried to be kept similar, in both experiment methods for a better comparison. As illustrated, Mullin's effect shows up as a downward shift (i.e. decrease in force) in displacement rate controlled experiments whereas it shows up as a right shift (i.e. decrease in stiffness) in force rate controlled experiments. In both experiment methods, repeating cycles resulted in less stiff and more compliant material.

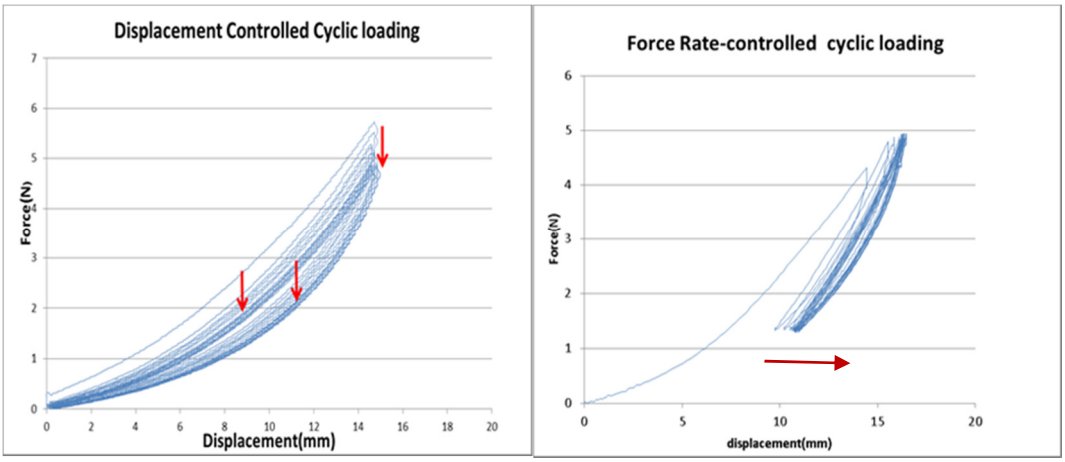

Figure 4.3-3. Force versus Displacement curves for indentation tests under displacement and load control for fifteen cycles .The period of both experiment was 90 s but in different subjects. Note the obvious shift to the right of the curves in the load controlled test.

4.3.1 Rate Dependence of the Response of Soft tissue During Load-Controlled Cyclic Loading

Normally, during in vitro investigation in which the tissue reaction to different load or displacement rates is looked for, a continuous loading history is refined through cyclic preconditioning (Fung, 1993). Then again, preconditioning is often not utilized as a part of in-vivo investigation, keeping in mind the end goal to represent the biomechanical properties of the tissue as would be experienced amid damage or clinical intercession; for instance, in vivo tests on skin are generally performed without preconditioning (Meijer et al., 1999; Escoffier et al., 1989). In vitro tests have likewise been performed without cyclic preconditioning, taking into consideration full recovery between tests (Provenzano et al., 2001) or quasi-static loading (Belkoff and Haut, 1991; Belkoff et al., 1995), or when the noncyclic, viscoelastic reaction is wanted (Lanir et al., 1993). In fact that preconditioning is an acknowledged part of mechanical testing of soft tissues (and also other soft materials including elastomers). Thus in this study the rate dependency of

mechanical responses of soft tissue was investigated without eliminating the preconditioning process in order to represent the real mechanical response of tissue. In this section, four experiments with different rates were conducted for investigating rate dependency of soft tissue during force rate cyclic loading.

The main motivation for doing these experiments was the interesting result in Giles et al., (2007). In the mentioned study, results from in-vitro tests on myocardium and skin showed that the tissues demonstrated an increment in nonlinear stiffness with a drop in loading rate. In other words, the quicker the test was performed, the more compliant the preconditioned material response was. This reaction is clearly not predictable from previous studies on soft tissues, in which displacement controlled tests show an increment in stiffness with an increment in strain. Figure (4.3-4) adopted from the mentioned article summarizes the tests and results in the article. Load- stretch relation of in vitro load controlled tests in one direction of equibiaxial tension tests on porcine dermis is illustrated in this figure. The tissue load was 250 g in different periods of 5, 10, 50 s. Each loading was in 20 cycles. Hence it was decided to check this observed anomalous behavior for first time with in-vivo experiments and force-rate controlled tests.

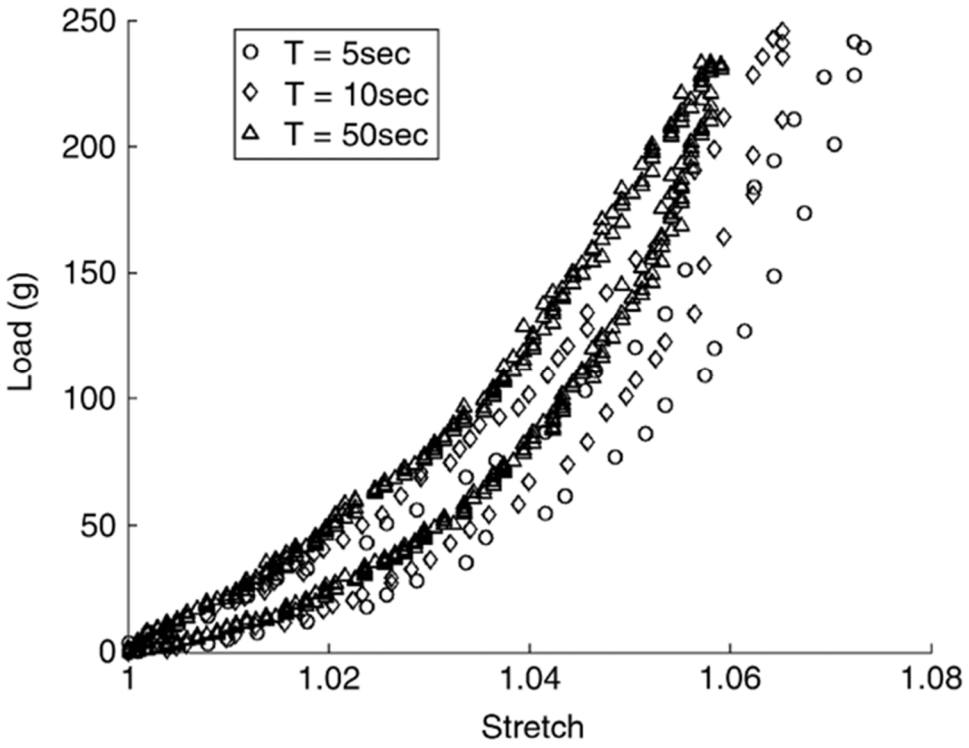

Figure 4.3-4. Load- stretch relation of in vitro load controlled tests in one direction of equibiaxial tension tests on porcine dermis, the tissue load was 250 g in different periods of 5,10,50 s. each loading was in 20 cycles. ***Adopted from Giles et al., (2007)***

In experiments carried out in this part of our study, it was tried to keep the inputs of the tests similar with the one proposed in the mentioned article, thus the input parameters of the tests were: 2N/s -8cycle-cycle time: 10 s, 1N/s -8cycle-cycle time: 20 s, 4N/s -8cycle-cycle time: 5 s, 0.5N/s -8cycle-cycle time: 40 s. The tests were conducted with elliptic tip, in both transverse and longitudinal direction on human forearm. The results for both orientation were the same thus results of experiments on transverse direction were provided here.

The maximum force for all tests was 10 N, the duration, thus the rate of experiments was different. Prior to each test with different inputs, 10 cycles of loading were carried out for preconditioning of tissue. It should be mentioned that in in-vivo force rate controlled cyclic loading, achieving a complete preconditioned tissue was not possible. Because of soft tissue viscoelasticity behavior, tissue immediately adapts

to the applied force by removing the fluid of ECM to the neighbor regions, then the force applied to the indenter tip drops and indenter again goes forward to catch the target force. There is always a space for indenter to go forward but for preventing any damage or pain to subject, preconditioning tests were conducted in a limit.

Force-time and force-displacement relations of the tests with 40s duration were demonstrated in Figures (4.3-5), (4.3.6), and (4.3-7).

First observation was that in the test with long duration (40 s for each cycle), that was applied in slowest force-rate, the displacement through the tissue seems to never stop (Figure4.3-7), but in the test with shorter duration (faster) (Figure 4.3-9) the tissue after 4^{th} cycle became preconditioned, and stayed at a steady amount. One reason for this observation can be that, in long duration indentations, indenter has time to restructure the tissue and move the fluids to neighboring parts and penetrate more.

This outcome was clear also in force-displacement graph of tests which hysteresis of the slower force rate (Figure 4.3-6) is more scattered than that of the faster force rate (Figure 4.3-8). This may be the consequence of the larger displacements and more restructuring of the tissue in slower force-rates in time. This means that the tissue acts like a solid in faster loading rates.

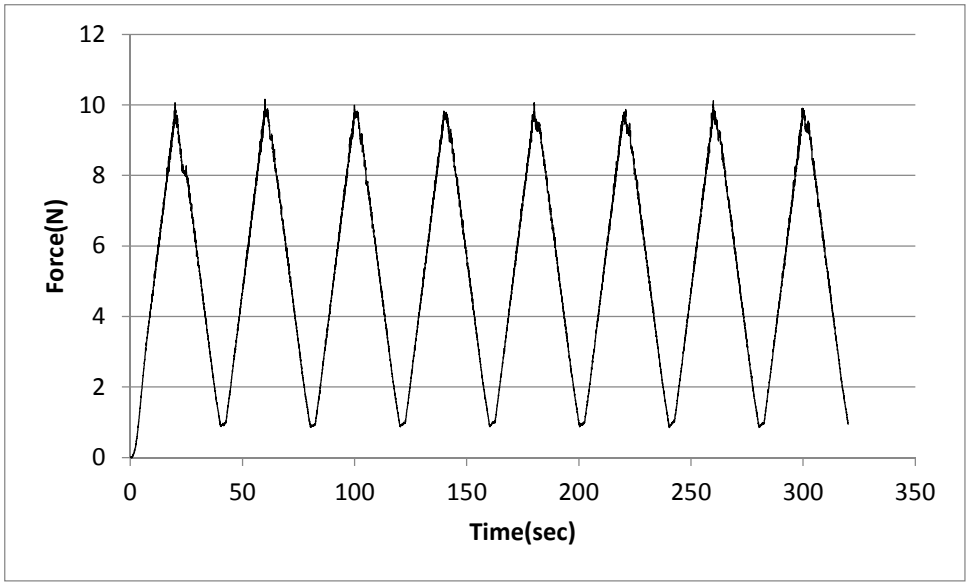

Figure 4.3-5 . Force- time relation of the force controlled cyclic loading with 0.5N/s -8cycle-cycle time: 40 s

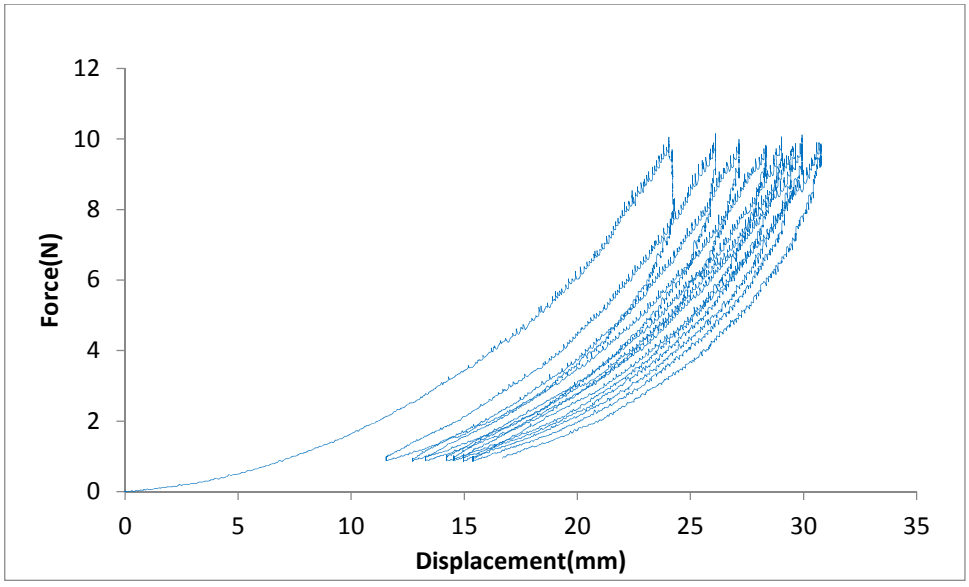

Figure 4.3-6. Force- displacement relation of the force controlled cyclic loading with 0.5N/s -8cycle-cycle time: 40 s

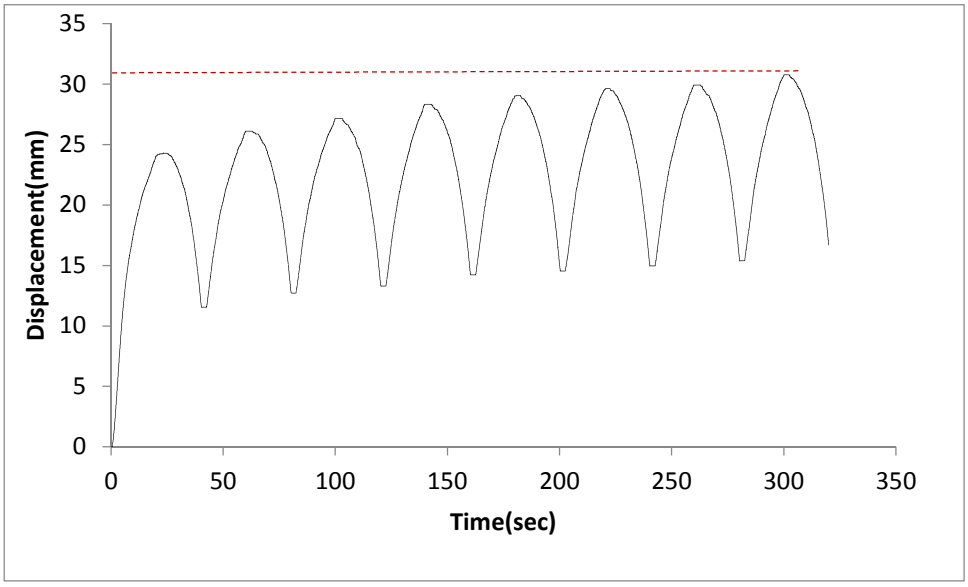

Figure 4.3-7. Displacement- time relation of the force controlled cyclic loading with 0.5N/s -8cycle-cycle time: 40 s

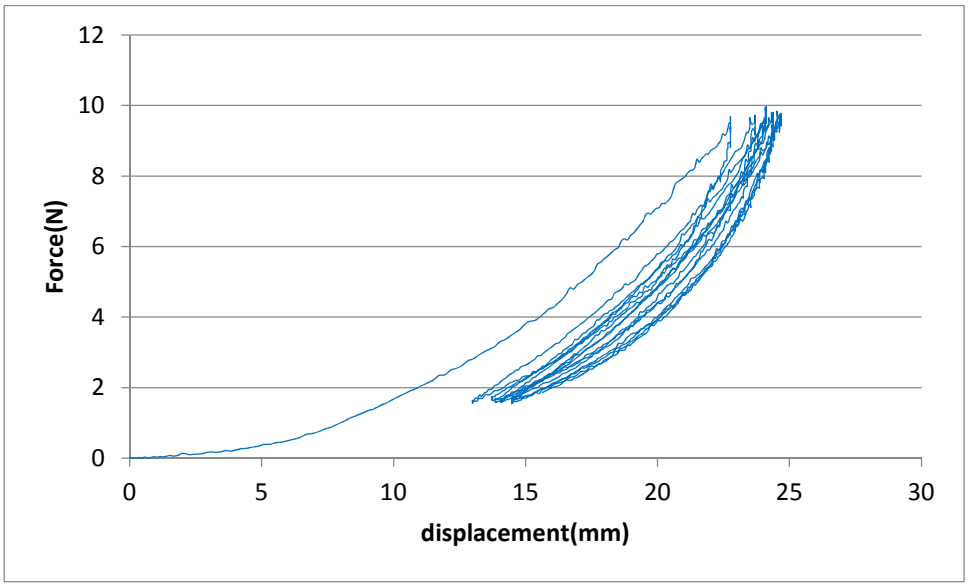

Figure 4.3-8. Force-displacement relation of the force controlled cyclic loading with 2N/s -8cycle-cycle time: 10 s

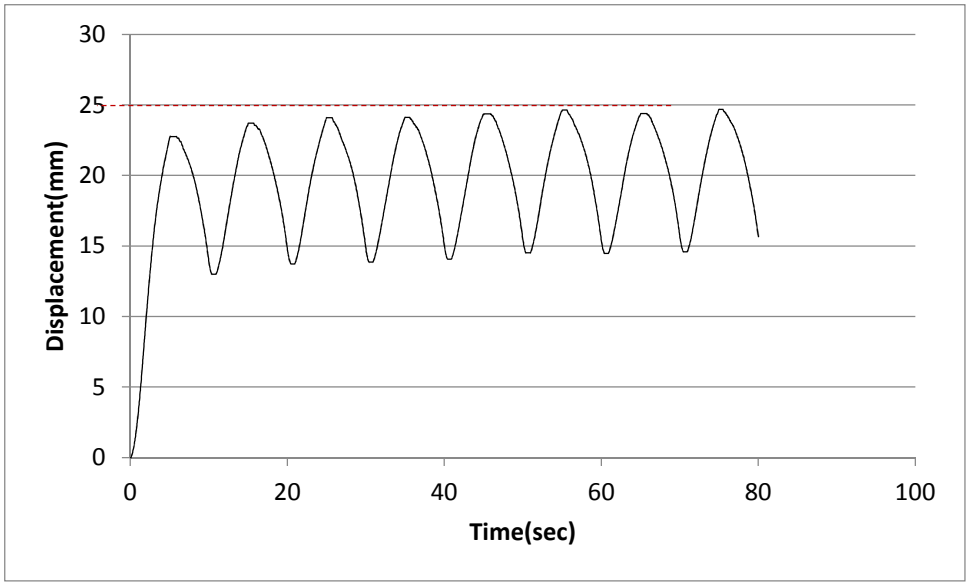

Figure 4.3-9. Displacement-time relation of the force controlled cyclic loading with 2N/s -8cycle-cycle time: 10 s

Finally, the comparison of the four different load rate experiments illustrated in Figure (4.3-10), demonstrated that tissue displayed an increase in nonlinear stiffness with an increment in force rate: the speedier a test is performed, the stiffer the material response is. As can be seen in Figure (4.3-10) when the displacement of last cycle in 5 s is about 23 mm, the displacement of last cycle of 40 s is around 30 mm. This reaction appears to conflict with that of in-vitro tests in aforementioned article and is in agreement with what is normally expected of soft tissues based on stretch or displacement controlled tests, in which an increased rate of loading, results in a stiffer material reaction.

Moreover, Chai et al., in their study for non-preconditioned tissue, mentioned that: "High testing rates and cyclic tests with high frequencies does not allow the tissue to fully respond, possibly causing less deformation and consequently higher stiffness results. This might explain the results found by Lee et al. (1991) where the dynamic stiffness was found to be higher than the static stiffness. In general, the stiffness values between static and dynamic mechanical studies were very different" (Chai,et al., 2014).

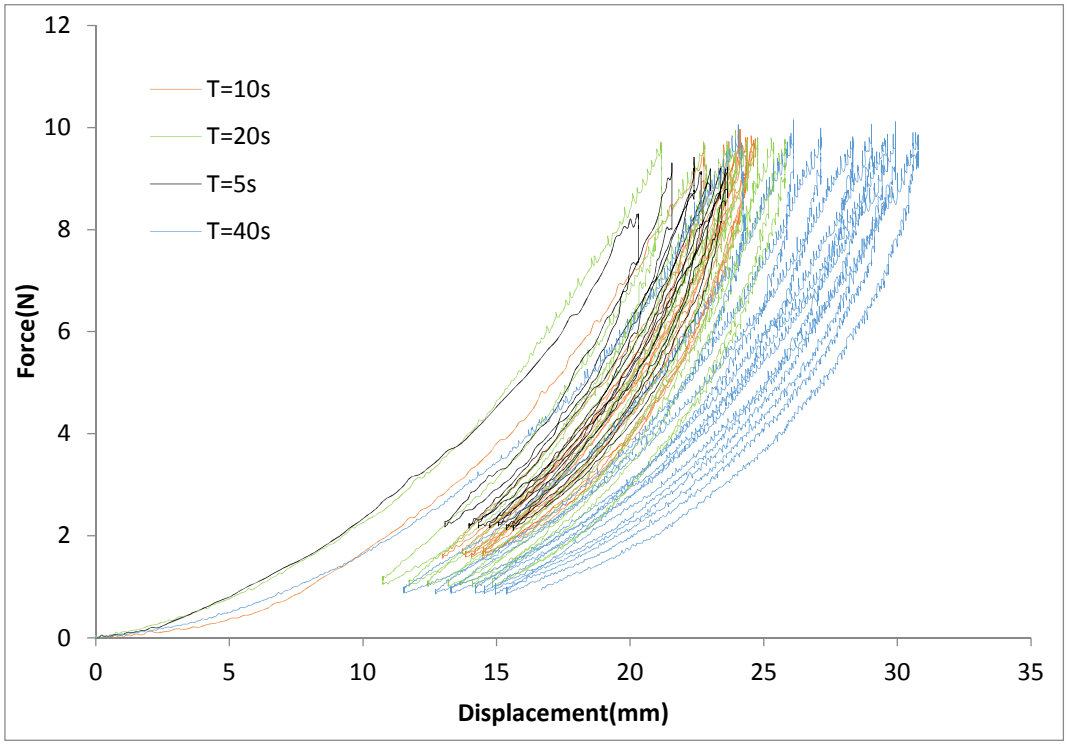

Figure 4.3-10.Comparison of force-displacement relations of four force controlled cyclic loading experiments on human forearm with different rates; 5, 10, 20, and 40 s. the tissue load was 10 N, each loading was in 8 cycles. 5 s corresponds to 4N/s, 10s corresponds to 2N/s, 20 s corresponds to 1 N/s and 40 s corresponds to 0.5 N/s

4.4 Relaxation tests

Stress Relaxation: In the event that a consistent displacement is applied to a soft tissue, the energy to keep the material in this position reduces over the time. The stiffness keeps on decreasing until the material achieves a balance in which the energy gets to be consistent.

It appears that speedier strain rates cause more elastic reactions and the material acts more like a solid (stiffer), though slower strain rates cause more liquid like conduct.

4.4.1 Relaxation tests with different displacement rate

In this section the behavior and response of soft biological tissues during the in-vivo indentation is provided.

In order to examine rate dependency 4 relaxation experiment with 4 different rates were conducted on human forearm; 1, 3, 5, and 10 mm/s. the other input parameters were the same in all experiments; relaxation time were 120 s, displacement were 20 mm, motor loop 20 ms. The written samples per second is 100 samples. These tests were carried out without eliminating preconditioning effect, and before each different test tissue is allowed to recover for 15 minutes. As mentioned before in-vivo relaxation tests are strongly sensitive to any muscle tonus or motion and even breathing harmony, thus in long relaxation durations (such as 120 s) undeniable varieties in the trend of relaxing curve were seen.

The comparison of results (Figure 4.4.1) showed that the stiffness (the response force) increased with faster displacement rates. As can be seen the sharper upward slopes were, the higher force responses were seen. This result is in agreement with the cyclic loading tests. In addition to this, in faster displacement rates more amount of relaxation in comparison to the slower displacement rates, were observed. The reason is that in higher displacement rates because of larger force response, the amount of stored stress in tissue is more. For example in the experiment with 10 mm/s speed (the fastest displacement rate), the relaxation period starts from 6.67 N that is above the other curves and ends in 4.17 N which is beneath other curves.

It can be seen that there was a substantial decrease in the force required to maintain the strain over time. This is typical in viscoelastic materials and suggests that the tissue is capable of adapting its internal structure to minimize the effect of the indentation.

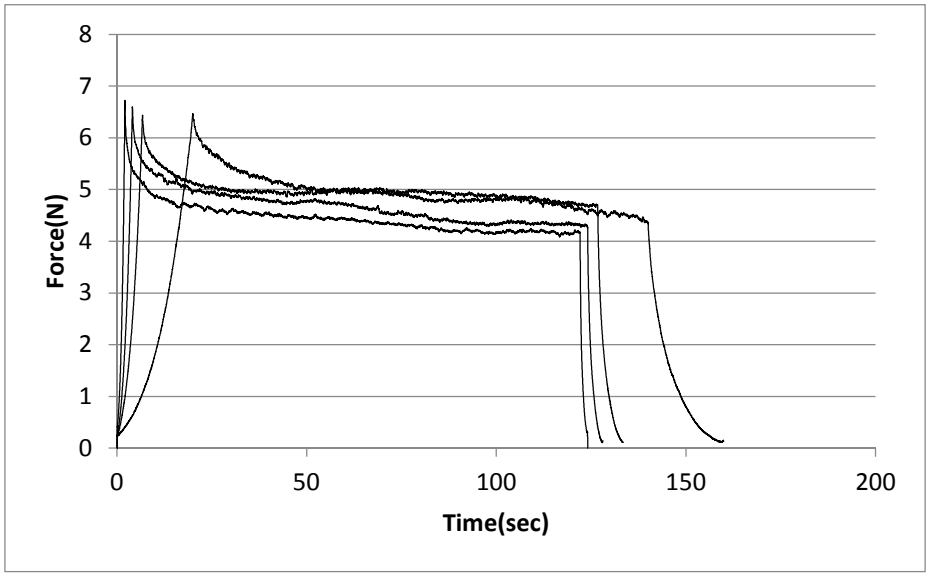

Figure 4.4-1 Comparison of the relaxation tests with different displacement rates.

4.4.2 Breathing and Heartbeat Effect in Relaxation Tests:

In relaxation tests, some bigger periodic fluctuations were observed despite very small pulses related to heartbeats. After examinations and some experiments on dummy objects instead of individuals, as it was anticipated from previous studies (Petekkaya.2008) the source of these fluctuation was breathing. The number of periodic fluctuations and breathing times were in harmony (Figure 4.4-2)

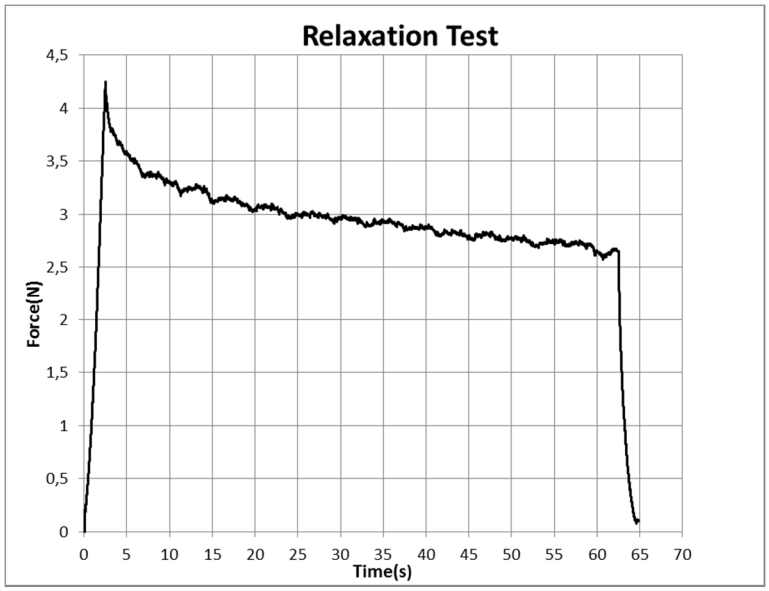

Figure 4.4-2 Relaxation test conducted on forearm with 5 mm/s speed, 6 mm displacement and 60 seconds relaxation duration

4.4.3 Relaxation Tests with Different Displacements

Another set of experiments was carried out in order to investigate the relaxation tests with the same rate, 5 mm/s and the same relaxation time, 120 sec, and different displacements, 15, 20 and 25 mm. Also between these experiments, the wait time was 15 minutes. As mentioned before it is known that in low displacement levels faster relaxation happened. As illustrated in Figures 4.4-3, 4.4-4, 4.4-5, the fastest relaxed tissue was in the experiment with lowest level of displacement (15 mm). It can be seen that after about 45 seconds, the tissue was approximately relaxed and the curve stayed at a steady amount until the end of the relaxation time. Bonifasi-lista et al., (2005) during in-vitro experiments on human ligaments resulted that relaxation happened quicker at the most minimal strain levels. We have earlier relaxed tissue in low displacements because the stored stress is lower. In fact, the process of relaxation is faster in high displacement levels. After comparing the relaxation curves of these three experiments it can be seen that amount of force drop in 45th second is increased with the increase in displacement level. This means that the larger relaxation happens in a short time in higher displacement levels that

means faster relaxation happens in large displacements, but since the amount of stored stress is more, this process takes more time. Even 120 seconds was not enough for a complete relaxation of the tissue with 25 mm displacement.

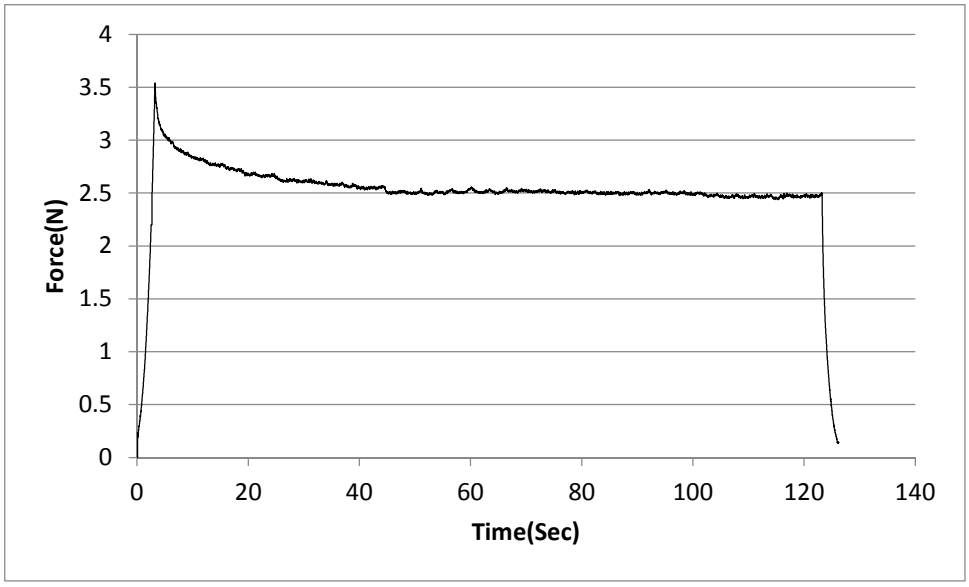

Figure 4.4-3 Relaxation test on human forearm with 120 s relaxation time,5 mm/s speed and 15 mm displacement on subject S

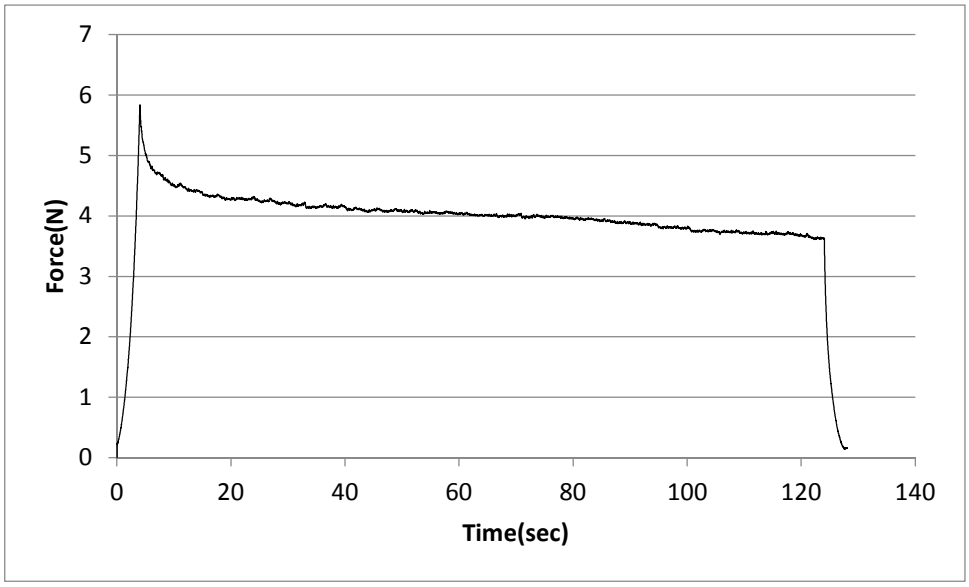

Figure 4.4-4. Relaxation test on human forearm with 120 s relaxation time, 5 mm/s speed and 20 mm displacement on subject S

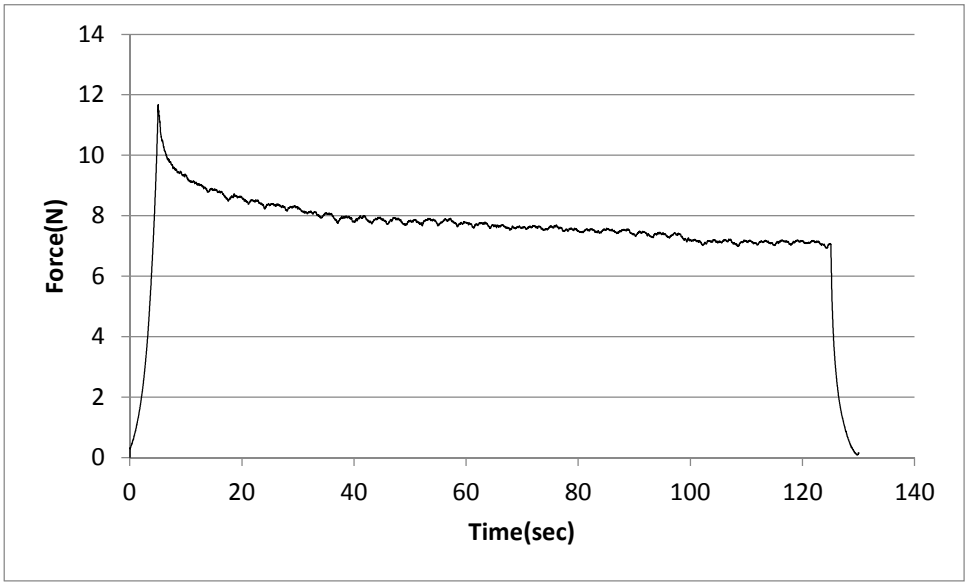

Figure 4.4-5. Relaxation test on human forearm with 120 s relaxation time, 5 mm/s speed and 25 mm displacement on subject S

Lokshin & Lanir, (2009) in their study mentioned that the level of strain and also the duration that strain is applying to tissue effects the following response of it, and in large strain levels the stress has larger decay. In this study in relaxation tests this fact was observable and larger strain levels resulted faster relaxation rate. Strain-dependency of soft tissues also was investigated in (Duenwald-Kuehl,et al, 2012) by experiments on tendons.

In addition in a study by Liu, (2006) in relaxation tests, tissue samples were loaded to different strains to observe its effects on stress relaxing over time. He resulted that "The reported strain-independent behavior in stress relaxation only occurred at certain strain levels". Strain-dependency or independency of stress relaxation curve, are investigated in literature specially for choosing a proper modeling equation, and for investigating the hypothesis of variables separation, namely the time and the strain separation in the relaxation function, which is widely used in soft tissue biomechanics.(Passaglia & Koppehrle, 1958)(Pioletti & Rakotomanana, 2000).

4.5 Creep Tests

In this section, creep experiments conducted on human arm, are provided. All presented experiments were conducted on the same position of the subject's arm, on the same day. In creep code as explained in section 3.2.4, firstly the test's target force was determined, then with the initiation of test, indenter device moves forward in a given speed (mm/s) in order to apply the target force to the tissue. After reaching this force, device tries to maintain this force throughout the required creep duration by a force controlled close loop. Because of creep phenomenon in biologic material, in order to maintain the target force, indenter tip has small forward and backward movement. By applying a constant force to a viscoelastic material, the displacement increases over time. Here the displacement, force, and time data were simultaneously recorded. Creep duration was chosen as 230 seconds. Creep in soft biological tissues appears to never stop because of internal restructuring (in living tissues) and other processes (Farshad et al., 1999), but this duration was taken as maximum because of limitations in carrying out the experiments, in-vivo (because of the subjects' toleration and avoiding discomfort and pain).

During creep experiments a problem was observed; an unwanted overshooting was happening in force, at the moment that target force reaches a lower threshold and exits displacement rate controlled open loop and enters into force rate controlled close loop.Then for solving this problem creep code was written in this way, that the indenter device enter into the closed loop before reaching the threshold domain. In this case, for example in an experiment illustrated in figure (4.5-1) that target force was10 N, indenter was entered into force rate controlled close loop in around 8 N. Before 8N, the speed of device was our input speed (3mm/s). In this way, the movement of device was more precise, and more dependable results were obtained. As illustrated in Figure (4.5-1) when the force was maintained at 10 N, the displacement during creep was increased from 24 mm in 10^{th} s to 26.6 mm in 230 s.

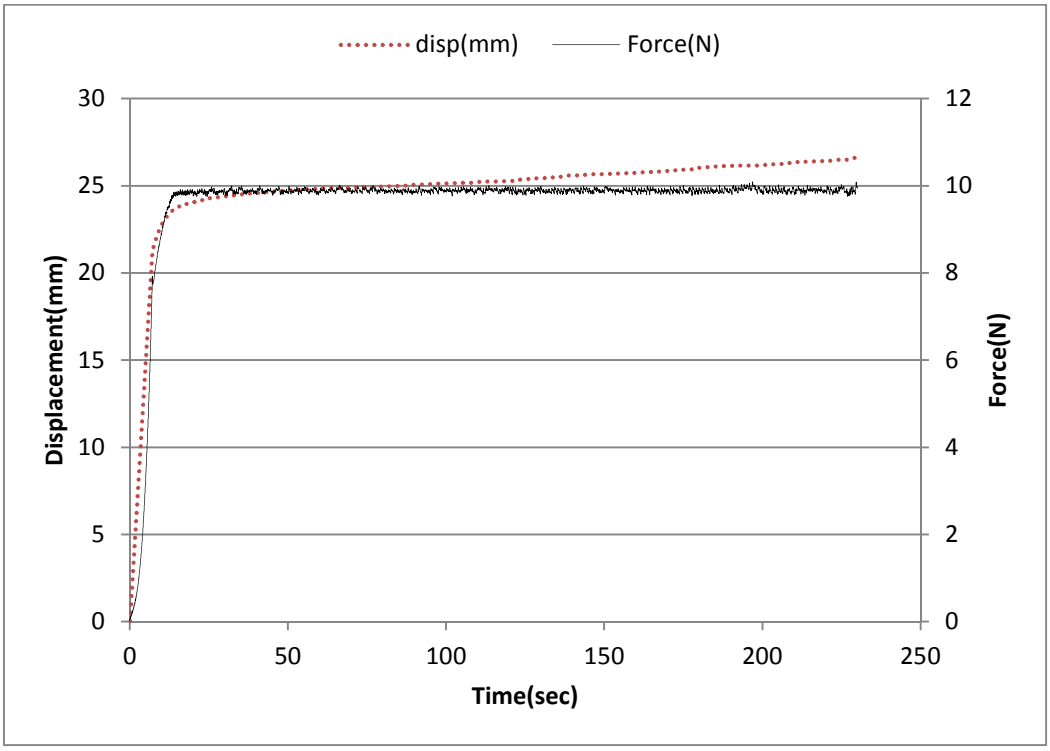

Figure 4.5-1.creep experiment with 10 N target force, 3mm/s initial speed of device.

Four creep experiments with different target force were conducted and the results were provided in Figure (4.5-2). The observations indicated that the larger target force was, the more displacement was applied to tissue during creep behavior (Figure 4.5-3). On the other hand, the moment of reaching target force is different in experiments. In larger target force, the larger portion of the displacement was travelled in 3mm/s speed but in smaller target force such as 0.9 N, whole travelled displacement was in force controlled close loop with a feedback checking. Thus, in order to obtain better results, the slope of displacement curve in creep duration for each experiment was calculated and shown in Table 4.5-1. The creep curve was assumed as a linear line from the start of creep duration up to the end of creep duration:

Table 4.5-1. The linear slope of displacement curve in creep duration.

Target forces	Creep start and ending Time(sec)	Creep start and ending Displacement(mm)	Linear slope
1 N	36.876_230	8.57_9.57	0.0052
3 N	21.202_230	13.81_15.71	0.0091
5 N	19.336_230	18.82_21.142	0.011
10 N	10.776_230	23.025_26.6	0.016

As shown in the Table 4.5-1, the slope of creep curve related to maximum force is more than others.

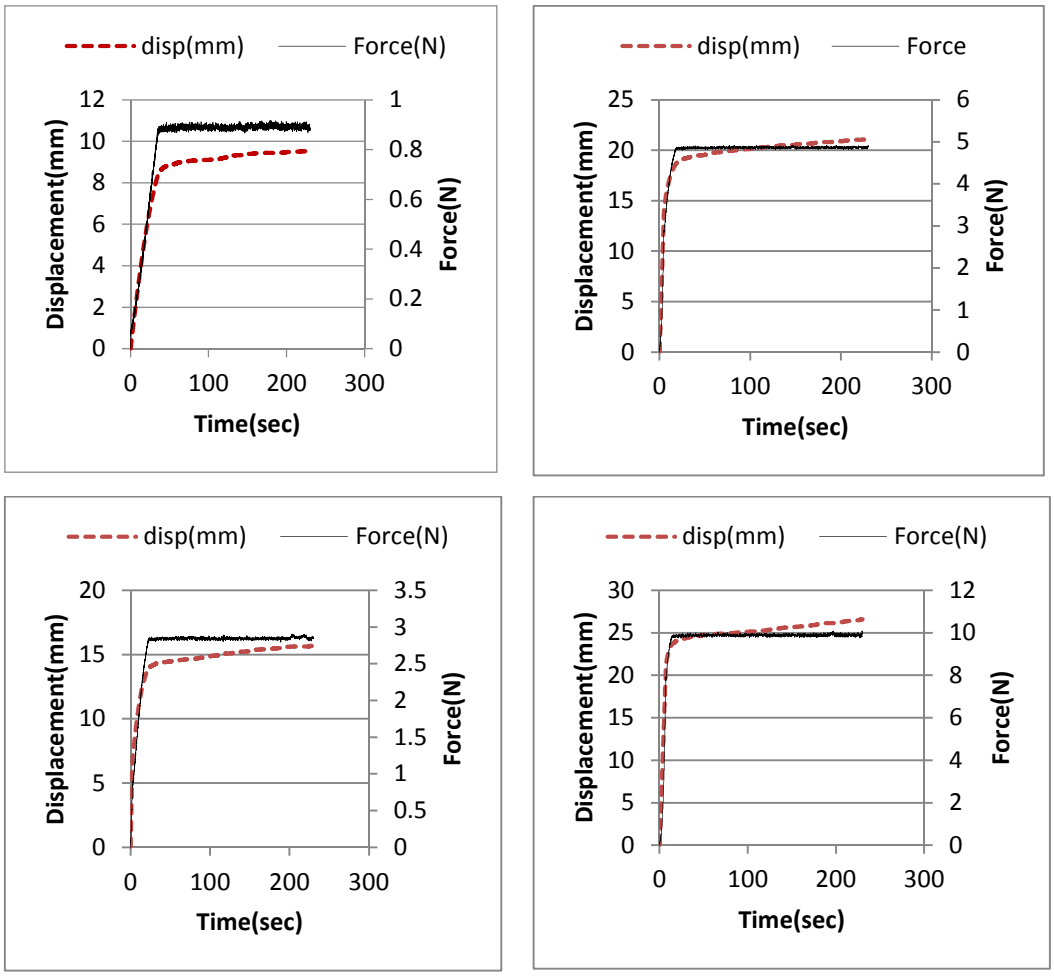

Figure 4.5-2.Creep tests with different target forces

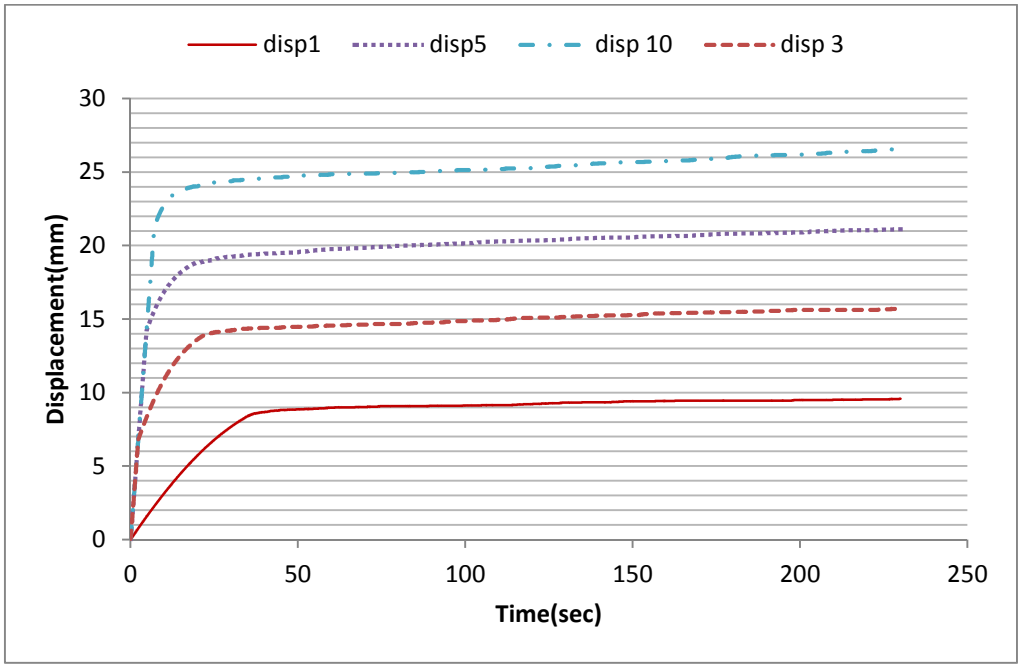

Figure 4.5-3.Displacement-time relation of creep experiments with four different target forces; 1, 3, 5 and 10 N

4.6 Determination of material directions and in-plane anisotropy

4.6.1 Investigation of biceps muscle anisotropy behavior by cyclic loading tests:

In order to investigate the anisotropy behavior of soft tissues, some successive cyclic loading experiments were observed with different angle orientation of tips on tissue. Firstly, the long axis of the ellipsoidal indenter tips was placed parallel to the longer axis of the biceps muscle and cyclic loading tests were conducted in every 30 degree up to 180 and a 210 degree for control. In these tests, for eliminating the preconditioning effect at first, 20 loops of cyclic loading were conducted at a pre-determined point of muscle, then the real tests were conducted consequently without waiting for the soft tissue to recover. Responses of biceps muscle in different indenter tip alignments, to the same displacement controlled cyclic loading test were examined .The tests were carried out at same point with 5

mm/s, 12 mm (test2) and 15 mm (test1) tissue displacement with an ellipsoidal indenter tip.

In results obtained from displacement controlled cyclic loading tests, by changing the alignment of indenter tip, the mean maximum force of the tissue was increased from 0˚to 90˚ and decreased from 90˚to 180˚. This means that the stiff direction of the muscle is at 90 degree and perpendicular to the contraction direction of muscle fibers and the compliant direction is in 0˚(Fig.4.6-1). In 0˚, the long axis of elliptic tip was positioned parallel to the long axis of biceps muscle and therefore parallel to the alignment direction of muscle fibers. In 90˚ the long axis of elliptic tip is perpendicular to long axis of the biceps muscle. As a result, the alignment direction of the muscle fibers and sarcomeres is a factor that determines the stiff and compliant direction of muscle; the direction parallel to fibers is the most compliant direction, and the direction perpendicular to fibers is the stiffest. This obtained trend in force-angle relation also was observed in experiments on other subjects.

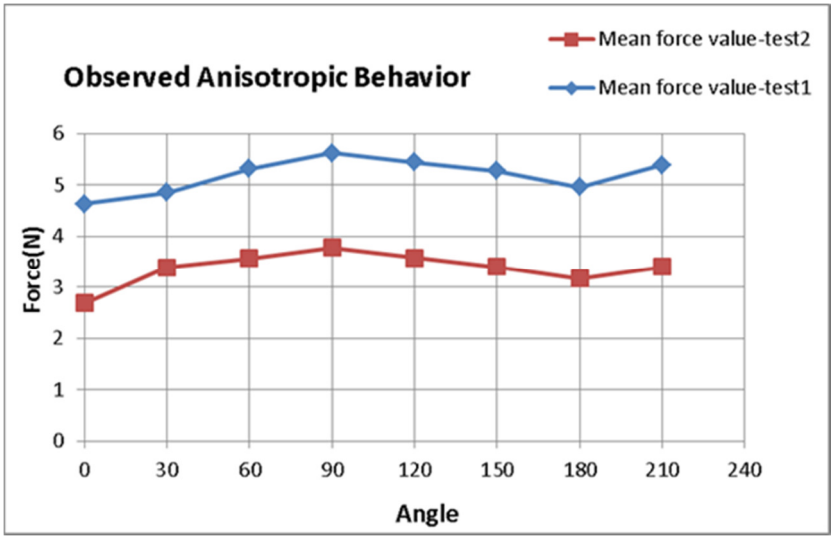

Figure 4.6-1. Response of biceps muscle in different indenter tip alignments, to the same displacement controlled cyclic loading test. The experiments were carried out at same point with 5 mm/s, 12 mm (test2) and 15 mm (test1) tissue displacement. The mean maximum response force(N) in different alignment of indenter tip increased from 0˚to 90˚.

4.6.2 Investigation of biceps muscle anisotropy behavior by relaxation tests:

In order to investigate the anisotropy behavior besides cyclic loading tests, relaxation tests were also conducted on biceps muscle.

For scrutinizing the anisotropic response of tissue, the constant parameters of 2 different equations were derived and compared. The equations are as follows:

$$\boldsymbol{F(t) = F_0[1 - \delta_1(1 - e^{-t/\tau_1}) - \delta_2(1 - e^{-t/\tau})]} \quad \text{.....4.6-1}$$

$$E(t) = \frac{\boldsymbol{E_1}}{\boldsymbol{\Gamma(1-\alpha)t^{\alpha}}} \quad \text{.....4.6-2}$$

$$E(t) = E_r + \frac{E_g - E_r}{(1+t/\tau)^{\alpha}} \quad \text{.....4.6-3}$$

The first equation (4.6-1) is a two-term Prony series used for simulating relaxation behaviors of the soft biological tissues. Constant Parameters in the equation have certain meanings based on the viscoelastic material model (Tönük and Silver-Thorn, 2004). Two different approaches are often adopted for investigate viscoelasticity: creep/stress relaxation (quasi-static/low- rate) and dynamic tests. The results from quasi-static tests are often correlated by means of Prony series (Brinson and Brinson, 2008), although other fitting techniques have been used, including a more generalized transfer function (between stress and strain) in Laplace space (Yu and Haddad, 1994), or splines (Tran et al., 2011).

It is concluded in the literature that the two term Prony series can better approximate the viscoelastic mechanical behavior such as relaxation, than one term or 3 term prony series. Palacio-Torralba et al., (2014).

F (t) = Output force

F_0 = Force at the start of relaxation

δ_1=Short-term relaxation magnitude

τ_1 =Short-term relaxation time constant

δ_2 =Long-term relaxation magnitude

τ_2 =Long-term relaxation time constant

t = time

The second equation (4.6-2) is Fractional Power law, where $0 \leq \alpha \leq 1$ and $E_1 = E\tau\alpha$. Here E is an elastic constant with the units of (N m^{-2}) and τ is a time constant with units of (seconds); thus E_1 had units of (Pascal) $(seconds)^{\alpha}$. The bounding values of α represent the discrete elements employed in conventional viscoelastic models (spring, E_1= E when $\alpha = 0$ and dashpot, $E_1 = E\tau\alpha = \eta$, the coefficient of viscosity, when $\alpha = 1$)

Fractional calculus is useful in the field of biorheology, in part, because many similar materials (polymers, gels, emulsions, composites and suspensions) show power-law responses to an applied stress or strain an example of such power-law behavior in elastic tissue was observed by Cariem and Magin. For viscoelastic measurements of the aorta, both in vivo and in vitro, and the analysis of resulted data was carried out using fractional order viscoelastic models (Craiem & Magin, 2010).

Third equation (4.6-2) is a modified Fractional Power Law (four parameter fractional order Zener model) that has one parameter more than the previous one, but results in better curve fitting (Demirci, 2012).

E_g=E(t=0)= glassy modulus

E_r=E(t$\rightarrow\infty$)=rubbery modulus

And τ (time constant) and α (the order of time derivative) are constants chosen for fitting the data. The arbitrary fractional order α which varies from zero to one is defined as the "Non-dimensional memory parameter" and the variation of this memory parameter allows the constitutive equation to shift from a representation of a solid state to fluid state. To be clear when α =0 the material has perfect memory

and represents a solid state and when $\alpha = 1$ the material has no memory defining the viscous fluid state

There is no limitation that α be an integer, the initial value is glassy modulus that gradually reduces to rubbery modulus during stress relaxation (Bagley, 1989)

The parameters of the model should be restricted to the conditions $E_g > E_r > 0$, $\tau > 0$, $0 < \alpha < 1$

Fractional order derivative α characterizes the power law response which is observed on most of the soft tissues. It is claimed in literature that, the relaxation data usually do not follow a simple exponential; however it is described by a power law expression.

It has been observed that employing fractional calculus principles to the linear viscoelasticity theory, the parameters necessary to describe the observed material behavior are significantly reduced compared to the integer order viscoelastic models (Enelund, Maehler, Runesson, & Joseffson, 1999), (Bagley & Torvik, 1983), (Schmidt & Gaul, 2002), (Wei & Shimizu, 2001) (Craiem & Armentano, 2006) (Welch, Rorrer, Duren, & JR., 1999).

As a part of this thesis, in addition to investigating the claim that fractional order material models are more proper to curve-fitting for quasi-static experimental data than integer order viscoelastic models such as Prony series, the parameters of fractional power law was obtained by curve fitting to the experiments conducted in different orientations with elliptic tips, to investigate the behavior of these parameters by angle change, thus investigating the anisotropy of the tissue.

For curve fitting, “Nonlinear Least Squares” method, and the “Trust-Region” algorithm were used in “Curve Fitting Tool” of MATLAB (Refer to Appendix D for more details). By minimizing the least squares error amount between the measured data and the model, the model parameters are identified optimally.

4.6.2.1 Examining the elastic and viscoelastic behavior of biceps muscle using Prony series

In order to examine the elastic behavior of tissue, firstly 6 successive experiments tests were carried out on biceps muscle with the same input parameters: 140 seconds relaxation time, 3 mm/s speed, and 25 mm displacement. The only different characteristic in these tests was the alignment angle of indenter tip on muscle surface which was with 30 degree intervals increased from 0˚.to 180˚.

Table 4.6-1. Material constants of relaxation tests in different orientations, on subject Z, with 140 seconds relaxation time, 3mm/s speed, and 25 mm displacement, obtained from two term Prony series

Alignment Angle(degree)	**F_0**	**δ_1**	**τ_1**	**δ_2**	**τ_2**	**SSE**	**R^2**
0	7.204	0.06203	0.2745	0.1368	33.95	0.7549	0.9315
30	7,092	0.05887	0.2619	0.1509	33.05	0.5384	0.9576
60	7,363	0.054762	0.1715	0.1574	33.39	0.5399	0.9563
90	7,629	0.05271	0.06444	0.1579	33.82	0.5406	0.9618
120	6,845	0.05673	0.09748	0.1214	33.97	0.6691	0.9235
150	6,486	0.06879	0.116	0.1474	43.2	0.7823	0.9456
180	5,825	0.07879	0.3092	0.1054	60.25	0.8167	0.8999

By analyzing constants obtained from relaxation tests (table 4.6-1) following conclusions was resulted:

- The obtained maximum force response just before the relaxation time was in 90 degree. This result is in agreement with the results obtained in cyclic loading tests and also in agreement with Petekkaya (2008) results.
- δ_1 was decreased from 0 degree to 90 degree and then started to increase from 90 degree to 180 degree.

- τ_1 also was decreased from 0 to 90 degree and then started to rise from 90 to 180 degree
- δ_2 had smooth changes with no specific trend in results, the maximum value was in 60 degree and the minimum value was in 180 degree.
- τ_2 had also partially the decreasing and then increasing trend.
- The difference between response force 0 and 90 degree shows that the experiment's condition was changed during the time. One hypothesis is that tissue was preconditioned during the experiments somewhere between 0 and 180 degree in addition to waiting between each experiment for 5 to 10 minutes for recovering, tissue cannot fully recover.

As aforementioned before, obtaining very different values (with more than 1 N difference) for immediate response force, in 0 degree and 180 degree means that the experiment conditions were not so stable. These experiments were conducted without any preconditioning and allowing tissue to recover for 15 minutes after each orientation test. But it seems that tissue was not fully recovered and somewhere during tests preconditioning also happened to some extent. Due to Lokshin and Lanir (2009), fully recovering of skin tissue takes several hours. Hence, in order to solve experiment's problem, prior to experiments, some dummy tests were carried out in all directions for preconditioning of the tissue, and for obtaining more stable and dependable data. The aim is moving the preconditioning effect to somewhere before real tests (instead of between the tests) and then starting the real experiments. The experiments were conducted in a random order of orientation to examine if this gradual preconditioning affects the results or not.
Hence, a series of relaxation experiments were carried out again on different subjects. Among the successful ones, because of the similarity, only the two set of them, was provided here. These two sets of experiments were conducted on subject N and G, by elliptic tip C. The results of these experiments were collected in table 4.6-2 and table 4.6-3.

Table 4.6-2. Two term Prony series fitting results for relaxation tests conducted on subject N, using elliptic tip C

Degree	F_0	δ_1	δ_2	τ_1	τ_2	SSE	R^2
0	4.915	0.08403	0.1099	0.5921	13.77	10.86	0.9438
30	5.129	0.0935	0.09686	0.7311	7.971	10.54	0.9213
60	6.356	0.127	0.1133	0.6165	9.463	16.74	0.9452
90	7.634	0.08728	0.1653	1.137	26.91	16.62	0.988
120	6.963	0.1655	0.1265	1.306	31.36	17.76	0.9802
150	6.536	0.09573	0.09286	0.4635	8.778	26.4	0.8712
180	5.062	0.07667	0.1119	0.7584	13.61	17.67	0.9199

Table 4.6-3. Two term Prony series fitting results for relaxation tests conducted on subject G, Using elliptic tip D

Degree	F_0	δ_1	δ_2	τ_1	τ_2	SSE	R^2
0	4.907	0.07922	0.08798	1.834	45.09	11.38	0.9452
30	4.663	0.0971	0.3183	7.524	467.3	6.862	0.9764
60	5.77	0.07584	0.1251	1.754	56.92	10.22	0.978
90	6.28	0.09311	0.09832	4.642	80.36	11.25	0.9749
120	5.818	0.07013	0.1158	2.475	46.3	4.717	0.9897
150	5.06	0.09715	0.113	5.532	131.8	5.272	0.9809
180	4.782	0.08733	0.3891	9.903	640.3	9.905	0.9636

In figure 4.6-2 and 4.6-3 the immediate relaxation force response of subject N and subject G were demonstrated in different orientations. As can be seen in both figures the force response is maximum in 90 degree alignment of tip on the bulk biceps muscle (perpendicular to the muscle contraction direction). This behavior was observed in all experiments. Moreover it is in agreement with results obtained

in cyclic loading tests. Thus the elastic behavior of tissue changes in different directions, and with indentation tests with an elliptic tip, the directions with maximum and minimum of elasticity behavior can be found. This kind of results can be used in improving the constitutive equation of soft biological tissues. It should be mentioned that the experiments with one abnormality or deviation in trend (because of muscle tonus or physiology of tissue in that point and orientation) were eliminated as unsuccessful experiments. It can be seen that in both set of experiments, 0 and 180 degree force responses are very close to each other even after conducting random order experiments.

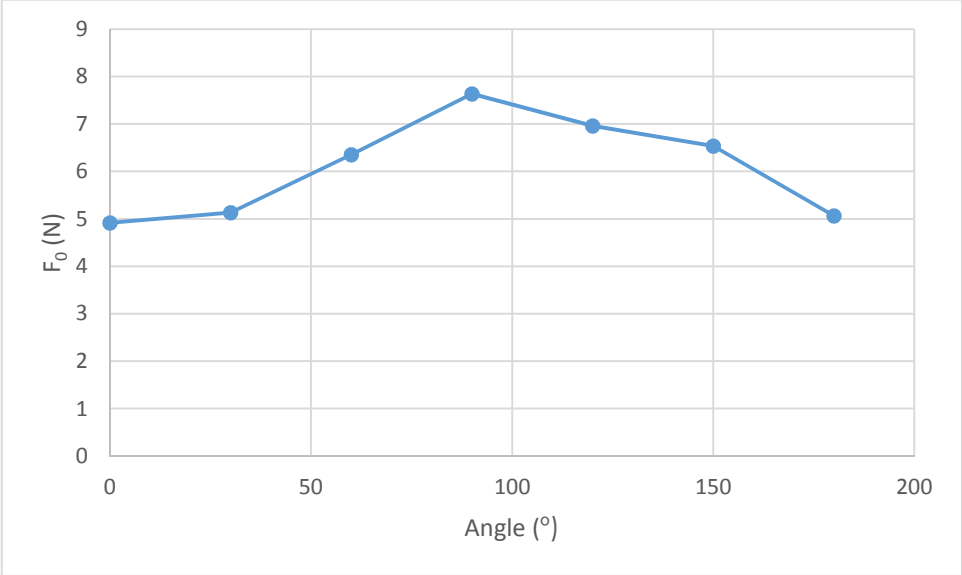

Figure 4.6-2. The immediate relaxation force response of subject N in different orientations.

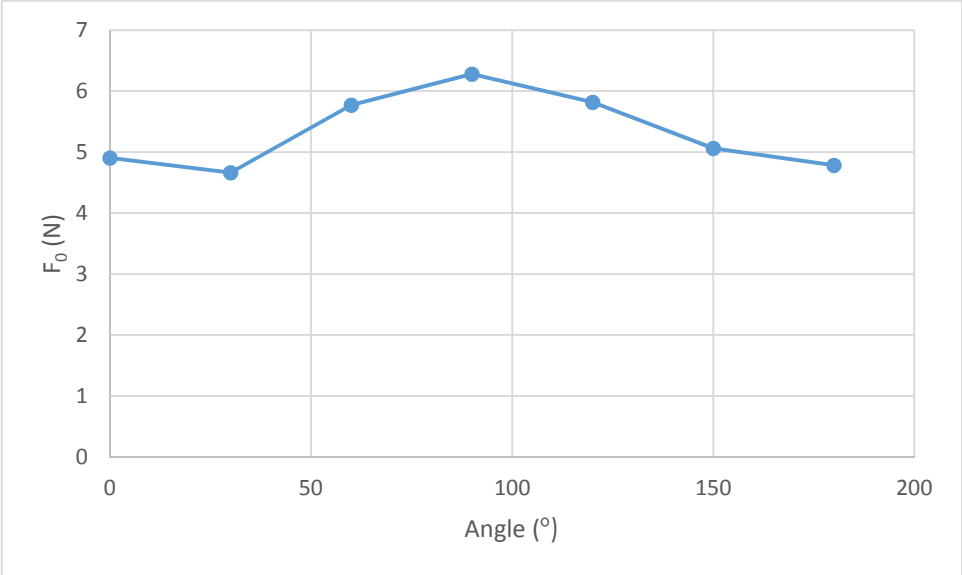

Figure 4.6-3. The immediate relaxation force response of subject G in different orientations.

An example of curve fitting in 120 degree from second set of relaxation tests (G) was provided in figure (4.6-4)

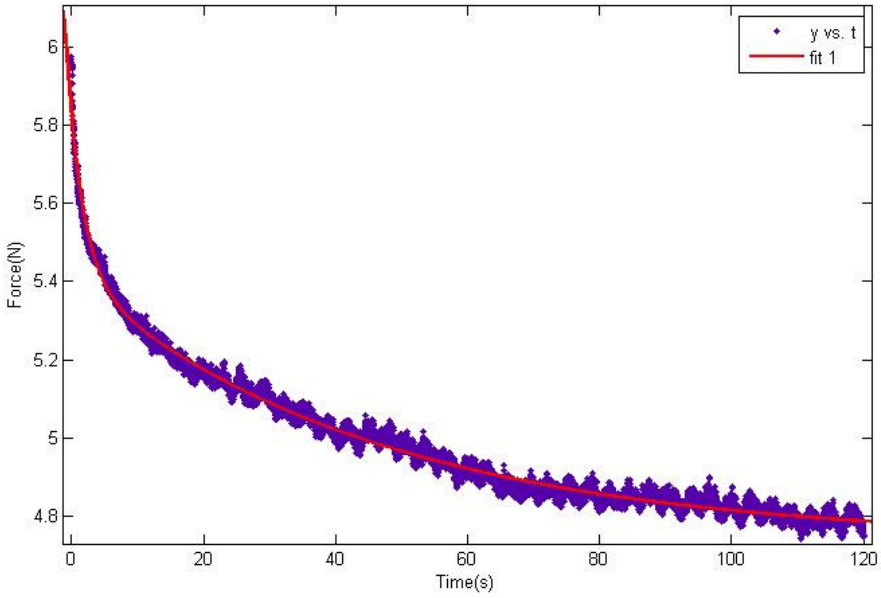

Figure 4.6-4. Relaxation test curve fitting using Prony series in 120 degree orientation from second set of tests (G)

Then the other parameters such as δ_1, τ_1, δ_2, τ_2 were examined. Interpretation of first set of relaxation experiments related to subject N were provided in this section;

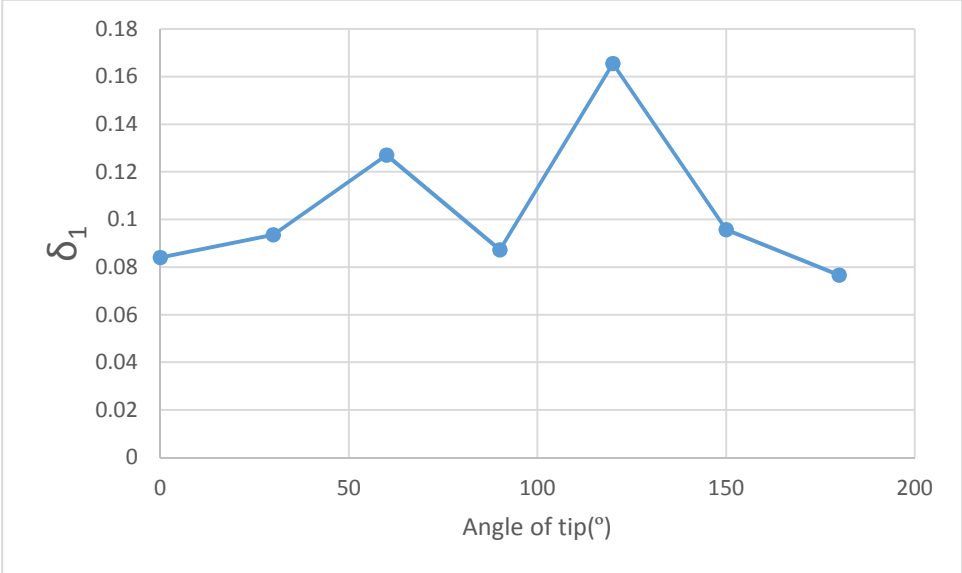

Figure 4.6-5.Short term relaxation magnitude in different orientations

Obtained short term relaxation magnitudes were illustrated in figure 4.6-5. Except than two deviations in 60 and 90 degree, all values are changing between 0.08 and 0.1, and have small variances. If the value appeared in 90 degree was not considered, then an increasing-decreasing trend could be observed. After all these any obvious trend was not detected in this graph.

For short term time constants demonstrated in figure (4.6-6), the maximum value happened in 120 degree, a trend similar to increasing-decreasing trend was observed but still there was many deviations.

An interesting result was observed for long term relaxation magnitude shown in figure (4.6-7). The trend and shape of it, was very similar to relaxation force response (F0). An increasing-decreasing trend with a maximum value at 90 degree.

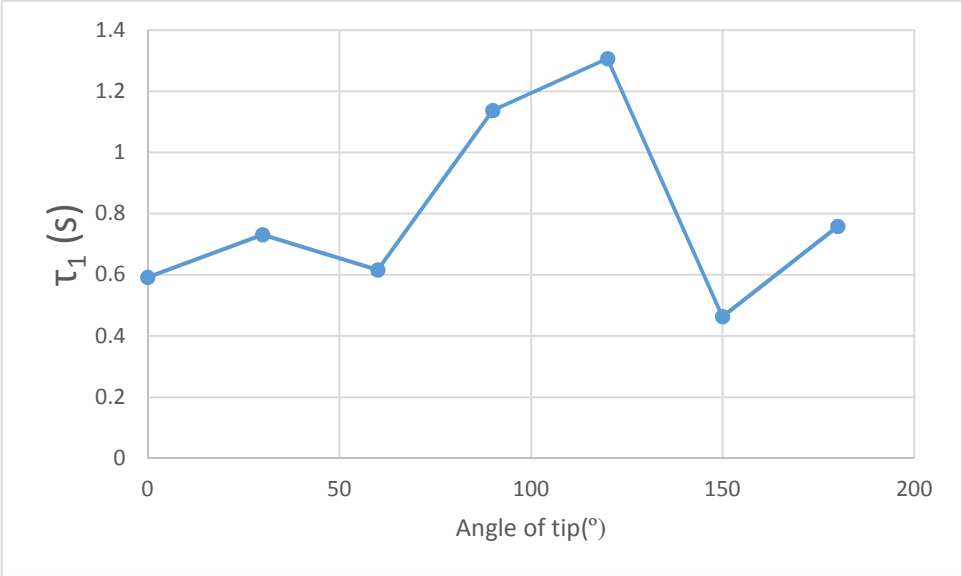

Figure 4.6-6. Short term time constant in different orientations

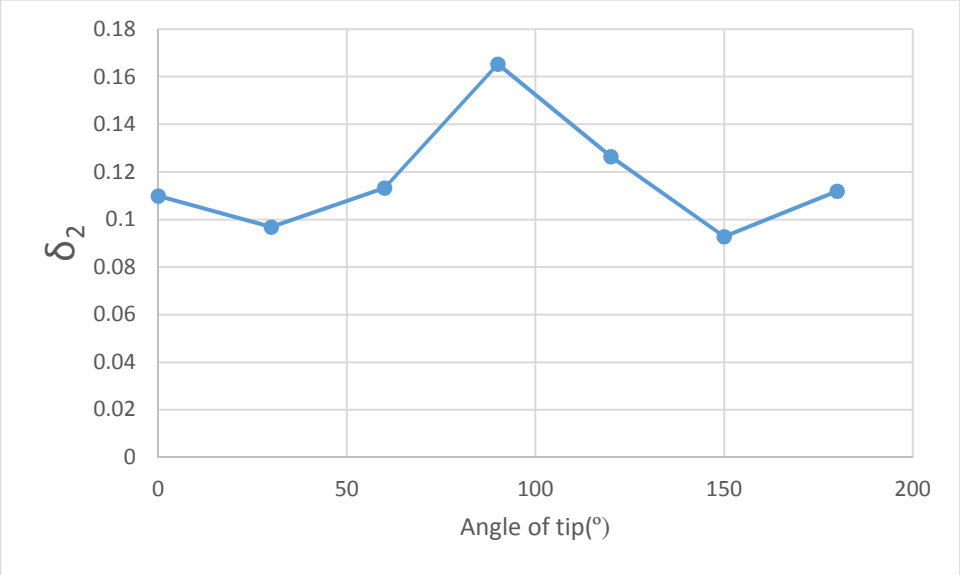

Figure 4.6-7. Long term relaxation magnitude in different orientations

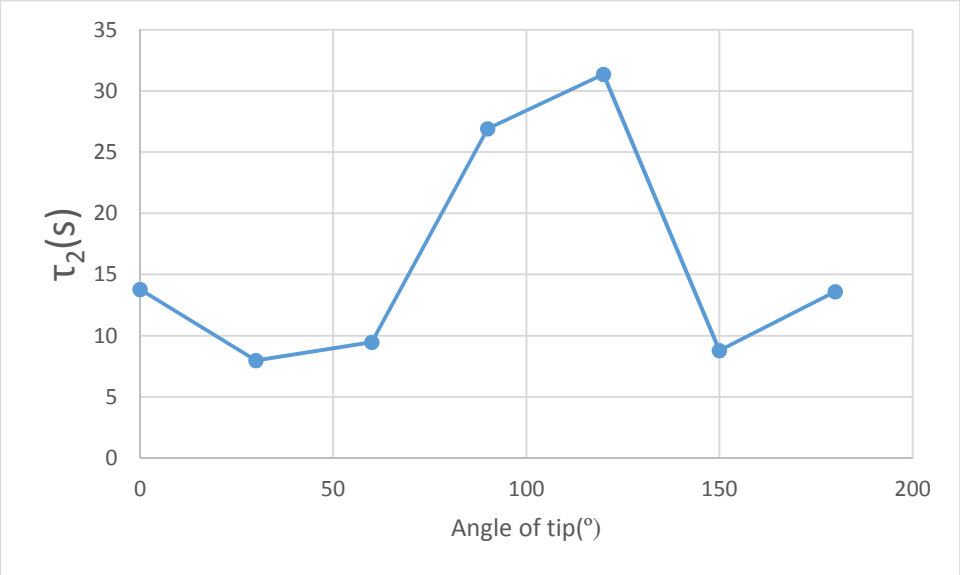

Figure 4.6-8. Long term Time constant in different orientations

Long term time constant had an approximately similar trend to short term time constant with large deviations at 90 and 120 degree (Fig.4.6-8). The maximum amount.

After examining these Prony series parameters of different set of relaxation tests in different indenter tip orientations on tissue, no similar, pure and precise result was obtained in different experiments set. As a proof for this claim the result of the other data set (Table 4.6-3) were provided in Figure (4.6-9).

As can be observed there was no similar characteristic or trend to the previous data. Even the observed similar trend of δ2 to F0 in previous set of data was not observed in this set. However there was still some relations in graphs, for example in large deviations they behave very similar such as values which appeared at 30 degree orientation.

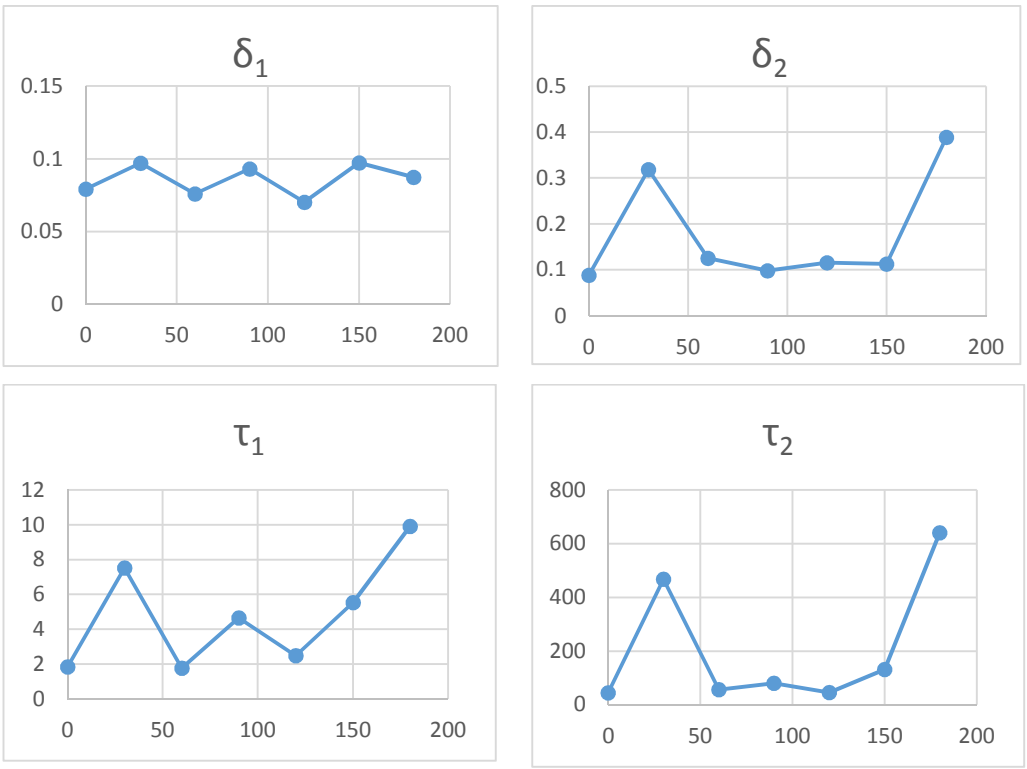

Figure 4.6-9. Second set of Prony series parameters (table 4.6-3) for relaxation tests in different orientations

It should be mentioned that in experiments using elliptic tip D more unstable results were obtained in comparison to the elliptic tip C and the reason for this could be

large axis of contact surface of tip with tissue. In this case factors such as curvature of tissue and different physiology in thickness of tissue under the tip surface may affect the results.

4.6.2.2 Examining the elastic and viscoelastic behavior of biceps muscle using fractional law.

The success of curve fitting of fractional order models compared to integer order models is investigated in Davis, et al (2006). It is known that the curve-fitting superior capability of the fractional order model does not come from the decreased number of parameter, but rather it is inherit to non-integer order derivative that provides a continuous and monotonic transition from elastic to viscous behavior.

In order to examine the elastic behavior of tissue, firstly 6 successive experiments were carried out on biceps muscle with the same input parameters: 120 seconds relaxation time, 3 mm/s speed, and 20 mm displacement. The only different characteristic in these tests was the alignment angle of indenter tip on muscle surface which was with 30 degree intervals increased from 0°.to 180° . The result were collected in Table 4.6-4. An example for curve fitting at 150 degree was provided at Figure 4.6-10

Table 4.6-4. Material constants of relaxation tests in different orientations on subject S, with 120 seconds relaxation time, 3mm/s speed, and 20 mm displacement, obtained from fractional power law.

Tip alignment(°)	E_g	E_r	τ	α	SSE	R
0	0.1664	0.1146	0.2074	0.1092	0.006129	0.9569
30	0.1883	0.1696	4.128	1	0.01399	0.8556
60	0.2134	0.02604	0.1989	0.03658	0.02098	0.9473
90	0.2265	0.0091	0.9438	0.01242	0.01237	0.983
120	0.1946	0.1639	2.649	0.4996	0.00895	0.9599
150	0.1795	0.1556	1.62	0.5808	0.007284	0.9335
180	0.1687	0.1368	2.084	0.3345	0.007907	0.9604

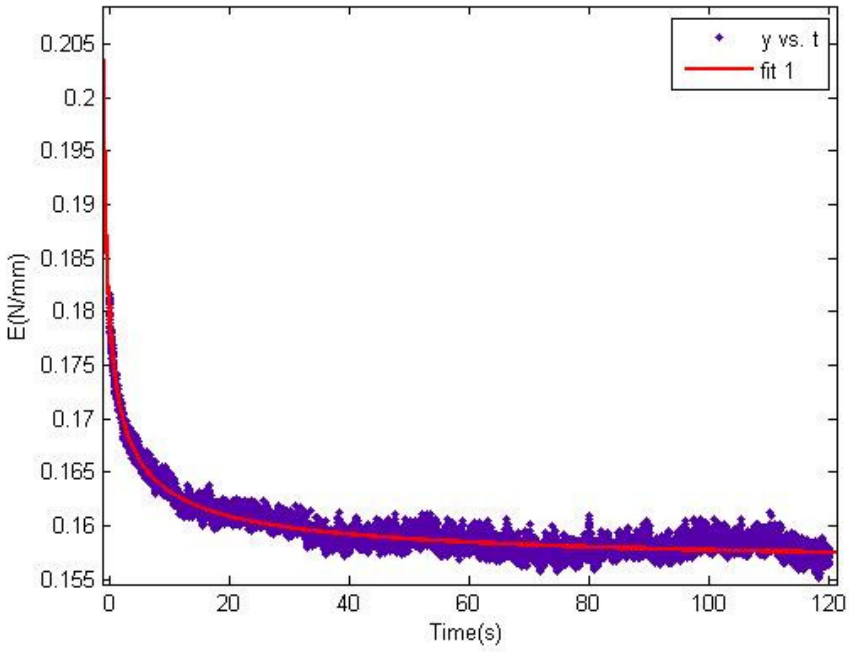

Figure 4.6-10 Relaxation test curve fitting, using fractional power law at 150 degree.

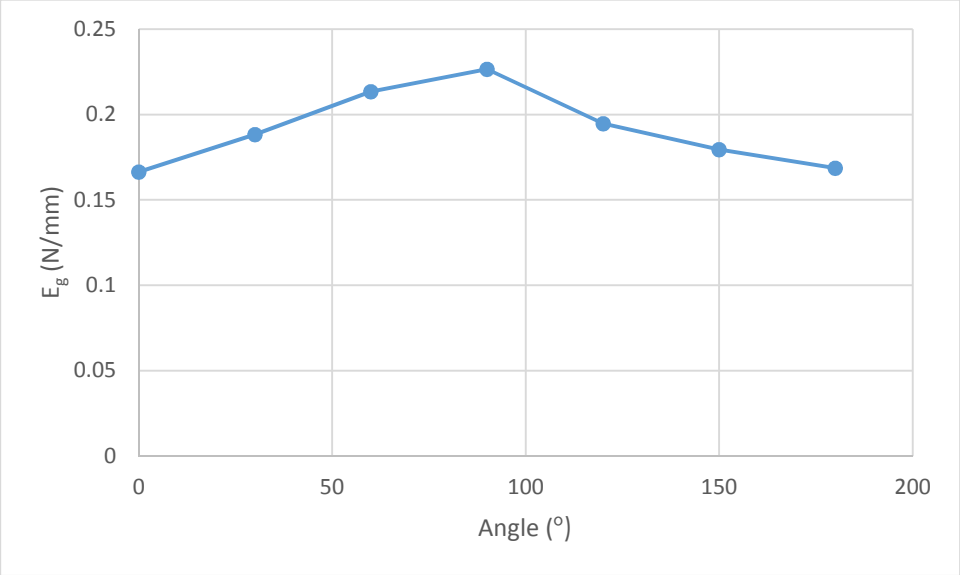

Figure 4.6-11.glassy modulus versus elliptic tip orientation

By analyzing relaxation test data obtained from fractional Power law, following conclusions was resulted:

- E_g was increased from 0 degree to 90 degree, the maximum amount of this parameter achieved on 90 degree, then it was decreased to its value (0.168 N/mm) at 180 degree. The obtained E_g trend which represents the elastic behavior of tissue is in agreement with the obtained F_0 trend in Prony series equation and also with other experiment protocols like cyclic loading.

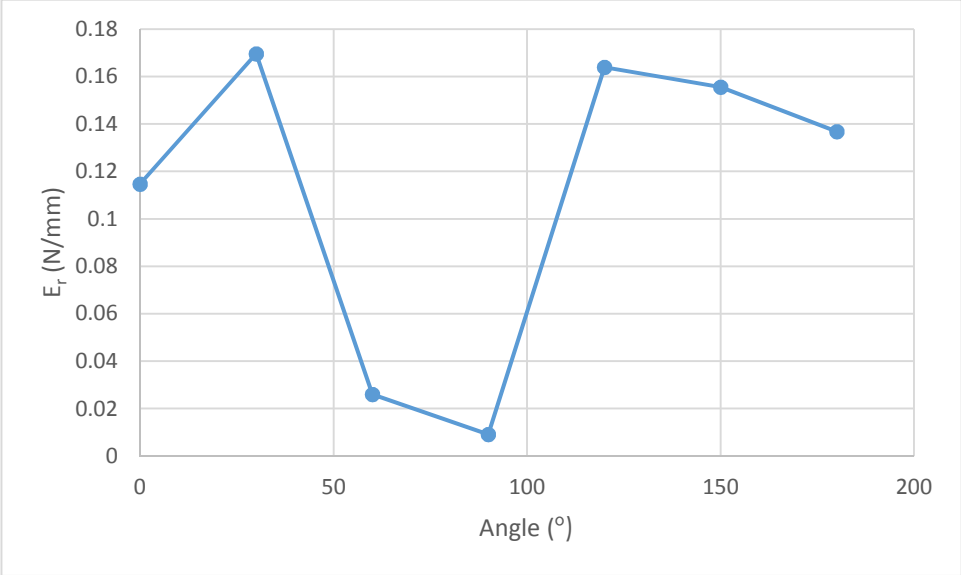

Figure 4.6-12, Rubbery modulus versus elliptic tip orientation

- As aforementioned before the E_g amounts decrease in time (infinity) to E_r amounts. For E_r values, it can be seen that large deviations happened in 60 and 90 degree orientations of indenter tip which value appeared in 90 degree was the minimum (Figure 4.6-12). Actually the value at 30 degree also was not so dependable, because the value of alpha was 1.

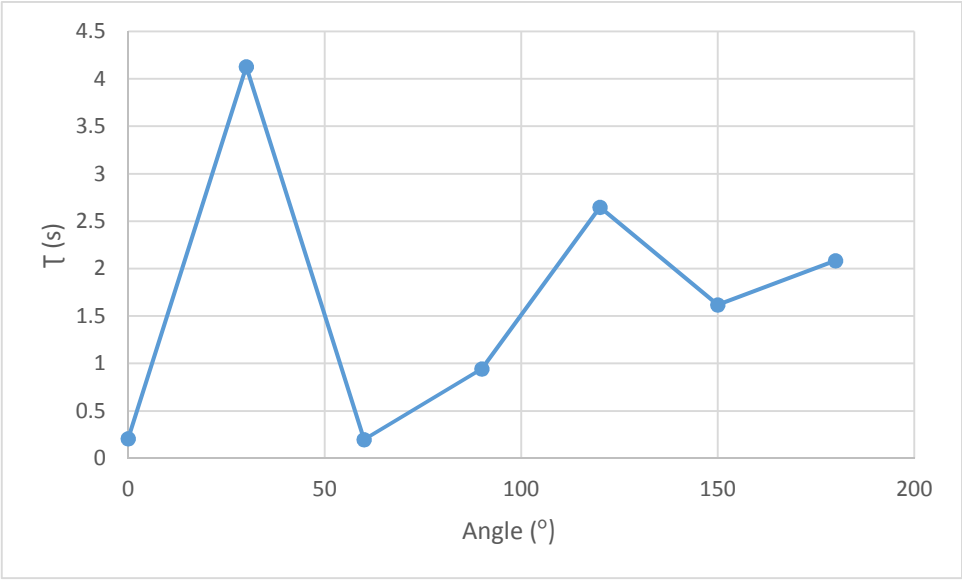

Figure 4.6-13. Time constant (s) versus elliptic tip orientation.

- Except than a large deviation in 30 degree, which was not so dependable, time constant had an increasing trend. The minimum amounts was at 60 (Figure 4.6-13).

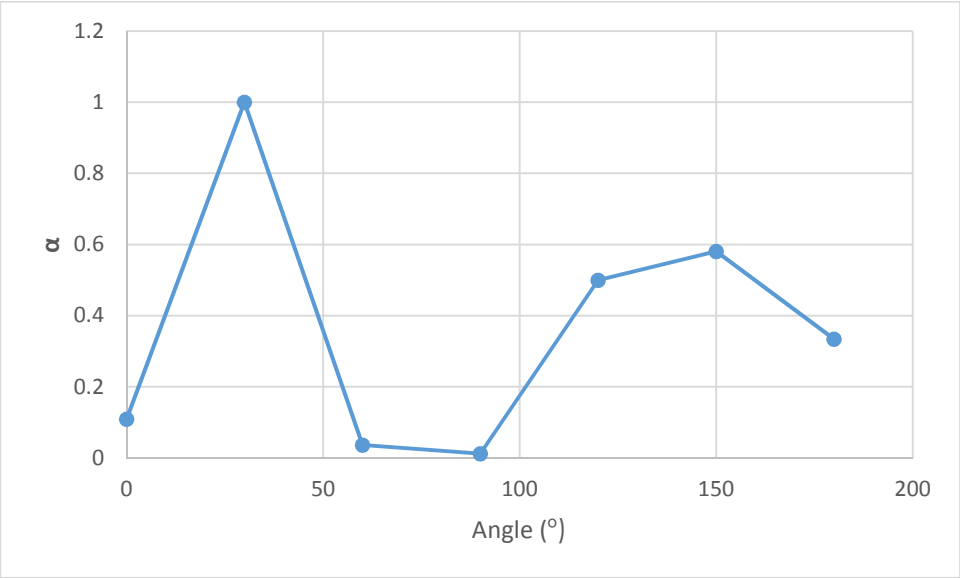

*Figure 4.6-14. Fractional order (**α**) amounts versus tip orientation*

- **α** that is fractional order, is known as "non-dimensional memory parameter". As illustrated in Figure (4.6-14) the trend of amounts of fractional order was very similar to the time constants trend. Here also there was a large deviation at 30 degree. If again the value at 30 degree was not considered, time constant values showed nearly an increasing trend. At the beginning tissue represents more solid-like behavior (close to 0) and in time it shifted to a more fluid-like representation (near 1)

The fractional power law results were not so stable and no clear trends was observed in different experiment sets. The fitting process was not better than Prony series.

4.6.3 Investigation of biceps muscle anisotropy behavior by creep tests:

In order to investigate the anisotropy behavior, creep tests also were conducted on biceps muscle. 6 successive experiments tests were carried out with the same input parameters: initial velocity 3 mm/s, experiment time 120 s, threshold for target force 0.01.

The only different characteristic in these tests was the alignment angle of indenter tip on muscle surface which was with 30 degree intervals increased from 0°.to 180º. For scrutinizing the anisotropic response of tissue, the constant parameters of two term Prony series were derived and compared. The Prony series used in creep is as following;

$$\boldsymbol{d(t) = d_0[1 + \delta_1(1 - e^{-t/\tau'_1}) + \delta_2(1 - e^{-t/\tau'_2})]} \qquad \textit{Equation 4.6-4}$$

d (t) = Output displacement

d_0 = displacement at the start of force fixing

δ_1=Short-term creep magnitude

τ_1 =Short-term creep time constant

δ_2 =Long-term creep magnitude

τ_2 =Long-term creep time constant

t = time

The results of conducted creep experiments were demonstrated in Table (4.6-5). The curve fitting process using Prony series, had better results in creep than in relaxation tests. Moreover clearer trends were observed in creep tests.

Table 4.6-5. Material constants of creep tests on subject G in different orientations for two term Prony series.

Alignment Angle(degree)	d_0(mm)	δ'_1	τ'_1(s)	δ'_2	τ'_2(s)	SSE	R^2
0	27.01	0.0114	4.402	0.0515	57.51	0.7224	0.9984
30	25.57	0.00852	2	0.08688	75.76	2.633	0.9967
60	25.09	0.01038	2.929	0.07974	85.13	1.642	0.9951
90	24.04	0.01626	6.61	0.137	201	3.661	0.9943
120	25.03	0.009734	3.848	0.07602	99.89	1.84	0.9914
150	25.91	0.007882	5.608	0.07243	85.68	1.829	0.9972
180	27.35	0.009884	1.12	0.05795	55.04	5.765	0.9895

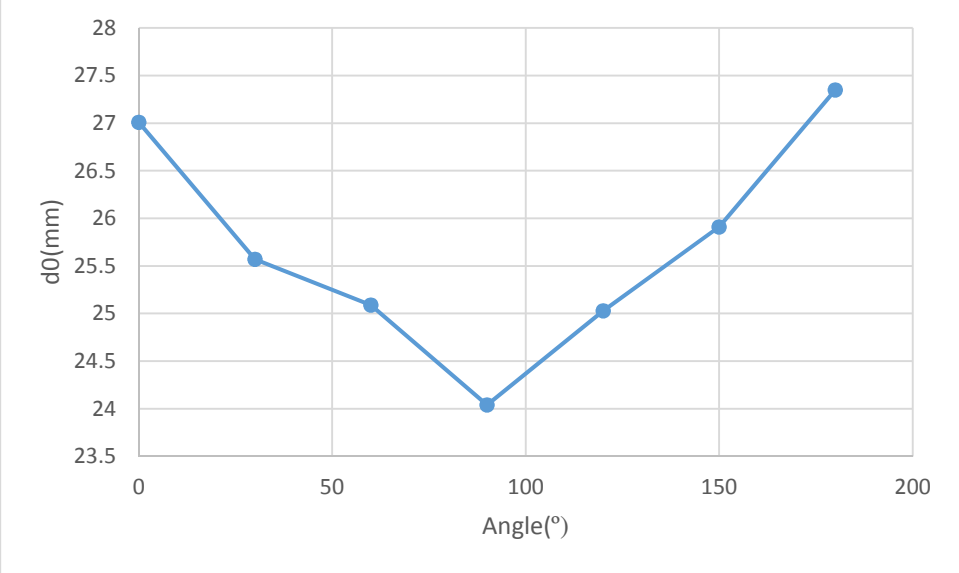

Figure 4.6-15.d_0 (displacement at the start of force fixing and creep) versus elliptic tip orientations

After examining the displacement amount of tissue at the start of creep (Figure.4.6-15), a decreasing-increasing trend was observed and the amount of displacement in 90 degree was the minimum, this means that stiffest direction is in 90 degree and it is in correspondence with the results obtained from relaxation force and cyclic loading response force.

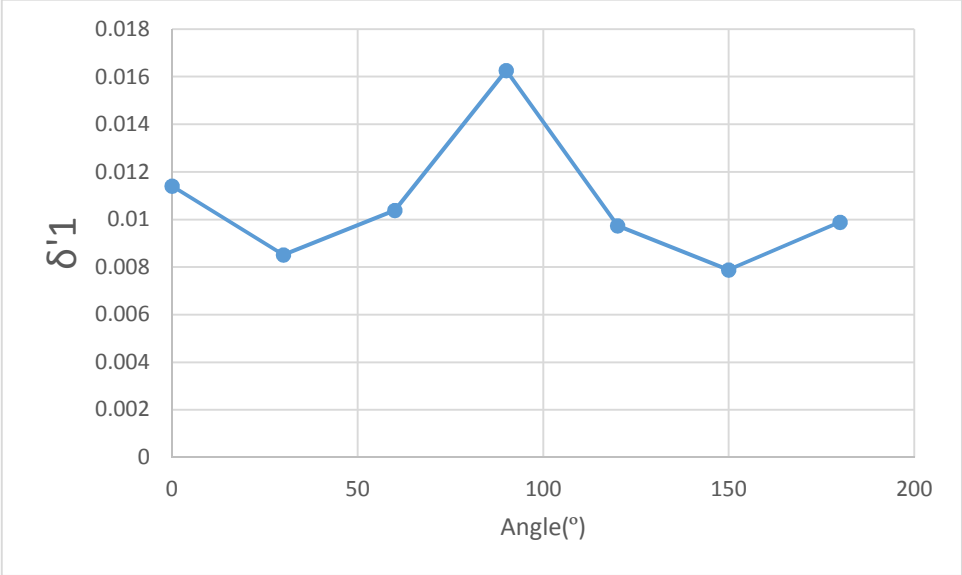

Figure 4.6-16. Short term creep magnitude (δ'1) versus elliptic tip orientation

δ'1 was changing with small variances and the amounts have an increasing-decreasing trend which maximum value appeared at 90 degree that had the minimum displacement (Fig 4.6-16).

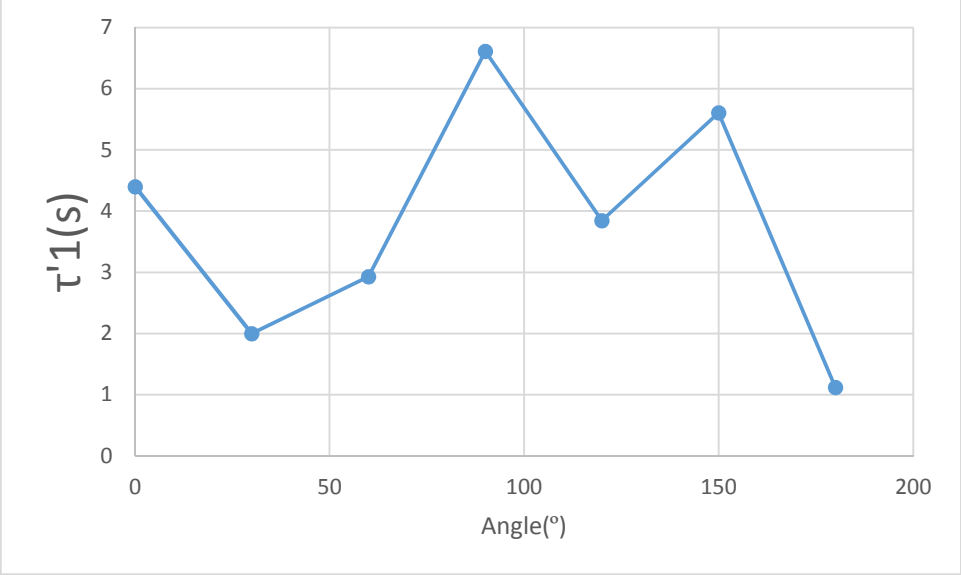

Figure 4.6-17. Short term time constant versus elliptic tip orientation

Short term time constant had a maximum amount at 90 degree again (figure 4.6-17).

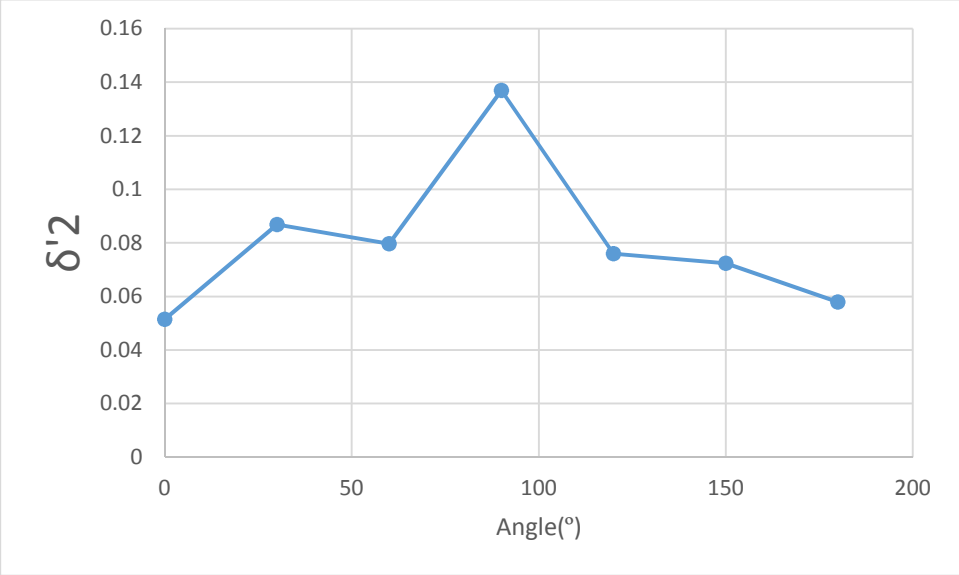

Figure 4.6-18. Long-term creep magnitude versus tip orientation on muscle

In long term creep magnitude a similar increasing-decreasing trend with maximum amount in 90 degree, where minimum displacement happened, was observed (Figure 4.6-18)

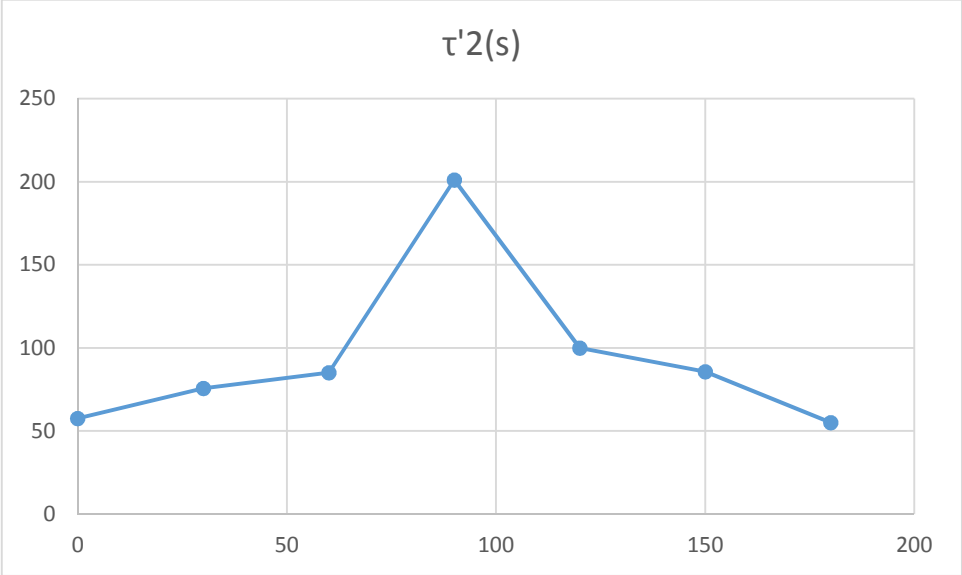

Figure 4.6-19. Long-term time constant versus elliptic tip orientation.

- τ'_2 Was changed between 50 s and 200 s and the maximum amount of this parameter was achieved in 90 degree. An increasing-decreasing trend was observed (Figure 4.6-19).

In Figure 4.6-20 an example for curve fitting of creep experiment at 0 degree was provided.

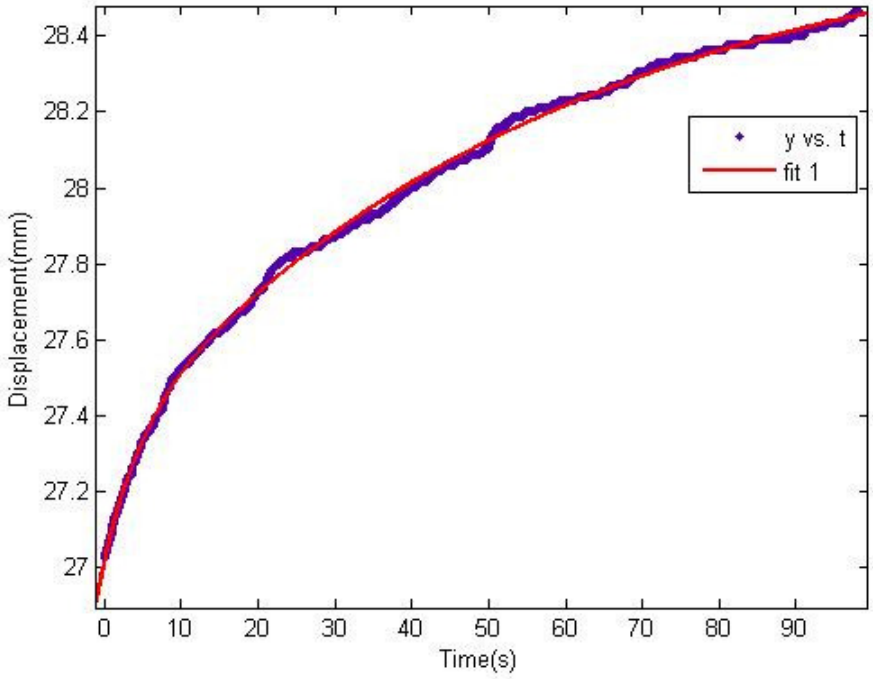

Figure 4.6-20.Creep experiment curve fitting using Prony series at 0 degree indenter tip alignment,

The results obtained from creep indicates that, the stiffest direction which the initial displacement before creep is minimum (90 degree), shows more significant changes in Prony series parameter values, in compare to the other directions. In 90 degree, because of stiffness, the tissue displacement is smaller than other alignments, the other parameters such as creep magnitude and time constant also have a significant deviation in 90 degree. The maximum deviation of short term time constant in this direction indicates that, in first phase of creep, tissue needs more time to dislocation compared to the other directions, and the slope of creep curve is softener, which the reason can be high stiffness in that direction. The long term time constant is also shows the same behavior which indicates the creep behavior as time goes to infinity. On the other hand both short term and long term creep magnitudes have usually a maximum deviation in stiffest direction which indicates that although initial fast displacement before creep is the least, in this direction, but it seems that tissue needs time to travel the more displacement like other direction. Thus in the direction

perpendicular to muscle contraction direction, although the tissue dislocation is the least at initial moment, but when time goes to infinity the dislocation of tissue in this direction will be the largest in compare to the other directions. This interesting result in creep was repeatable in almost all of conducted experiments.

CHAPTER 5

DISCUSSION AND CONCLUSION

This study consists of two phases, firstly the driving software of the existing indenter device was written and improved in LabVIEW environment. The test protocols such as displacement-rate cyclic loading, relaxation and creep was completed. Then for conducting the precise and dependable in-vivo experiments on soft biological tissues, the movement precision of the indenter tip was checked and improved in all protocols by debugging process. In addition a new protocol that is novel among in-vivo in-house indentation set-ups was added to the other test protocols which is force-rate controlled cyclic loading protocol.

The second phase study was conducting in-vivo experiments, using mentioned protocols on human arm. In order to examining the anisotropic behavior of tissue and for being able to conduct tests in different orientations, elliptic tips and alignment fixer was designed and produced. After conducting creep and relaxation tests in different angle alignment for determining anisotropy behavior of soft tissue, resulted experimental data was used to obtain the constants of the Prony series which is capable of modelling these experiments. In addition, the constants of the fractional power law that is known to be a better fit to relaxation data compared to Prony series, was obtained. Then anisotropic response of the tissue was examined by utilizing the constants found for the Prony series and fractional power law.

The main results of this work is:

The main observation made at the end of the experiments was the nonlinear behavior displayed by the tissues. In other words, it was observed that, hysteresis developed at the cyclic loading, stress decreased under constant strain, and the strain increased under constant stress, and under cyclic loading-unloading, tissue has displayed the preconditioning (Mullin's) effect.

Another important conclusion derived with regard to the preconditioning effect was that, the preconditioning effect related to the hysteresis magnitudes in cyclic loading was more clearly observable in comparison to force-time graphs. Difficulties and problems of conducting tests in-vivo (such as subject's muscle movement and irregular breathing, etc.) affects force-time graph more than hysteresis area magnitude. Even when the force values remained at an equilibrium level by repeating cycles, hysteresis magnitudes were decreased gradually. This second type preconditioning was detected firstly by Petekkaya (2008). Thus for modeling and simulating applications, instead of force-time relation, observing of hysteresis area leads to more precise results.

Fung (1984) claimed that magnitude of hysteresis areas are insensitive and independent to displacement-rate in cyclic loading tests. In this study it was observed that hysteresis magnitude is dependent to displacement-rate, which in faster loading-unloading process the hysteresis magnitudes were larger thus energy loss was more.

Another important outcome of this study was about force-rate controlled cyclic loading. It was observed that in cyclic loading and unloading while the force rate was changed the travelled displacement amount did not seem to stop and reach to an equilibrium level by passing time and repeating cycles. The reason for this can be the restructuring of the soft tissue and moving the fluids of ECM (Extracellular Matrix) to the neighbor regions thus in every cycle indenter tips needs to travel more to catch the identified target force in that current time. Farshad et al (1999) in his study mentioned a never stopping creep behavior in living tissues which is also a force-controlled protocol. This behavior was more significant in slow force rates which tissue had sufficient time for applying changes inside itself for adapting to the imposed force. Because of this behavior in slow rates, the cycles in

displacement-force graphs were spreading over displacement axis where in fast force-rates these cycles were more centralized. However clear preconditioning in terms of displacement-time was not seen during in-vivo tests. This behavior can be different during conducting in-vitro tests.

In addition, after observing cyclic loading experiments with different force-rates it was concluded that faster tests results a stiffer response of tissue and the slower tests results a compliant response of tissue. This fact is in contrast with a famous obtained result as anomalous behavior of soft tissue(Giles et al., (2007) under supervision of JE.Bischoff) during in-vitro force rate controlled experiments, and is in agreement with displacement-rate controlled experiments obtained both in this study and Petekkaya (2008).

In relaxation experiments the effect of different rates and displacement amount was scrutinized. In faster initial loadings, initial response force was observed to be larger. This result is in agreement with the cyclic loading and hysteresis results. Variation of the relaxation also examined with conducting relaxation tests with different displacement amounts. Although in many studies the strain level independency of relaxation curve was assumed, but in this study it was observed that, in large displacements, relaxation rate is more, for instance until a specific time, the force dropping amount is larger compared to the low level displacements, but when in low displacement levels, after a specific time, tissue was approximately relaxed, in high displacement levels the tissue continue to relaxing after that specific time for longer durations.

In creep tests it was observed that in larger target forces, creep rate was faster. This means that after applying a large force, during a specific time, tissue shows more creep amount (displacement amount), compared to small forces.

Within this study, anisotropic behaviors of biceps muscle were also screened. When the anisotropic response of the tissue were investigated, separate evaluations were performed for the cyclic loading-unloading tests, relaxation and creep tests through observing the trend of force in Prony series and glassy and rubbery modulus and other parameters in fractional power law, and parallel results with each other were obtained. Based on these results, while the angle between the long axis of the elliptic

surface of the indenter tip and the contraction direction of the biceps muscle increases, the stiffness of the tissue increases and reaches to its peak value at 90º angle. This behavior confirmed a periodical character and it also tended to decrease again inside interval starting from 90º and ending with 180º.

The last remark produced in this research came to realization by identifying the constants of both two-term Prony series, and fractional power law, competent at modelling of the attained experimental data. Better fitting outcomes for test data was attained with Prony series. Fractional power law constants had very unstable behavior. For creep experimental data Prony series curve fitting was very satisfying and most of the times with very good r-squared.

Anisotropic behavior of biceps muscle was analyzed with observing the trend of obtained constants for both mentioned models.

To conclude, with all the experiments completed, behavior of the soft biological tissue particularly human arm muscles and bulk tissue were analyzed at detail. Apart from this, responses in the soft biological tissues were much better comprehended. Considering the obtained results in the computer simulations, will help attaining much more idealistic final outcomes.

5.1 Future work

Some improvements can be carried out as a future work;

-It should be mentioned that in force-rate controlled results the first cycle is different than other cycles and the lower force amount reaches around 1N and it does not get closer to the zero. This error can be minimized more for being able to conduct more complicated experiments.

-For creep protocol, separating creep curve, (from the moment that indenter reaches to target force and tries to keep the force constant) from the initial ramp of the experiment that is mostly displacement-rate controlled will make the analyzing process of the recorded data easier.

REFERENCES

Ahearne, M., Yang, Y., Then, K. Y., & Liu, K. K. (2007). An indentation technique to characterize the mechanical and viscoelastic properties of human and porcine corneas. Annals of biomedical engineering, 35(9), 1608–16. doi:10.1007/s10439-007-9323-9

Ahn, B., & Kim, J. (2010). Measurement and characterization of soft tissue behavior with surface deformation and force response under large deformations. Medical image analysis, 14(2), 138–48. doi:10.1016/j.media.2009.10.006

Al-ja'afreh, T., Zweiri, Y., Seneviratne, L., & Althoefer, K. (2008). A new soft-tissue indentation model for estimating circular indenter "force–displacement" characteristics. Proceedings of the Institution of Mechanical Engineers, Part H: Journal of Engineering in Medicine, 222(5), 805–815. doi:10.1243/09544119JEIM319

Argatov, I.I., Mishuris, G. S., & Paukshto, M. V. (2015). Cylindrical lateral depth-sensing indentation testing of thin anisotropic elastic films. European Journal of Mechanics - A/Solids, 49, 299–307. doi:10.1016/j.euromechsol.2014.07.009

Bagley, R. L. (1989). Power law and fractional calculus model of viscoelasticity. AIAA Journal, 27(10), 1412–1417. doi:10.2514/3.10279

Bagley, R. L., Torvik, P. J. (1983). Fractional calculus—a different approach to the analysis of viscoelastically damped structures. AIAA Journal, vol. 21, no. 5, pp. 741–748.

Barrett, S. R. H., Sutcliffe, M. P. F., Howarth, S., Li, Z. Y., & Gillard, J. H. (2009). Experimental measurement of the mechanical properties of carotid atherothrombotic plaque fibrous cap. Journal of biomechanics, 42(11), 1650–5. doi:10.1016/j.jbiomech.2009.04.025

Basdogan, C. (2012). Dynamic Material Properties of Human and Animal Livers, Soft Tissue Biomechanical Modeling for Computer Assisted Surgery, Springer Series on Studies in Mechanobiology, Tissue Engineering, and Biomaterials, Vol. 11, pp. 229-241, Ed: P. Yohan.

Belkoff, S. M., Haut, R. C., (1991). A structural model used to evaluate the changing microstructure of maturing rat skin. J. Biomech. 24(8):711-720.

Belkoff, S. M., Naylor, E. C., Walshaw, R., Lanigan, E., Colony, L., & Haut, R. C. (1995). Effects of subcutaneous expansion on mechanical properties of porcine skin. The Journal of surgical research, Volume: 58, Issue: 2, Pages: 117-123.

Bilston, L. E. (Ed.), "Neural Tissue Biomechanics", *Springer*, 2011.

Bischoff, J. E. (2004). Static Indentation of Anisotropic Biomaterials Using Axially Asymmetric Indenters—a Computational Study. Journal of Biomechanical Engineering, 126(4), 498. doi:10.1115/1.1785808

Bonifasi-lista, C., Lake, S. P., Small, M. S., & Weiss, J. A. (2005). Viscoelastic properties of the human medial collateral ligament under longitudinal , transverse and shear loading, 23, 67–76.

Borodich, F. M., Keer, L. M., & Korach, C. S. (2003). Analytical study of fundamental nanoindentation test relations for indenters of non-ideal shapes. Nanotechnology, 14(7), 803–808. doi:10.1088/0957-4484/14/7/319

Brinson, H. F., Brinson, L.C. Polymer Engineering Science and Viscoelasticity. Springer, New York, 2008.

Carson, W. C., Gerling, G. J., Krupski, T. L., Kowalik, C. G., Harper, J. C., & Moskaluk, C. a. (2011). Material characterization of ex vivo prostate tissue via spherical indentation in the clinic. Medical engineering & physics, 33(3), 302–9. doi:10.1016/j.medengphy.2010.10.013

Chai, C.-K., Speelman, L., Oomens, C. W. J., & Baaijens, F. P. T. (2014). Compressive mechanical properties of atherosclerotic plaques--indentation test to characterise the local anisotropic behaviour. Journal of biomechanics, 47(4), 784–92. doi:10.1016/j.jbiomech.2014.01.018

Chao, C. Y. L., Zheng, Y. P., Huang, Y. P., & Cheing, G. L. Y. (2010). Biomechanical properties of the forefoot plantar soft tissue as measured by an optical coherence tomography-based air-jet indentation system and tissue ultrasound palpation system. Clinical biomechanics (Bristol, Avon), 25(6), 594–600. doi:10.1016/j.clinbiomech.2010.03.008

Chen, W. M., Phyau-Wui Shim, V., Park, S. B., & Lee, T. (2011). An instrumented tissue tester for measuring soft tissue property under the metatarsal heads in relation to metatarsophalangeal joint angle. Journal of biomechanics, 44(9), 1801–4. doi:10.1016/j.jbiomech.2011.03.031

Choi, a. P. C., & Zheng, Y. P. (2005). Estimation of Young's modulus and Poisson's ratio of soft tissue from indentation using two different-sized indentors: Finite element analysis of the finite deformation effect. Medical & Biological Engineering & Computing, 43(2), 258–264. doi:10.1007/BF02345964

Choi, S. T., Jeong, S. J., & Earmme, Y. Y. (2008). Modified-creep experiment of an elastomer film on a rigid substrate using nanoindentation with a flat-ended cylindrical tip. Scripta Materialia, 58(3), 199–202. doi:10.1016/j.scriptamat.2007.09.036

Cox, M. A. J., Driessen, N. J. B., Boerboom, R. A., Bouten, C. V. C., & Baaijens, F. P. T. (2008). Mechanical characterization of anisotropic planar biological soft tissues using finite indentation: experimental feasibility. Journal of biomechanics, 41(2), 422–9. doi:10.1016/j.jbiomech.2007.08.006

Craiem, D., & Magin, R. L. (2010). Fractional order models of viscoelasticity as an alternative in the analysis of red blood cell (RBC) membrane mechanics. Physical biology, 7(1), 13001. doi:10.1088/1478-3975/7/1/013001

Craiem, D. O., Armentano, R. L. (2006). Arterial viscoelasticity: a fractional derivative model. Conf Proc IEEE Eng Med Biol Soc 1: 1098-1101.

Davis, G. B., Kohandel, M., Sivaloganathan, S., Tenti, G. (2006). The Constitutive Properties of the Brain Parenchyma Part 2. Fractional Derivative Approach, Medical Engineering & Physics, 28: 455-459.

Dimitriadis, E. K., Horkay, F., Maresca, J., Kachar, B., & Chadwick, R. S. (2002). Determination of elastic moduli of thin layers of soft material using the atomic force microscope. Biophysical journal, 82(5), 2798–810. doi:10.1016/S0006-3495(02)75620-8

Duchemin, G., Maillet, P., Poignet, P., & Dombre, E. (2005). A Hybrid Position / Force Control Approach for Identification of Deformation Models of Skin and Underlying Tissues, 52(2), 160–170.

Ebenstein, D. M., Coughlin, D., Chapman, J., Li, C., & Pruitt, L. a. (2009). Nanomechanical properties of calcification, fibrous tissue, and hematoma from atherosclerotic plaques. Journal of biomedical materials research. Part A, 91(4), 1028–37. doi:10.1002/jbm.a.32321

Eder, M., Raith, S., Jalali, J., Volf, A., Settles, M., Machens, H. G., & Kovacs, L. (2013). Comparison of Different Material Models to Simulate

3-D Breast Deformations Using Finite Element Analysis. Annals of Biomedical Engineering. doi:10.1007/s10439-013-0962-8

Enelund, M., Maehler, L., Runesson, K., Joseffson, B. L. (1999). Formulation and integration of the standard linear viscoelastic solid with fractional order rate laws International Journal of Solids and Structures, 36 (16), 2417-2442.

Escoffier, C, De Rigal, J., Rochefort, A., Vasselet, R., Lévêque, J. L., Agache, P. G. (1989). Age-related mechanical properties of human skin: an in vivo study. J. Invest. Dermatol. 93, 353-357.

Farshad, M., Barbezat, M., Flu, P., Schmidlin, F., Graber, P., & Niederer, P. (1999). Material characterization of the pig kidney in relation with the biomechanical analysis of renal trauma. Journal of Biomechanics, 32, 417–425.

Feng, Y., Okamoto, R. J., Namani, R., Genin, G. M., & Bayly, P. V. (2013). Measurements of mechanical anisotropy in brain tissue and implications for transversely isotropic material models of white matter. Journal of the Mechanical Behavior of Biomedical Materials, 23, 117–32. doi:10.1016/j.jmbbm.2013.04.007

Fu, Y. B., & Chui, C. K. (2014). Modelling and simulation of porcine liver tissue indentation using finite element method and uniaxial stress-strain data. Journal of biomechanics, 47(10), 2430–5. doi:10.1016/j.jbiomech.2014.04.009

Fung, Y. C. (1973). Biorheology of soft tissues. Biorheology. Jun;10(2):139-155.

Fung, Y. C. (1984). Structure and Stress-Strain Relationship of Soft Tissues. American Zoologist, 24:13-22.

Fung, Y. C., "Biomechanics: Mechanical Properties of Living Tissues", *Springer-Verlag*, New York, 1993.

Fung, Y. C., Liu, S. Q. (1993). Elementary mechanics of the endothelium of blood vessels. J Biomech Eng. Feb;115(1):1-12.

Fung, Y.C. Biodynamics: Circulation. *Springer-Verlag*, New York, 1984.

Gefen, A., & Margulies, S. S. (2004). Are in vivo and in situ brain tissues mechanically similar? Journal of biomechanics, 37(9), 1339–52. doi:10.1016/j.jbiomech.2003.12.032

Giles, J. M., Black, A. E., & Bischoff, J. E. (2007). Anomalous rate dependence of the preconditioned response of soft tissue during load controlled deformation. Journal of biomechanics, 40(4), 777–85. doi:10.1016/j.jbiomech.2006.03.017

Hayenga, H. N., Thorne, B. C., Peirce, S. M., & Humphrey, J. D. (2011). Ensuring congruency in multiscale modeling: towards linking agent based and continuum biomechanical models of arterial adaptation. Annals of biomedical engineering, 39(11), 2669–82. doi:10.1007/s10439-011-0363-9

Holzapfel, G. A., "Computational Biomechanics of Soft Biological Tissue", *Wiley*, 2004.

Hrapko, M., van Dommelen, J. A. W., Peters, G. W. M., Wismans, J. S. H. M. (2008). The influence of test conditions on characterization of the mechanical properties of brain tissue. J. Biomech. Eng. 130, 0310031 – 03100310

Huang, N. F., Okogbaa, J., Lee, J. C., Jha, A., Zaitseva, T. S., Paukshto, M. V., Cooke, J. P. (2013). The modulation of endothelial cell morphology, function, and survival using anisotropic nanofibrillar collagen scaffolds. Biomaterials, 34(16), 4038–47. doi:10.1016/j.biomaterials.2013.02.036

Iivarinen, J. T., Korhonen, R. K., Julkunen, P., & Jurvelin, J. S. (2011). Experimental and computational analysis of soft tissue stiffness in forearm using a manual indentation device. Medical engineering & physics, 33(10), 1245–53. doi:10.1016/j.medengphy.2011.05.015

Jirasek, M. Z., Bazant, P., "Inelastic Analysis of Structures", *Wiley*, 2001.

Karduna, A. R., & Halperin, H. R. (1997). Experimental and Numerical Analyses of Indentation in Finite-Sized Isotropic and Anisotropic Rubber-like Materials, 25.

Kauer, M., Vuskovic, V., Dual, J., Szekely, G., & Bajka, M. (2002). I nverse finite element characterization of soft tissues, 6, 275–287.

Korhonen, R. K., Saarakkala, S., Juha, T., Laasanen, M. S., Kiviranta, I., & Jurvelin, J. S. (2003). Experimental and numerical validation for the novel configuration of an arthroscopic. Phys. Med. Biol., 48, 1565–1576.

Kroon, M., & Holzapfel, G. A. (2008). A new constitutive model for multi-layered collagenous tissues. Journal of biomechanics, 41(12), 2766–71. doi:10.1016/j.jbiomech.2008.05.033

Lake, S. P., & Barocas, V. H. (2012). Mechanics and kinematics of soft tissue under indentation are determined by the degree of initial collagen fiber alignment. Journal of the mechanical behavior of biomedical materials, 13, 25–35. doi:10.1016/j.jmbbm.2012.03.017

Lee, R. T., Richardson, S. G., Loree, H. M., Grodzinsky, A. J., Gharib, S. A., Schoen, F. J., & Pandian, N. (1991). Prediction of Mechanical Properties of Human Atherosclerotic Tissue by High-Frequency Intravascular Ultrasound Imaging An In Vitro Study.

Lokshin, O., & Lanir, Y. (2009). Viscoelasticity and preconditioning of rat skin under uniaxial stretch: microstructural constitutive characterization. Journal of biomechanical engineering, 131(3), 031009. doi:10.1115/1.3049479

Luo, G., Houston, V. L., Garbarini, M. A., Beattie, A. C., & Thongpop, C. (2011). Finite element analysis of heel pad with insoles. Journal of biomechanics, 44(8), 1559–65. doi:10.1016/j.jbiomech.2011.02.083

Mak, A. F., Liu, G. H., Lee, S. Y. (1994). Biomechanical assessment of below-knee residual limb tissue. J Rehabil Res Dev. 1994 Aug;31(3):188-98.

Meijer, R., Douven, L.F.A., Oomens, C. W. J. (1999). Characterisation of anisotropic and nonlinear behaviour of human skin in vivo. Comput. Methods Biomech. Biomed. Engin., 2:13–27.

Moerman, K. M., Sprengers, A. M. J., Nederveen, A. J., & Simms, C. K. (2013). A novel MRI compatible soft tissue indentor and fibre Bragg grating force sensor. Medical engineering & physics, 35(4), 486–99. doi:10.1016/j.medengphy.2012.06.014

Namani, R., Feng, Y., Okamoto, R. J., Jesuraj, N., Sakiyama-Elbert, S. E., Genin, G. M., & Bayly, P. V. (2012). Elastic characterization of transversely isotropic soft materials by dynamic shear and asymmetric indentation. Journal of biomechanical engineering, 134(6), 061004. doi:10.1115/1.4006848

Nava, A., Mazza, E., Furrer, M., Villiger, P., & Reinhart, W. H. (2008). In vivo mechanical characterization of human liver. Medical image analysis, 12(2), 203–16. doi:10.1016/j.media.2007.10.001

Pailler-Mattei, C., Bec, S., & Zahouani, H. (2008). In vivo measurements of the elastic mechanical properties of human skin by indentation tests. Medical engineering & physics, 30(5), 599–606. doi:10.1016/j.medengphy.2007.06.011

Palacio-Torralba, J., Hammer, S., Good, D. W., Alan McNeill, S., Stewart, G. D., Reuben, R. L., & Chen, Y. (2014). Quantitative diagnostics of soft tissue through viscoelastic characterization using time-based instrumented palpation. Journal of the mechanical behavior of biomedical materials, 41C, 149–160. doi:10.1016/j.jmbbm.2014.09.027

Pandolfi, A., & Vasta, M. (2012). Fiber distributed hyperelastic modeling of biological tissues. Mechanics of Materials, 44, 151–162. doi:10.1016/j.mechmat.2011.06.004

Pelletier, H., Krier, J., & Mille, P. (2006). Characterization of mechanical properties of thin films using nanoindentation test. Mechanics of Materials, 38(12), 1182–1198. doi:10.1016/j.mechmat.2006.02.011

Peña, E., Peña, J. a, & Doblaré, M. (2008). On modelling nonlinear viscoelastic effects in ligaments. Journal of biomechanics, 41(12), 2659–66. doi:10.1016/j.jbiomech.2008.06.019

Petekkaya, A. T. & Tönük, E. (2010).Yumuşak doku mekanik davranışının modellenebilmesi için yerinde (in-vivo) indentör deneyleri Makina Tasarım ve İmalat Dergisi, 10, 19-31.

Petekkaya, A. T. (2008). In vivo indenter experiments on soft biological tissues for identification of material models and corresponding parameters. Ankara: Thesis submitted to the Graduate School of Natural and Applied Sciences of Middle East Technical University

Prevost, T. P., Jin, G., de Moya, M. A., Alam, H. B., Suresh, S., & Socrate, S. (2011). Dynamic mechanical response of brain tissue in indentation in vivo, in situ and in vitro. Acta biomaterialia, 7(12), 4090–101. doi:10.1016/j.actbio.2011.06.032

Rees, D. W. A., "Basic Engineering Plasticity: An Introduction with Engineering and Manufacturing Applications", *Butterworth-Heinemann*, 2006.

Roan, E., & Vemaganti, K. (2011). Strain rate-dependent viscohyperelastic constitutive modeling of bovine liver tissue. Medical & biological engineering & computing, 49(4), 497–506. doi:10.1007/s11517-010-0702-2

Roylance, D., "Mechanical Properties of Materials", *MIT*, 2008.

Rubin, M. B., & Bodner, S. R. (2002). A three-dimensional nonlinear model for dissipative response of soft tissue, 39, 5081–5099.

Samur, E., Sedef, M., Basdogan, C., Avtan, L., & Duzgun, O. (2007). A robotic indenter for minimally invasive measurement and characterization of soft tissue response. Medical image analysis, 11(4), 361–73. doi:10.1016/j.media.2007.04.001

Sandrin, L., Fourquet, B., Hasquenoph, J. M., Yon, S., Fournier, C., Mal, F., Palau, R. (2003). Transient elastography: a new noninvasive method for assessment of hepatic fibrosis. Ultrasound in Medicine & Biology, 29(12), 1705–1713. doi:10.1016/j.ultrasmedbio.2003.07.001

Schmidt, A., & Gaul, L. (2002). Parameter Identification and FE Implementation of a Viscoelastic Constitu- tive Equation Using Fractional Derivatives. Proc. Appl. Math. Mech., 1(1), 153–154.

Seifzadeh, A., Oguamanam, D. C. D., Trutiak, N., Hurtig, M., & Papini, M. (2012). Determination of nonlinear fibre-reinforced biphasic poroviscoelastic constitutive parameters of articular cartilage using stress relaxation indentation testing and an optimizing finite element analysis. Computer Methods and Programs in Biomedicine, 107(2), 315–26. doi:10.1016/j.cmpb.2011.07.004

Spilker, R. L. (1992). A Finite Element Analysis of the Indentation Stress-Relaxation Response of Linear Biphasic Articular Cartilage. Journal of Biomechanical Engineering, 114, 191–201.

Suh, J. F., Youn, I., & Fu, F. H. (2001). An in situ calibration of an ultrasound transducer : a potential application for an ultrasonic indentation test of articular cartilage, 34, 1347–1353.

Tai, K., Qi, H. J., & Ortiz, C. (2005). Effect of mineral content on the nanoindentation properties and nanoscale deformation mechanisms of bovine tibial cortical bone, 6, 947–959.

Tholey, G., Desai, J. P., & Castellanos, A. E. (2003). Evaluating the Role of Vision and Force Feedback in Minimally Invasive Surgery : New Automated Laparoscopic Grasper and a Case Study 1, 198–205.

Tidius, P., "Skeletal Muscle Damage and Repair", *Hardcover*, 2008.

Tönük, E., & Silver-Thorn, M. B. (2004). Nonlinear Viscoelastic Material Property Estimation of Lower Extremity Residual Limb Tissues. Journal of Biomechanical Engineering, 126(2), 289. doi:10.1115/1.1695575

Toyras, J., Lyyra-Laitinen, T., Niinimaki, M., Lindgren, R., Nieminen, M. T., Kiviranta, I., & Jurvelin, J. S. (2001). Estimation of the Young ' s

modulus of articular cartilage using an arthroscopic indentation instrument and ultrasonic measurement of tissue thickness, 34, 251–256.

Tracqui, P., Broisat, A., Toczek, J., Mesnier, N., Ohayon, J., & Riou, L. (2011). Mapping elasticity moduli of atherosclerotic plaque in situ via atomic force microscopy. Journal of structural biology, 174(1), 115–23. doi:10.1016/j.jsb.2011.01.010

Tran, A. B., Yvonnet, J., He, Q. C., Toulemonde, C., Sanahuja, J. (2011). A simple computational homogenization method for structures made of linear heterogeneous viscoelastic materials. Comput. Meth. Appl. Mech. Eng. 200, 2956–2970.

Van Dommelen, J. a. W., van der Sande, T. P. J., Hrapko, M., & Peters, G. W. M. (2010). Mechanical properties of brain tissue by indentation: interregional variation. Journal of the mechanical behavior of biomedical materials, 3(2), 158–66. doi:10.1016/j.jmbbm.2009.09.001

Walraevens, J., Willaert, B., De Win, G., Ranftl, A., De Schutter, J., & Sloten, J. Vander. (2008). Correlation between compression, tensile and tearing tests on healthy and calcified aortic tissues. Medical engineering & physics, 30(9), 1098–104. doi:10.1016/j.medengphy.2008.01.006

Wang, X., Schoen, J. a, & Rentschler, M. E. (2013). A quantitative comparison of soft tissue compressive viscoelastic model accuracy. Journal of the mechanical behavior of biomedical materials, 20, 126–36. doi:10.1016/j.jmbbm.2013.01.007

Welch, S. W. J., Rorrer, R. A. L., Duren Jr., R. G. (1999). Application of time-based fractional calculus methods to viscoelastic creep and stress relaxation of materials. Mechanics of Time-Dependent Materials 3 (3), 279-303.

Wu, Z., Baker, T. A., Ovaert, T. C., & Niebur, G. L. (2012). NIH Public Access, 44(6), 1066–1072. doi:10.1016/j.jbiomech.2011.01.039.

Yao, W., Yoshida, K., Fernandez, M., Vink, J., Wapner, R. J., Ananth, C. V, Myers, K. M. (2014). Measuring the compressive viscoelastic mechanical properties of human cervical tissue using indentation. Journal of the Mechanical Behavior of Biomedical Materials, 34, 18–26. doi:10.1016/j.jmbbm.2014.01.016

Yin, Y., Ling, S. F., & Liu, Y. (2004). A dynamic indentation method for characterizing soft incompressible viscoelastic materials. Materials Science and Engineering: A, 379(1-2), 334–340. doi:10.1016/j.msea.2004.02.055

Yu, P., Haddad, Y. M. (1994). On the dynamic system identification of the response behaviour of linear viscoelastic materials. Int. J. Press. Vessels Pip. 67, 45–54.

Zhang, J., Michalenko, M. M., Kuhl, E., & Ovaert, T. C. (2010). Characterization of indentation response and stiffness reduction of bone using a continuum damage model. Journal of the mechanical behavior of biomedical materials, 3(2), 189–202. doi:10.1016/j.jmbbm.2009.08.001

Zhang, J., Niebur, G. L., & Ovaert, T. C. (2008). Mechanical property determination of bone through nano- and micro-indentation testing and finite element simulation. Journal of biomechanics, 41(2), 267–75. doi:10.1016/j.jbiomech.2007.09.019

Zhang, M. G., Cao, Y. P., Li, G. Y., & Feng, X. Q. (2014). Spherical indentation method for determining the constitutive parameters of hyperelastic soft materials. Biomechanics and modeling in mechanobiology, 13(1), 1–11. doi:10.1007/s10237-013-0481-4

Zhang, M., Zheng, Y. P., & Mak, A. F. T. (1997). Estimating the effective Young's modulus of soft tissues from indentation tests—nonlinear finite element analysis of effects of friction and large deformation. Medical Engineering & Physics, 19(6), 512–517. doi:10.1016/S1350-4533(97)00017-9

Zheng, Y., Mak, A. F. T., & Lue, B. (1999). Objective assessment of limb tissue elasticity : Development of a manual indentation procedure, 36(2).

Zheng, Y.P., Choi, Y. K. C., Wong, K., Chan, S., and Mak, A. F. T. Biomechanical assessment of plantar foot tissue in diabetic patients using an ultrasound indentation system. Ultrasound in Medicine and Biology 26(3): 451-456, 2000.

Zysset, P. K., Guo, X. E., Ho, C. E., Moore, K. E., & Goldstein, S. A. (1999). Elastic modulus and hardness of cortical and trabecular bone lamellae measured by nanoindentation in the human femur, 32, 1005–1012.

APPENDICES

A.INDENTER SET UP DETAILS

A.1. Circuit Diagram

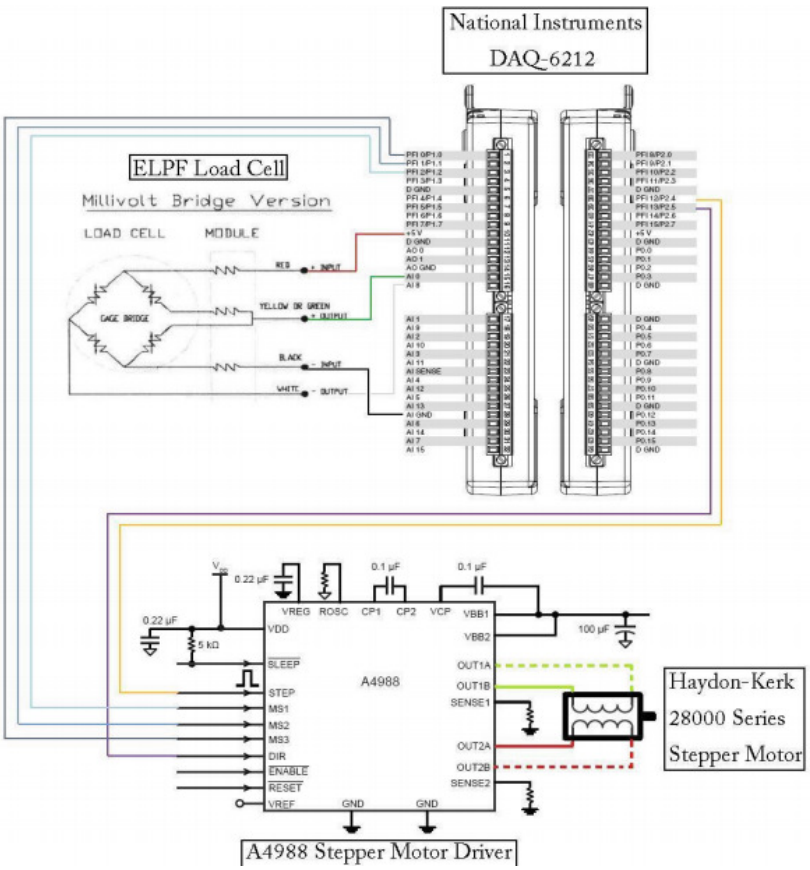

Figure A 1.Indenter circuit diagram

The circuit diagram of the system designed includes Natianol Instruments Data Acquisition Card-6212, ELPF Load Cell, A4988 Stepper Motor Driver, and Haydon-Kerk 28000 Series Stepper Motor. Further specifications for these parts will be given in Appendix. Note that the STEP input is used to generate pulse train that drives the stepper motor, and given to the motor driver from the data acquisition card. Also, DIR input determines the direction in which the motor rotates, and it is given in the same way as STEP input. MS1,MS2, and MS3 inputs are employed to decide upon which step resolution (full,half, or quarter) is used.

Adopted from ME407 Mechanical Engineering Design project: soft tissue indenter.

A.2. Signal Amplifying Circuitry

Readings of the differential output pairs of the load cell changes from 0 to 2.1982 mv/V in its full range. Therefore, when the load cell is fed with an input voltage of 5V it can give an output up to

$$\frac{2.1982mV}{V} * 5V = 10.991mV$$

Although the data acquisition card is capable of dividing -200mV and +200mV range into 2^{16} bits, in order to increase the resolution of data acquisition, and amplifier circuitry is used. The purpose of this circuitry is to amplify 0 mV-10.991 mV range to a level higher than 200 mV (at least 20 times) so that the NI USB-6212 card is capable of dividing full range of load cell data into 2^{16} bits.

To achieve this goal, an instrumentation amplifier AD620N is used for amplifying the signal. Other than its common use in the market, this instrumentation amplifier is much more stable compared to a regular operational amplifier. Moreover, it gives a very linear output and the working range of the device is in the desired level (min: -Vs+1.9 ; max:+Vs-1.2 for a supply voltage of Vs=±5V). AD620 is also a low cost, high accuracy instrumentation amplifier that requires only one external resistor to set gains of 1 to 1000 with a very low level of noise.

The connection diagram of the circuitry used that is an OPAMP circuit can be given as following;

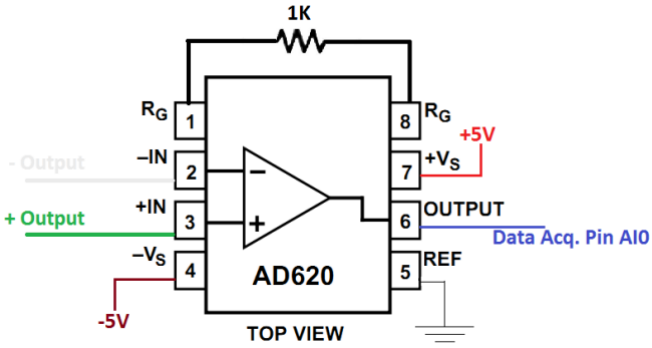

Figure A 2. OPAMP circuit

Where ± output pins are simply the outputs of the load cell. Note that the gain of the system is selected as 50 (as 1k Ω resistor is connected) which can simply be changed by changing the RG resistor. The formula for the calculation of amplifier gain is;

$$G = \frac{49.4\ k\Omega}{R_G} + 1$$

(Adopted from ME407 Mechanical Engineering Design project: soft tissue indenter)

B.OPERATIONAL CODES

B.1.Filtering

After receiving the data from load cell, in order to get rid of its noise, acquired voltage values from the load cell (in mV) are filtered. Then the filtered values are converted into newton [N] (Figure A.3).

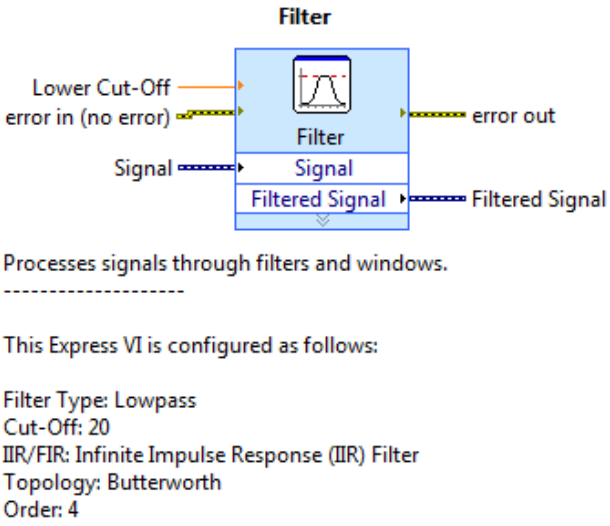

Figure.B. 1.Filter vi

The example input and output signal is as following:

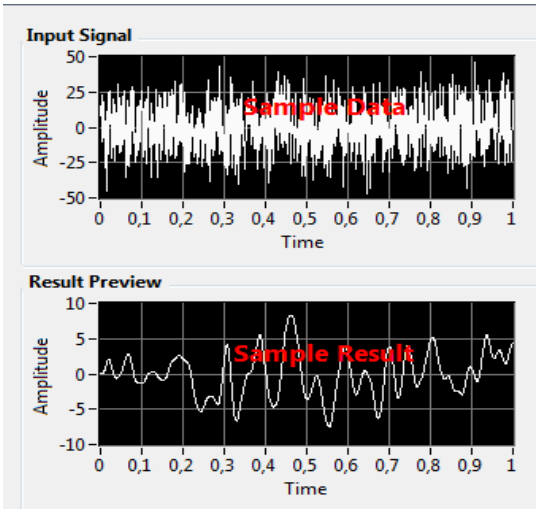

Figure.B. 2..Input and output signal to filter

B.2.Load-cell offset

This code was written for measuring the existent force on loadcell before experiments. Through this code the load-cell force was measured up to required input time such as 10 seconds, using sample- clock.vi and AI-voltage-based.vi, then the mean value of this measured force was calculated by Mean.vi and was given as output. This value was subtracted from the recorded force values during experiments. The front panel and block diagram of code is demonstrated in following Figure:

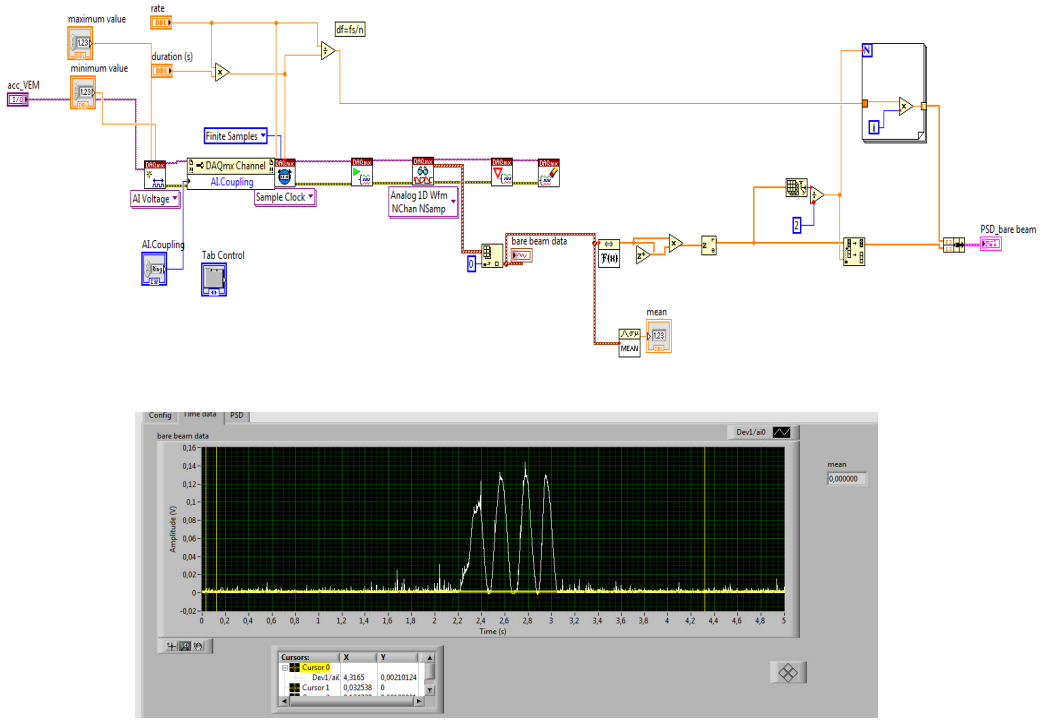

Figure.B. 3.Load-cell offset code and GUI

B.3.Indenter Device Manual Control:

This code was written to move the indenter to the desired position (backward or forward) in a desired input speed. It was controlled by two Boolean keys, Dir and Run

Dir:
T: REVERSE
F: FORWARD

RUN:
T: DRIVES MOTOR
F: STOPS

The related block diagram is demonstrated in following Figure:

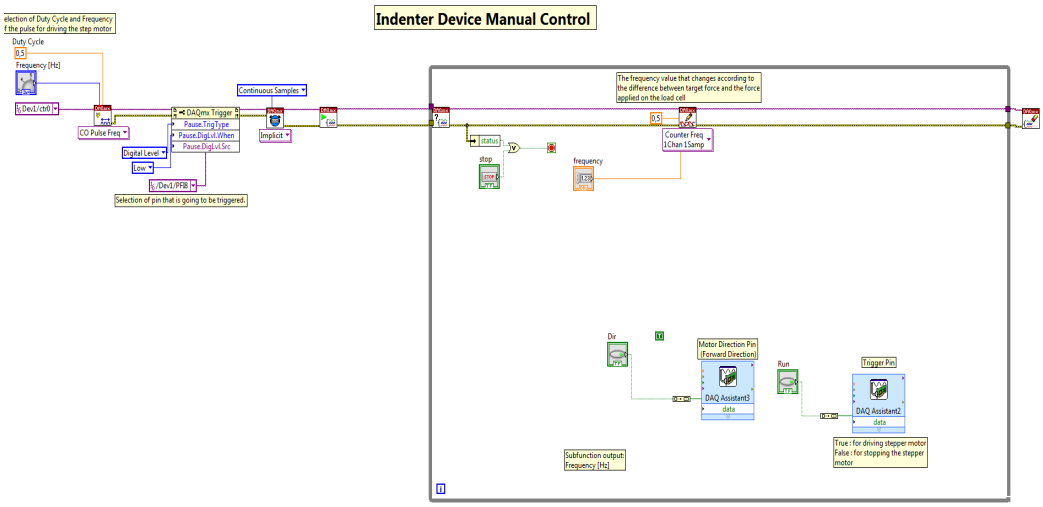

Figure.B. 4.Indenter manual control

B.4.The sub-vi's used in block diagrams:

Error sub-vi

A sub-function which calculates the amount of error between target and real force values in [mV], multiplies this difference with a proportional gain constant for converting this difference into output frequency.

Input: Reference Voltage [mV], Real Voltage Value [mV], Value of maximum load (50N) in [mV]

Output: Frequency [Hz]

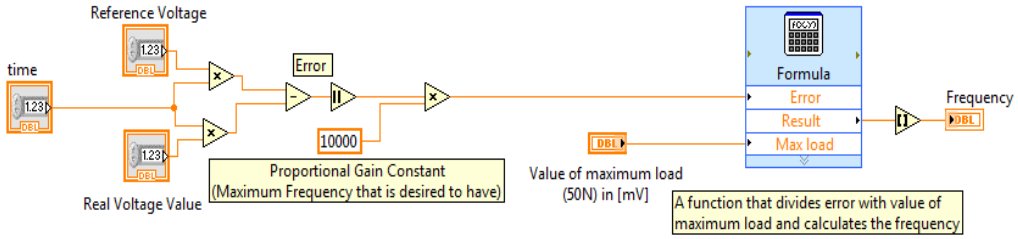

Figure.B. 5. Error sub-vi

StepsRequired sub-vi

A subfuntion which converts the input displacement [mm] into number of steps for the stepper motor by dividing the displacement by the amount of displacement per one full step.

Input: Displacement [mm]

Output: Number of Steps Required

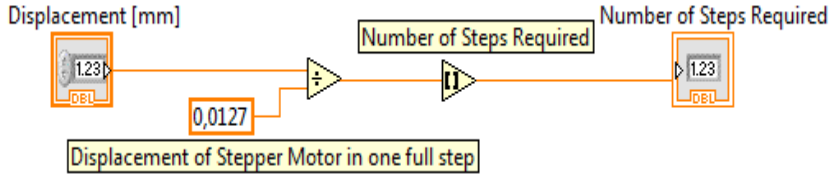

Figure.B. 6. StepsRequired sub-vi

VelocityConvertor-vi

A sub-function which converts the input velocity [mm/s] into stepper motor frequency by dividing the velocity by the amount of displacement per one full step.

Input: Velocity [mm/s]

Output: Frequency [Hz]

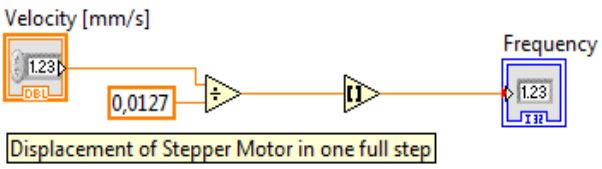

Figure.B. 7. VelocityConvertor-vi

DirectionSelection sub-vi:

A sub-vi which calculates the total number of cycles passed and then generates a boolean output for selecting the direction of stepper motor. Total number of steps passed is divided into number of steps required, and then the remainder is compared with the error (as some steps might be missed due to sampling frequency and waiting time). Parity of number of cycles passed is checked and if they are identical, step motor is driven forward, else backward.

Inputs: Number of Steps Passed, Number of Steps Required, Error

Outputs: Number of cycles passed, Forward Signal (T/F), Backward Signal (T/F)

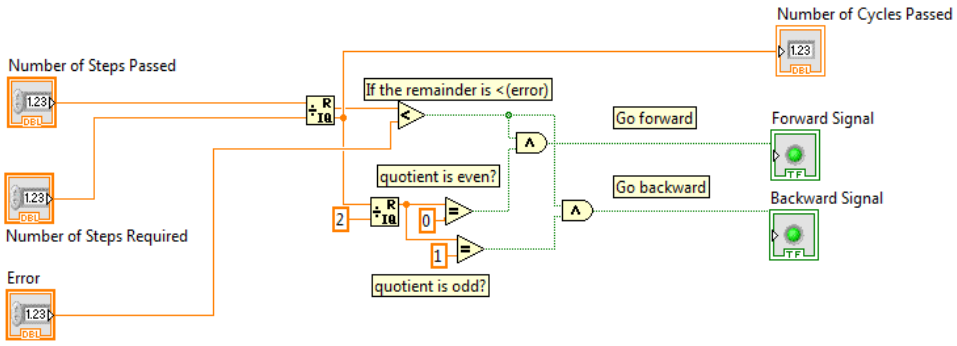

Figure.B. 8. DirectionSelection sub-vi

ForceConvertor-vi

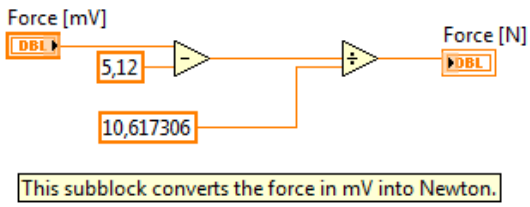

Figure.B. 9.ForceConvertor-vi

Step Calculator sub-vi

A sub-vi which calculates the total number of steps passed. The number of loops is multiplied by the stepper motor frequency and then is multiplied by the waiting time to obtain total number of passed steps.

Inputs: Duration [ms] to wait, Frequency [Hz], Number of loops

Outputs: Number of passed steps

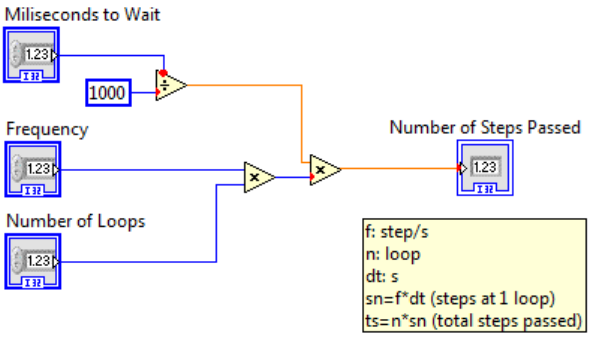

Figure.B. 10. Step Calculator sub-vi

StepCalculator sub-vi

This subfunction calculates the number of steps passed at each loop and adds to counters

Step current=step passed+sgn*ds

Where: ds=current frequency*dt

Sgn is a coefficient that determines the required direction. If the output of [forward and backward] array is forward (true,false signals) that corresponds to zero in 1D array, then the sgn=1 , and if the output of 1D array is 1 that means the input signal is (False,True) that means the requirement for backward direction, then the sgn amount will be -1 , in stop case the sgn will be 0.

Inputs: Frequency [Hz], Elapsed time from previous iteration (dt), steps past

Outputs: displacement [mm], Current step

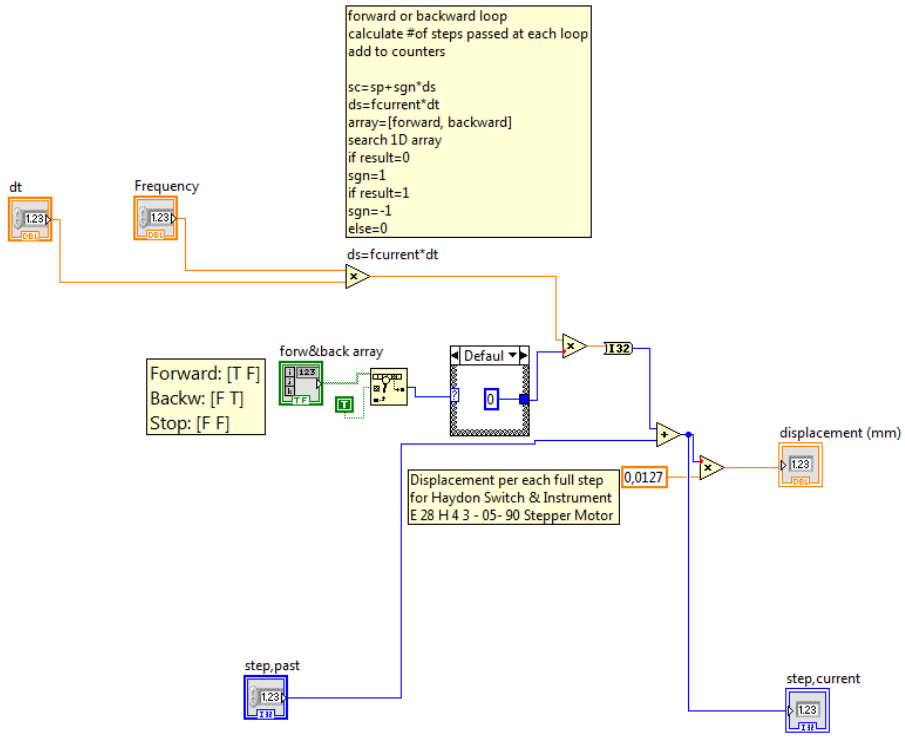

Figure.B. 11. StepCalculator sub-vi

Displacement Calculation:

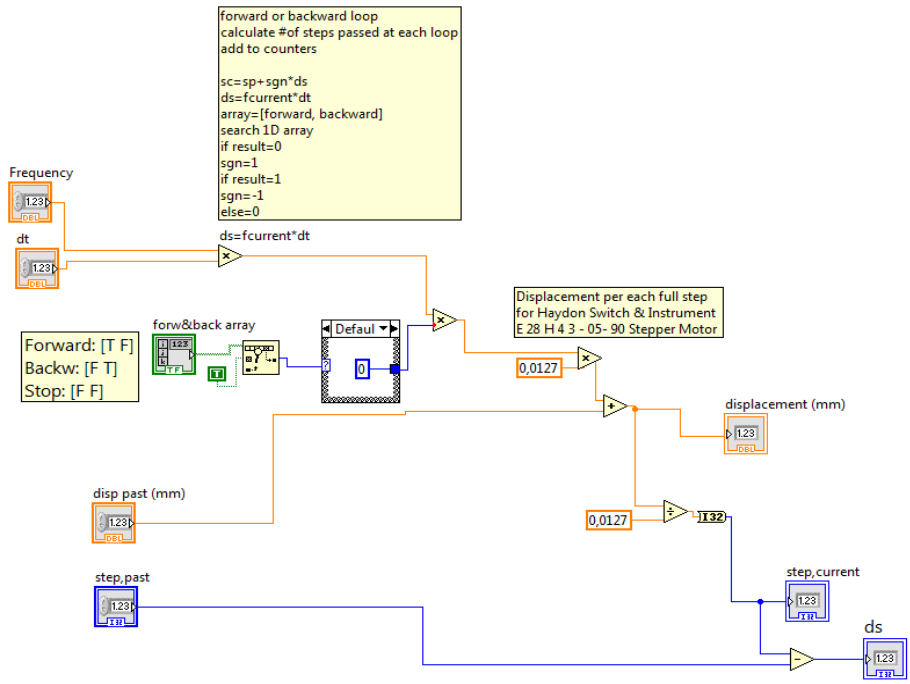

Figure.B. 12. Displacement Calculation code

SubForce Sub-vi

A sub-function which takes force [N] as its input from the user, converts it into [mV] units and calculates its upper and lower threshold levels for force controlled applications.

Input: Force [N]

Output: Force [mV]

Thresholds: +-1%

For tension case zero offset is around 0,000577289 V whereas for compression case it is around

0,00046662V

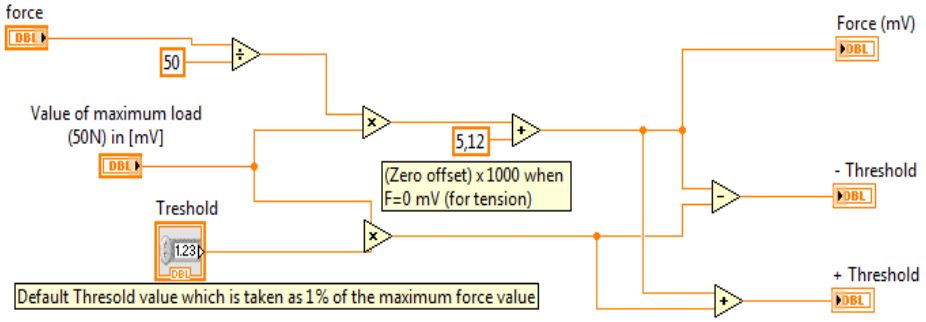

Figure.B. 13.SubForce Sub-vi

B.5.Displacement- rate controlled cyclic loading test block diagram:

After taking the necessary inputs from the graphical user interface, velocity which is taken as mm/s is converted into frequency, in which the stepper motor will be driven at by the help of a velocity converter sub vi. After obtaining the frequency and specifying the duty cycle to be 0.5, pulses are created from the pulse generator block. This block is connected to the counter pin of NI USB-6212 card which is the pin that creates steps for driving the stepper motor. There is a trigger block connected to the pulse generator. The purpose of this block is either to drive the stepper motor or to stop the stepper motor.

The trigger block checks if the digital I/O pin 33 is high or low. If this pin is high, than pulses are continuously generated from the counter pin and the stepper motor goes forward or backward according to the state of the direction pin of the stepper motor driver card. Making trigger pin low stops pulse generation and therefore it stops the stepper motor. After taking the displacement input and starting the test, StepsRequired sub vi block calculates the necessary number of steps required to reach the desired input displacement value. All other blocks are put inside of a while loop in order to obtain real time data acquisition. In this loop, there is a wait sub vi that adds a delay to the system in order not to miss steps and a step calculator sub vi that counts the number of steps passed. The output of this sub vi is then taken as input for the DirectionSelection sub vi. This sub vi compares the required number of steps with the number of steps passed and gives a Boolean output directly to digital I/O pin 39 which is connected to the direction pin of the motor driver card. Therefore, after reaching the desired displacement the state of the direction pin is reversed therefore motor starts to move in the reverse direction. There is also a counter within the DirectionSelection sub vi, which counts how many cycles have passed. This result is then compared with the input number of cycles and if they are equal the state of the trigger pin is made low which stops the pulse generation, therefore the stepper motor. During the whole cyclic loading test, load cell is continuously read from the analog inputs AI0-AI8 which are differential pairs that take the difference between the two load cell output pins. These inputs are then

filtered by a lowpass filer and ForceConverter vi then takes the value of maximum load as its input, converts the data read from the load cell from mV to N scale. This block is then connected to the waveform chart and the change of force vs. time is displayed in the graphical user interface.

The block diagram of this experiment is shown in following page:

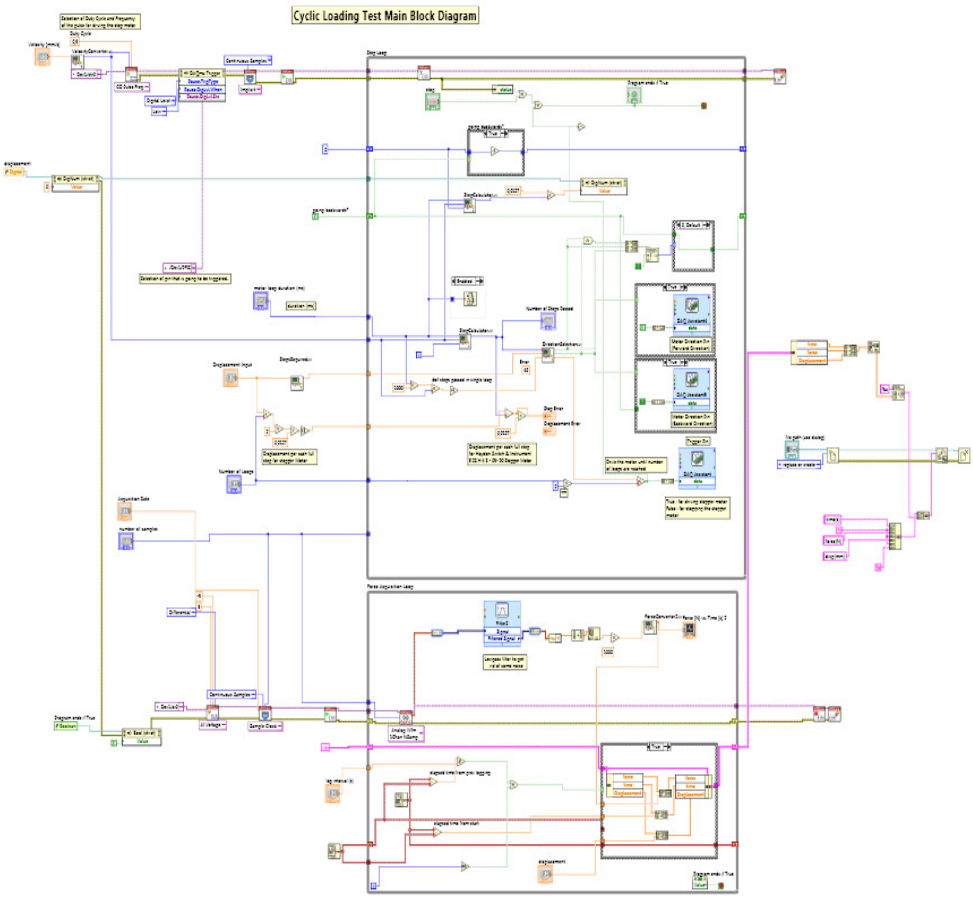
Cyclic Loading Test Main Block Diagram

B.6.Displacement controlled cyclic loading code flowchart:

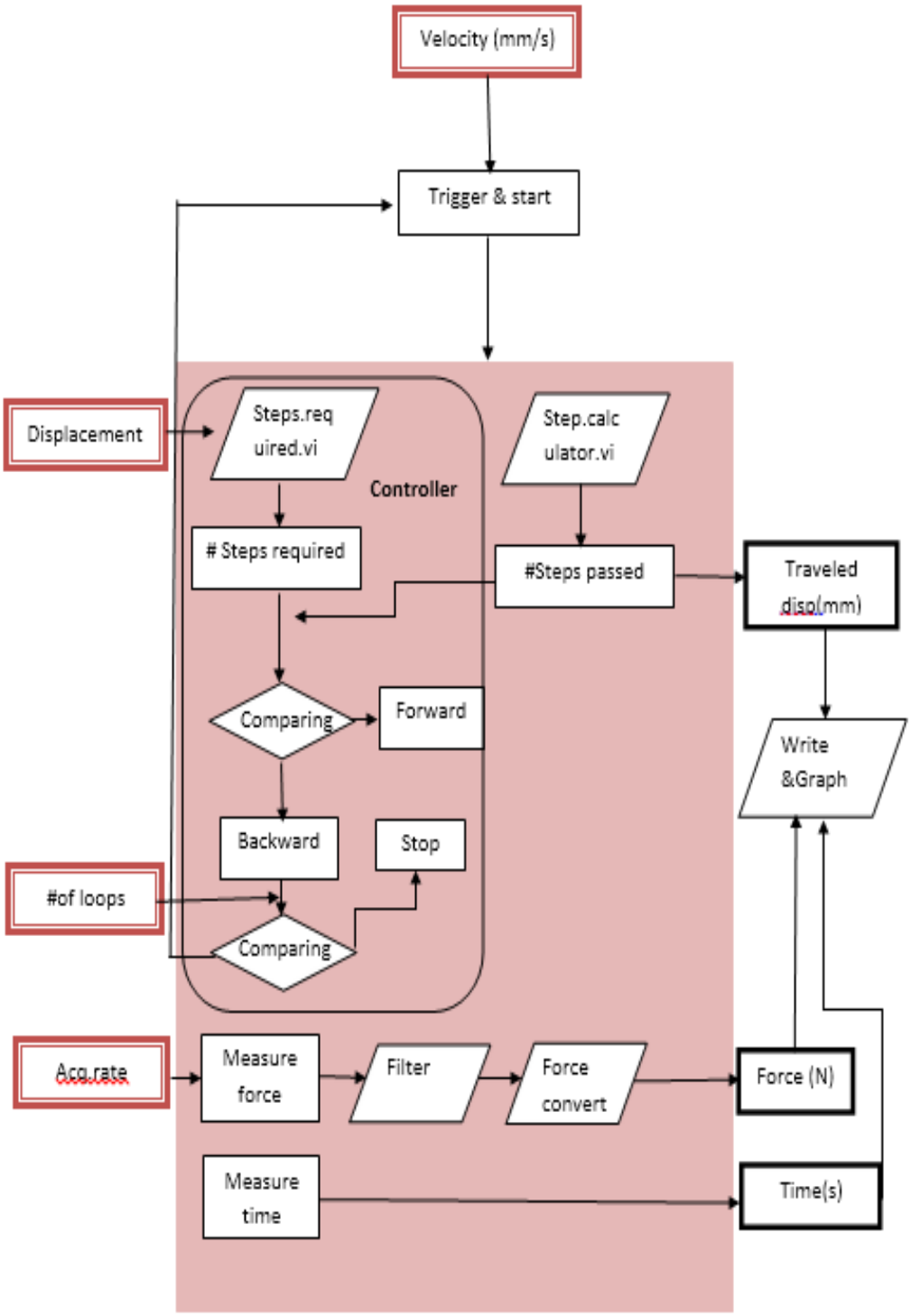

B.7.Force controlled cyclic loading test block diagram:

This block diagram is used for force-rate controlled cyclic loading test of soft tissue indenter setup. Duration for cycles [s], force threshold amount and force-rate value [N/s] which will be kept constant by a P-controlled closed loop system can be given as inputs by the user. One of the counter pins of NI USB-6212 data acquisition card is used for driving the stepper motor. Two differential analog pins are used to read load cell data continuously. After receiving the data, in order to get rid of its noise, acquired voltage values from the load cell (in mV) are filtered. Those filtered values are converted into newton [N] and compared with the input force value at current time. After comparing these, a signal is generated and sent to the motor direction pin in order to choose the desired direction (either forward or reverse). If the applied force is not in the desired range, a digital I/O pin is triggered which enables pulse generation from the counter pin for driving the motor.

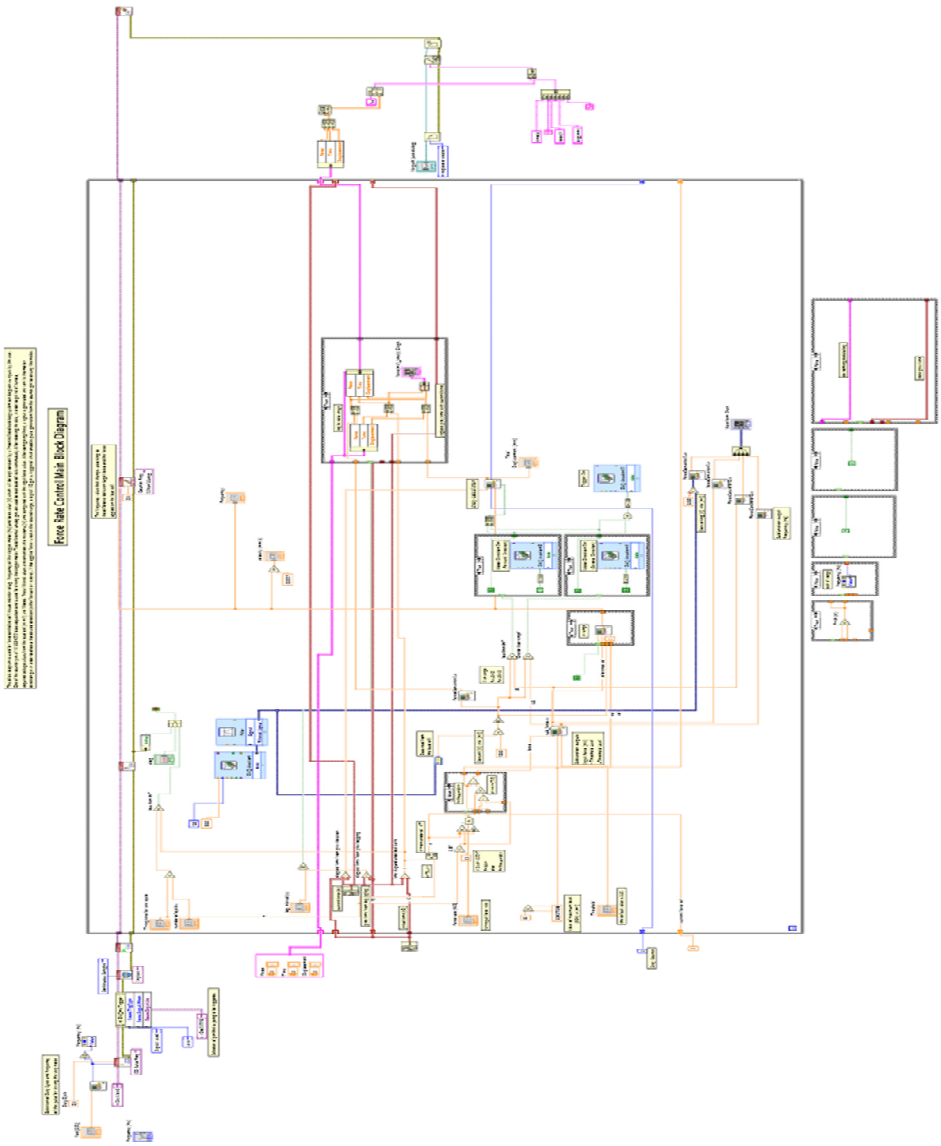
Rotor Rate Control Main Block Diagram

B.8.Fore-rate controlled cyclic loading flowchart:

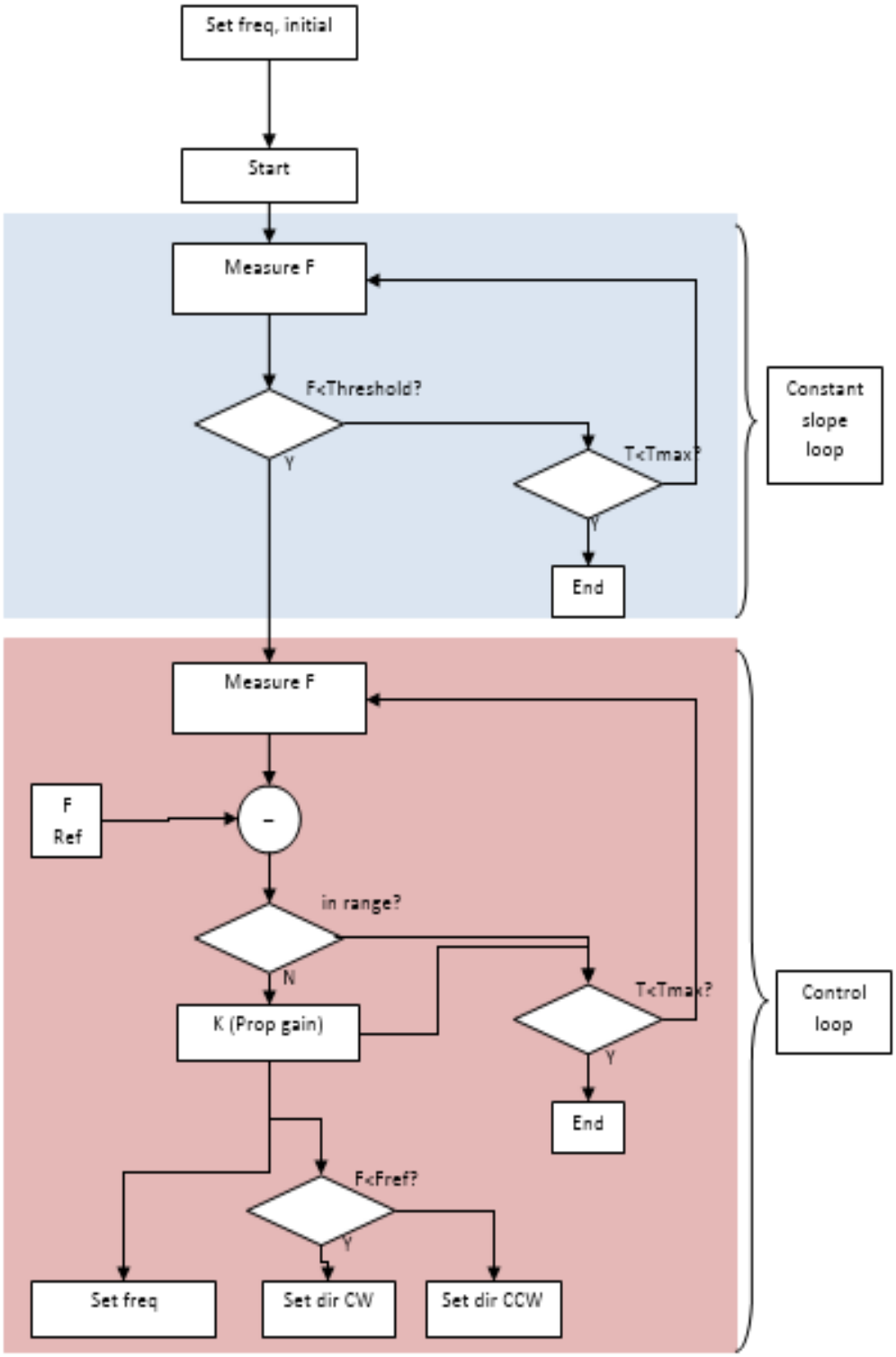

B.9.Creep test block diagram

This block diagram is used for force controlled creep test for soft tissue indenter setup. initial speed value [mm/s] ,experiment time, target force value [N] which will be kept constant by a proportional-controlled closed loop system, and threshold value of target force, can be given as inputs by the user. One of the counter pins of NI USB-6212 data acquisition card is used for driving the stepper motor. Two differential analog pins are used to read load cell data continuously. After receiving the data, in order to get rid of its noise, acquired voltage values from the load cell (in mV) are filtered. Those filtered values are converted into newton [N] and compared with the input force value. After comparing these, a signal is generated and sent to the motor direction pin in order to choose the desired direction (either forward or reverse). If the applied force is not in the desired range, a digital I/O pin is triggered which enables pulse generation from the counter pin for driving the motor.

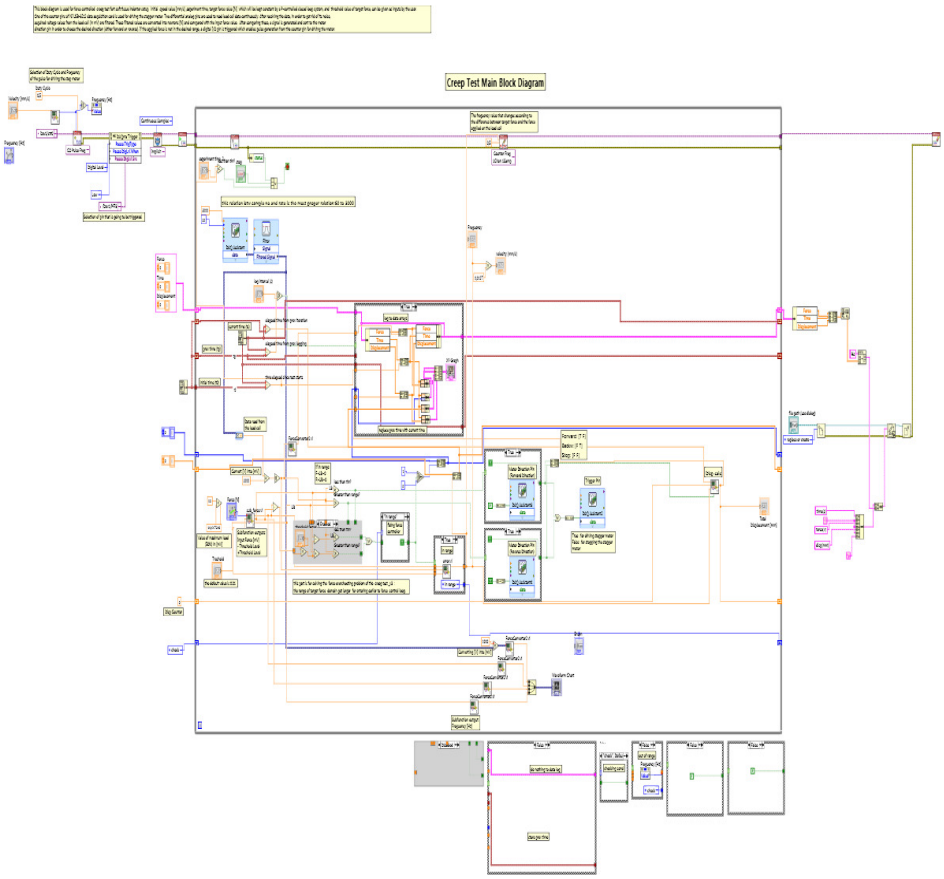
Creep Test Main Block Diagram

B.10.Creep code flowchart:

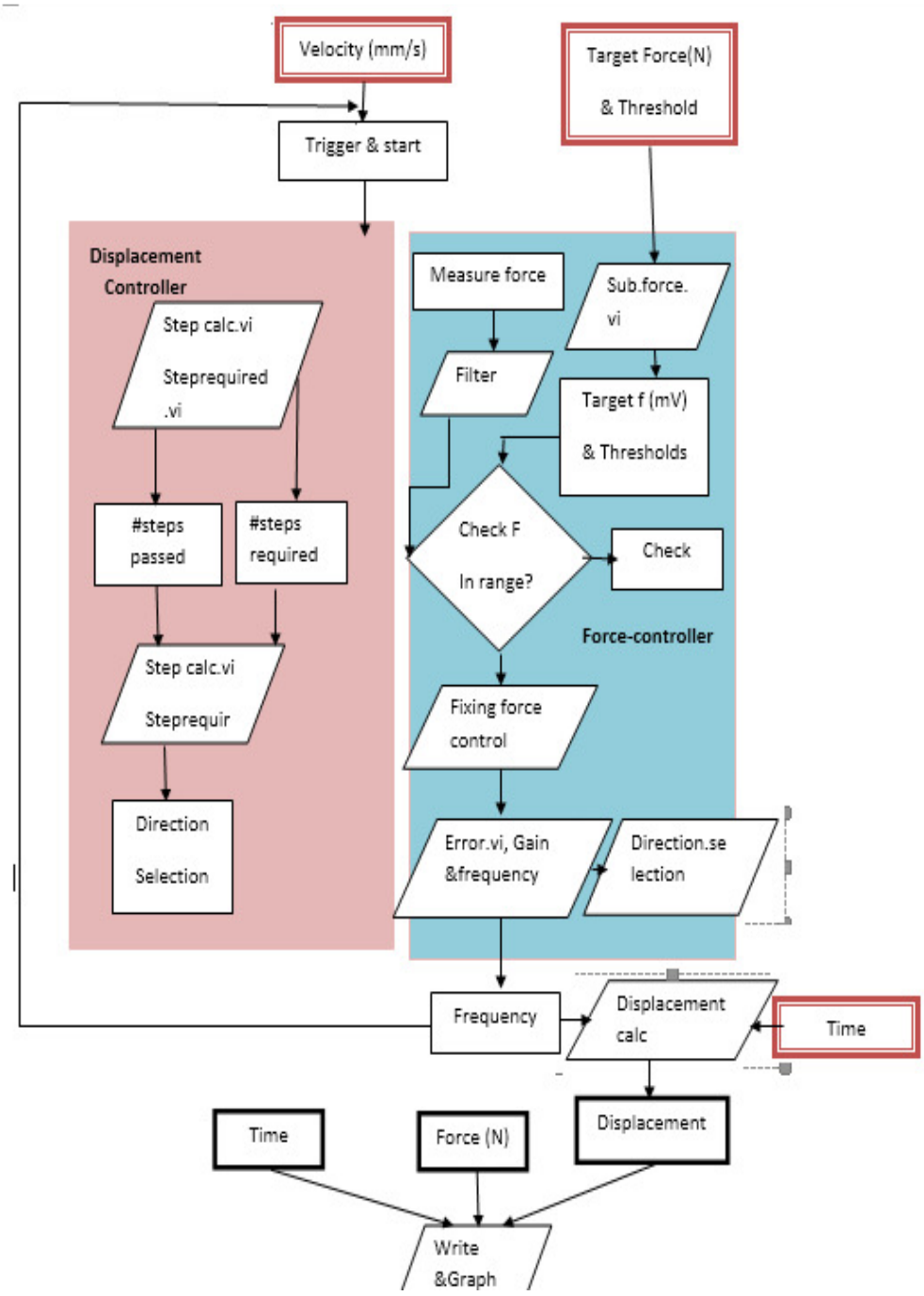

B.11.Relaxation test block diagram:

The algorithm that is used for the open loop relaxation test is quite similar to the one used for cyclic loading test. After taking the necessary inputs from the graphical user interface, velocity which is taken as mm/s is converted into frequency, by the help of a velocity converter sub vi. After obtaining the frequency and specifying the duty cycle to be 0.5, pulses are created from the pulse generator block. Pulses are generated again by changing the state of the digital I/O pin which is used as the trigger pin. Making the state of this pin high, drives the stepper motor until the desired position is reached. The input displacement value is converted into required step number by StepsRequired sub vi and this value is again compared with the number of steps that has already passed which is calculated by StepCalculator sub vi. If motor has not reached the desired position, it is driven towards forward until the number of steps becomes equal to the required number of steps. When they are equal, DirectionSelection sub vi creates a backward signal that makes the state of the second case structure true. Within this case structure, motor remains stationary until relaxation time duration is reached then its direction is reversed and the motor is triggered again until it fully retracts to its original position. All these actions are enclosed by a while loop which enables real time data acquisition. During the whole relaxation test, from the analog inputs AI0-AI8 which are differential pairs, load cell is continuously read and then filtered by the lowpass filter block. ForceConverter.vi then, converts the data read from the load cell from [mV] to [N] scale. This block is then connected to the waveform chart and the change of force vs. time is displayed in the graphical user interface.

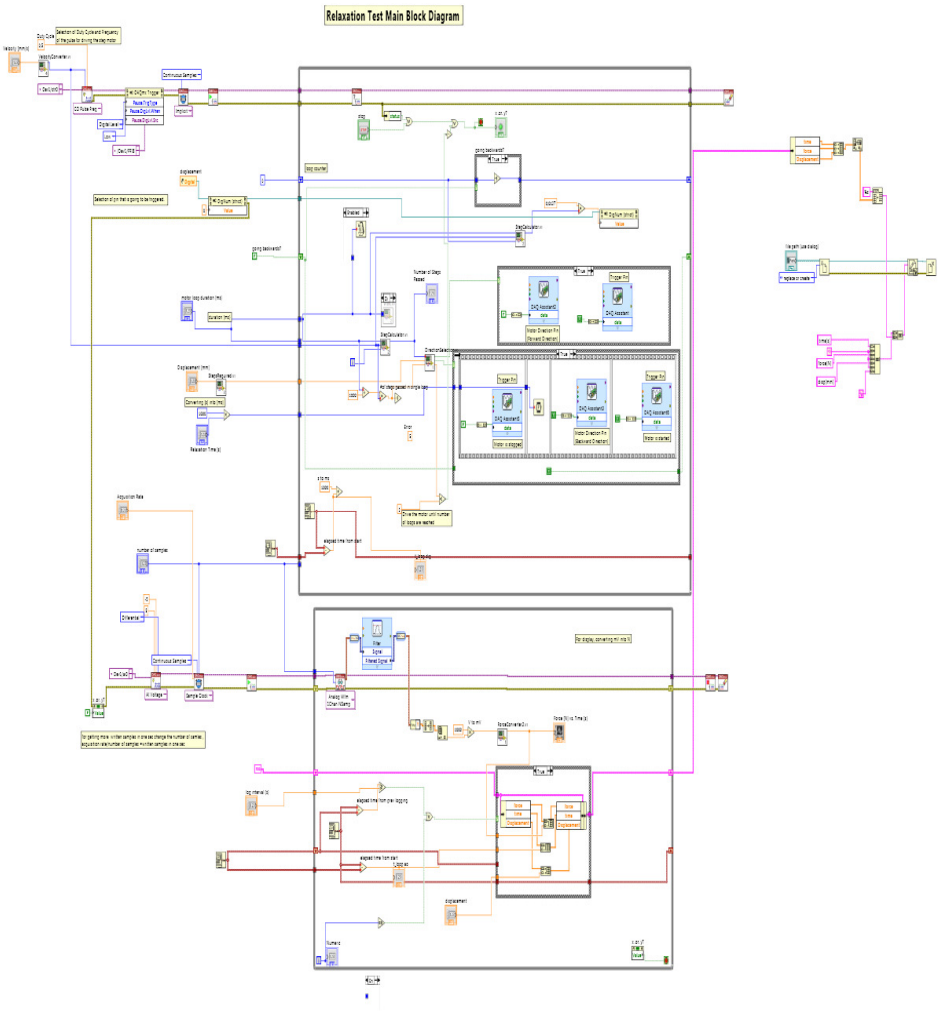
Relaxation Test Main Block Diagram

B.12.Relaxation code flowchart:

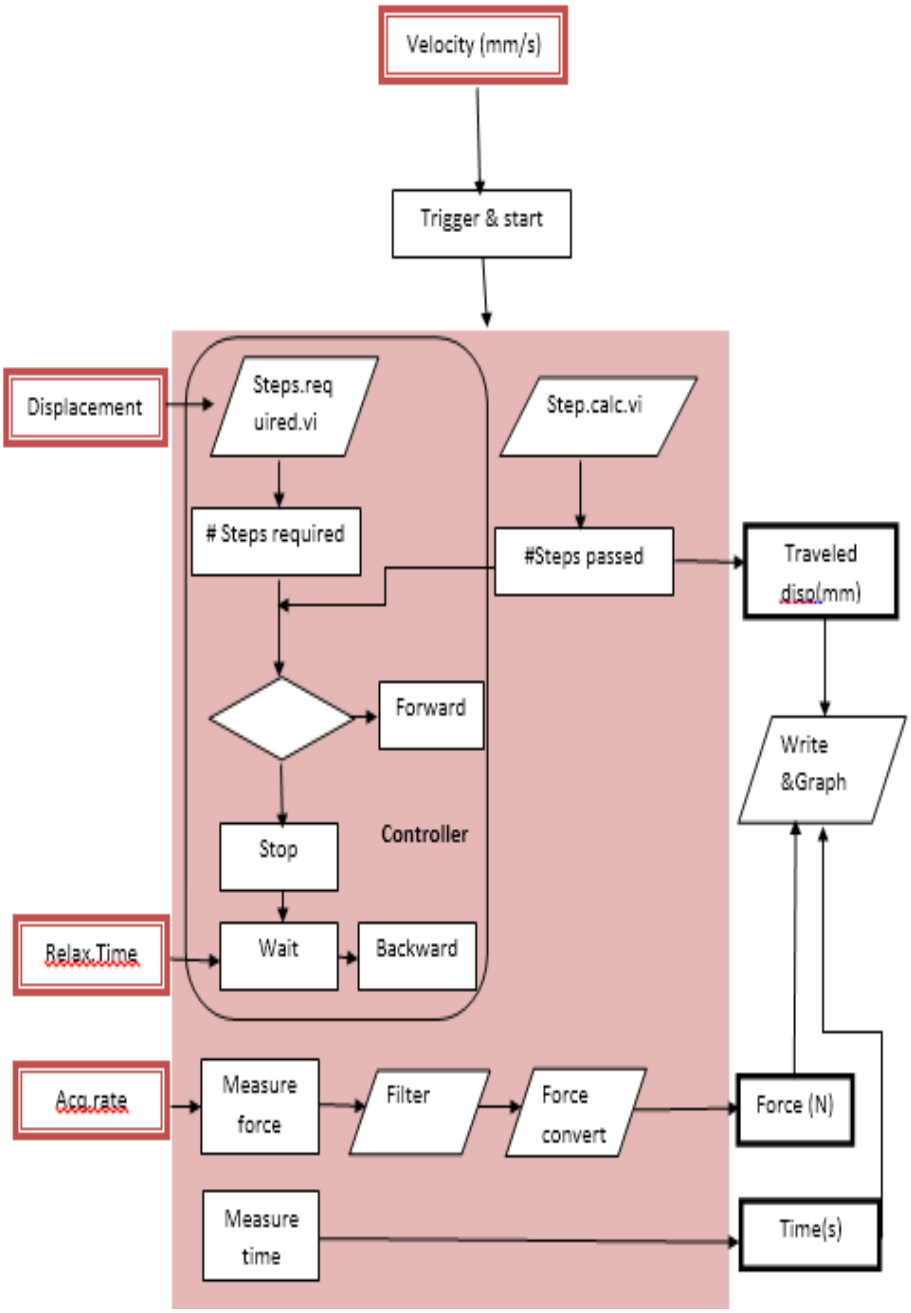

C.USER MANUAL

Operation Manual

- Connect the USB cable of the Data Acquisition Card to the computer that will be worked with, and check the light of the Data Acquisition Card near the USB cable socket if it is turned on,
- Connect the power cable of the stepper motor using the specified adapter,
- Place arm of patient on the arm fixing part such that bony parts of arm near wrist and elbow touch the fixed pins, and then gently screw the moving pins to the fixed pins until all possible motions of arm are restricted,
- Open Step motor manual control.vi and adjust the position of the indenter tip by running the program and pressing the buttons on the system,
- Open the test program of the related experiment on LabVIEW,
- Enter the required inputs for the experiment.

To run the Soft Tissue Indenter,

- Click the run button of the front panel of the LabVIEW.
- Change the “Motor loop duration” between 20 ms and 100 ms, due to input values. Do NOT decrease this value lower than 20 ms in order to accurate movement of device.
- In creep test the “Threshold factor” is for pre-entering into force controlled closed loop. The proper value for this factor is values between 2 and 4.
- In force-controlled codes (creep and force rate controlled cyclic loading) the maximum written number of samples was kept as 50 samples per second, with 60 to 3000 data points and rate values. Lower than 60 may cause errors.

To obtain the output data,

- Right click on the Waveform Chart on LabVIEW, and export the graph to the desired platform such as Excel or Simplified Image.
- Also written force, time, and displacement data are available in text files with defined path in each experiment's code.
- Change the value of "number of samples" and "rate" for changing the number of written samples in one seconds. For example with 50, and 5000 values the written number of samples per second is 100 sample.
- Also log interval value is used for decreasing the number of written samples. For obtaining the maximum data in defined rate of sampling, this value should be zero.

Necessary Precautions,

- Do not exceed the force level of the load cell which is 50N during the experiment. Otherwise, the load cell can be damaged,
- Do not supply more than 12V to the stepper motor. Otherwise, the stepper motor can be damaged,
- Unplug the power cable for the stepper motor when it is not in operational mode. Otherwise, the stepper motor can get extremely hot.

Maintenance Manual

- Check all the wire connections between the data acquisition card, the stepper motor, and the load cell,
- Lubricate the rail guide regularly,
- Check the bolt connections,

D.MATLAB ALGORITHM USED FOR CURVE FITTING

For curve fitting of experimental data to the relaxation and creep models, Cftool of MATLAB (2010b) was used. The related MATLAB code is as following:

```
clc
clear all
    [filename, pathname] = uigetfile( ...
    {'*.xlsx;*.dat;*.txt','Data Files
(*.xlsx,*.dat,*.txt)';
     '*.*',  'All Files (*.*)'}, ...
     'Select a data file');
Data = importdata(fullfile(pathname,filename)); %data
file may include any characters plus a set of data
(x,y)

Data=(Data.data.Sheet1);

t = Data(:,1);
y = Data(:,2); %same as E(t)
% axis([0 2 -0.5 6])
% hold on
plot(t,y,'ro')
title('Data points')
% hold off
cftool
%F = @(x,xdata)x(1)*exp(-x(2)*xdata) + x(3)*exp(-
x(4)*xdata); % desired function
%F= @(x,xdata)x(1)+(x(2)-x(1))/()

%x0 = [1 1 1 0]; % initial guess for parameters


%[x,resnorm,~,exitflag,output] = lsqcurvefit(F,x0,t,y)

%hold on
%plot(t,F(x,t))
%hold off
%Er+(Eg-Er)/(1+x/Tav)^alpha
% E1/gamma(1-alpha)*(x^alpha)
```

```
%F0*(1-delta1*(1-exp(-x/tav1))-delta2*(1-exp(-x/tav2)))
%d0*(1+deltaprim1*(1-exp(-x/tavprim1))+deltaprim2*(1-
exp(-x/tavprim2)))
% run the code,then import the excel file in two
column(t and y)
```

After running this code and importing the required excel data in fitting > fit editor, type of fit was chosen as "Custom Equations", then in New> General Equations part, the related formula was pasted. The following figure is an example for Prony series equation and it's parameters for relaxation experiment.

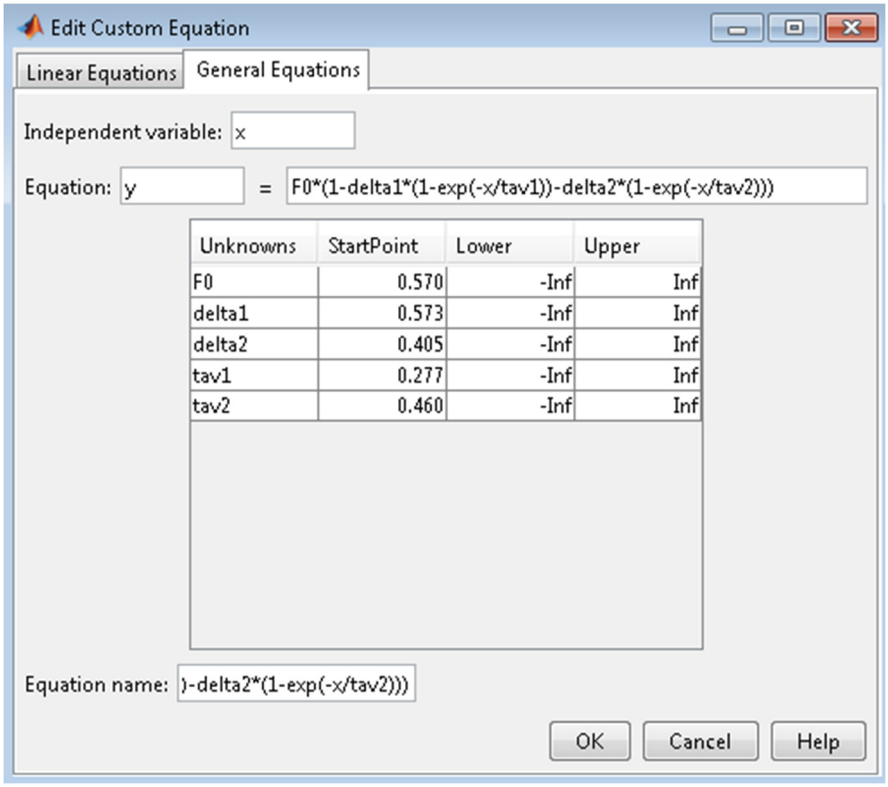

Figure. D. 1.Custom Equations window

Cftool has different fitting algorithms. Trust Region Method is the most powerful one and is the evolution of Levenberg-Marquardt. This method is the default method for non-linear curve fitting and is able to follow the negative curvature of objective function. This method can accept bounds on the fit parameters in contrast

to the Levenberg-Marquardt method though without a requirement for good initial guesses this method is able to fit the model very better than the other methods. In the Curve Fitting app, click the Fit Options button to open the Fit Options dialog box. The following window will be appear:

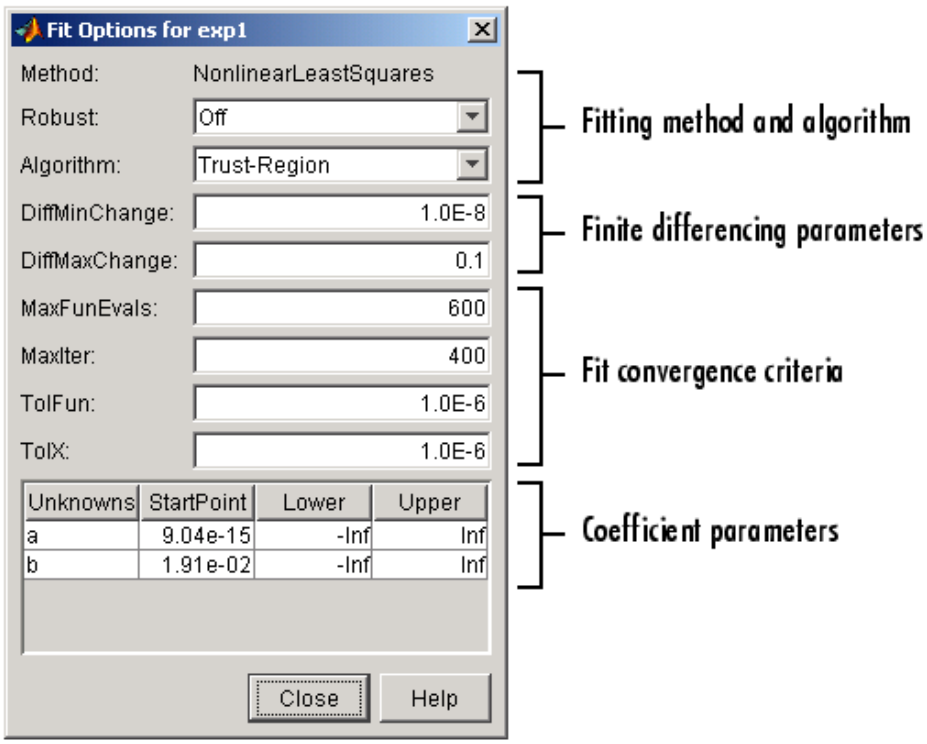

Figure. D. 2. Fit options window

The meaning of appeared parameters in “Fit Options” window, are as following:

Fitting Method and Algorithm

Method — The fitting method.

The method is automatically selected based on the library or custom model you use. For nonlinear models, the method is NonlinearLeastSquares.

Robust — Specify whether to use the robust least-squares fitting method.

Off — Do not use robust fitting (default).

On — Fit with the default robust method (bisquare weights).

LAR — Fit by minimizing the least absolute residuals (LAR).

Bisquare — Fit by minimizing the summed square of the residuals, and reduce the weight of outliers using bisquare weights. In most cases, this is the best choice for robust fitting.

In in this study, the Robust fitting was not used.

Algorithm — Algorithm used for the fitting procedure:

Trust-Region — This is the default algorithm and must be used if you specify Lower or Upper coefficient constraints.

Levenberg-Marquardt — If the trust-region algorithm does not produce a reasonable fit, and you do not have coefficient constraints, try the Levenberg-Marquardt algorithm.

Finite Differencing Parameters

DiffMinChange — Minimum change in coefficients for finite difference Jacobians. The default value is 10-8.

DiffMaxChange — Maximum change in coefficients for finite difference Jacobians. The default value is 0.1.

Note that DiffMinChange and DiffMaxChange apply to:

Any nonlinear custom equation, that is, a nonlinear equation that you write

Some of the nonlinear equations provided with Curve Fitting Toolbox software

However, DiffMinChange and DiffMaxChange do not apply to any linear equations.

Fit Convergence Criteria

MaxFunEvals — Maximum number of function (model) evaluations allowed. The default value is 600.

MaxIter — Maximum number of fit iterations allowed. The default value is 400.

TolFun — Termination tolerance used on stopping conditions involving the function (model) value. The default value is 10-6.
TolX — Termination tolerance used on stopping conditions involving the coefficients. The default value is 10-6.
These values were increased due in order to obtain a successful convergence.

Coefficient Parameters

Unknowns — Symbols for the unknown coefficients to be fitted. For Prony series the number of these parameters were 5 and for fractional power law there were 4 parameters to be identified.
StartPoint — The coefficient starting values. The default values depend on the model. For custom models, default values are randomly selected within the range [0,1].
Lower — Lower bounds on the fitted coefficients. The tool only uses the bounds with the trust region fitting algorithm. The default lower bounds for most library models are -Inf, which indicates that the coefficients are unconstrained. For Fractional Power Law this bound for α parameter was 0. For Prony series fitting to creep and relaxation experimental data this bound is used for τ_1 and τ'_1, and for τ_2 and τ'_2 parameters as 10^{-5}. In some cases because of error in finding the fit, for τ_2 and τ'_2 this amount was chosen as 3 or 5, because the amount of these parameters are more than 50 and this bounding helps to Matlab to find the fit.
Upper — Upper bounds on the fitted coefficients. The tool only uses the bounds with the trust region fitting algorithm. The default upper bounds for all library models are Inf, which indicates that the coefficients are unconstrained. In Fractional Power Law this bound is 1 for α and for τ_2 and τ'_2 this bound was chosen as 10^5, again for preventing the fitting errors.

At the end of successful fitting the parameters were obtained. The goodness of fit were defined by obtained SSE (sum of squared errors between the model and

experimental data) and R^2 (R-squared) amounts. The R-squared amount for exact fit is 1, thus better fits have R-squared amounts closer to 1.

E.PUBLICATIONS

Süleyman Demirel Üniversitesi
Fen Bilimleri Enstitüsü Dergisi
Suleyman Demirel University
Journal of Natural and Applied Science
18(SI: Biomechanics), 10-20, 2014

Indentation and Observation of Anisotropic Soft Tissues Using an Indenter Device

Parinaz ASHRAFI [*1,2], Ergin TÖNÜK [1,2,3]
[1] Department of Biomedical Engineering, Middle East Technical University, 06800 Ankara, Turkey
[2] BIOMATEN, CoE in Biomaterials and Tissue Engineering, METU, 06800 Ankara, Turkey
[3] Department of Mechanical Engineering, Middle East Technical University, 06800 Ankara, Turkey

(Received: 12 September 2014, Accepted: 27 November 2014)

Keywords
Indentation
Soft Tissue Modeling
Anisotropic Tissue

Abstract: Soft tissues of human body have complex structures and different mechanical behaviors than those of traditional engineering materials. There is a great urge to understand tissue behavior of human body. Experimental data is needed for improvement of soft tissue modeling and advancement in implants and prosthesis, as well as diagnosis of diseases. Mechanical behavior and responses change when tissue loses its liveliness and viability. One of the techniques for soft tissue testing is indentation, which is applied on live tissue in its physiological environment. Indentation affords several advantages over other types of tests such as uniaxial tension, biaxial tension, and simple shear and suction, thus it is of interest to develop new indentation techniques from which more valid data can be extracted. In this study a new indenter device was designed and constructed. Displacement and force rate cyclic loading, and relaxation experiments were conducted on human arm. The in-vivo force rate controlled cyclic loading test method which is novel is compared with the traditional displacement controlled cyclic loading tests. Anisotropic behavior of tissue cannot be determined by axi-symmetric tips, therefore ellipsoid tips were used for examining anisotropy and in-plane material direction of bulk soft tissues.

Eşyönsüz Yumuşak Dokuların İndentör Cihazı Kullanılarak İndentasyonu ve Gözlemi

Anahtar Kelimeler
İndentasyon
Yumuşak Doku Malzeme
Eşyönsüz Doku

Özet: İnsan bedeninde iskelet dışındaki neredeyse tüm dokular yumuşak dokulardır. Yumuşak dokuların mekanik davranışı çoğu mühendislik malzemesinden farklı ve daha karmaşıktır. Yumuşak doku mekanik özelliklerinin belirlenmesi ve malzeme modeli oluşturulması implantlar, protez ve ortezler ve hatta tanı koyma açısından önemlidir. Öte yandan yumuşak dokuların canlılığını kaybetmesi ile mekanik özelliklerinde farkedilir değişiklikler meydana gelir. Yumuşak doku mekanik özelliklerini belirlemek için kullanılan deneysel yöntemlerden birisi de indentasyondur. İndentasyonun tek veya iki eksenli çekme, kayma, emme gibi yöntemlere göre belirli avantajları olduğu bilindiğinden daha iyi veri almak üzere yeni indentasyon deneyleri geliştirlmesine gerek duyulmuştur. Bu çalışma kapsamında yeni bir indentör cihazı tasarlanıp üretilmiş, devirli yükleme, gevşeme ve sünme deneyleri yapılarak deneysel veriler incelenmiştir. İndentör cihazının göncellenen yapısı nedeniyle toplanan veri daha temizdir. Mullin (alışma) etkisi, viskoelastisite, eşyönsüzlük gibi özellikler gözlenebilmektedir. Sünme ve kuvvet denetimli yükleme deneyleri bu sistem aracılığıyla yapılabilmektedir. Dokuların eşyönsüz özelikleri olduğu bilindiğinden eksenel simetrik olmayan uçlarla düzlemsel eşyönsüzlük hakkında bilgi edinilmektedir. Ayrıca kuvvet denetimli deneyler ile yer değiştirme denetimli deney sonuçları incelenmiştir.

* Corresponding author: Parinaz.Ashrafi@metu.edu.tr

1. Introduction

Soft biological tissues have complex structures with complicated physiology .They display very different mechanical behavior in comparison to the traditional engineering materials. For improvement of soft tissue constitutive modeling and improvement in implants and prosthesis designing, as well as diagnosis of diseases, it is needed to perceive the mechanical behavior of soft tissues. For this there is a need for reliable constitutive equations that formulate and model the material behavior. Mechanical modeling relies on parameters that must be determined from experiments with determined boundary conditions, so to allow the inverse problem to be solved. Due to this aim it is needed to carry out tests and collect experimental information about the mechanics of the material. Recorded time-force-displacement data and determined geometry and boundary conditions were the input data used to evaluate the mechanical properties and to determine the constitutive model.

Many models exist in literature but because of the peculiar behavior of the live soft biological tissues, a completely acceptable model has not been proposed yet. Most of the existing models hardly simulate all experimentally observed behavior and some models are deficient in modeling even basic features (Zheng et al., 1999), and that is due to lack of the reliable experimental results. It is possible to conduct mechanical experiments on soft biological tissues by different methods. Most of the experimental data reported in the literature so far have been obtained ex vivo (Ahn & Kim, 2010; Carson et al., 2011; Fu & Chui, 2014; Seifzadeh et al., 2012; Zhang et al., 2014). Ex vivo measurements are obviously easier to perform and conditions can be made more repetitive these data are less accurate for realistic mechanical modeling since the properties of a living organ can change after removal from its natural environment with e.g. an intact blood perfusion and adequate water content of the tissue (Nava et al., 2008). In this study, in-vivo tests were conducted. In the in-vivo tests organ is studied at its original place and while it is alive. These two basic factors make in-vivo method as an ideal approach because firstly mechanical behavior and responses change when tissue loses its liveliness and viability. Secondly surrounding of the tissue, has great influence on the mechanical behavior of the tissue, thus the response of tissue in its original place is different than of it in separate place. Fung(1984) explains this fact during tests on blood vessels. In the studies carried out on pig brain (Gefen & Margulies, 2004) and on pig liver (Ottensmeyer et al., 2004) different in-vivo and ex-vivo test methods were conducted and compared. In Geffen and Margulies the nearest result to in-vivo test obtained in the ex-vivo perfused test and for stable cases, it showed a deviation of 17%. This deviation was above 50% forunperfused ex-vivo test.For these reasons, research in this area has been recently focused on examination of mechanical behavior of soft tissues in a living state and within the body(in vivo)(Carter et al., 2001; Kauer 2001; Ottensmeyer, 2001; Samur et al., 2007).

Nevertheless there are some identified disadvantages of in-vivo indentation that should also be considered; For avoidingany detriment and harm, tests are carried out only on external organs of subjects, such as skin, though studies on the internal organs by employing non-invasive methods are alsopossible, yet the nonlinear properties of tissue would not be properly characterized and only a linear stress-strain relation would be observed. (Ottensmeyer 2002). Another difficulty is that due to not having a regular geometry of cross-section of tissue sample, boundary conditions, and loading direction, instead of simple calculation oneneeds advanced techniques like inverse finite element method for obtaining stress-strain relations (Hu et al., 2011; M Kauer, 2002; Kim, 2004; Samani & Plewes, 2004; Tönük & Silver-Thorn, 2004)

It is possible to carry out experimentsonsoft biological tissues by using different devices. Nava et al. (2008) used an aspiration device to conduct in-vivo suction tests on human liverduring open surgery. Compressive force exerted by the surgeon during the measurements in order to ensure a good initial contact between aspiration device and liver surface caused uncertainties.Indentation tests are frequently used in the investigation of the mechanical properties of soft biological tissues (Choi & Zheng, 2005; Korhonen, 2003; Yin et al., 2004). Pailler-Mattei et al. (2008) used an original light load indentation device to study in vivo the mechanical properties of human skin. Cox et al. (2008) used indentation tests with varying indenter sizes on linear elastic rubbers and compared to tensile tests on the same specimen for modeling of synthetic heart valve. Eight carotid atherothrombotic plaque samples harvested from patients were studied by indentation tests by Barrett et al. (2009). In Ahn & Kim, (2010), soft tissue indentation loading experiments on porcine livers were performed to measure the surface deformation and force response of tissue with various indentation depths and two different tip shapes. Fath El Bab et al. (2010) proposed a sensor with two probes configuration to address dependency on the pushing distance. Carson et al. (2011) used spherical indentation tests for ex vivo material characterization of prostate tissue. In Chao et al. (2010) a tomography-based air-jet indentation system was used for examination of forefoot plantar soft tissue and compared with resulting obtained from tissue ultrasound palpation system. W.-M. Chen et al (2011) developed an instrument-driven tissue

tester that includes a portable motorized indenter within a special foot positioning apparatus for in vivo tests. Van Dommelen et al. (2010) conducted indentation experiments for comparing white matter and grey matter brain tissue.Iivarinen et al. (2011) compared the indentation stiffness ofin relaxed, physically stressed and oedemic human forearm by using a hand held stiffness meter. An optoelectromechanical tissue indenter was used by Luo et al. (2011) during experiments on human heel. Prevost et al. (2011) compared the results of in-vitro, in-vivo and in in-situ indenter tests on porcine brain tissue. Fu & Chui, (2014) combined compression and elongation data obtained from in vitro tests on porcine liver tissue for indentation simulations.

Indentation can be used in all test methods such as, in-vivo, ex-vivo, thus comparative studies are feasible. Zhang et al. (2014) conducted in vitro swine brain indentation tests. Yao et al. (2014) developed a spherical indentation technique to measure the time-dependent material properties of human cervical tissue taken from patients undergoing hysterectomy.

Indentation is the most suitable technique for in-vivo test method. During indentation tests viscoelasticity, relaxation, creep and in-plane anisotropy can be observed therefore important mechanical properties of tissue can be examined. Indentation affords several advantages over other types of in vivo tests such as uniaxial tension, biaxial tension, simple shear and suction, thus it is of interest to develop new indentation techniques from which more valid data can be extracted (Bischoff, 2004). During these tests the tip of indenter device moves forward toward the tissue and simultaneously records time, tissue reaction force and tip displacement.

In this study an indenter device was designed and constructed. Common soft tissue behaviors such as preconditioning effect and anisotropy were observed. The in-vivo force rate controlled cyclic loading test method which is novel is compared with the traditional displacement controlled cyclic loading tests.

Most biological tissues are characterized by anisotropy (Kroon & Holzapfel, 2008; Pandolfi & Vasta, 2012; Peña et al. 2008). Since soft tissues are composed of different materials, like elastin and collagen, in different combinations, soft tissue properties are direction dependent (Samur et al, 2007). The anisotropic characteristics of soft tissues arise due to the preferred orientation and distribution of the collagen fibers (Lokshin & Lanir, 2009). For example, transverse anisotropy is observed in nanofibrillar collagen scaffold that mimic the structure of collagen organization in blood vessels (Huang et al., 2013; Argatov et al., 2015). This important characteristic cannot be observed by using circular indenter tips, the use of axially symmetric tips for estimating material properties ignores pronounced anisotropy. Feng et al. (2013) proposed combination of dynamic shear tests with subsequent asymmetric indentation tests on the same sample, to measure the anisotropy of brain tissue. Bischoff (2004) in a computational study used ellipsoidal tips, and displayed anisotropy in his results. Petekkaya (2008) used these ellipsoidal tips in his experimental study.

2. Materials and Methods

2.1. Subjects and Equipment

A group of eight young subjects all having a normal healthy condition (age 25-29) voluntarily contributed to the study. The experiments were performed under the approval of the Ethics Committee of Middle East Technical University (Ankara- Turkey).

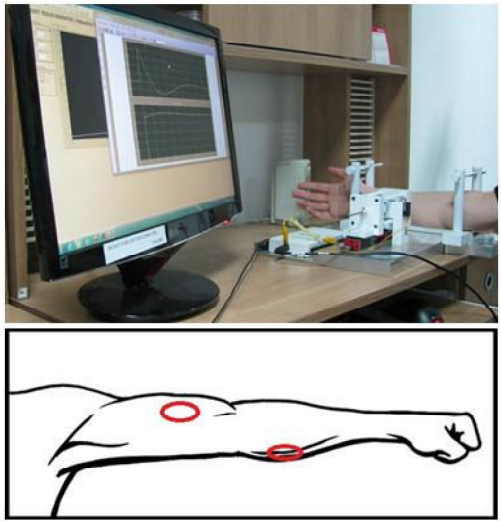

Figure 1. Indenter device set up and indentation regions on arm.

Experimental data was acquired using a soft tissue indenter designed and manufactured in METU. It is designed to make in vivo (on live body) measurements on human arm. After fixing the arm device indents a predetermined point on it with forward and backward movements. The arm is at rest and lay on a mechanical support during each experiment. Indenter set up and indentation regions on arm are presented in Figure (1). The indentation force, displacement, and time are measured and controlled via a load cell, step motor and data acquisition system. For this Haydon switch hybrid stepper motor (28000 series size 11), Honeywell ELPF-T1-M-50N load-cell and AD620 amplifier was selected. For real time data collection a computer code with a graphical user interface was developed in LabVIEW programming software (version 11.0) and NI-6212 (16-bit resolution) data acquisition card

with chosen input sampling rate between 50 to 100 samples per second (S/s) was used. Resolution requirements for force and displacement were 5mN and 2μm. Ellipsoidal tip made of a polymer (polyamide) wasused for indenting tissue during experiments. The top and front view of the contact surface of tip is illustrated in Figure (2). The dimensions are: Rx=6mm, Ry=1.5 mm, Rz=1.5 mm

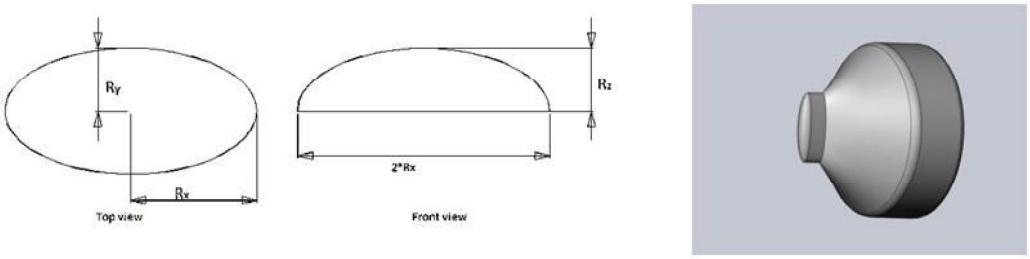

Figure 2. Indenter tip used in anisotropy tests; R_x=6mm, R_y=1.5 mm, R_z=1.5 mm

2.2. Experiment Procedure

2.2.1. Displacement rate controlled cyclic loading experiments

In this test, various scrutiny were made using two groups of data that are force-time and force-displacement. Soft biological tissues display preconditioning effect (Mullin's effect) under cyclic loading. During first load cycles tissue is more stiff and resistant to force, by repeating the cycles the reaction of tissue changes and shows repeatable and comparatively compliant response.

In "displacement rate controlled mode", the amount of displacement is kept constant and force vs. time and force vs. displacement characteristics of the soft tissue are examined. Motor speed [mm/s], the displacement [mm] and number of cycles have to be taken as inputs by the help of the graphical user interface in LabVIEW. 5mm/s motor speed,15 mm displacement and 15 loops were chosen as inputs for the tests.

2.2.2. Force rate controlled cyclic loading experiments

In "force rate controlled mode", the amount of force rate is kept constant [N/s], and displacement-time and force-displacement characteristics of the soft tissue areexamined. For example if input is 1 N/s and the cycle duration time is 10s, in 5s the indenting force linearly increases to 5N (the peak force of cycle) and then it linearly decreases back to zero force. The test is repeated until the desired number of cycles is reached. Therefore, in order to perform this test, parameters such as force rate [N/s], the time duration for every cycle, and number of cycles have to be taken as inputs by the help of the graphical user interface. In addition to these inputs the value of threshold to define tolerance domain of target force is also defined as user's input parameter. The values used for the experiments were, force rate1.8N/s, duration was 6s for every cycle,15 loops, and a force tolerance of 0.01 N were chosen as inputs for the tests.

2.2.3. Relaxation experiments

In this test, after initial indentation the amount of displacement (penetration into tissue) was kept constant and the response of tissue was observed. After going forward and reaching the required input displacement into the soft tissue, the stepper motor and indenter tip was dwelled until input relaxation timeis reached and then at the end of this time indenter device is retracted. The input parameters to this test are the amount of displacement [mm], the speed of the motor [mm/s] and relaxation time [s]. Here the tests were conducted on forearm with 5 mm/s motor speed,6 mm displacement and 60 seconds relaxation duration. Due to sensitivity, relaxation experiments should be conducted in a noiseless environment. They are extremely influenced by muscle movements during relaxation time.

2.2.4. Determination of material directions and in-plane anisotropy

In literature, flat-ended cylindrical (Choi et al., 2008), spherical (Dimitriadis 2002), conical (Pelletier et al., 2006), pyramidal (Borodich et al., 2003) and cylindrical lateral (Argatov et al., 2015) that uses the lateral contact of a cylindrical indenter are widely used. The response of tissue to loads are different depend on the direction, this behavior cannot be determined by axi-symmetric tips, therefore ellipsoid tips which are theoretically examined by Bischoff (2004), and first experimentally used byPetekkaya et al. (2010) were used.

The long axis of the ellipsoidal indenter tips was placed parallel to the longer axis of the biceps muscle and cyclic loading tests were conducted in

every 30 degree up to 180 and a 210 degree for control. In these tests, for eliminating the preconditioning effect at first, 20 loops of cyclic loading were conducted at apre-determined point of muscle then the real tests were conducted consequently without waiting for the soft tissue to recover. Response of biceps muscle in different indenter tip alignments, to the same displacement controlled cyclic loading test were examined. The tests were carried out at same point with 5mm/s, 12 mm (test2) and 15mm (test1) tissue displacement with an ellipsoidal indenter tip. Displacement values of biceps muscle in every 30 degree indenter tip alignments, to the same force controlled cyclic loading test were examined. The tests were carried out at same point with 1N/s force rate,5 loops and 100s total experiment time.

3. Results

3.1. Displacement Rate Controlled Cyclic Loading Test Results

Mullin's effect in force-time graph shows up as a decrease in force; the force value drops progressively as time goes by and tends to an equilibrium value as time goes to infinity (Figure 3). Because of breathing and sensitivity of loadcell, in last cycles the exact equilibrium constant force was impossible to catch.

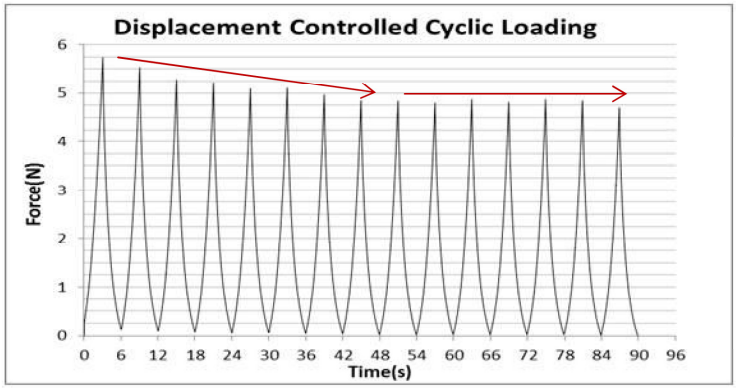

Figure 3. Displacement controlled cyclic loading test with 5 mm/s velocity,15 mm displacement and15 loops

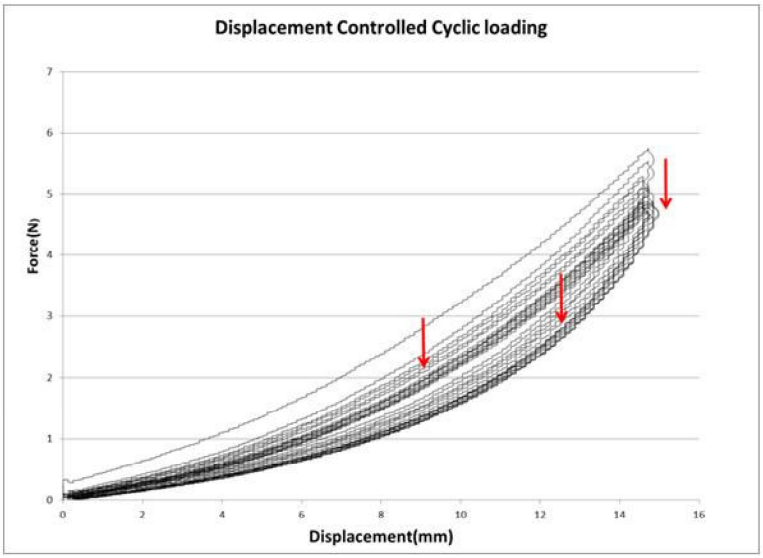

Figure 4. The observed downward shift in Hysteresis of cyclic loading test

3.2. Force Controlled Cyclic Loading Test Results

Mullin's effect on soft tissue during force controlled cyclic loading test was examined. The illustrated preconditioning effect observed in displacement-time and force-displacement graph is different than of it in displacement rate controlled cyclic loading tests. In displacement-time graph, as expected there was an increase in the displacement with progressing cycles that means a decrease in stiffness of tissue. Here we were trying to keep the force rate constant. In every cycle indenter sets out the movements in order to catch the target force pertinent to that current time, thus the peak forces were the same. Due to breathing, difficulties of in vivo tests, and good sensitivity of loadcell, we normally cannot see the exact equilibrium force (Figure 5).

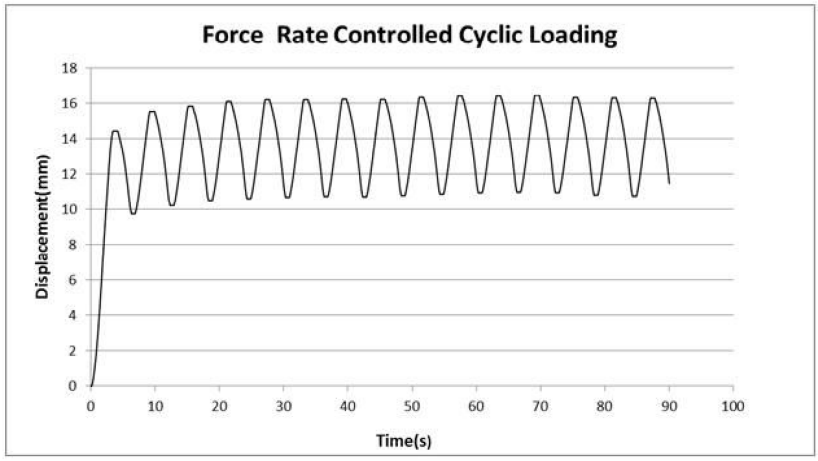

Figure 5. Force rate controlled cyclic loading test with 1.8N/s, 6s for every cycle and15 loop

In force-displacement graph of this experiment preconditioning was illustrated distinctly. There was a shift to right in curves by repeating cycles and during the last cycles almost repeating curves occurred. In addition to increase in the maximum displacements of the tissue (stretch), a decrease was observed in magnitude of hysteresis by increasing number of cycles and an approach to a repeatable pattern (Figure 6).

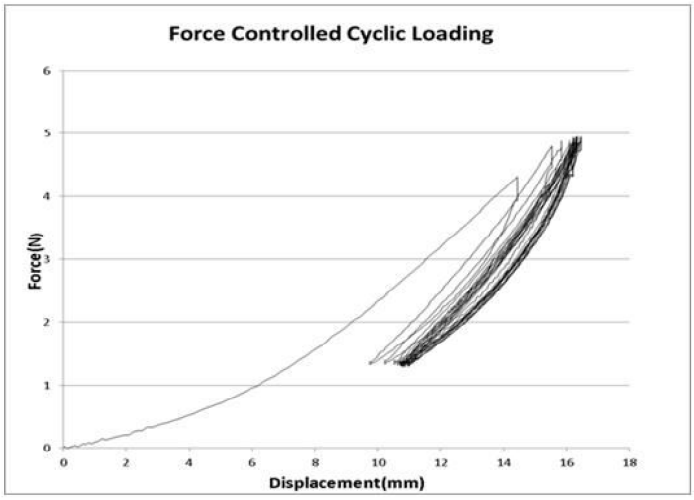

Figure 6. Obvious shift to right in maximum displacements by repeating cycles

In Figure (7), force-displacement relation under displacement rate control and load rate control for fifteen cycles is illustrated. The period of both experiment was 90 s but in different subjects. Mullin's effect shows up as a downward shift (i.e. decrease in force) in displacement rate controlled experiments whereas it shows up as a right shift (i.e. decrease in stiffness) in force rate controlled.

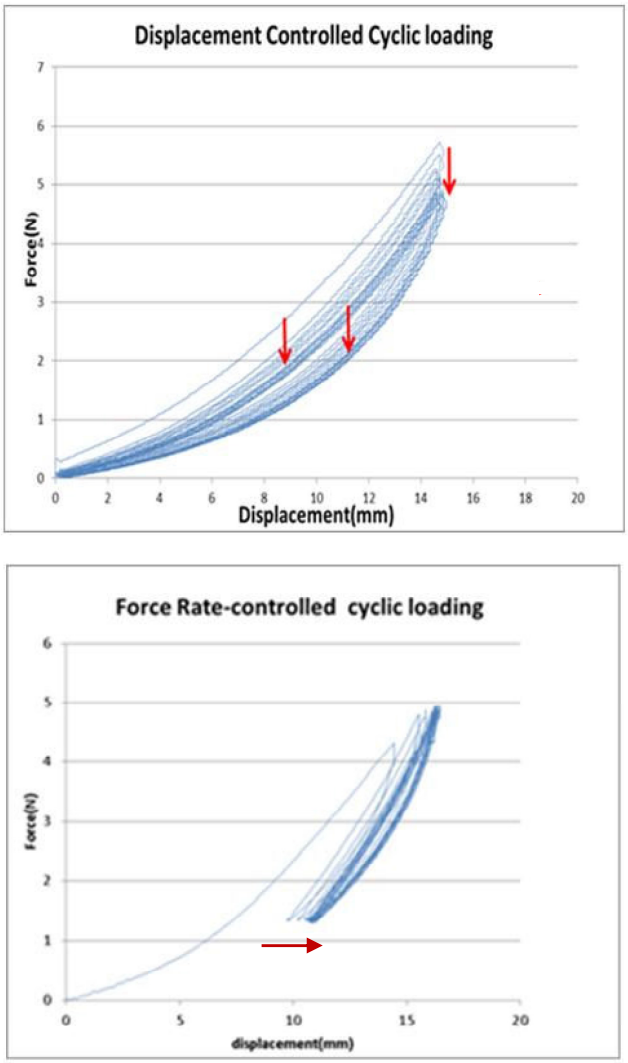

Figure 7. Force versus Displacement curves for indentation tests under displacement and load control for fifteen cycles. The period of both experiment was 90 s but in different subjects. Note the obvious shift to the right of the curves in the load controlled test.

3.3. Relaxation Experiment Results

In relaxation tests some periodic fluctuations were observed despite to the very small pulses related to heartbeats. After examinations and some experiments on dummy objects instead of individuals, as it was anticipated from previous studies (Tonuk.2004 and Petekkaya.2008) the source of these fluctuation was because of breathing. The number of periodic fluctuations and breathing times were in harmony. In relaxation tests, during constant imposed deformation, the resulting force drops progressively as time goes by and tends to an equilibrium value as time goes to infinity (Figure 8).

indenter travels less to catch the target force(Figure 10).

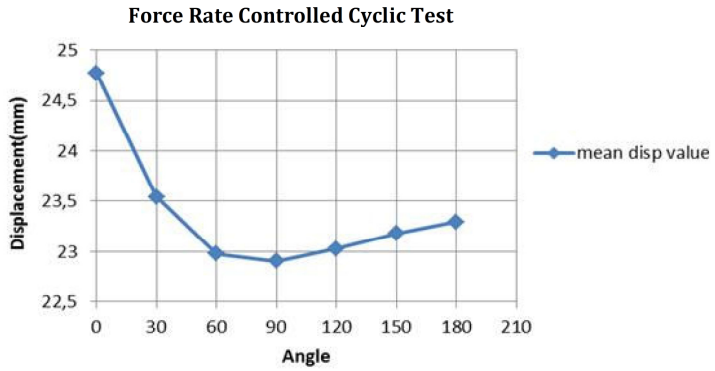

Figure 10. Displacement values of biceps muscle in different indenter tip alignments, to the same force controlled cyclic loading test. The tests were carried out at same point with 1N/s force rate, 5 loops and 100s total experiment time

4. Conclusion

This investigation is an experimental study to examine mechanical behavior of human soft tissues. One of the main reasons of doing material tests on soft biological tissues is to obtain a precise constitutive equation which can be used in finite element simulations of mechanical interaction of human body with surrounding. Better design of prosthesis, orthoses, identification of diseases, accident protection of passengers etc. are all based on accurate simulations where the bottle neck is material model. In this study in-vivo indentation experiments by an in-house indenter device were conducted on human arm muscles. Displacement rate and force rate cyclic loading, and relaxation experiment protocols were used. This study demonstrates the difference between Mullin's effect during in-vivo force rate controlled cyclic loading and the traditional displacement controlled test method. Ellipsoidal tip was used to examine in-plane anisotropy and material direction of bulk soft tissues. It was observed that the stiffer material direction is perpendicular to contraction direction of muscle in both displacement rate and force rate cyclic loading protocols. In addition it was observed that in relaxation tests, during constant imposed deformation, the resulting force drops slowly as time progresses and tends to an equilibrium value as time goes to infinity.

References

Ahn, B., & Kim, J., 2010. Measurement and characterization of soft tissue behavior with surface deformation and force response under large deformations. Medical Image Analysis, 14(2), 138–148.

Argatov, I. I., Mishuris, G. S., & Paukshto, M. V., 2015. Cylindrical lateral depth-sensing indentation testing of thin anisotropic elastic films. European Journal of Mechanics - A/Solids, 49, 299–307.

Barrett, S. R. H., Sutcliffe, M. P. F., Howarth, S., Li, Z.-Y., Gillard, J. H., 2009. Experimental measurement of the mechanical properties of carotid atherothrombotic plaque fibrous cap. Journal of Biomechanics, 42(11), 1650–1655.

Bischoff, J. E., 2004. Static Indentation of Anisotropic Biomaterials Using Axially Asymmetric Indenters—a Computational Study. Journal of Biomechanical Engineering, 126(4), 498.

Borodich, F. M., Keer, L. M., Korach, C. S., 2003. Analytical study of fundamental nanoindentation test relations for indenters of non-ideal shapes. Nanotechnology, 14(7), 803–808.

Carson, W. C., Gerling, G. J., Krupski, T. L., Kowalik, C. G., Harper, J. C., Moskaluk, C. A., 2011. Material characterization of ex vivo prostate tissue via spherical indentation in the clinic. Medical Engineering & Physics, 33(3), 302–309.

Carter, F. ., Frank, T. ., Davies, P. ., McLean, D., Cuschieri, A., 2001. Measurements and modelling of the compliance of human and porcine organs. Medical Image Analysis, 5(4), 231–236.

Chao, C. Y. L., Zheng, Y.-P., Huang, Y.-P., Cheing, G. L. Y., 2010. Biomechanical properties of the forefoot plantar soft tissue as measured by an optical coherence tomography-based air-jet indentation system and tissue ultrasound palpation system. Clinical Biomechanics (Bristol, Avon), 25(6), 594–600

Chen, W.-M., Phyau-Wui Shim, V., Park, S.-B., Lee, T., 2011. An instrumented tissue tester for measuring soft tissue property under the metatarsal heads in relation to metatarsophalangeal joint angle. Journal of Biomechanics, 44(9), 1801–1804.

Choi, A. P. C., Zheng, Y. P., 2005. Estimation of Young's modulus and Poisson's ratio of soft tissue from indentation using two different-sized indentors: Finite element analysis of the finite deformation effect. Medical & Biological Engineering & Computing, 43(2), 258–264.

Cox, M. A. J., Driessen, N. J. B., Boerboom, R. A, Bouten, C. V. C., Baaijens, F. P. T., 2008. Mechanical characterization of anisotropic planar biological soft tissues using finite indentation: experimental feasibility. Journal of Biomechanics, 41(2), 422–429.

Dimitriadis, E. K., Horkay, F., Maresca, J., Kachar, B., Chadwick, R. S., 2002. Determination of elastic moduli of thin layers of soft material using the atomic force microscope. Biophysical Journal, 82(5), 2798–2810.

Fath El Bab, A. M. R., Sugano, K., Tsuchiya, T., Tabata, O., Eltaib, M. E. H., Sallam, M. M., 2010. New compensation technique for the soft tissue stiffness measurements using two sensor probes configuration. Procedia Engineering, 5, 1304–1307.

Feng, Y., Okamoto, R. J., Namani, R., Genin, G. M., Bayly, P. V., 2013. Measurements of mechanical anisotropy in brain tissue and implications for transversely isotropic material models of white matter. Journal of the Mechanical Behavior of Biomedical Materials, 23, 117–132.

Fu, Y. B., Chui, C. K., 2014. Modelling and simulation of porcine liver tissue indentation using finite element method and uniaxial stress-strain data. Journal of Biomechanics, 47(10), 2430–5. doi: 10.1016/j.jbiomech.2014.04.009

Gefen, A., Margulies, S. S., 2004. Are in vivo and in situ brain tissues mechanically similar? Journal of Biomechanics, 37(9), 1339–1352.

Hu, J., Klinich, K. D., Miller, C. S., Rupp, J. D., Nazmi, G., Pearlman, M. D., Schneider, L. W., 2011. A stochastic visco-hyperelastic model of human placenta tissue for finite element crash simulations. Annals of Biomedical Engineering, 39(3), 1074–1083.

Iivarinen, J. T., Korhonen, R. K., Julkunen, P., Jurvelin, J. S., 2011. Experimental and computational analysis of soft tissue stiffness in forearm using a manual indentation device. Medical Engineering & Physics, 33(10), 1245–1253.

Kauer, M., No, D. E. T. H. (n.d.). Inverse Finite Element Characterization of Soft Tissues with Aspiration Experiments Inverse Finite Element Characteriza- tion of Soft Tissues with Aspiration, (14233).

Kauer, M., Vuskovic, V., Dual, J., Szekely, G., Bajka, M., 2002. I nverse finite element characterization of soft tissues, 6, 275–287.

Kim, J.,2004. Virtual Environments for Medical Training : Graphic and Haptic Simulation of Tool-Tissue Interactions By Virtual Environments for Medical Training :

Korhonen, R. K., Saarakkala, S., Juha, T. (n.d.). Experimental and numerical validation for the novel configuration of an arthroscopic, 1565.

Kroon, M., & Holzapfel, G. A., 2008. A new constitutive model for multi-layered collagenous tissues. Journal of Biomechanics, 41(12), 2766–71.

Lokshin, O., Lanir, Y., 2009. Viscoelasticity and preconditioning of rat skin under uniaxial stretch: microstructural constitutive characterization. Journal of Biomechanical Engineering, 131(3), 031009. doi:10.1115/1.3049479

Luo, G., Houston, V. L., Garbarini, M. A., Beattie, A. C., Thongpop, C., 2011. Finite element analysis of heel pad with insoles. Journal of Biomechanics, 44(8), 1559–1565.

Nava, A., Mazza, E., Furrer, M., Villiger, P., Reinhart, W. H., 2008. In vivo mechanical characterization of human liver. Medical Image Analysis, 12(2), 203–216.

Ottensmeyer, M. P., 2001. Minimally Invasive Instrument for In Vivo Measurement of Solid Organ Mechanical Impedance by.

Ottensmeyer, M. P., Kerdok, A. E., Howe, R. D., Dawson, S. L., 2004. The Effects of Testing Environment on the Viscoelastic Properties of Soft Tissues, 3078, 9–18.

Pailler-Mattei, C., Bec, S., Zahouani, H., 2008. In vivo measurements of the elastic mechanical properties of human skin by indentation tests. Medical Engineering & Physics, 30(5), 599–606.

Pandolfi, A., Vasta, M., 2012. Fiber distributed hyperelastic modeling of biological tissues. Mechanics of Materials, 44, 151–162.

Pelletier, H., Krier, J., Mille, P., 2006. Characterization of mechanical properties of thin films using nanoindentation test. Mechanics of Materials, 38(12), 1182–1198.

Peña, E., Peña, J. A., Doblaré, M., 2008. On modelling nonlinear viscoelastic effects in ligaments. Journal of Biomechanics, 41(12), 2659–2666.

Prevost, T. P., Jin, G., de Moya, M. A., Alam, H. B., Suresh, S., Socrate, S., 2011. Dynamic mechanical response of brain tissue in indentation in vivo, in situ and in vitro. Acta Biomaterialia, 7(12), 4090–4101.

Samani, A., Plewes, D., 2004. A method to measure the hyperelastic parameters of ex vivo breast tissue samples. Physics in Medicine and Biology, 49(18), 4395–4405.

Samur, E., Sedef, M., Basdogan, C., Avtan, L., Duzgun, O., 2007. A robotic indenter for minimally invasive measurement and characterization of soft tissue response. Medical Image Analysis, 11(4), 361–373.

Seifzadeh, A., Oguamanam, D. C. D., Trutiak, N., Hurtig, M., Papini, M., 2012. Determination of nonlinear fibre-reinforced biphasic poroviscoelastic constitutive parameters of articular cartilage using stress relaxation indentation testing and an optimizing finite element analysis. Computer Methods and Programs in Biomedicine, 107(2), 315–326.

Structure and Stress-Strain Relationship of Soft Tissues Author(s): Y. C. Fung Stable URL : http://www.jstor.org/stable/3882748 . Your use of the JSTOR archive indicates your acceptance of the Terms & Conditions of Use , available at . content in a t. (2014), 24(1), 13–22.

Tönük, E., Silver-Thorn, M. B., 2004. Nonlinear Viscoelastic Material Property Estimation of Lower Extremity Residual Limb Tissues. Journal of Biomechanical Engineering, 126(2), 289. doi:10.1115/1.1695575

Van Dommelen, J. A. W., van der Sande, T. P. J., Hrapko, M., Peters, G. W. M., 2010. Mechanical properties of brain tissue by indentation: interregional variation. Journal of the Mechanical Behavior of Biomedical Materials, 3(2), 158–166.

Yao, W., Yoshida, K., Fernandez, M., Vink, J., Wapner, R. J., Ananth, C. V, … Myers, K. M., 2014. Measuring the compressive viscoelastic mechanical properties of human cervical tissue using indentation. Journal of the Mechanical Behavior of Biomedical Materials, 34, 18–26.

Yin, Y., Ling, S.-F., Liu, Y., 2004. A dynamic indentation method for characterizing soft incompressible viscoelastic materials. Materials Science and Engineering: A, 379(1-2), 334–340.

Zhang, G. Y., Wittek, A., Joldes, G. R., Jin, X., Miller, K., 2014. A three-dimensional nonlinear meshfree algorithm for simulating mechanical responses of soft tissue. Engineering Analysis with Boundary Elements, 42, 60–66.

Zheng, Y., Mak, A. F. T., Lue, B., 1999. Objective assessment of limb tissue elasticity : Development of a manual indentation procedure, 36(2).

F.RESEARCH ETHICS COMMITTEE APPROVAL

UYGULAMALI ETİK ARAŞTIRMA MERKEZİ
APPLIED ETHICS RESEARCH CENTER

DUMLUPINAR BULVARI 06800
ÇANKAYA ANKARA/TURKEY
T: +90 312 210 22 91
F: +90 312 210 79
ueam@metu.edu.tr
www.ueam.metu.edu.tr

ORTA DOĞU TEKNİK ÜNİVERSİTESİ
MIDDLE EAST TECHNICAL UNIVERSITY

Sayı: 28620816/ 400 -2047

10.11.2014

Gönderilen : Y.Doç. Dr. Ergin TÖNÜK
Makine Mühendisliği

Gönderen : Prof. Dr. Canan Sümer
IAK Başkanı Vekili

İlgi : Etik Onayı

Danışmanlığını yapmış olduğunuz Biyomedikal Muhendisligi Bölümü öğrencisi Parinaz Ashrafi'nin "Material Identification of Soft Tissues by Indenter Experiments and Inverse Finite Element Modelling of Viscoelastic Behavior by Fractional Calculus Including in-plane Anisotropy" isimli araştırması "İnsan Araştırmaları Komitesi" tarafından uygun görülerek gerekli onay verilmiştir.

Bilgilerinize saygılarımla sunarım.

Etik Komite Onayı

Uygundur

10/11/2014

10 Kasım 2014

Prof.Dr. Canan Sümer
Uygulamalı Etik Araştırma Merkezi
(UEAM) Başkanı Vekili
ODTÜ 06531 ANKARA